MOLECULAR DYNAMICS STUDY OF THERMAL DISORDER IN A BICRYSTAL MODEL

by

Tue Nguyen

B.S., Physics, M.I.T. (1984)
B.S., Computer Science, M.I.T. (1985)
B.S., Electrical Engineering, M.I.T. (1985)
B.S., Mathematics, M.I.T. (1985)
B.S., Nuclear Engineering, M.I.T. (1985)
M.S., Nuclear Enginerring, M.I.T. (1986)

SUBMITTED TO THE DEPARTMENT OF NUCLEAR ENGINEERING IN PARTIAL FULFILLMENT OF THE REQUIREMENTS FOR THE DEGREE OF

DOCTOR OF PHILOSOPHY

at the

MASSACHUSETTS INSTITUTE OF TECHNOLOGY

September 1988

Signature of Author _____
Department of Nuclear Engineering
September 27, 1988

Certified by _____
Sidney Yip
Professor of Nuclear Engineering
Thesis Supervisor

Accepted by _____
Allan F. Henry
Chairman, Department Committee on Graduate Students

MOLECULAR DYNAMICS STUDY OF THERMAL DISORDER IN A BICRYSTAL MODEL

by

Tue Nguyen

Submitted to the Department of Nuclear Engineering on September 27, 1988 in partial fulfillment of the requirements for the degree of Doctor of Philosophy.

Abstract

The question of whether or not the grain boundary (gb) interface will melt at a temperature distinctly below the bulk melting point T_m has been longstanding. Experiments have shown that there is no evidence of gb premelting but resolution limitations preclude detailed observations of the onset of thermal disordering at the gb before it melts. Molecular dynamics (MD) simulation results regarding this question of gb premelting are divided, because different techniques and models have been used.

This thesis attempts to resolve this issue by a careful MD study of a (310) $\theta = 36.86^o$ <001> symmetrical tilt bicrystal model using an Embedded Atom Method (EAM) aluminum potential. The melting temperature T_m is first determined using the criterion of coexistence of the solid and liquid phases. Then the gb structure is studied directly to determine whether or not there is gb premelting. Finally the thermal disorder behavior of the gb structure below melting is examined.

Based on the explicit results concerning structural order, energy and mobility obtained from the present simulations, we find that our bicrystal model shows no evidence of premelting (complete melting below T_m). Both the surface and the gb interface exhibit thermal disorder at temperatures below T_m with complete melting occurring at or very near T_m. Concerning the details of the onset of melting, the data show considerable disordering in the interfacial region starting at about 0.93 T_m. The interfaces exhibit metastable behavior in this temperature range, and the temperature variation of the interfacial thickness suggests that the disordering induced by the interface is a continuous transition, a behavior that has been predicted by a theoretical analysis. Our results also indicate a close similarity between the disordered behavior at the external surface and at the internal surface (gb) having the same orientation.

The conclusion of our work regarding the absence of gb premelting is consistent with the most recent experimental observations and also in agreement with various simulation results which indicate that gb melting should occur at T_m.

Thesis Supervisor: Sidney Yip
Title: Professor of Nuclear Engineering

Acknowledgement

I would like to thank my thesis supervisor, Prof. Sidney Yip, for his guidance, friendship and assistance through all aspects of my graduate study at M.I.T.

I thank Drs. Paul S. Ho and Thomas Kwok of IBM T.J. Watson Research Center for the financial and moral support, insightful discussions and suggestions while I was at IBM. I would like to thank Dr. Ho for being my thesis reader and for allowing me to use the IBM supercomputer facility where the majority of the simulation runs presented in this thesis were made.

I thank Drs. D. Wolf, J. Lutsko and S. Phillpot of ANL for invaluable discussions that are instrumental to the development of this project. Together we have developed the MD program used in this work. I am also thankful to Dr. Wolf who made the EAM potential capability possible and provided Cray time for the simulation study.

I thank R. Craig Williamson, Program Manager of the DOE Radioactive Waste Management Fellowship program, for all his support and understanding in my fellowship period. I am also thankful to him for giving me an extension of the fellowship.

I thank Prof. M. Kazimi for his useful advise in financial aid matter.

I thank Prof. O. Harling for guidance and support in my years at M.I.T.

I thank S.M. Foiles for his effort in fitting the aluminum EAM potential and making it available to me.

I thank Cindy Nitta for helpful friendship.

I thank my colleagues, Kin Cheung and Tze Poon, for support and friendship.

The research was performed under appointment to the Radioactive Waste Management Fellowship program administered by Oak Ridge Associated Universities for the U.S. Department of Energy.

Table of Contents

List of Figures

List of Tables

Chapter 1

Introduction

Interfacial phenomena play a critical role in many important thermodynamic and mechanical properties of materials such as strength, ductility, creep behavior, diffusion, intergranular fracture, segregation, etc. One of the most common interfaces is grain boundary (gb) which is the interface between two single crystals of different orientations.

In the study of gb properties in metals, there is a longstanding question of whether or not the gb interface will melt at a temperature distinctly below the bulk melting point T_m. This problem of gb premelting, defined in this thesis to be the melting at the gb at temperature below melting, has been addressed as early as 1947.[1] Much later (1972) a review[2] based on experimental measurements and evidence prior to 1972 concluded that both theoretical arguments and exprimental observations could not resolve unambiguously the question of gb premelting. More recently (1987), this subject has been again reviewed [3,4] and gotten essentially the same conclusion that further studies, both theoretical and experimental, are needed to settle this problem. A related phenomenon is the melting at an external surface (the surface premelting problem) which is also not completely understood.[5]

The basic difficulty in the study of the gb premelting phenomenon is the atomic scale of the gb region core. Therefore various experiments have used indirect methods to understand the gb structures at high temperatures such as the gb sliding and migration experiments[6-8] or rotating spheres experiments.[9,10] The disadvantage of the indirect approaches is that in general they are much harder to analyze and interpret, and often the results are not conclusive. For example, the gb sliding and migration experiments[11] have shown that the activation energy associated with the sliding rate of the bicrystals changes at a certain temperature T_c which ranges between 0.7 to 0.9 T_m for high angle gb. This

change was attributed to a gb structural transformation. However there is no information available on the structure of the gb therefore one cannot say if this transformation is the gb premelting transition. The rotating spheres on-a-hot-plate experiments [9-10] have led to the conclusion that essentially all gb could not have been completely melted up to .99 T_m because of the rotation of the spheres due to the dependence of their energy on crystal misorientation. However this does not exclude the possibility that the gb region is highly disordered and the atomic positions at the interface still correlated with the single crystal material in the two grains adjoining the boundary.

More recently, direct observations of the gb structures at temperatures near T_m have been performed[12,13] by hot stage TEM to locate grain boundary dislocations (gbd) and to observe the partially melted polycrystalline aluminum specimen. Results from gbd observations indicate that gb structures remain ordered up to .96 T_m. Observations of the partially melted polycrystalline aluminum specimen lead to the conclusion that there is no complete gb melting in aluminum below .999 T_m. However this technique does not offer any information on the thermal disorder of the gb which preceeds the complete melting process.

Difficulties and limitations of experimental techniques so far have precluded any information on the atomistic scale in the temperature range close to T_m. Therefore computer modeling is especially important and has been used exclusively for studying gb structures and behavior at high temperatures. However, simulation results regarding the question of gb premelting are divided, because different techniques and models have been used.[14] Explicit evidence showing the gb behavior below T_m upon which different simulation workers can agree is still lacking. 2-d lattice gas model study of Kikuchi and Cahn[15] has suggested a gradual transition which leads to complete melting at T_m. More recently molecular dynamics (MD) simulations have been carried out to investigate the behavior of the bicrystals at finite temperatures. The advantage of MD calculations is that,

in principle, the only assumptions involved are classical Newtonian mechanics and specific interatomic potentials for the material being simulated. In practice, there are limitations due to the finite system size and duration of the simulation. Nonetheless, it is quite generally accepted that atomistic simulations can provide the most detailed information about the structural and dynamical behavior of models of relatively simple material systems.

Recent MD studies have revealed pronounced structural disorder in idealized model at a temperature distinctly lower than that where the bulk lattice becomes disordered. MD simulations of $\Sigma = 7$[16] and $\Sigma = 13$[17] two dimensional bicrystals indicate a structural transition occurring at approximately .7 T_m to .8 T_m, where T_m is the melting temperature of the reference system, a perfect 2d lattice in this case. The interpretation that the transition is gb melting is based on the temperature variation of the enthalpy and on structure information in the forms of instantaneous atomic configurations.

There exists also a number of MD studies of 3d bicrystal models, all showing the phenomenon of structural disorder at temperature significantly below T_m. Ciccotti et al.[18-20] studied the temperature dependence of a high angle Σ 5 gb using Lennard-Jones (LJ) pair potential and obtained results which appear to be in qualitative agreement with Kikuchi and Cahn. Their results indicated the onset of a gradually disordering transition at 0.5 T_m. However, because of their border condition (periodic border condition, PBC) mutual annihilation of the gb occurred at 0.9 T_m, thus direct information on the gb structure near T_m could not be obtained.

Broughton and Gilmer[21] have also investigated gb premelting in several tilt gb by calculating interface excess free energy through harmonic analysis of the ground state configurations and comparing with MD results. They found gb premelting only in the high angle gb at T_m while the other gb remain ordered up to T_m. They concluded that gb premelting is not a true phase transition at temperature below T_m since the thermodynamic

parameters are continuous functions of temperature. Also the quasi-liquid (disordered region at the interface) must retain some crystalline symmetry because of the small gb region below T_m.

In contrast to these results, Deymier et al.[22] have studied 2d and 3d bicrystals and found evidence for a first order phase transition at 0.8 T_m through excess free energy calculations. Also Nguyen et al.[23,24] have studied an aluminum bicrystal at high temperature and found gb premelting at temperature as low as 0.7 T_m. However, they have overestimated the melting temperature T_m, thus their interpretation of the gb premelting phenomenon is not valid. We will return to this point in chapter 4.

Lutsko and Wolf[25] also studied gb disordering at high temperature and found that twist gb structure is ordered up to 0.85 T_m. They also suggested that the frustration of gb migration in 3d periodic border condition could cause the thermal disordering in the gb structure.

The purpose of this thesis is to study the gb premelting phenomenon by a careful MD study of a specific bicrystal model using state-of-the-art MD techniques. The objective is to first determine the melting temperature T_m for the potential used, then the gb structure is studied directly to decide whether or not there is gb premelting. Finally the thermal disorder behavior of the gb structure below melting is examined.

The thesis is divided as follows. Chapter I gives the introduction, background, and objective of this thesis. Chapter II describes the MD simulation technique and the bicrystal model with emphasis on the difficulties of proper border conditions and realistic interatomic potential functions. Chapter III discusses the thermal disorder in a bulk crystal model. Chapter IV determines the melting temperature T_m and examines the thermal disorder of the free surface in a model with free surface. Chapter V examines the thermal disorder in the bicrystal model and discusses factors which could affect the results of the model. Chapter VI offers comparison and interpretation of present results in light of the previous simulation studies. Chapter VII gives the conclusions.

Chapter 2

Simulation technique

With the advances in supercomputers and theoretical studies of interatomic potentials, molecular dynamics (MD) is gaining acceptance as a standard simulation tool for the investigation of material behavior and properties, especially in areas where experiments are difficult such as interfacial phenomena. The main difficulties of the experimental techniques in studying interfacial phenomena are (i) the extent of the interface is of order of few atomic layers, so atomic resolution is required, (ii) the mobility of these interfaces is high, especially at high temperature, so during the course of the experiment, the interface can migrate out of the observed section of the sample, and (iii) there are many parameters which could affect the measurement. A sample of a bicrystal could contain an impurity concentration resulting from material processing technique or from segregation from the bulk. It could have inherent strains from heat treatment process. There could also be elastic and plastic deformation, all of which have to be taken into account for an accurate interpretation of the data.

The effects of these numerous variables can be separated in MD studies. The advantage of an MD approach is that different models can be used to isolate the effects of different parameters, thus it is possible to effectively eliminate the problem of competing effects in studying a complex process. For example a pure system model with no impurity or defects could be used to study the geometry and structural dependence of interfacial properties. Compositional effects could be studied by using pure alloy systems. The effects of impurity then can be studied by adding impurities into the model.

In this chapter, a brief description of the MD technique is presented. Then the bicrystal model used in this work will be described with emphasis on the border condition and potential function.

2.1 Molecular dynamics method

Standard molecular dynamics technique is employed in this work. The MD technique has been extensively described elsewhere,[26] together with its applications to gb simulation,[27] therefore only a brief description of the technique is presented here.

The basic idea of MD is to generate atomic trajectories by numerical integration of Newton's equations of motion for N atoms, i.e. to solve numerically a set of N x d coupled nonlinear second order differential equations where N is the number of atoms and d is the dimension. Properties can be calculated from the atoms' positions and velocities. The MD simulation technique is summarized in a flowchart in Fig. 2-1.

The advantage of MD is the availability of the gb structures at the microscopic scale. MD simulation also gives a vast amount of data about the movement of individual atoms in the gb region which is not accessible from experiments. These atomistic data offer detailed information of gb behavior which will give basic understanding in term of atomic structure and kinetics.

The main limitations of the MD technique are the interatomic potential functions and border conditions for the simulation cell which will be discussed extensively in the next sections. Other limitations are the size and time scales of the simulation which are a compromise between the simulation reality and computational resource.

Interatomic potential function is an indispensible ingredient in MD simulation because it is the basic assumption of the technique. Recent advances in interatomic potentials for fcc metal[28-30] have given more realistic potential functions especially in regions with defects like surfaces or gb. Border conditions are also important in MD simulation. Because of limitation due to finite size system which is a consequence of computer resource limitation, border conditions are chosen so that the effects of the border are negligible. New, improved border conditions[31,32] have successfully removed many restrictions and possible artifacts of the early models.

2.2 Bicrystal model

2.2.1 Geometry

The grain boundary model is an aluminum bicrystal (310) $\theta = 36.86^{o}$ <001> symmetrical tilt structure ($\Sigma = 5$) as shown in Fig. 2-2. In specifying the geometry of the model, coordinate axes are chosen such that the x direction is along the [130], the y direction [001], and the z direction [310]. The system has periodic borders along the x and y directions. Along the z direction, free border condition is used. The interatomic potential used is an EAM potential fitted to aluminum properties. The detailed description of this border condition and potential function will be presented in the next section.

Σ 5 tilt gb has been studied extensively in previous works including gb structure, energy,[33,34] and dynamics.[18,19] Σ 5 tilt gb of bcc metal (iron) has been studied also in the past.[35] It is natural to extend our study to fcc metal to study the effect of different crystal structures. Aluminum is chosen because of the current interest in aluminum metal connecting lines in integrated circuits. Electromigration damage in fine metal lines (mostly made of aluminum) is a direct consequence of their microstructure (through gb diffusion) and geometry.[36] Geometry dependence of electromigration damage has been studied extensively,[37] but theoretical study of the effect of gb diffusion on electromigration is still very limited.

The model is composed of 1920 atoms with 2 and 32 CSL units in the x and z directions respectively, and a y dimension of 3 lattice constants. The small size of the gb plane is chosen to ensure a planar gb, thus minimizing effects due to curved gb plane. The large size of the simulation cell in the z direction is to allow adequate bulk material between the gb plane and the surfaces.

The Σ=5 symmetric tilt gb structure created by the coincident site lattice method is not stable due to the small separation between a pair of atoms in each of the two CSL units

across the boundary in every other (001) plane (see Fig. 2-2). Standard procedure is to remove one atom from the close pair.[33,34,18] One atom is then removed from every close pair in the initial configuration of the Σ 5 tilt gb structure. Relaxation is necessary after removing atoms in the simulation cell to allow for possible translation, expansion or contraction of the two crystals. Relaxation is automatically carried out at all temperatures in this model because the top and bottom crystals are allowed to move with respect to each other in all three directions. The free surfaces allow the expansion or contraction of the two crystals in the z direction. The periodic condition in the x and y directions and the lack of constraints of the two crystals allow them to move along the x and y directions also.

2.2.2 Interatomic potentials

The main theoretical limitation of MD is the availability of the interatomic potentials describing the forces between atoms. The accuracy of the simulation results depends heavily on the prescribed potentials.

In this study two types of potentials are used to investigate interfacial behaviors and properties of metals: empirical potentials and the Embedded Atom Method potentials[30].

The empirical potential used in this study is the Morse potential, fitted to vacancy formation energy of aluminum[38] shown in Fig. 2-3

$$V=D_o(\exp(-2\alpha(r-r_o))-2\exp(-\alpha(r-r_o))) \tag{2.1}$$

where the potential parameters D_0, α, r_0 depend on the potential range cutoff. In this study a Morse potential with a range cutoff of 1.49 a_0 that lies between 4th and 5th nearest neighbor is used. For this cutoff, the Morse potential parameters are

$$D_0 = 0.115759 \text{ eV}$$

$$\alpha = 2.350012 \text{ A}^{-1}$$

$$r_0 = 2.876333 \text{ A}$$

Morse type potentials are widely used to simulate metals[39-41] in early studies mainly because nothing else was available.

The main advantage of empirical potentials is that they are simple and easy to use. However empirical potentials do not represent metals well and its applications are rather controversial. The assumption of pair interaction for many empirical potentials is insufficient since non local interaction might be important. Electronic contributions are ignored or at best are lumped together in the atom interaction. Short range interaction of empirical potentials due to the limitation of computational resources could also affect the simulation results since long range interaction in metals due to ion-ion interaction (Friedel oscillation) can be significant for some properties.[42]

Despite these disadvantages, empirical potentials perform fairly well in simulations. The effects of the short range cutoff, though a necessity due to the constraint of computational resources, should be studied in view of the calculations of grain boundary energies at zero temperature which show a sensitive variation at short cutoffs.[43] In that study, it is also shown that grain boundary energies and structures vary greatly for different potentials. It therefore suggests that empirical potentials can only give qualitative behaviors of materials.

Together with the truncation at short range, shifting the potential to achieve smoothness across the range cutoff is essential to avoid unphysical effects due to the discontinuity at the range cutoff. The shifted potential will have zero potential and force at the range cutoff

$$V_{shifted}(r)=V_{unshifted}(r)-V_{unshifted}(r_{cutoff})-V'_{unshifted}(r)\times(r-r_{cutoff}) \tag{2.2}$$

where the apostrophe denotes derivative with respect to r. As a result the shifted potential will be slightly different from the unshifted potential.

Improved interatomic potential functions for metals have become available recently

following the development of the embedded atom method (EAM).[28-30] Although the resulting potentials are still effectively fitted to known properties of metals, the variation with local electron density is explicitly taken into account through density functional formalism, and this eliminates the major objections to the empirical potentials: the neglect of the electronic contributions, the Cauchy discrepancy and the cohesive energy-vacancy formation dilemma.[44] Another potential model, equivalent to the EAM, using the second moment approximation to the tight binding method has been independently developed by Finnis and Sinclair.[45] Also Oh and Johnson[46] has proposed simple functional forms for EAM potentials to replace its current complex forms available only in numerical table.

The EAM potentials for fcc metals have given very encouraging results in a number of calculations of material properties.[47] They provided a good description of phonons [48] and liquid metal structure.[49] They also have been used to study hydrogen interaction with metals.[50] It described well the surface segregation in NiCu alloys system,[51] the equilibrium segregation at internal defects,[52] and alloy grain boundary properties.[53]

The interatomic potential used in this work is an EAM potential developed by Foiles. [54] The potential has been fitted to the elastic constants, sublimation energy, lattice constants and vacancy formation energy of pure aluminum.

$$E_{tot} = \sum_i F_i\left(\sum_{j \neq i} \rho_i(r_{ij})\right) + \frac{1}{2}\sum_{i \neq j} \Phi_{ij}(r_{ij}) \tag{2.3}$$

where E_{tot} is the total energy of the system, r_{ij} is the distance between atom i and atom j, $\rho_j(r_{ij})$ is the electron density contributed by atom j to atom i, and Φ_{ij} is the pair interaction between atom i and atom j.

The pair interaction term Φ_{ij} is fitted to a Morse potential form (equation (2.1)) with the values

$$D_0 = 0.25959 \text{ eV}$$

$$\alpha = 2.65803 \text{ A}^{-1}$$

$$r_0 = 1.88067 \text{ A}$$

The atomic electron density ρ_j is calculated from the Hartree-Fock calculations of Clementi and Roetti[55] but using only the longest range parts of these functions for computational ease. The embedding function F_i is determined by requiring that the homogeneous deformation of the fcc lattice obeys the simplified equation of state proposed by Rose et al.[56] The pair potential function Φ_{ij} and the density function ρ_j are cutoff at a distance of 5.45 A (between fourth and fifth nearest neighbors) and a constant shift is added to the function so that they go continuously to zero at the cutoff.

The potential functions $F_i(\rho)$, $\rho_j(r)$ and $\Phi_{ij}(r)$ are shown in Fig. 2-4, 2-5 and 2-6 respectively.

2.2.3 Border conditions for bicrystal models

Bicrystal models are commonly used to analyze and interpret physical properties of grain boundary solids.[57] In defining a bicrystal model one has to consider both the geometric structure of the interface (grain boundary) and the interatomic potential functions through which the particles are assumed to interact. The effects of the interatomic potential functions have been discussed in previous section. This section will concentrate on the geometrical structure of the interface. Simulation calculations must be performed on a simulation cell with specified dimensions, geometry and border condition. These specifications in turn determine the spatial extent of the crystalline material on either side of the interface and the relation between the system under direct simulation and a specimen on the macroscopic scale. Since cells of varying size and border conditions of different types have been used, an appreciation of the cell-specific effects is helpful when discussing the physical significance of simulation results.

Bicrystal models are generally based on the coincident-site-lattice concept which assumes perfect matching of atomic positions at the interface.[58,59] In this construction the

two halves of the bicrystal are single crystals which have been rotated relative to each other about an axis which lies either in the plane of the interface (tilt boundary) or normal to the plane (twist boundary). For reasons of computational economy, it is common to consider high-angle boundaries to take advantage of the smaller periodic structural units. This means choosing boundaries with a low value of Σ, where Σ is the inverse density of the coincident-site-lattice points. A number of tilt boundaries have been investigated on the grounds that these are low-energy boundaries and are therefore special.[60] Thus far MD studies have been concerned only with tilt boundaries. However, there are cogent reasons for studying twist boundaries[60]. From a geometrical analysis it has been shown that a symmetrical tilt boundary is a special case of twist boundary (180^{o} angle of rotation and some translation). Moreover, the most important parameters governing the grain boundary energy are shown to be the interplanar spacing normal to the interface and the area of the planar unit cell in the plane of the interface, the boundary plane. It follows from these considerations that studies of twist boundaries can best lead to a general understanding of interfacial properties.

The development of appropriate border conditions for atomistic calculations is another important issue. The basic function of the border conditions imposed on the simulation cell is to keep the computational burden within reasonable limits without introducing artificial constraints on the bicrystal system. This means the borders must ensure that the interface is properly surrounded by bulk matter while keeping the simulation cell size to a minimum. In the two (x and y) directions parallel to the interface, the periodic nature of the coincident-site-lattice model makes the use of periodic border condition a natural choice. In the perpendicular (z) direction it is not clear what border condition is the most appropriate. Early studies have employed periodic borders[16-19,21,22] or fixed borders,[24,62] each with some unsatisfactory consequences. Recently, methods which permit the simulation cell to expand or contract in the z direction as well as independent x-y

translations for the two halves of the bicrystal have been proposed.[31,32] Free border model also has shown reasonable results using the EAM potential since the EAM potential stabilizes the surface quite well.[61] In this study, these border conditions will be discussed.

A good bicrystal model should contain only one interface since the interaction between interfaces is unknown, unless one is studying this interaction. Therefore the periodic border condition in the direction perpendicular to the interface plane is undesirable because it introduces a second interface in the simulation cell. These two interfaces will interact and at sufficiently high temperatures, thermally activated boundary migration will lead to the annihilation of the two interfaces.[62] This undesirable effect can be minimized by using large enough simulation cell so the the interaction between these two interfaces is kept to a negligible level, at least at the outset of the simulation. However this could render the simulation cell to be unnecessarily too large. Other undesirable feature of the periodic border condition is that grain boundary expansion will occur at the expense of the bulk crystal, i.e., in order to make room for the expansion of the interface, the bulk has to be squeezed together, thus raising the pressure and also distorting the structure of the bulk materials. This effect could be avoided by using Parrinello-Rahman (PR) boundary condition[63] which allows the cell to expand or contract in the z direction according to the stresses produced in the cell. However this is not totally satisfactory because strictly speaking, PR boundary condition is only applicable to homogeneous system. For a non-homogeneous system like the bicrystal model, PR boundary condition will relieve the stresses in the grain boundary region by uniformly expanding the whole system, effectively using the negative pressure in the bulk region resulting from this unnecessary and unphysical expansion to compensate for the high pressure in the grain boundary region. In principle this mechanism of relieving stresses in the bicrystal model is not satisfactory but one could argue that eventually the bulk could return to the ideal crystal state and then the stresses in the grain boundary region is relieved. This question still needs to be resolved as to how it would affect the simulation.

To achieve a bicrystal model that contains only one interface, the top and bottom bulk materials need to be decoupled. A Region I-Region II treatment will accomplish this goal. The basic idea of this border treatment is to divide the simulation cell (so-called Region I) into a central interface region which contains the grain boundary, bounded at either end by a buffer region (see Fig. 2-7).

This computational cell in which Newton's equations of motion are solved explicitly for every atoms is then surrounded by a so-called Region II which simulates the embedding of the interface region into a bulk ideal crystal environment. To accomplish this the atom positions in region II are chosen to be a replica of the atom positions in the corresponding buffer. The advantage of this Region I-Region II treatment is that there will not be a second grain boundary interface although in general there will be additional interfaces between Region I and Region II. The effect of these extra interfaces will be small because they are embedded in bulk ideal crystal. Their presence is due to the difference in behavior of atoms in Region I and Region II.

There are different models resulting from this border treatment. The first is the fixed border condition?[35] In this border condition, the atoms in Region II are held fixed throughout the simulation. The constraint on the cell imposed by the fixed borders is in principle highly undesirable. However in practice the actual effects on the behavior of the interfacial region are small if sufficiently large bicrystal model is used. The main objection to the fixed border condition is similar to that of the periodic border condition, namely the fixed atoms in Region II will not allow the expansion of the interfacial region. Worse yet, it does not even permit the relative translations (in the boundary plane, x-y directions) of the two halves of the bicrystal, which is considered to be important especially for tilt grain boundaries. To compensate for these effects, starting interfacial structure need to be carefully determined to ensure proper amount of translations and expansion of the grain boundary. This could be done easily at T = 0K using energy minimization technique. It is

assumed that the translations will not be a function of temperature, though this assumption is not tested. For the grain boundary expansion, it is known that at higher temperature there is more expansion. Therefore the predetermined grain boundary expansion at T = 0K will not be correct at higher temperatures. To study this effect, two simulation cells of different sizes in the z direction need to be used. Any property which is significantly affected by the fixed borders will show variations with cell size; conversely, if the same property values are obtained from both models this would provide numerical evidence that the border effects on that property are not serious.

Another Region I-Region II border treatment is the semiperiodic border condition (SPB).[31] In the fixed border condition the atom positions in Region II are a replica of the atom positions in the corresponding buffer only at the beginning of the simulation run, because at a later time the buffer atoms will move while the Region II atoms will not. In the semiperiodic border condition the atom positions in Region II are always a replica of the atoms positions in the corresponding buffer, i.e., atoms in Region II are always the image of atoms in the corresponding buffer. The advantage of this semiperiodic border condition is that atoms in Region II behave as if they are in a bulk ideal crystal environment and they are not held at T = 0K as in the case of the fixed border condition. Since the top and bottom buffers are decoupled and could move independently, translations and expansion of the grain boundary region are allowed. A disadvantage of this border is that surface heating occurs in the region adjacent to Region II since atoms moving in the border regions will do work on the atoms in the buffer regions. This heating can be suppressed by rescaling the temperature separately in these regions. The temperature rescaling scheme giving the best uniform properties (potential energy, temperature) across these surfaces is to divide the outer buffers, the regions to rescale the temperature separately, into two regions according to the repulsive and attractive part of the interatomic potential and then rescaling them separately.

Another variation of the Region I-Region II border treatment is being proposed.[32] In this border condition, the Region II atoms are held fixed with respect to each other. However, they can move as a whole in response to the forces in the x and y directions and the stress in the z direction.

Free border condition is also being proposed where Region II is a vacuum. The advantage of the free border condition is the capability of relieving stress generated from the gb region. The free surfaces at both ends of the simulation cell will allow the expansion of the gb region. Translations of the upper and lower crystals in the bicrystal model are also possible without any constraints. The disadvantage is that the interaction between the external surfaces and the internal interface as well as the range of this interaction are not known. Therefore the behavior of the internal interface could be influenced by the surfaces. The surface behavior therefore needs to be studied separately and then compared to that of the bicrystal model.

Free border model is mainly used in this work to study the thermal disorder behavior of the gb interface. However other border conditions, fixed border and semiperiodic border, are also examined to evaluate the dependency of the gb behavior on border conditions.

2.2.4 Local property calculations

Since the behavior of the gb region is of primary interest, it is essential that this region can be identified and separated from the bulk region. Thus the simulation cell is divided into equal layers along the z direction, each having a length of 1/2 CSL (0.79 a) and containing 30 atoms at the outset. The size of these layers is small enough to allow the distinction between surface region and bulk region, yet large enough to have good statistics. An estimate of the standard deviation of a system with size N is $1/\sqrt{N}$. For a layer of 30 atoms, the standard deviation is about 18%. There are 64 layers in this model. At T=0K,

the gb interface is situated in the central layers, layer 32 and 33. The two free surfaces are at the two outermost layers, layer 1 and layer 64. Elementary lattice sums[64] have suggested that the fifth and subsequent layers (approximately 4 lattice constants from the surface) are not likely to be perturbed appreciably by the free surface, so one could consider the surface regions to extend about 5 layers from the surface. The layers between the gb and the surfaces therefore should behave like bulk material. In the course of the simulation runs, their properties are calculated and compared with bulk properties to ensure that the model has enough bulk material between the gb interface and the surfaces.

We are primarily interested in those physical properties which are well defined at any temperature and which reveal some aspects of the structural order. We therefore consider a thermodynamic property, the potential energy U, two structural properties, the static structure factor $S(\underline{K})$ and the radial distribution function g(r), and atomic mobility in terms of mean squared displacement (MSD) Δr^2 and the diffusion coefficient D. Also the stress tensor π and the hydrostatic pressure P are monitored to ensure that the system is in stress free condition. These are defined as

$$U = \frac{1}{2} < \sum_{i,j \in L} u(r_{ij}) > \quad (2.4)$$

$$S(\underline{K}) = \frac{1}{N^2} \mid \sum_{i \in L} exp(i\underline{K} < \underline{r}_i >) \mid^2 \quad (2.5)$$

$$\rho g(r) = < \frac{1}{N} \sum_{i,j \in L} \frac{\delta(r - r_{ij}, \Delta r)}{V(\underline{r}_i, r, \Delta r)} > \quad (2.6)$$

$$\Delta r^2 = < \sum_{i \in L} (r_i(t) - r_i(0) - r_{cm}(t) + r_{cm}(0))^2 > \quad (2.7)$$

$$D = \frac{1}{6}\frac{<\Delta r^2>}{t} \tag{2.8}$$

$$\Omega\pi = <\sum_{i \in L} m\underline{v}_i\underline{v}_i - \sum_{i,j \in L} \frac{\partial u(r_{ij})}{\partial \underline{r}_{ij}}\underline{r}_{ij}> \tag{2.9}$$

$$P = Trace(\pi) = \frac{1}{3}(\pi_{11}+\pi_{22}+\pi_{33}) \tag{2.10}$$

where u is the interatomic pair potential, $\underline{r}_i$ is the position of atom i, r_{ij} is the scalar distance between atom i and j, m is the atom mass, t is the time, $\underline{v}_i$ is the velocity of atom i, Ω is the volume of layer L, $V(r_i,r,\Delta r)$ is the volume of a spherical shell inside the layer L with center $\underline{r}_i$, radius r and shell thickness of Δr, ρ is the bulk density, $\underline{K}$ is a prescribed wave vector, chosen in this work to be along the y direction, N is the number of atoms in layer L, r_{cm} is the center of mass position of layer L. In these expressions, the ensemble average denoted by the angular bracket < > will be treated as a time average over the simulated trajectories and δ is a modified delta function defined as

$$\delta(r,\Delta r) = \begin{cases} 1 & if -\Delta r/2 \le r \le \Delta r/2 \\ 0 & otherwise \end{cases} \tag{2.11}$$

Our expression differs somewhat from the conventional definition of the structure factor $S(\underline{K})$ in that the particle position $\underline{r}_i$ is replaced by $<\underline{r}_i>$. By using a time-averaged position we find $S(\underline{K})$ is more free of the effects of thermal motions.

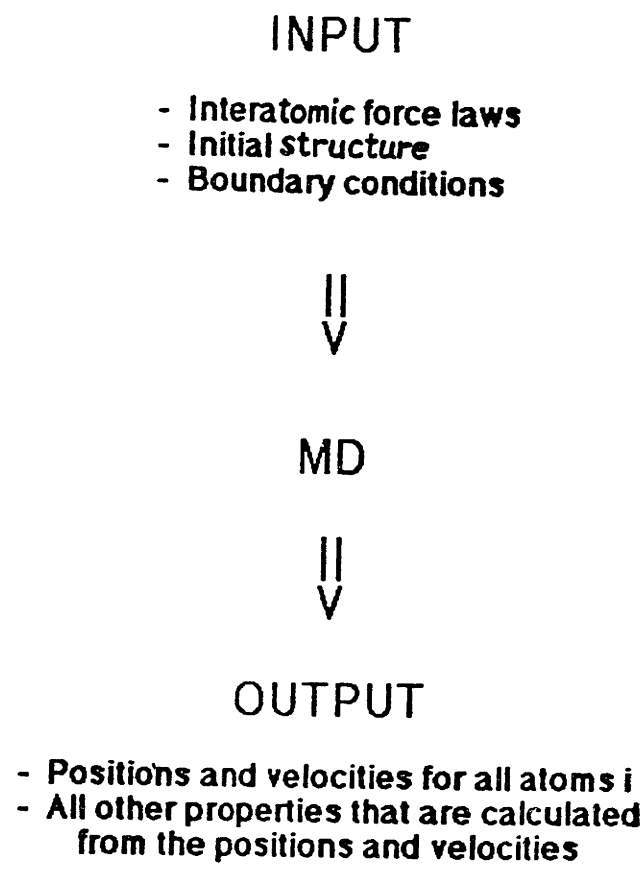

Figure 2-1: Flowchart for MD simulation

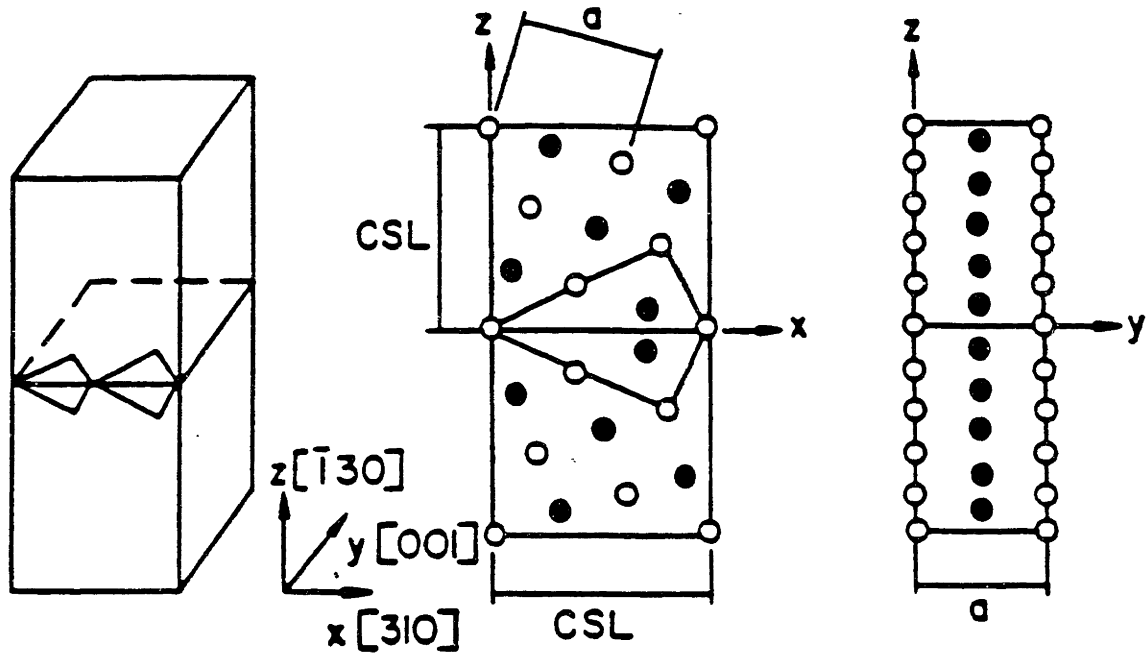

Figure 2-2: Bicrystal simulation model

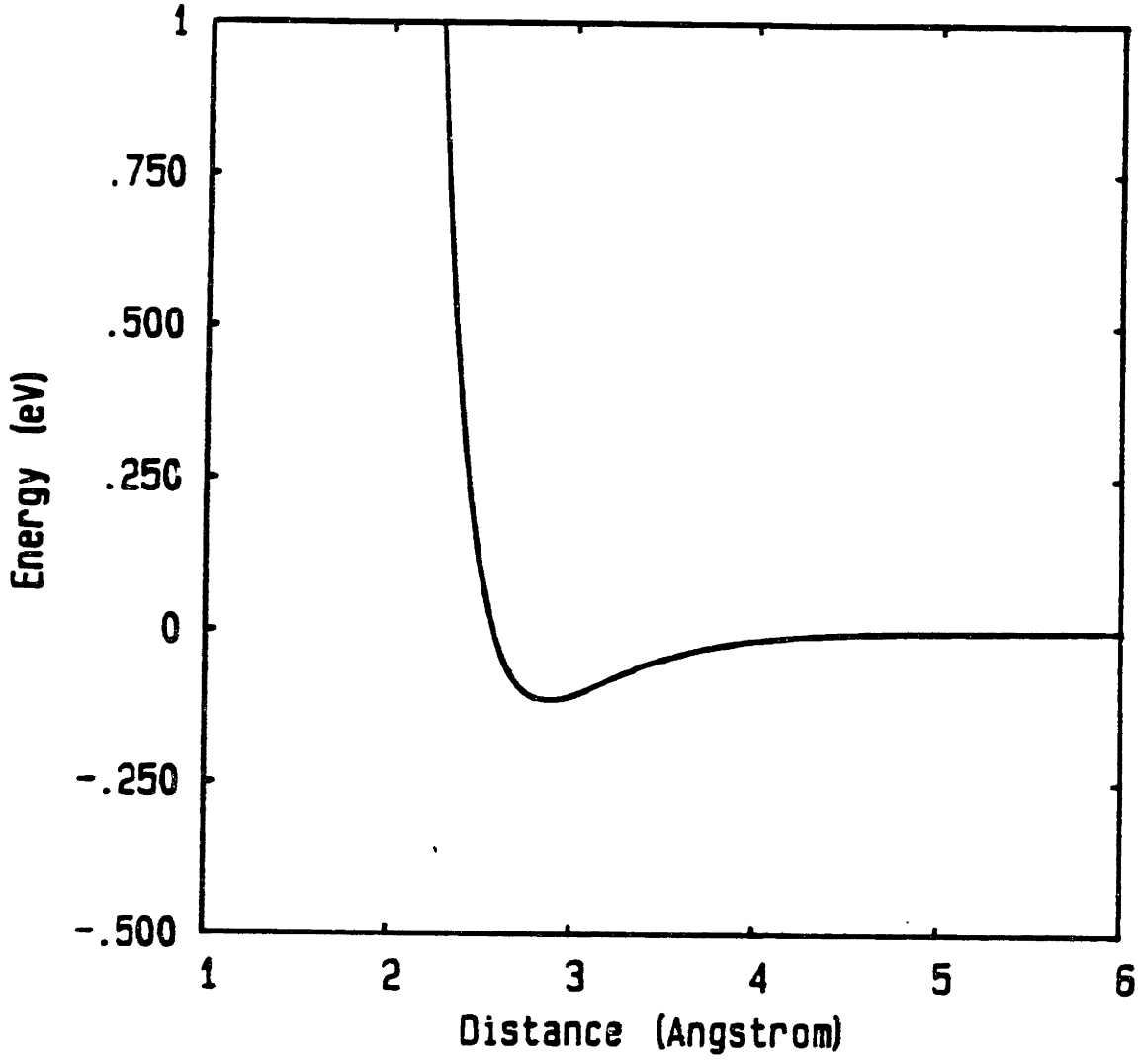

Figure 2-3: Morse potential function

Morse potential fitted to vacancy formation energy of aluminum. The difference between the shifted and unshifted potentials is not discernable in this figure.

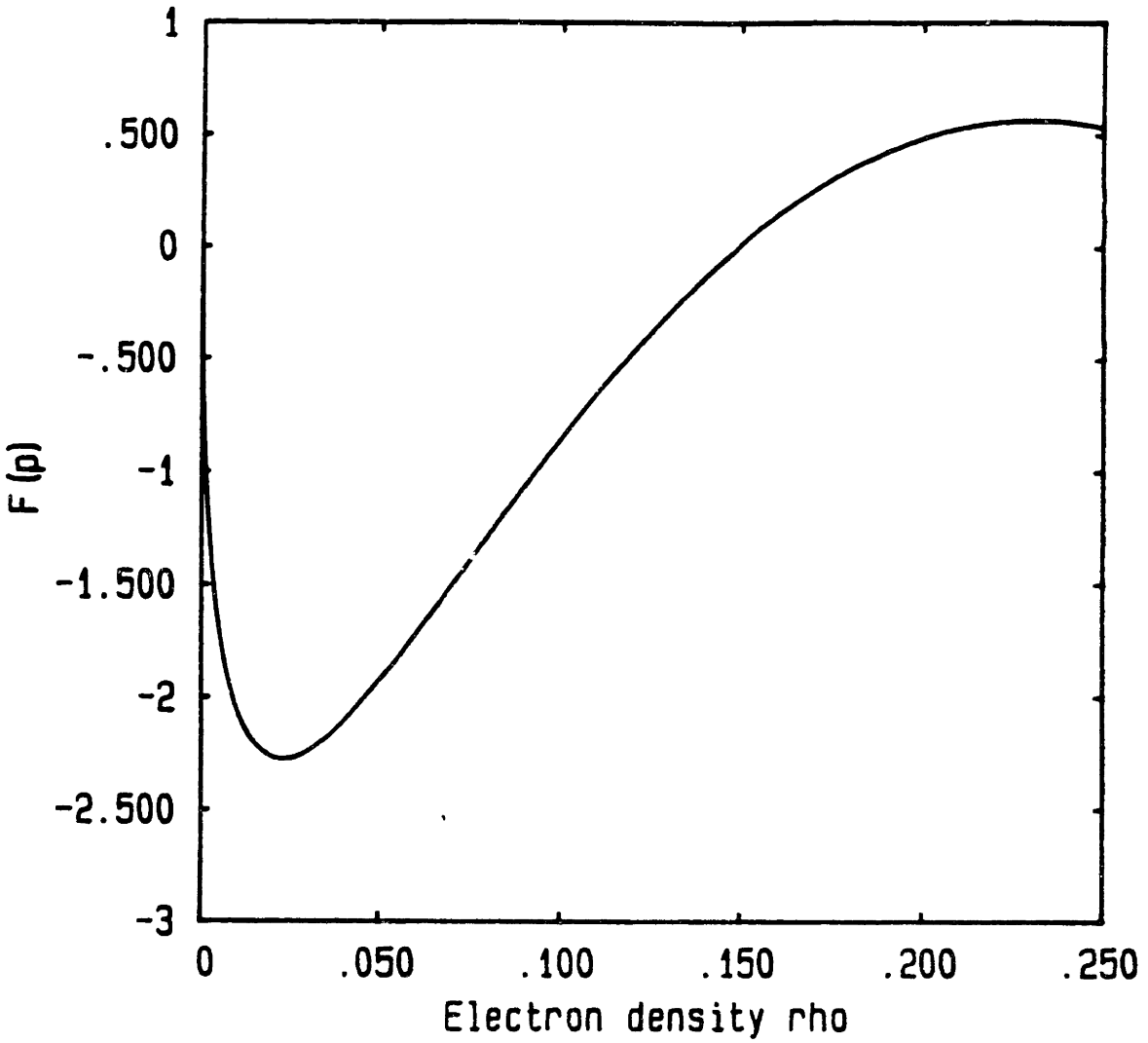

Figure 2-4: F(ρ) for aluminum EAM potential

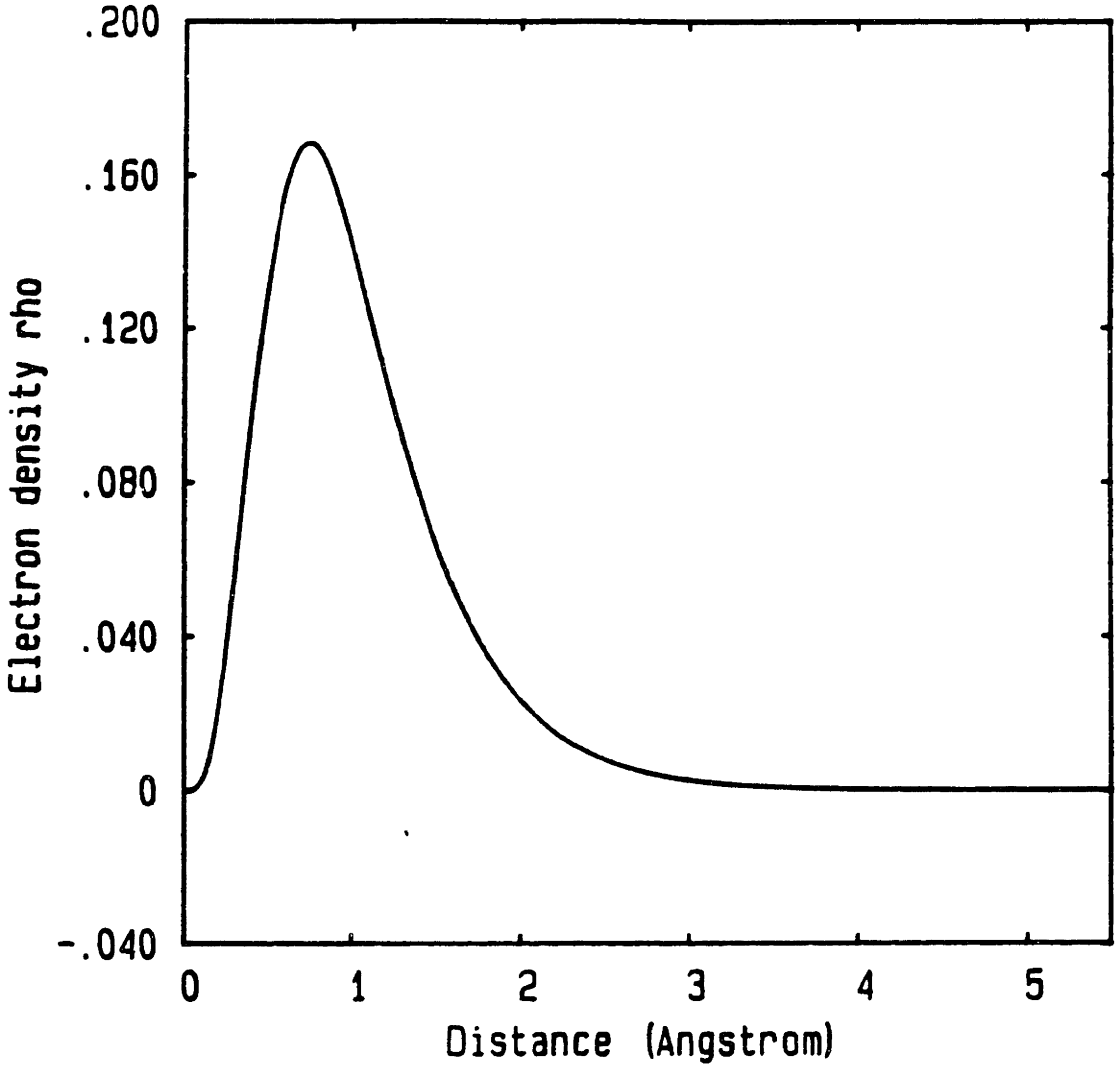

Figure 2-5: $\rho(r)$ for aluminum EAM potential

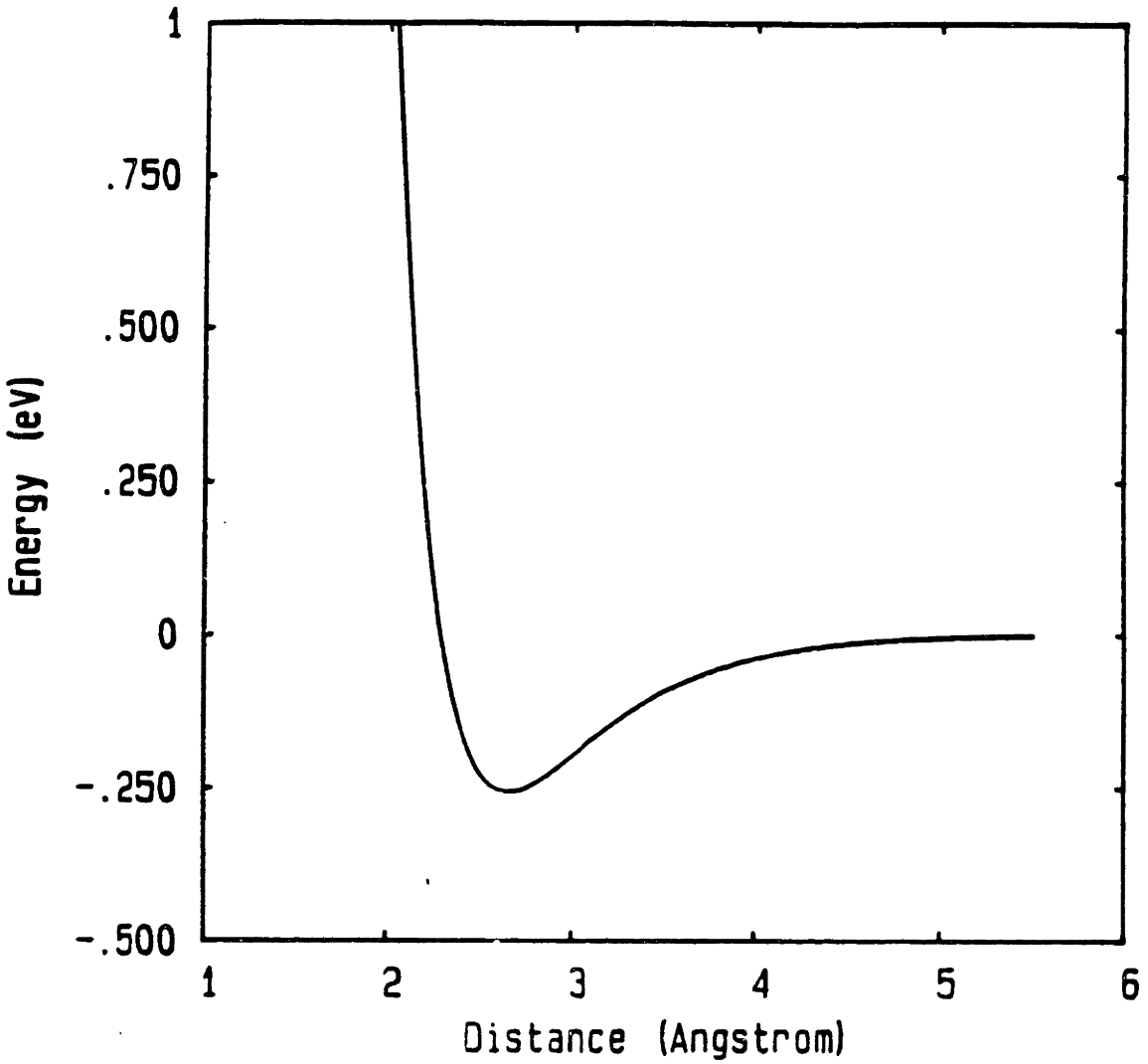

Figure 2-6: $\Phi(r)$ for aluminum EAM potential

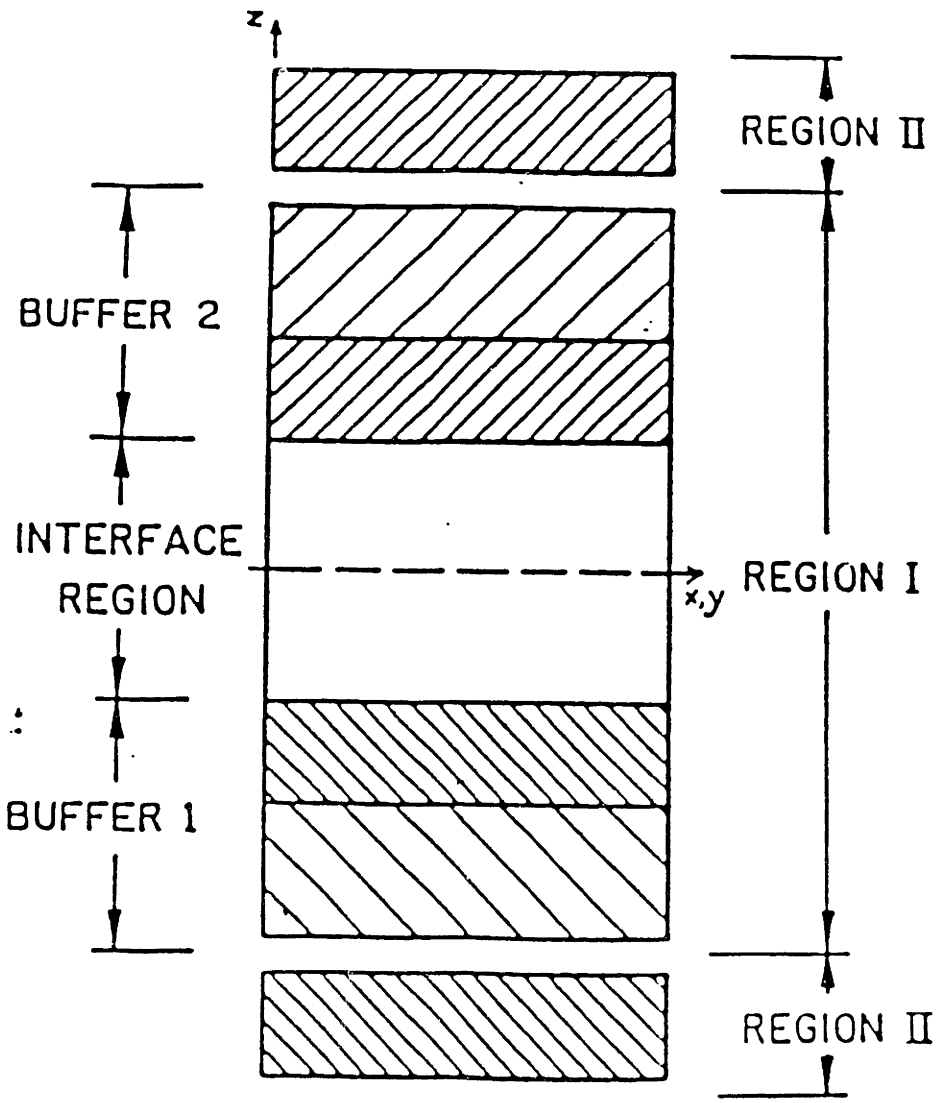

Figure 2-7: Region I - Region II separation for bicrystal model

Chapter 3

Thermal disordering in bulk crystal

The bicrystal model has a gb interface in the middle and two free surfaces at the ends of the simulation cell as described in previous chapter. To properly evaluate the interactions of the gb with the free surface, the behavior of the surface needs to be understood first. Thus, a reference model with the same orientations as the bicrystal model but without the gb is constructed and the behavior of the surface is studied. Another use of the reference model which is equally important is the determination of the thermodynamic melting temperature. It has been demonstrated[65,66] that the melting temperature obtained from simulation model with planar defect (gb) using the criterion of zero propagation velocity of the liquid region is very close to that obtained from free energy calculation.

An upper bound of the melting temperature can be obtained using 3d periodic single crystal model. Since this model does not have any defect or surface, there is higher energy barrier when the system changes from ordered state to disordered state.

The thermal disordering in a bicrystal model study will consist of three chapters, this chapter and the next two chapters. It is organized as follows. In this chapter, thermal disordering in a 3d bulk crystal model is studied. This will give the upper bound of the melting temperature, the highest temperature that a system can stay in solid state for a reasonable simulation time (ten to hundred of thousand time steps). In the next chapter, chapter 4, we will calculate the melting temperature using the reference model and examine the behavior of the surface at temperatures below melting. In chapter 5 we will will study the behavior of the gb interface in a bicrystal model at temperatures below melting.

It has been thought for some time that under normal condition, it is impossible to superheat a solid. The only way to achieved superheating in early studies[67] is to apply heat

at the interior of the material and let the heat diffuse to the surface. In that way a temperature gradient is set up where the surface is cooler than the center, and the superheating solid then can be obtained in the middle of the material. Recent experiments [68] has shown that by eliminating the material surface and other defect by using a small single crystal sphere and coating it with a material of higher melting temperature, superheating can be achieved. This demonstrates that melting originates from the surface or defect and in their absence, superheating can occur.

The purpose of this chapter is to calculate the upper bound of the melting temperature, called T_s, the highest temperature that a material in the model can undergo superheating.

Simulations are carried on a single aluminum crystal system using 3d periodic model containing 108 atoms arranged in the fcc structure. Since the known melting temperature of aluminum is 933K, the simulation runs cover the temperature range of 400K to 1400K to bracket this temperature as summarized in Table 3-I. Constant temperature is maintained by rescaling the atomic velocities at every time step. Also temperature is increased by rescaling the atomic velocities to achieve the desired temperature. Each run, which consists of 20000 time steps except the runs at 900K and 950K which consist of 80000 time steps, is made at zero stress (Parrinello-Rahman boundary condition)[63], and the initial atomic configuration is taken from the end of the preceding run.

The potential energy resulted from this model follows a straight line variation with temperature up to 950K. At 1000K the energy increases to a distinctly higher value almost instantaneously (after about 1000 time steps). Therefore the runs at 900K and 950K are made considerably longer (80000 time steps each) to see if the energy at these temperatures increases. At time step 50000 the energy in the 950K run increases to a higher value. But the run at 900K still has the same energy value even at the end of the simulation run (time step 80000). At the same time with the increase in the energy at temperature 950K, the

Temp (K)	Potential energy (eV)	Structure factor S(K)	MSD (a2)	Lattice expansion (a)	Lattice constant (A)	Pressure (eV/a3)
400	-3.525	0.998	0.003	1.01098	4.094	-0.0005
600	-3.493	0.997	0.005	1.01760	4.121	0.0008
700	-3.476	0.998	0.006	1.02116	4.136	-0.0011
800	-3.457	0.996	0.008	1.02529	4.152	0.0019
900	-3.436	0.995	0.013	1.03003	4.172	0.0007
950	-3.418#	0.993#	0.013*	1.03239	4.181	0.0010
950	-3.345	0.005	1.05*	1.05120	4.257	0.0010
1000	-3.335	0.010	2.89*	1.05430	4.270	-0.0008
1100	-3.315	0.011	8.93*	1.05992	4.293	-0.0039
1200	-3.290	0.008	18.9*	1.06669	4.320	-0.0012
1300	-3.273	0.010	26.4*	1.07144	4.339	-0.0001
1400	-3.248	0.009	37.7*	1.07908	4.370	-0.0027

Table 3-I: 3d periodic single crystal model results

Metastable state.

* Not equilibrium value. This value is taken at the end of the simulation run and still increases.

a (4.05A) is the lattice constant of Al at room temperature (298K). Structure factor S($\underline{K}$) is calculated from averaged positions of atoms over 1000 time steps. The wave vector $\underline{K}$ is chosen along the [001] direction of the fcc structure. Pressure unit (eV/a3) is equivalent to 24.1 kbar.

system configuration becomes structurally disordered as indicated by the static structure factor $S(\underline{K})$. Also the mean squared displacement increases sharply and appears to be unbounded. We regard this collection of properties as indicating lattice instability and consider the transition to occur at 950K for the present model.

As noted above, this transition temperature T_s is only the highest temperature that the present model can undergo superheating. For this model, the material can undergo superheating for 50000 time steps or roughly 100 psec at this temperature. The material is still solid at 900K over this time period. However it is possible that at this temperature the material at a later time could transform to the liquid state.

The potential energy and structure factor values for temperatures below T_s are the characteristic properties of the bulk aluminum solid at that temperature. These data will be used to determine that the solid material in the reference or bicrytal models to be studied later are indeed bulk material. The variation of potential energy with temperature establishes two energy branches, a solid branch and a liquid branch as shown in Fig. 3-1 with the heat of fusion is estimated to be 9.2 kJ/mol as compare to the experimental value of 10.79 kJ/mol. The cohesive energy for this model is -3.55 eV at room temperature (300K) as compared with the experimental value of -3.58 eV. These comparisons show that the potential model is reasonably realistic.

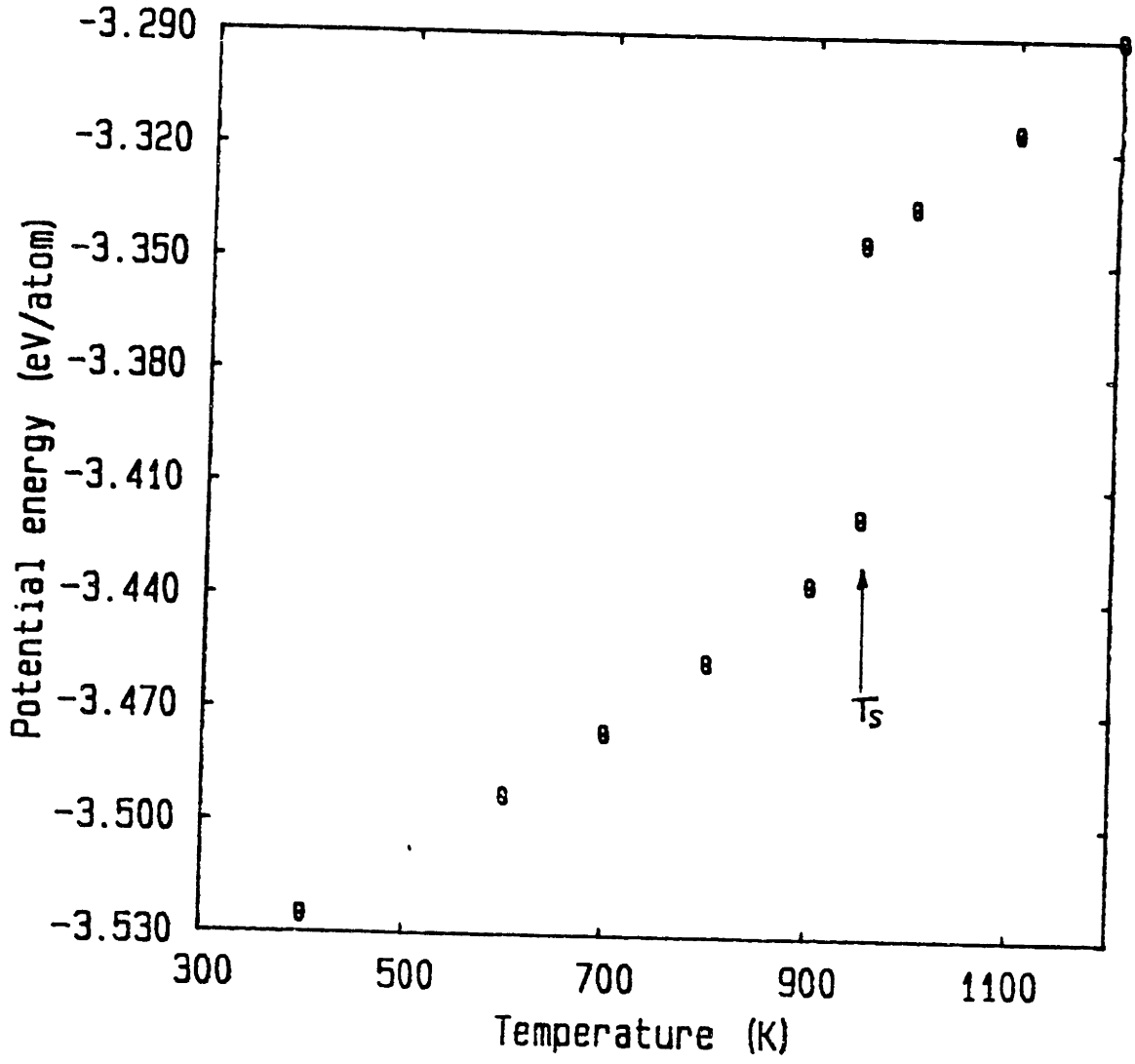

Figure 3-1: Potential energy for the single crystal model

Chapter 4

Thermal disorder in a model with free surface

It is now believed that melting begins at the solid surface or solid-solid interface.[69] Under normal condition, superheating of a solid is almost impossible. But when the surface is eliminated by coating with different material having higher melting temperature, superheating can be achieved.[68] This suggests that melting is a surface initiated process and the onset of disordering occurs below the melting temperature. Experiment has shown that the surface disordering can occur well below the bulk melting temperature of lead and the totally disordered surface film thickness increases rapidly as the temperature approaches melting temperature.[70] Recent theoretical analysis also suggests that a semi infinite system undergoing a first order transition in the bulk may exhibit critical behavior at its surface, i.e. surface properties behave continuously although bulk properties are discontinuous.[71]

Molecular dynamics simulation is well suited to obtain the detailed information at the atomistic level for the surface behavior at temperature below melting. However not all the simulation results are in agreement. While some computer simulation results[72,73] suggest surface melting occurs at temperature well below melting temperature and its thickness increases as the temperature approaches melting temperature, other result[74,5] suggests only surface roughening, i.e. the surface retains some of its crystalline structure up to a temperature close to the melting temperature.

The focus of this chapter is the study of the structure and kinetics of the free surface up to T_m. The intention is to provide a complete understanding of the free surface behavior at this temperature range for the evaluation and interpretation of the bicrystal model results which will be presented in the next chapter. However the study of the thermal disordering at the free surface is also significant in itself in view of the importance of the understanding

of the role of the surface in the melting process which is currently not completely understood. There is still not complete agreement on how the surface behaves below melting temperatures among computer simulation studies and among experimental observations.[75,70]

An equally important topic in this chapter is the determination of the thermodynamic melting temperature. The proper determination of T_m is obviously crucial to this work. In our previous studies[23,24] we took the temperature at which there is a discontinuous change (a jump) in the potential energy of a perfect crystal model with periodic borders to be the melting point T_m. Subsequently we realized that this temperature is the point at which the lattice becomes mechanically unstable, and this lattice instability temperature represents superheating of the system. If we call this temperature T_s, then we know that $T_m < T_s$. This error in the identification of T_m in our previous work lead to the claim that our results showed gb premelting.

In this thesis we will follow a different method of determining the melting point. The basic definition of T_m is the temperature at which the free energy curves for the solid and liquid phases intersect; it can be determined by direct free energy calculations (using MD) as done recently in the case of a three-body potential for silicon[76] and an EAM potential for copper.[66] An indirect method of determining T_m without the calculation of free energy has been used successfully at Argonne National Laboratory (ANL).[65,66] This method calculates T_m by extrapolating to zero the propagation velocity of the solid-liquid interface at temperatures above T_m. The basic idea of this method is the coexistence of the solid and liquid phases at T_m, or in other words the dynamic equilibrium of the solid-liquid interface. We have used this method in the present work.

This chapter is organized as followed. The first section describes the model of a single crystal with free surfaces. The second section gives a summary of all the simulation runs in this series. The third section discusses the determination of the melting temperature

of our model. The fourth and fifth sections examine in considerable detail the structure and kinetics of the surface behavior at temperatures above and below T_m respectively.

4.1 Model of a crystal with free surface

The model, called reference model, is an aluminum single crystal model with two (310) planar free surfaces as shown in Fig. 4-1. Aluminum and (310) free surfaces are chosen for this study because this model will later serve as a reference model (hence the name reference model) for the bicrystal model described in chapter 2 which is made of the same material and having the same orientations. The bicrystal model also has two free surfaces, together with a grain boundary, therefore a reference model is needed to study the interaction of the free surface with the grain boundary.

The reference model is composed of 1926 atoms with 2 and 32 CSL units (CSL unit = 1.58 a, where a is the lattice constant) in the x and z directions respectively, and a y dimension of 3 lattice constants. The large size of the simulation cell in the z direction is to allow adequate bulk material between the two surfaces to ensure that they do not interact with each other. Later results show that with this system size, the two surfaces behave independently, thus confirming that the system size is indeed adequate. The small ratio of surface to volume is chosen to avoid bulk driven premelting effect[74] which could change the phase diagram of the material studied. It has been observed[74] that for large surface to volume ratio, the thermodynamic data for the bulk material lie well inside the liquid domain with respect to the solid liquid coexistence line and thus will lead to premelting effect.

4.2 Summary of simulation runs

The upper bound of the melting temperature T_s for this potential function is established to be 950K from the 3d periodic model data presented in previous chapter. Therefore the temperature range studied using the reference model is below 950K. The simulation runs are carried out from 400K to 925K as summarized in Table 4-I.

All the runs in this series were run on the IBM 3900, with approximately 45 cpu minutes for 1000 timesteps. The total computer time for this series is estimated to be about 400 cpu hours.

Constant temperature is maintained by rescaling the atomic velocities at every time step. Each run is made at constant area in the xy plane and free surface in the z direction, with the lattice constant chosen to give essentially zero pressure at the given temperature. The lattice constants are obtained from the 3d periodic single crystal model (see Table 3-I). With this procedure the pressure of the system is found to fluctuate somewhat with increasing temperatures. The pressure fluctuation reflects a sensitivity of the pressure to the chosen lattice constant, although the effect is not considered to be serious. We could adjust the lattice constant to keep the pressure strictly constant[77] but we believe that it will not affect the results. The initial atomic configuration is taken from the final configuration of the preceeding run if the surfaces are still well ordered, i.e. there is no disordered layer. If the surface shows the existence of any disordered layer, the lower temperature configuration with well ordered surfaces will be used as initial configuration.

The temperature and pressure of the system are fairly uniform at all times and temperatures. Typical temperature and pressure profiles for the system at 825K at time step 30000 are shown in Fig. 4-2 and 4-3 respectively. The data are time averaged over 1000 time steps. The fluctuation is about 15% as estimated for a layer of 30 atoms.

In the next three sections, we will use the data from these runs to determine the

Temp (K)	#time step	Total time (psec)	Potential energy ordered (eV/atom)	Potential energy disordered (eV/atom)	Pressure (eV/a3)
400	5000	10.42	-3.525(5)	*	-0.020(20)
500	5000	10.45	-3.510(5)	*	-0.022(20)
600	5000	10.49	-3.493(7)	*	-0.024(20)
700	5000	10.53	-3.476(7)	*	-0.015(20)
750	5000	10.55	-3.467(11)	*	-0.022(40)
800	67000	141.61	-3.457(12)	-3.385(15)#	-0.021(30)
825	120000	253.93	-3.452(12)	-3.380(15)#	-0.023(20)
850	168000	355.91	-3.448(12)	-3.370(15)#	-0.022(30)
875	147000	311.78	-3.440(15)$	-3.365(15)%	-0.025(30)
900	16000	33.97	-3.438(15)$	-3.357(15)%	-0.020(20)
925	15000	31.89	-3.425(15)$	-3.351(15)%	-0.021(30)

Table 4-I: Reference model simulation runs

The parentheses denote error bars. Ex: -3.525(5) means -3.525± 0.005. a is the lattice constant at room temperature (4.05 A). The pressure unit eV/a3 is equivalent to 24.1 kbar.

* Not existed. For the length of the run, the surface does not have any region of highly disordered and high energy.

Metastable state. High energy, highly disordered layers formed at some times.

% High energy, highly disordered layers formed and propagated.

$ Unstable state. At later time this will become high energy state.

thermodynamic melting temperature and to study the structure and kinetics of the surface region at temperature above and below melting temperature.

4.3 Determination of melting temperature

The 3d periodic single crystal model gives the thermal behavior of bulk material. However due to the lack of defect sites, this model could undergo superheating. It therefore only gives the upper bound of the melting temperature T_s. To obtain thermodynamic melting temperature, defined as the temperature at the crossing of the temperature variation of the solid and liquid phase free energy curves, one could calculate directly the free energy of the system from MD simulations. Other method of calculating the melting temperature T_m which does not involve the calculation of the free energy is to use model with defect region since melting will nucleate from the defect sites and propagate inward. This propagation will allow the determination of the thermodynamic melting temperature using the criterion that at this temperature the system is in a two-phase state, or in other words, the propagation velocity is zero.[65] Same values for the melting temperatures (within error bar) have been obtained using these two methods, free energy calculation and zero propagation of velocity of the liquid region initiated from a planar defect (gb), in silicon model with Stillinger & Weber potential[65] and in copper model with an EAM potential.[66]

The criterion used to determine melting temperature in this study is that of the second method, i.e. zero propagation of the defected liquid region. The basic idea of this method is the coexistence of the solid and liquid regions at T_m. Above T_m, the liquid phase is thermodynamically favored, therefore it will spread with time and eventually the high energy state (supercooled solid) will disappear. At T_m, the solid liquid interface is in dynamic equilibrium and there will be no propagation of the liquid region.

The range cutoff for the interatomic potential used is 1.35 lattice constants or between third and fourth nearest neighbor distance. Therefore atoms in the first one or two

layers from the surface do not have the same number of neighbor interactions as atoms in the bulk region. The potential energy in these regions is much higher than that of the bulk material. These layers are excluded from all energy calculations because their high energy values only reflect the effects of the solid vapor interface.

Except for these surface layers, there are two distinct regions in the reference model, a low-energy, ordered region and a high-energy, disordered region as shown in Fig. 4-4 through the potential energy and structure factor profiles. The data in this figure are averaged over 1000 time steps for temperature 875K at time steps 30000. One sees that the ordered region is always in the middle of the simulation cell which is the crystalline solid region since the atoms are in well defined fcc lattice positions and their energies are similar to those of the 3d model as shown in Table 3-I. The disordered regions are at the surfaces. Their energies are higher than that of the bulk region but still significantly lower than that of the first layer of the free surface. At low temperatures (400K - 750K), there is no disordered region for the length of the simulation runs. Between 800K and 850K, the disordered regions are in metastable state, meaning that they are forming at some times and disappearing at other times. However, once formed these regions will exist for at least a few thousand time steps so that their properties can be calculated. At 875K and above, the disordered regions are propagating inward from the surface. Potential energies for the two regions are shown in Table 4-I in two separate columns for the ordered and disordered regions.

The potential energy values are plotted versus the temperature in Fig. 4-5 together with the values from the 3d model. One sees that they form two separate branches, the solid branch consisted of all energy values from the ordered region and the liquid branch consisted of all energy values from the disordered region. The energy values from these two models are very similar in the solid branch, showing that the ordered region in the reference model is indeed bulk material. In the liquid branch, the temperature ranges

studied for these two models do not overlap since we have purposely chosen to examine the reference model only at temperatures below T_s which is 950K. However, the data from the reference model extends smoothly into those obtained using the 3d model. One sees a hysteresis loop in the 800K - 950K range which contains the true melting temperature. Similar hysteresis loops also have been obtained with different systems, silicon model using Stillinger & Weber potential,[78] LJ model, etc.

Structure factor $S(\underline{K})$ is a measure of structural disorder along the $\underline{K}$ direction. A value of unity signifies a completely ordered structure while a value of zero means totally disordered structure along the direction of the chosen wave vector $\underline{K}$. A typical structure factor profile has been shown in Fig. 4-4. One sees disordered regions at the two ends of the simulation cell as characterized by an essentially zero value of the structure factor. The middle of the cell is in very well ordered as shown by $S(\underline{K})$ values close to unity. For the purpose of defining the size of the disordered region, the full width at half maximum criterion will be used as shown in Fig. 4-4. Since the value of the structure factor is always unity in the ordered region, and zero for a completely disordered region, the half maximum value is 0.5. Therefore the full width at half maximum criterion to determine the thickness of the disordered region is equivalent to the criterion that any layer having structure factor smaller than 0.5 is considered to be disordered.

The thickness of the disordered region at the surface defined as above is plotted as a function of time for temperatures between 850K and 925K in Fig. 4-6. At 850K the surface region is in metastable state. Even though there are some disordered layers in the surface region at 850K, this behavior is confined to a few layers in extent and appear not to spread in time in the rather long interval of simulation. Also at 850K the surface becomes very ordered at certain times. In constrast, at 875K and above, the thickness of the disordered regions grows steadily with time. Based on this behavior, the melting temperature is therefore judged to be between 850K and 875K for this potential function.

For a more accurate determination of the melting temperature, the propagation velocities of the surface disordered region at temperatures above 875K are plotted in Fig. 4-7. A fit through these velocities gives a zero propagation velocity at temperature (865± 15)K which will be taken to be the melting temperature for our model in this work.

4.4 Surface behavior above melting temperature

Detail structural and kinetics behavior of the surface at temperature 875K, slightly above T_m, is now examined. The purpose of this study is twofold. The first is to show that the disordered region which is defined based only on structural information also has the energy and mobility of a liquid. This will allow us to confirm that Fig. 4-6 is indeed showing the growth of a liquid region initiated from the surface. The second purpose is to establish a behavior characteristic of a liquid. This will be useful later when we analyze the surface behavior at temperatures below T_m.

The system behavior at 875K is changing with time. Potential energy and structure factor profiles averaged over 1000 time steps are shown in Fig. 4-8 and 4-9 respectively for the system at different time steps (50000, 70000 and 90000). One can see a growth of a region of high energy from the surfaces. The potential energy of this disordered surface region is found to have the same value as the liquid branch of the potential energy curve shown in Fig. 4-5.

Detail structures of the ordered disordered interface at these time steps are shown in Fig. 4-10. The atomic positions are time averaged over 1000 time steps. The interface is fairly sharp for this averaging, with the ordered region in complete order and the disordered region in complete disorder. One sees the advance of the interface as a function of time. Fig. 4-11 shows the interfacial region on a longer time scale. This figure contains three figures covering 20000 time steps each and starting at time steps 50000, 70000 and 90000 respectively. One sees a growth of the disordered region. Fig. 4-10 and 4-11 cover only

the middle region of the simulation cell. The surface is much farther to the right and the center of the simulation cell is farther to the left.

Structural information is also provided by the radial distribution function g(r). Fig. 4-12 and 4-13 show the g(r) of the two regions across the interface. In Fig. 4-12 the instantaneous atom positions are used while in Fig. 4-13 the 1000 time step time averaged positions are used. In Fig. 4-12 the data are accumulated for 1000 time steps at 10 time step interval. This covers the time step from 50000 to 51000. In Fig. 4-13 the data are accumulated for 50000 time steps at 1000 time step interval. This data covers the time step range of 50000 to 100000. g(r) for the disordered region are the same in both figures as shown in Fig. 4-12(a) and 4-13(a). In the ordered region, the time averaged data in Fig. 4-13(b) shows clearly the peaks associated with the neighbors of the fcc structure. The instantaneous data in Fig. 4-12(b) also shows the neighbor peaks but with much overlapping between them. The fourth neighbor peak is only seen in Fig. 4-13(b). This is because the time averaged positions are not affected by the thermal motion. In the disordered region, one sees the disappearance of the second neighbor peak in both Fig. 4-12(a) and 4-13(a). Also the third and fourth peaks are combined together to form a broad peak which is now the second neighbor peak for the liquid. This is the characteristic of a liquid structure.

The mobility of the atoms in the interface region is shown in Fig. 4-14 for the same time steps (50000, 70000 and 90000). In these figures, two consecutive 1000 time step time averaged atom positions are connected to show the movement of these atoms. One sees large movements of the atoms in the liquid region. The mobility of the disordered region is also shown in Fig. 4-15 through the xy (parallel to the interface) and z (normal to the interface) components of the MSD. One sees the propagation of the high mobility region from the surface as characterized by the MSD at different layers in the disordered region. The slopes of these MSD curves for different layers are similar. The diffusion

coefficient, calculated from these slopes, is $(4.4 \pm 0.6) \times 10^{-5}$ cm^2/sec. This can be compared to a calculation of diffusion coefficient using pseudopotential potential for liquid aluminum which gives also 4.4×10^{-5} cm^2/sec.[79]

4.5 Surface behavior below melting temperature

This section is the main focus of this chapter. The section consists of two parts. In the first part, the structure and kinetics of the surface region is examined in detail at temperatures below T_m. In the second part, we will study the time averaged behavior of the surface region at the temperature range below T_m.

The melting temperature has been determined to be 865K in the above section using the criterion of zero propagation of the liquid region initiated at the surface. The temperature range slightly below T_m is of interest because the thermal disordering at the surface would become most pronounced at this temperature range. Among the temperatures studied below T_m, the highest temperature is 850K. However this temperature is not a good choice to study the surface behavior below T_m because it is just about within error bar of the melting temperature ($T_m = 865 \pm 15$ K). Therefore we choose the temperature of 825K to study the thermal disordering phenomenon. The surface behavior at 850K and also at 800K also will be considered but less detail will be presented.

Potential energy and structure factor profiles averaged over 1000 time steps are shown in Fig. 4-16 and 4-17 respectively at 825K and at different time steps (25000, 45000, 62000 and 98000). One sees that the region of high energy and the region of disordered structure are closely correlated. One also sees metastability in these surface regions as they grow and shrink. Often the surface ordered and disordered regions are formed long enough (order of 10000 time steps) so that their potential energy can be calculated separately. When the surface region is transforming from ordered to disordered structure or vice versa,

its energy value is also changing between these values. The potential energies of the ordered and disordered regions are found to have the same values as the solid and liquid branches respectively of the potential energy vs temperature curve shown in Fig. 4-5.

Detailed configurations of the surface regions at these time steps are shown in Fig. 4-18 for the surface on the right. The atom positions are time averaged over 1000 time steps. The surface region couldbe quite ordered at some times (time steps (25000, 98000) and quite disordered at other times (time steps 45000, 62000). Fig. 4-19 shows the atom trajectories of the two surfaces at time steps 45000 at a shorter time scale. The data are accumulative over only 500 time steps. One sees the different behavior exhibiting by the two surfaces. While the surface on the right is very much ordered, the one on the left is quite disordered. Between the disordered surface region and the ordered substrate, there seems to be a intermediate region where the atoms are disordered but still have a faint resemblance of the underlying substrate. Fig. 4-20 and 4-21 show the surface regions on the right and left respectively at a longer time scale. These figures each contains four figures covering 20000 time steps each and starting at time steps 15000, 35000, 52000 and 85000 respectively. The region near the surface (shown clearest at the surface on the left at time steps 45000 and 62000 in Fig. 4-21(b) and 4-21(c)) is completely disordered and does not seem to recognize the underlying sudstrate structure. There is also an intermediate region between the outer surface and the bulk substrate where the atoms show much movement but one can still see the underlying bulk structure.

Further information on the structure of the surface region at these time steps are obtained through the radial distribution function g(r). Fig. 4-22 and 4-23 show the g(r) of the two regions across the interface. In Fig. 4-22 the instantaneous atom positions are used while in Fig. 4-23 the 1000 time step time averaged positions are used. In Fig. 4-22 the data are accumulated for 1000 time steps at 10 time step interval. This covers the time step from 45000 to 46000. In Fig. 4-23 the data are accumulated for 40000 time steps at 1000

time step interval. This data covers the time step range of 35000 to 75000. These four figures (Fig. 4-22(a), 4-22(b), 4-23(a) and 4-23(b)) are very similar to those of temperature 875K (above melting) for both ordered and disordered regions as described earlier in Fig. 4-12(a), 4-12(b), 4-13(a) and 4-13(b).

At later time (time step 98000) the surface structure is becoming quite ordered. This information is also reflected in the g(r) as shown in Fig. 4-24. Data in this figure is obtained the same way as data in Fig. 4-23 for the same surface region, except at a later time (time steps 75000 to 105000). One sees in this figure a growth of the second peak and a much sharper third peak which shows that this region is indeed become more ordered.

The mobility of the atoms in the right and left surface regions at these time steps (25000, 45000, 62000 and 98000) are shown in Fig. 4-25 and 4-26. In these figures, two consecutive 1000 time step time averaged atom positions are connected to show the movement of these atoms. These movements are very similar to those at 875K when the surface regions become disordered as in time steps 45000 and 62000 of the left surface (Fig. 4-26(b) and 4-26(c)).

The mobility of the disordered region is also shown in Fig. 4-27 through the xy and z components of the MSD. The z component of the MSD is presented separately because of the finite size of the disordered region in the z direction. Therefore one does not expect that the MSD in the z direction will be similar to that of the other two directions. One sees the propagation of the high mobility region from the surface as characterized by the MSD at different layers in the disordered region. At later time (after time step 75000) the MSD levels off, meaning the region is then recrystalized. The slopes of these MSD curves for different layers are similar. The diffusion coefficient for the disordered and mobile region, extracted from the linearly increased protion of the MSD curves, is 2.4×10^{-5} cm^2/sec (Recall that the liquid diffusion coefficient at 875K is 4.4×10^{-5} cm^2/sec).

MSD profile of the system at time step 45000 is shown in Fig. 4-28. These data are

time averaged over 1000 time steps. From these data one can extract the vibrational amplitude which is just the square root of the MSD. One sees a flat region in the center of the cell, signifying that the simulation cell is indeed large enough to have a significant amount of bulk material between the two surfaces. The vibrational amplitude of the surface region is much higher than that of the bulk region, which is expected because of the solid vapor interface.

Fig. 4-29 shows the movement of the atoms near the surface. A vacancy is created by an atom moving to the surface. An atom nearby is moving in to fill the vacancy and a surface atom is preparing to occupy the vacancy this atom left behind. This way a vacancy is formed and annihilated in a few hundred time steps. This movement occurs quite frequently, almost every few thousand time steps. For the vacancy to survive, it has to move deep into the bulk region, where it will have virtually no chance of being annihilated. Fig. 4-30 shows the presence of such a vacancy in the bulk region. This mechanism is much rarer. Over almost 400000 time steps of simulation runs at various temperatures, only 2 or 3 vacancies succeed.

When the surface structure is ordered, the vacancy exchange mechanism described above is responsible for the mobility of the surface atoms. However the time scale for the surface to become disordered is quite short, of the order of 1000 time steps (approximately 2 psec) as shown in Fig. 4-36 and 4-37 for the surface disordered thickness at temperatures 800K and 825K respectively. The transition from an ordered surface (small thickness) to a disordered surface or vice versa is always very fast. Fig. 4-31 shows two surface structure mobility separating by 1000 time steps. Lines are draw to connect two consecutive atom positions which are time averaged over 1000 time steps. The change from an ordered surface structure to a disordered surface structure is accomplished in just 1000 time steps.

The surface behavior at 825K has been described in considerable detail. The main feature of this behavior is the metastability of the surface region. It could be quite ordered (solid like) for some times and disordered (liquid like) at other times.

The same behavior is also observed at other temperatures below T_m. Shown in Figs. 4-32 through 4-35 are the surface structures at 800K (right and left surfaces) and 850K (right and left surfaces) respectively. Each figure is an accumulation atom positions for 20000 time steps at various time steps. This behavior is similar to that of 825K as shown previously in Fig. 4-20 and 4-21.

It has been shown that below the melting temperature, there is a temperature range in which there exists a disordered region. In contrast to the steady growth of the disordered (liquid) region at temperatures above melting, the disordered region below T_m is in a metastable state; the surface region is sometimes ordered and other times disordered. One has seen this behavior in various temperatures below T_m.

The thickness of the disordered region is another indication of metastable behavior of the surface region since there is a strong correlation between structure, energy and mobility of the surface region as shown earlier at temperature 825K. At temperature below T_m, the disordered region grows to a certain size and then shrinks to a completely ordered region, and then grows again a a later time. This behavior is observed at 800K and 825K as shown in Fig. 4-36 and 4-37 respectively and at 850K as shown in Fig. 4-6. The disordered region thickness at 825K and above in these figures are from one surface of the model. The other surface behaves essentially in the same way. We have found that the two disordered regions do not grow or shrink at the same time. They appear to behave independently of each other. For example, the other surface of the system at 800K is ordered for all the length of the simulation run as shown in Fig. 4-38. This, together with the fact that the disordered region at 800K at the other surface is smaller than those of 825K and 850K, implies that the temperature of 800K is very close to the onset of the formation of the disordered region at the surface.

From the foregoing data one can extract an average thickness for the disordered region as shown in Fig. 4-39. The error bar is taken from the standard deviation of the

thickness values. One sees a rapid but apparently continuous increase of the thickness as the temperature approaches the melting temperature. These data could be readily fitted to a $\log(T_m - T)$ or a power law $(T- T_m)^{-n}$ variation.

The diffusion coefficients of the disordered surface region are plotted in Fig. 4-40 for temperatures below and above T_m as function of $1/T$.

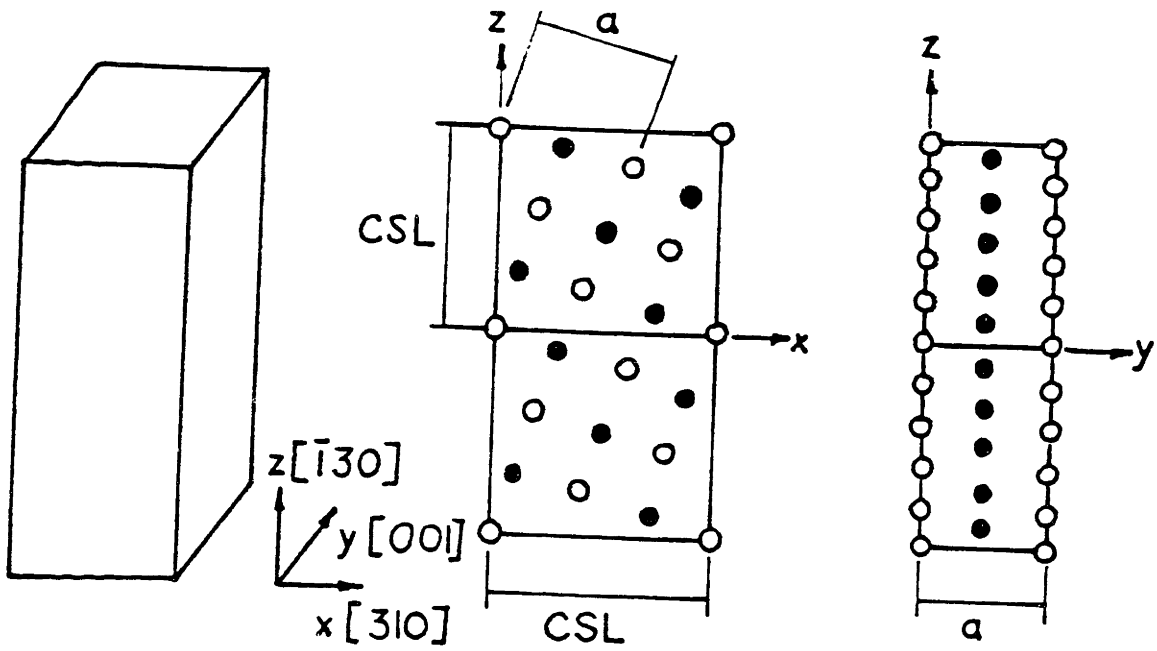

Figure 4-1: Geometry of the reference model

Shown are the xz and yz projections of the model. The x,y directions are periodic and the z direction is free. The size of this figure is 1 and 2 CSL units in the x and z directions respectively, and 1 lattice constant in the y direction. The actual system size used in this work is 2 and 32 CSL units in the x and z directions respectively and 3 lattice constants in the y direction.

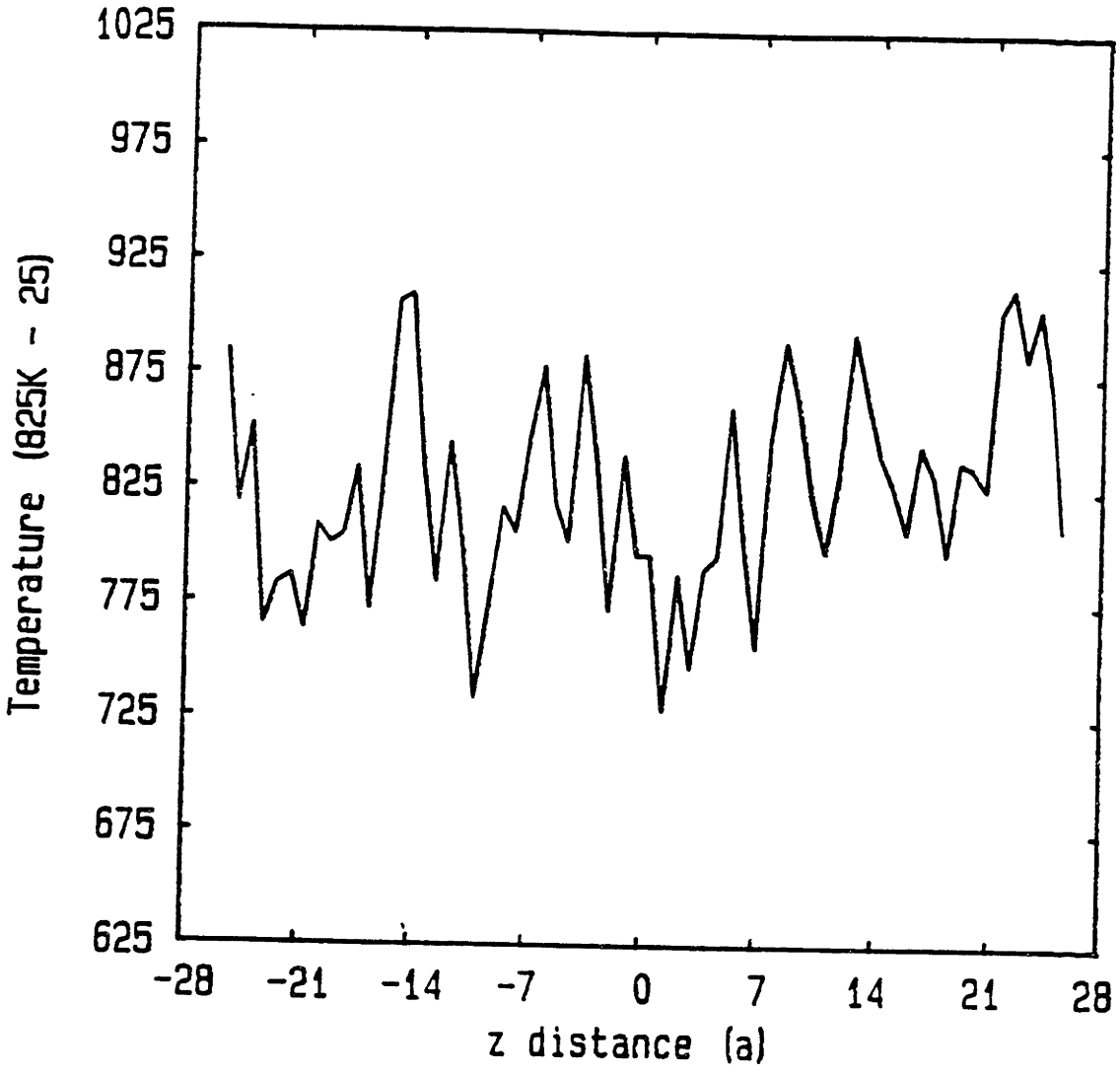

Figure 4-2: Temperature profile at 825K

These data are taken at time step 30000 with 1000 time steps averaging. a is 4.05 A.

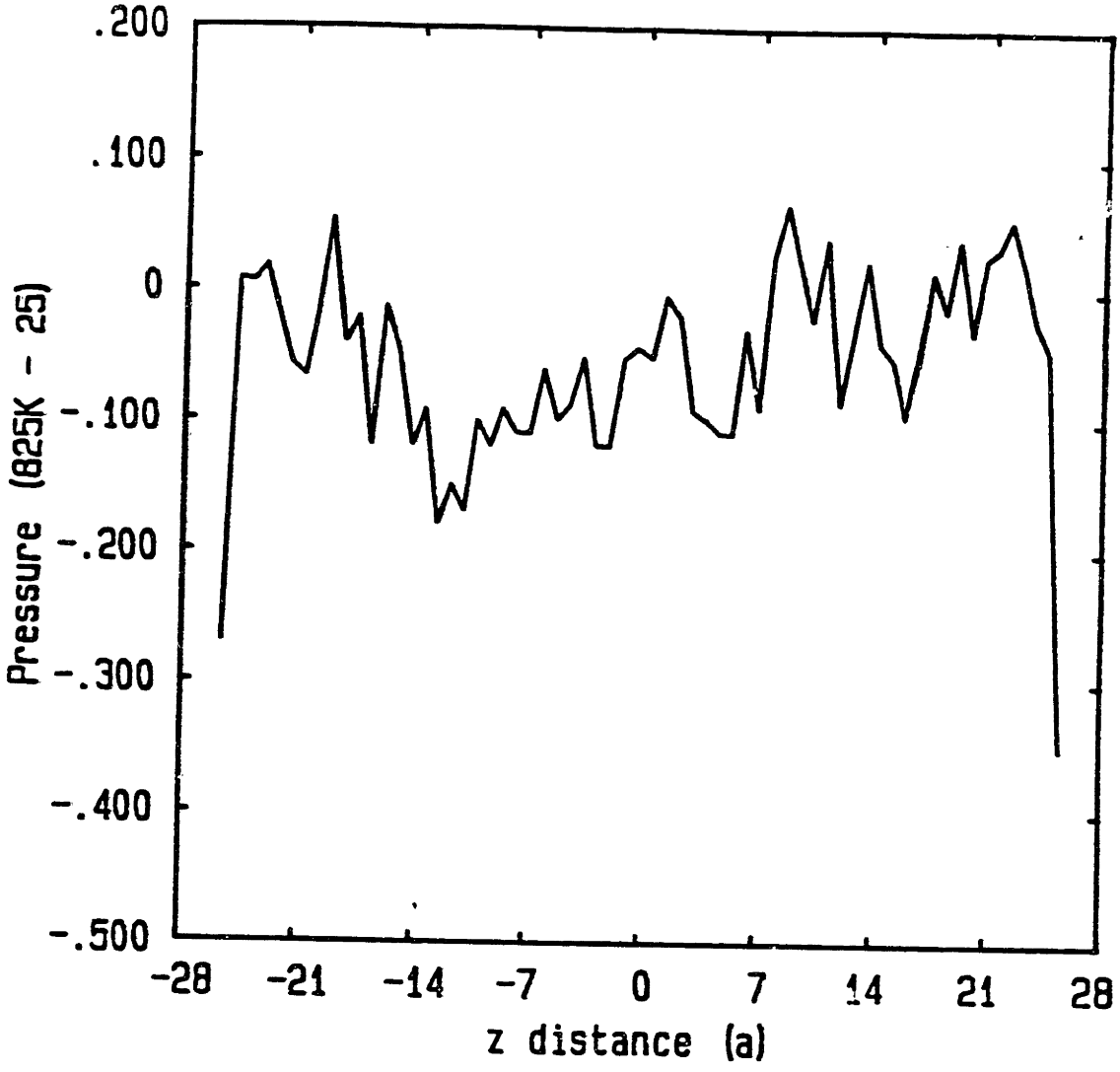

Figure 4-3: Pressure profile at 825K

These data are taken at time step 30000 with 1000 time steps averaging. a is 4.05 A.

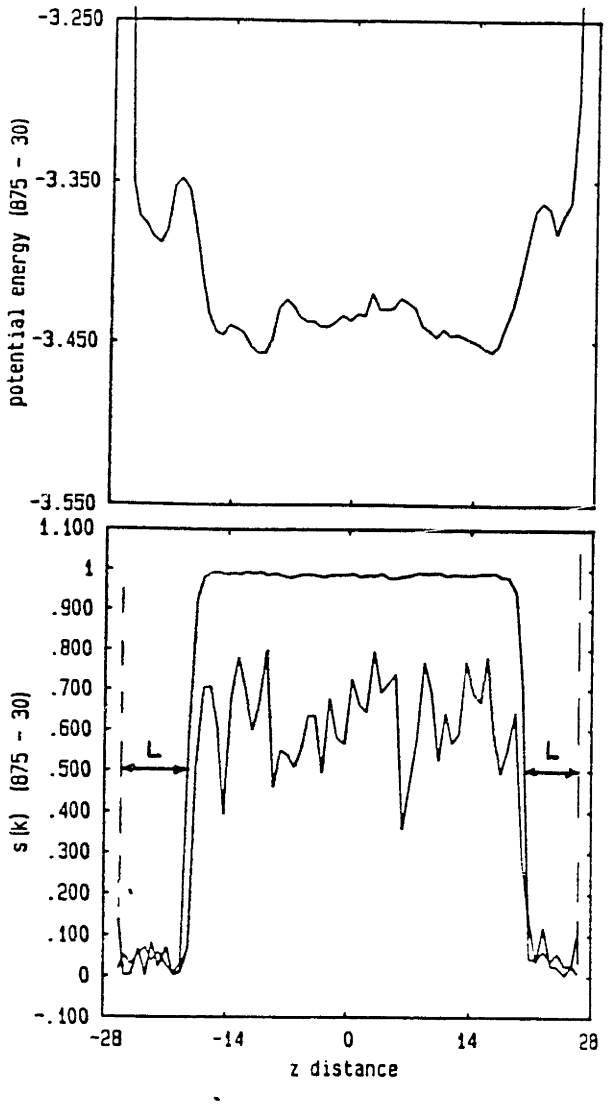

Figure 4-4: Typical potential energy and structure factor profiles

These data are taken at temperature 875K at time step 30000 with 1000 time steps averaging. a is 4.05 A.

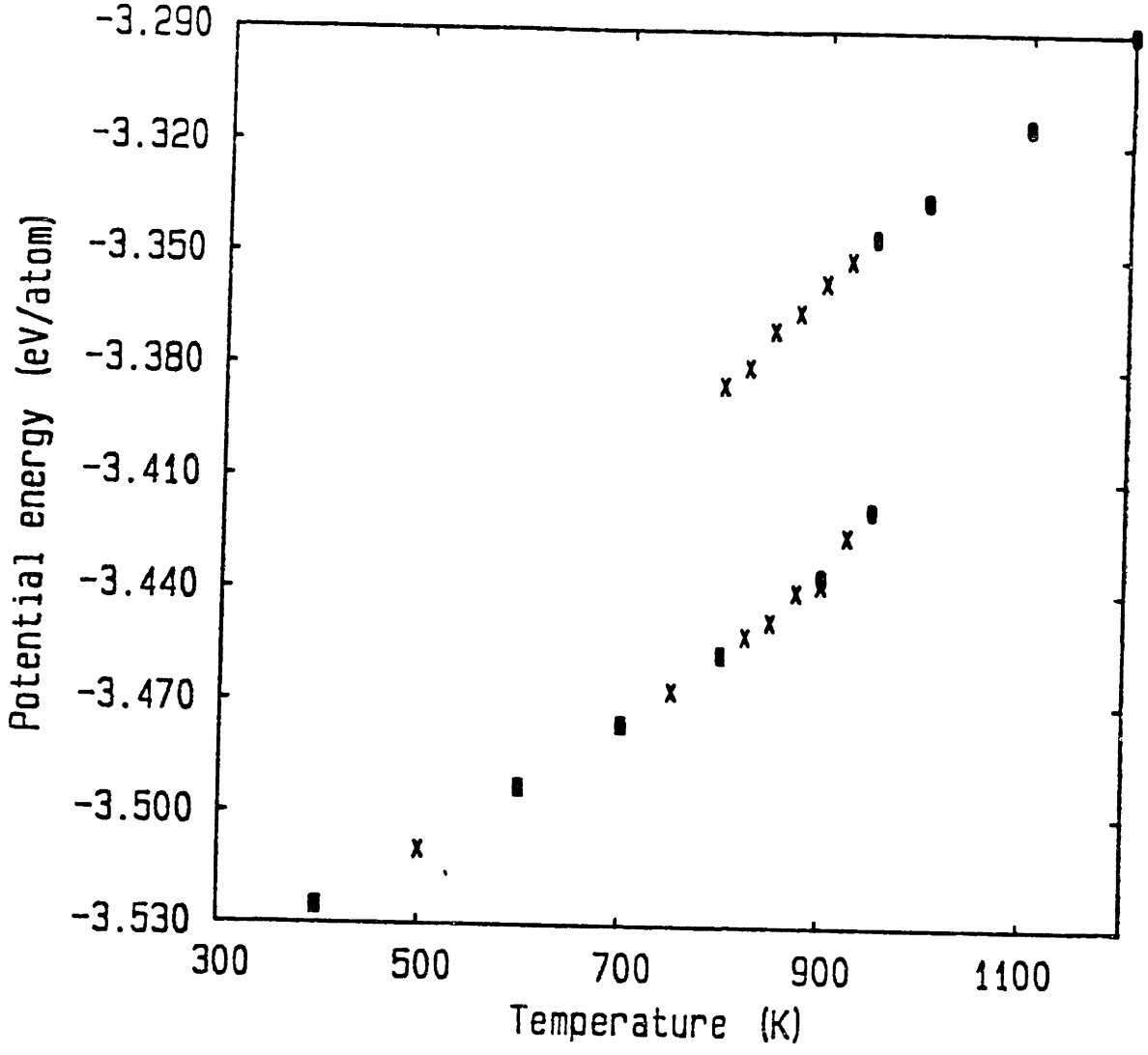

Figure 4-5: Potential energy vs temperature

Solid circles are data from the 3d single crystal model. Crosses are data from the ordered and disordered regions of the reference model. Solid squares are where a solid circle and a cross overlap.

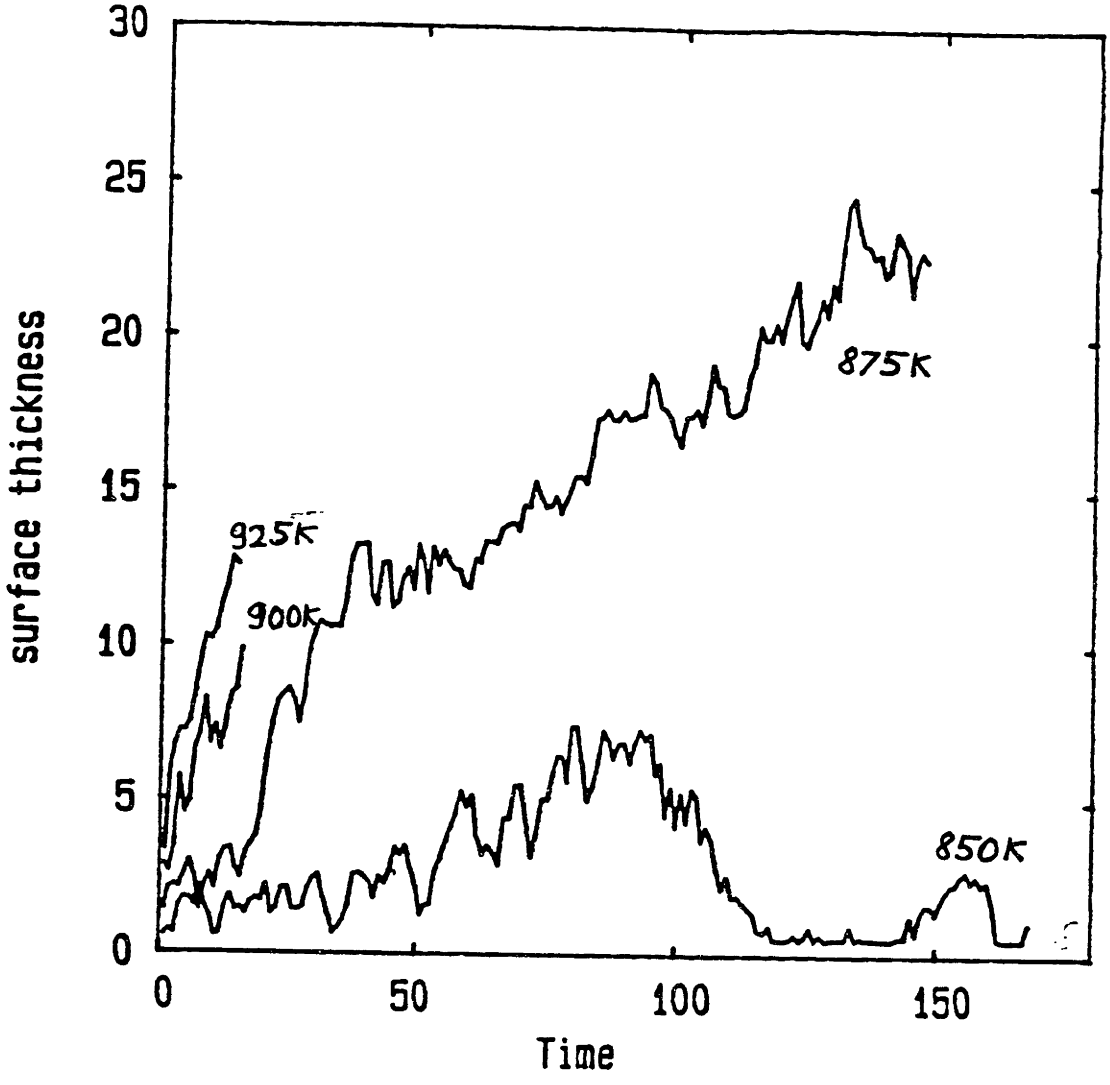

Figure 4-6: The growth of the surface disordered region

The time axis is in unit of 1000 time steps, or approximately 2.1 psec. The thickness is in unit of layer (0.79 lattice constants)

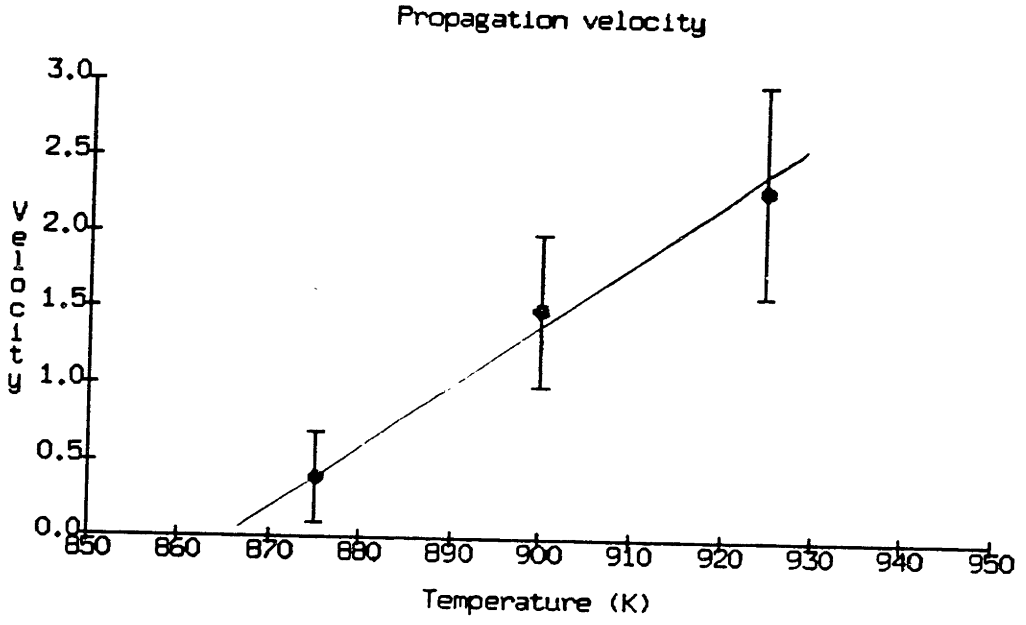

Figure 4-7: Propagation velocities of the disordered regions

The solid line is a linear fit through the data points.

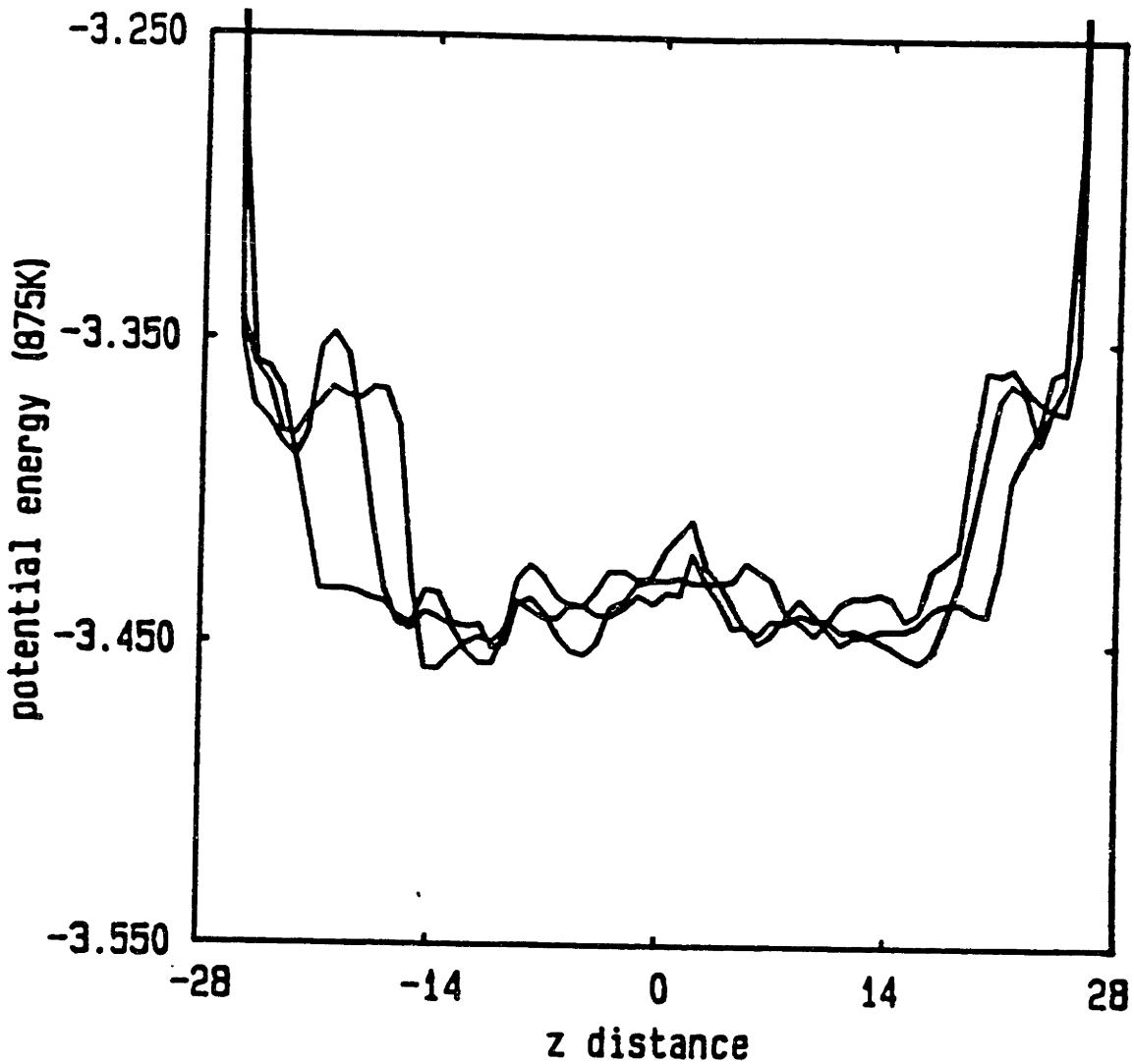

Figure 4-8: Potential energy profiles at 875K

Potential energy profile of the system at 875K for 3 different time steps (50000, 70000 and 90000). The data are averaged over 1000 time steps. The distance is in unit of a (4.05 A).

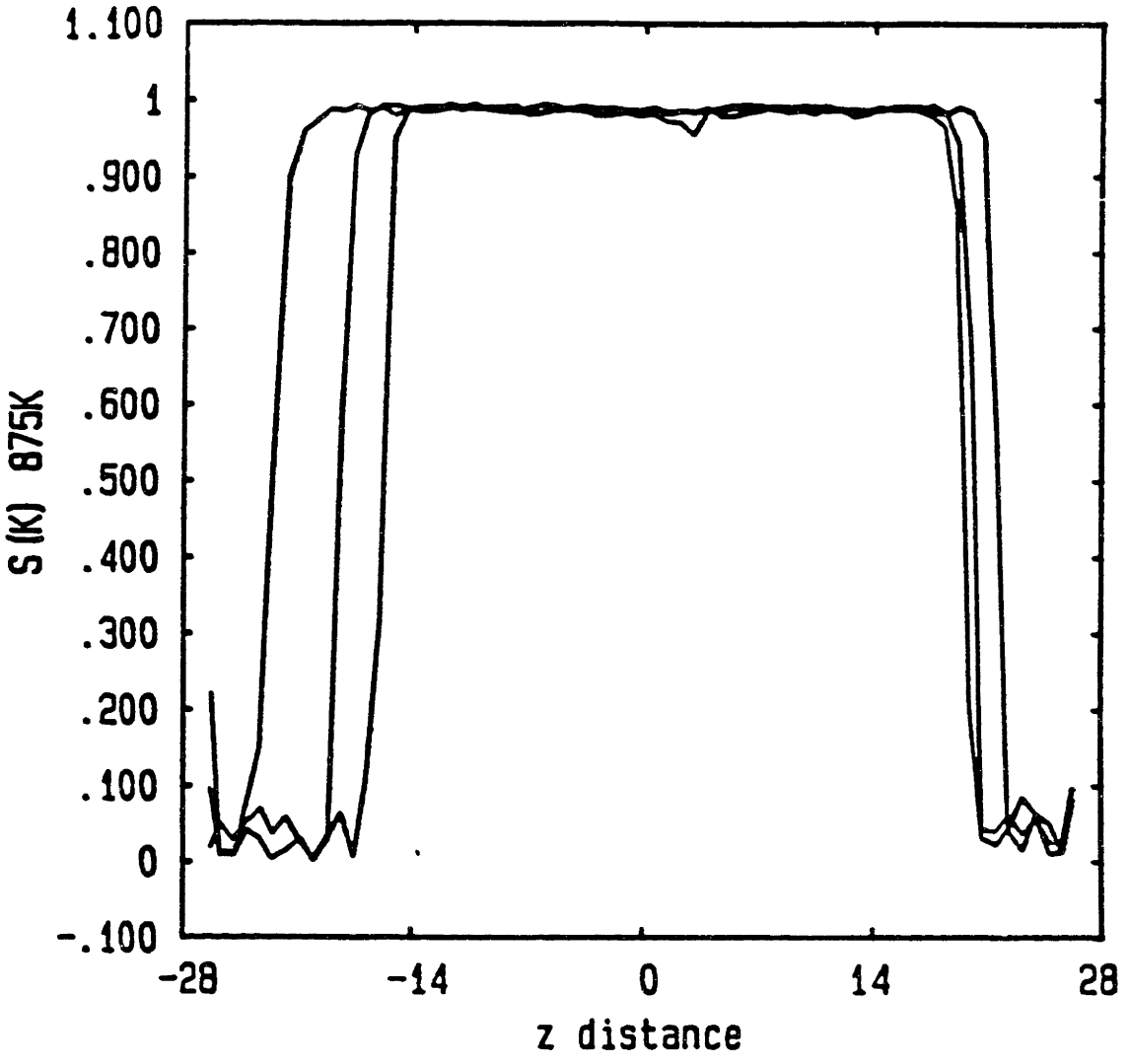

Figure 4-9: Structure factor profiles at 875K

Structure factor profile of the system at 875K for 3 different time steps (50000, 70000 and 90000). The data are averaged over 1000 time steps. The distance is in unit of a (4.05 A).

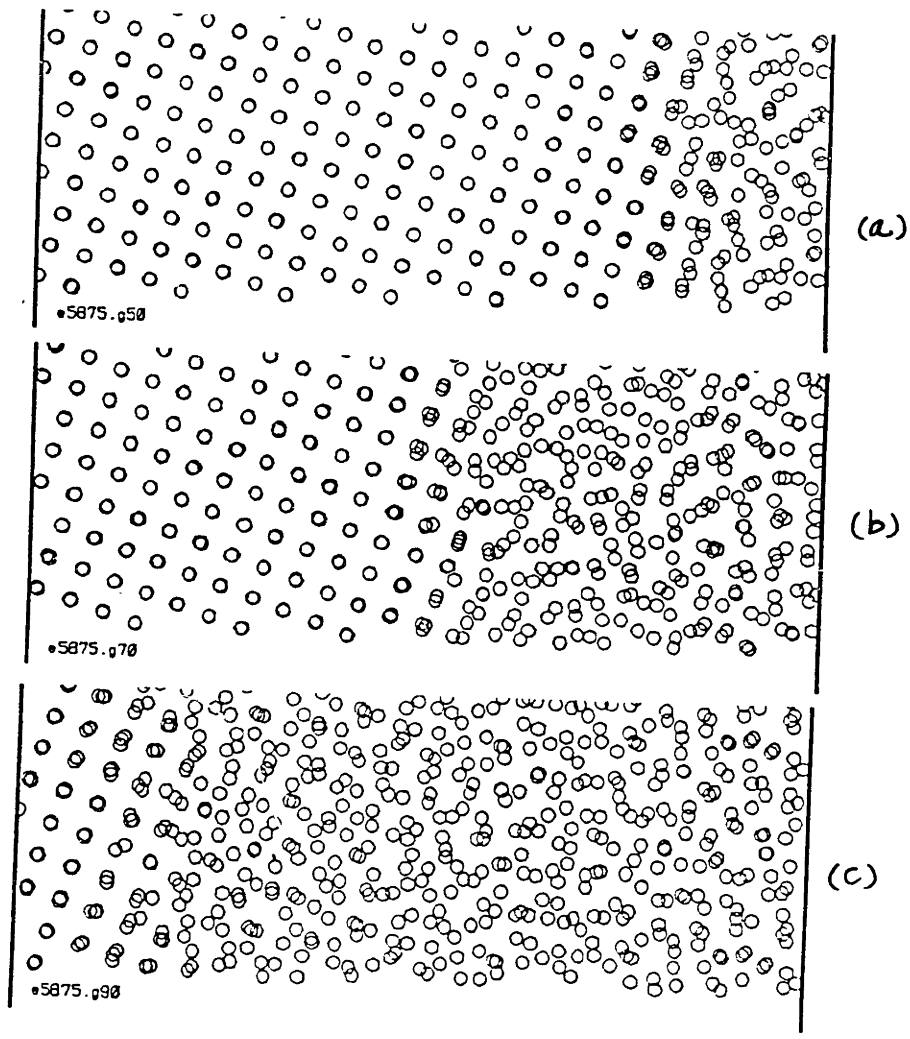

Figure 4-10: Atom positions at 875K

Detail structures of the ordered disordered interface at 875K for 3 different time steps (a) 50000, (b) 70000 and (c) 90000. The atom positions are averaged over 1000 time steps.

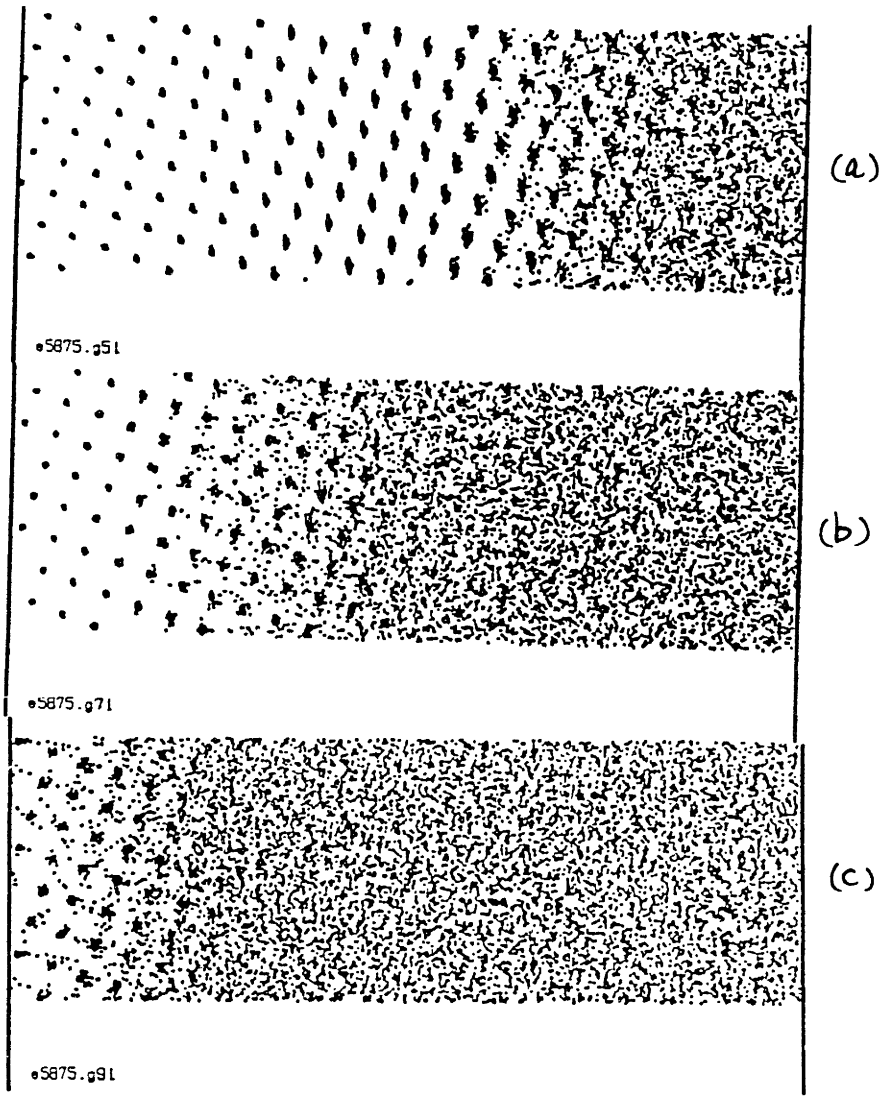

Figure 4-11: Structure at 875K

Accumulation of atom positions at the interface for 20000 time steps at 875K for 3 different time steps (a) 50000, (b) 70000 and (c) 90000. The atom positions are averaged over 1000 time steps.

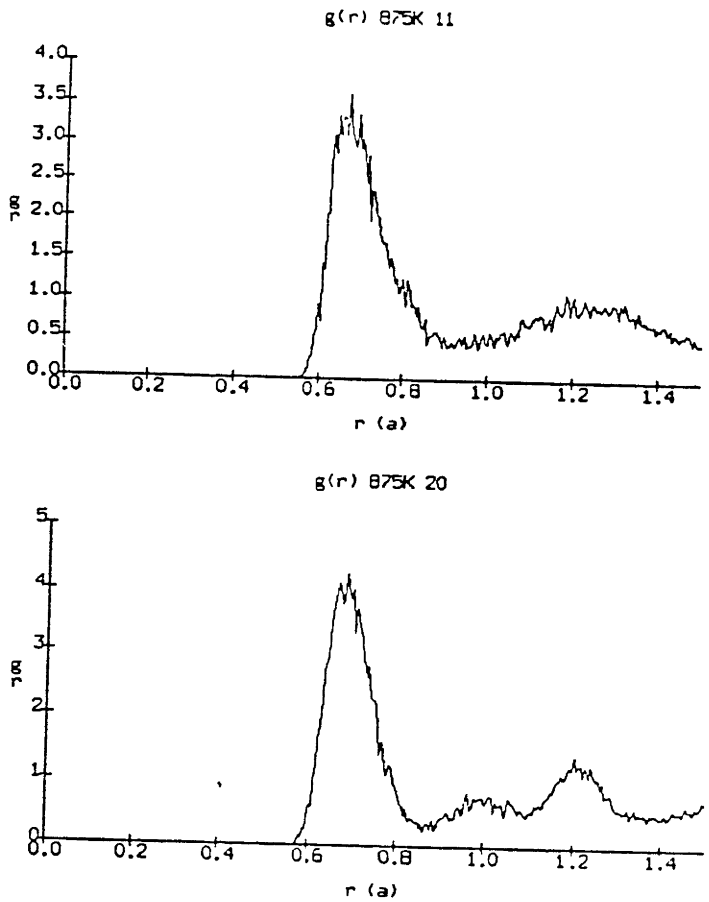

Figure 4-12: Instantaneous radial distribution function at 875K

g(r) for regions across the interface (a) disordered region, (b) ordered region. The data are accumulated for 1000 time steps with 10 time step interval at time step 50000. The atom positions are instantaneous positions.

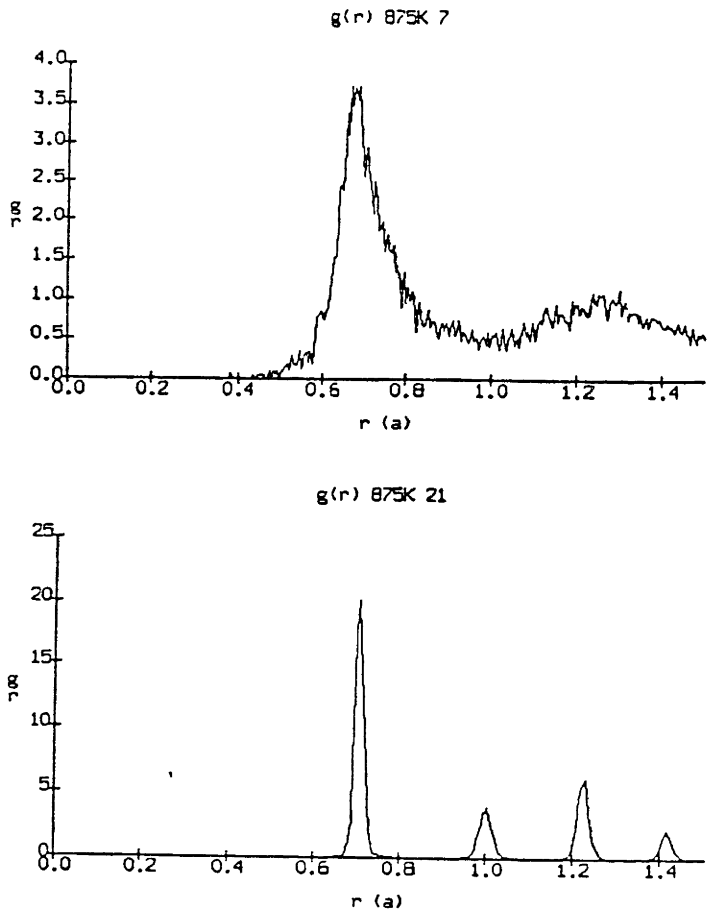

Figure 4-13: Time averaged radial distribution function at 875K

g(r) for regions across the interface (a) disordered region, (b) ordered region. The data are accumulated for 50000 time steps with 1000 time step interval at time step 50000. The atom positions are averaged over 1000 time steps.

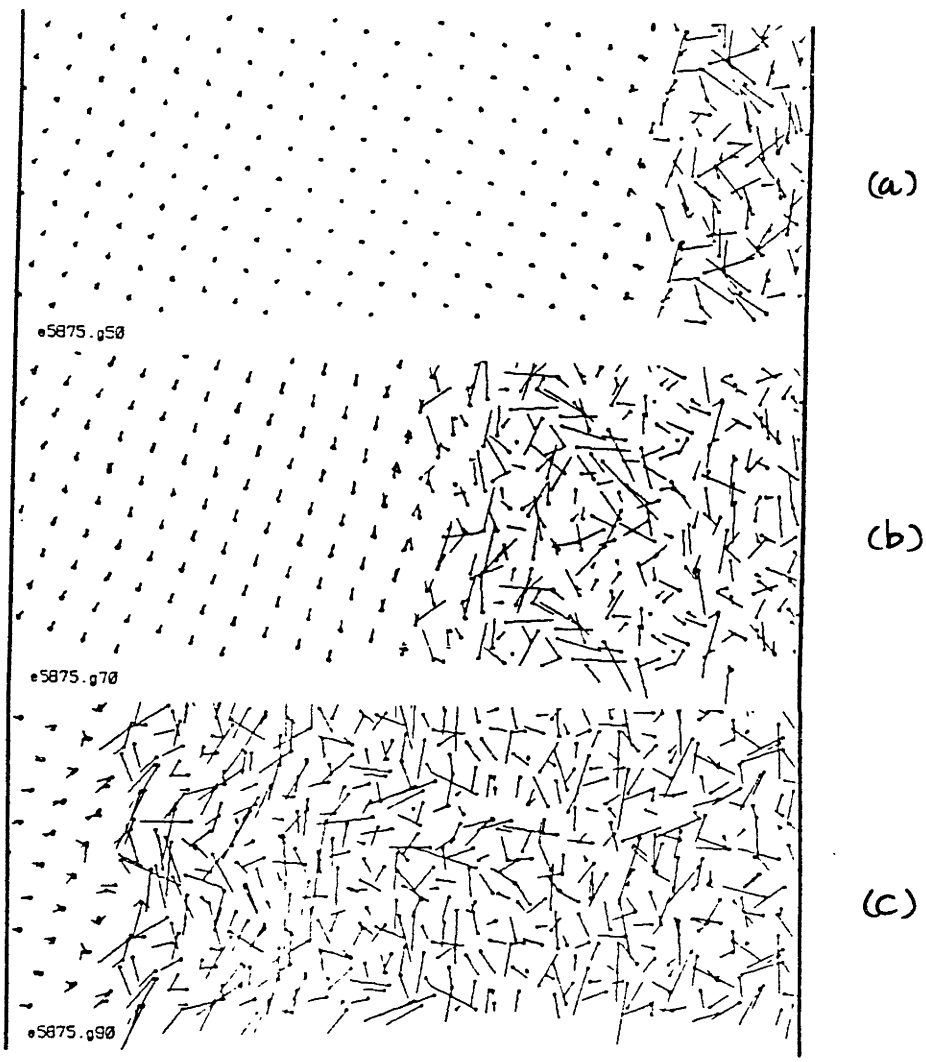

Figure 4-14: Mobility of the disordered region at 875K

Mobility of the disordered region at 875K at different time steps (a) 50000, (b) 70000 and (c) 90000. The lines are connecting two consecutive atom positions which are averaged for 1000 time steps.

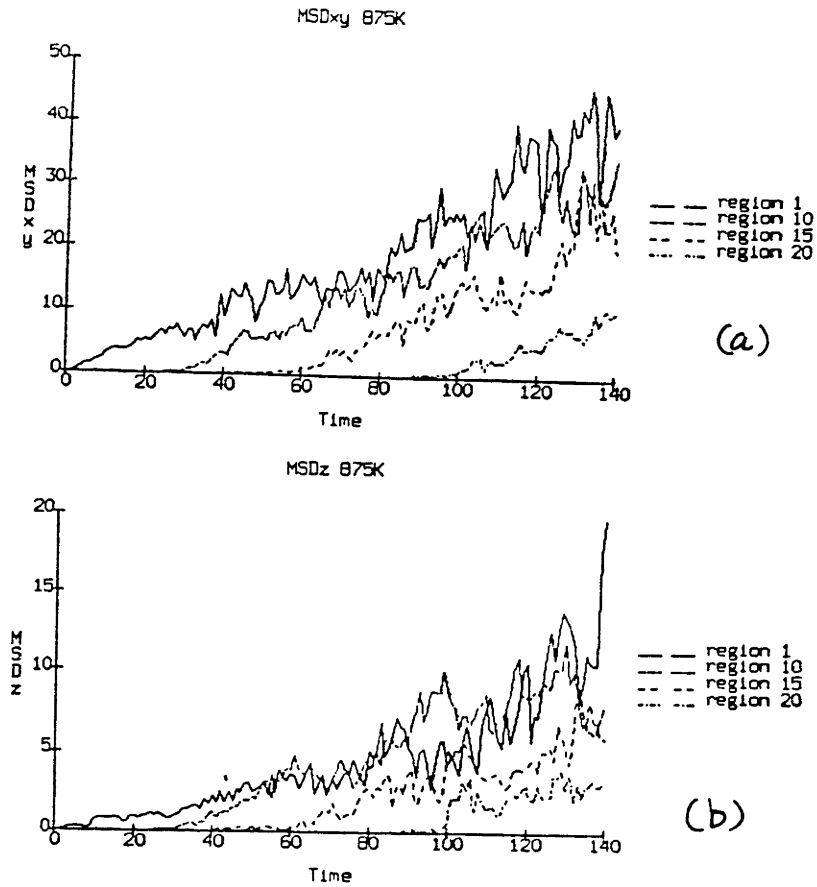

Figure 4-15: MSD at 875K

(a) xy component (b) z component. The data are for different layers in the surface region.

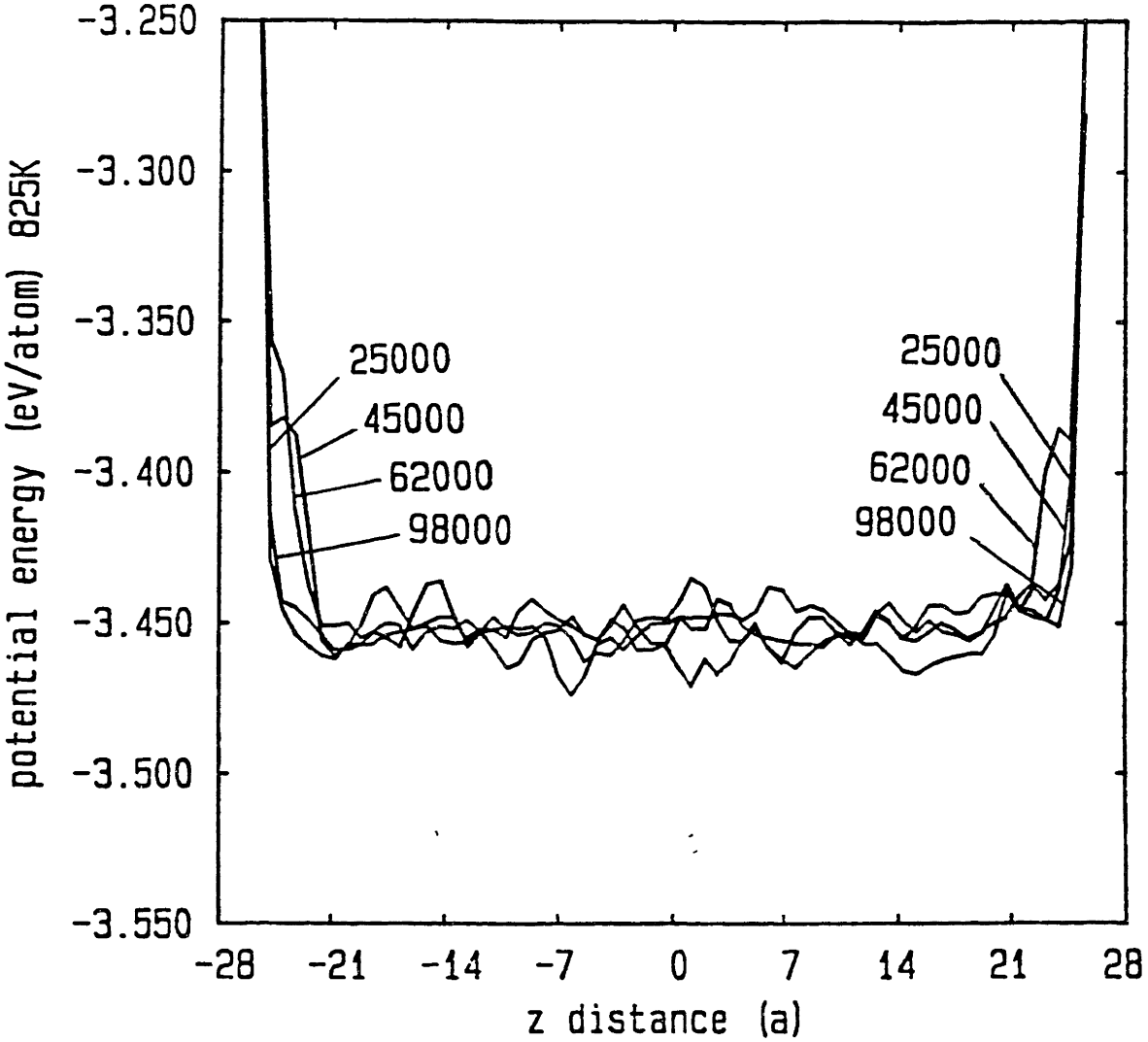

Figure 4-16: Potential energy profiles at 825K

Potential energy profiles of the system at 825K for 4 different time steps (25000, 45000, 62000 and 98000). The data are averaged over 1000 time steps. The distance is in unit of a (4.05 A).

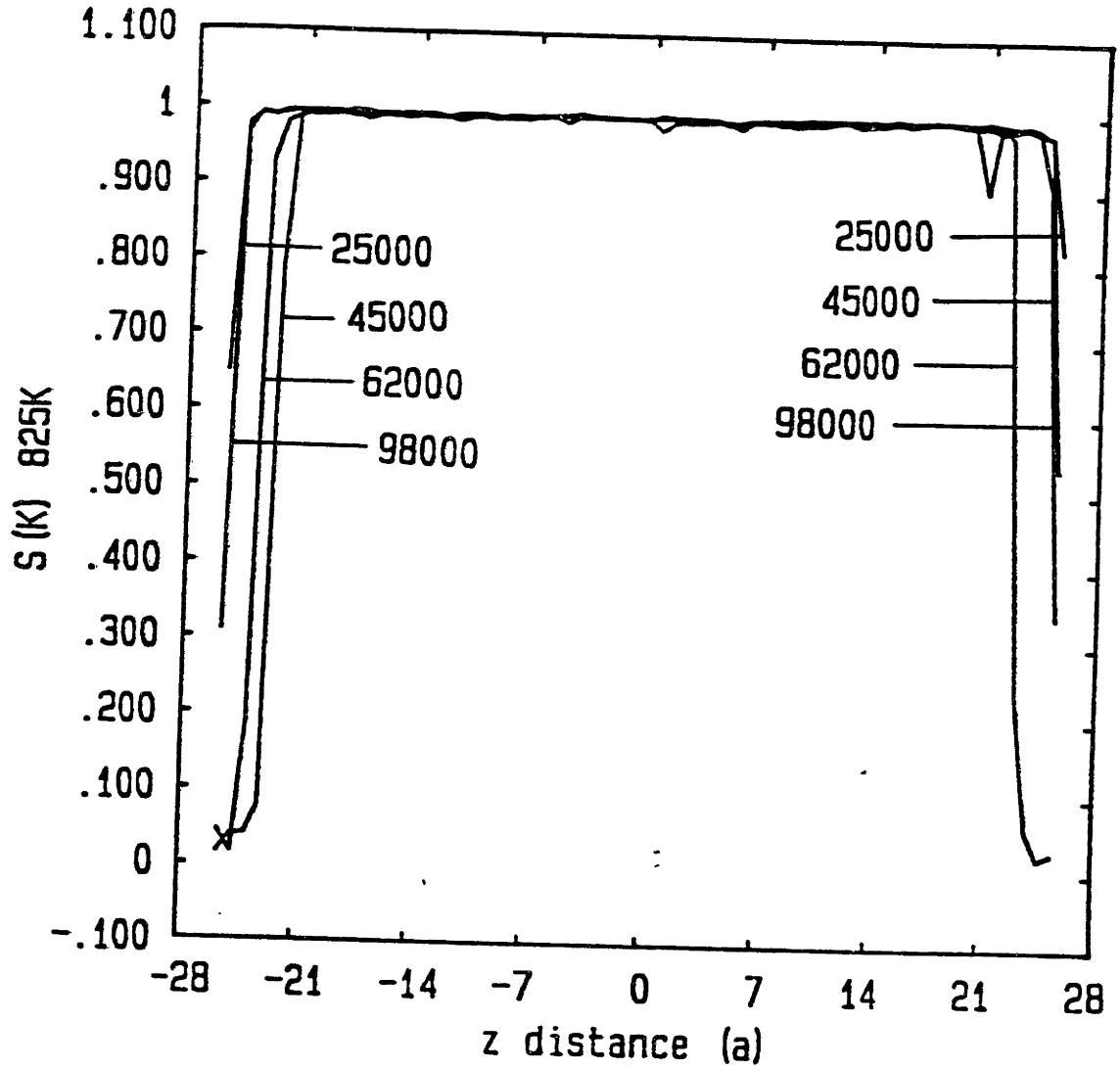

Figure 4-17: Structure factor profiles at 825K

Structure factor profiles of the system at 825K for 4 different time steps (25000, 45000, 62000 and 98000). The data are averaged over 1000 time steps. The distance is in unit of a (4.05 A).

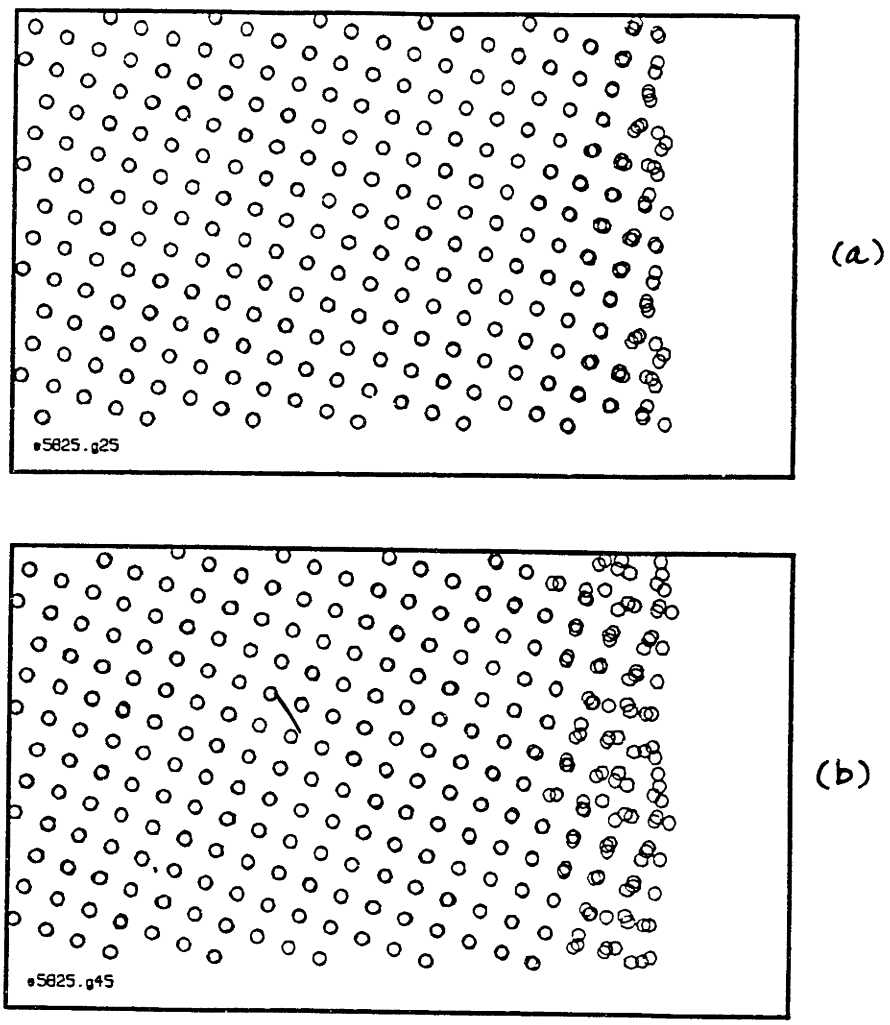

Figure 4-18: Atom positions at 825K

Detail structures of the ordered disordered interface at 825K for 4 different time steps (a) 25000, (b) 45000 (c) 62000 and (d)98000. The atom positions are averaged over 1000 time steps.

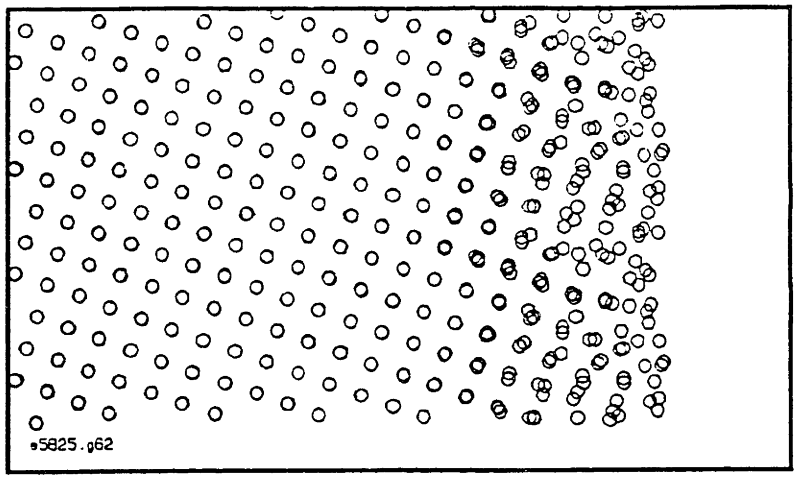

(c)

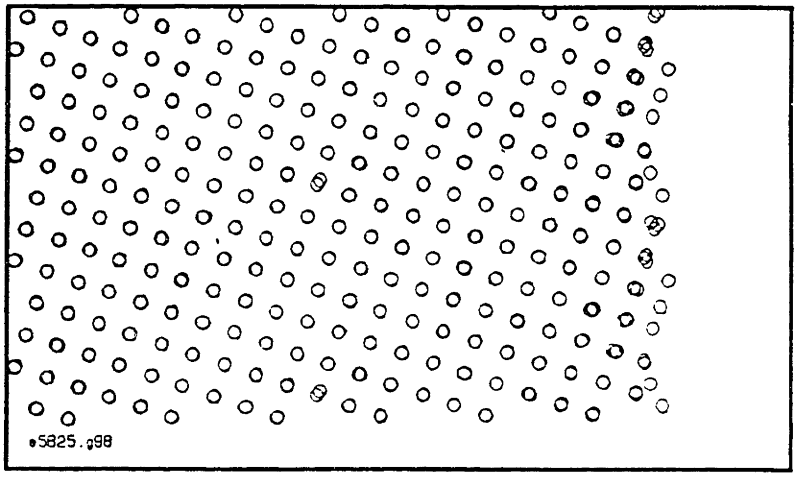

(d)

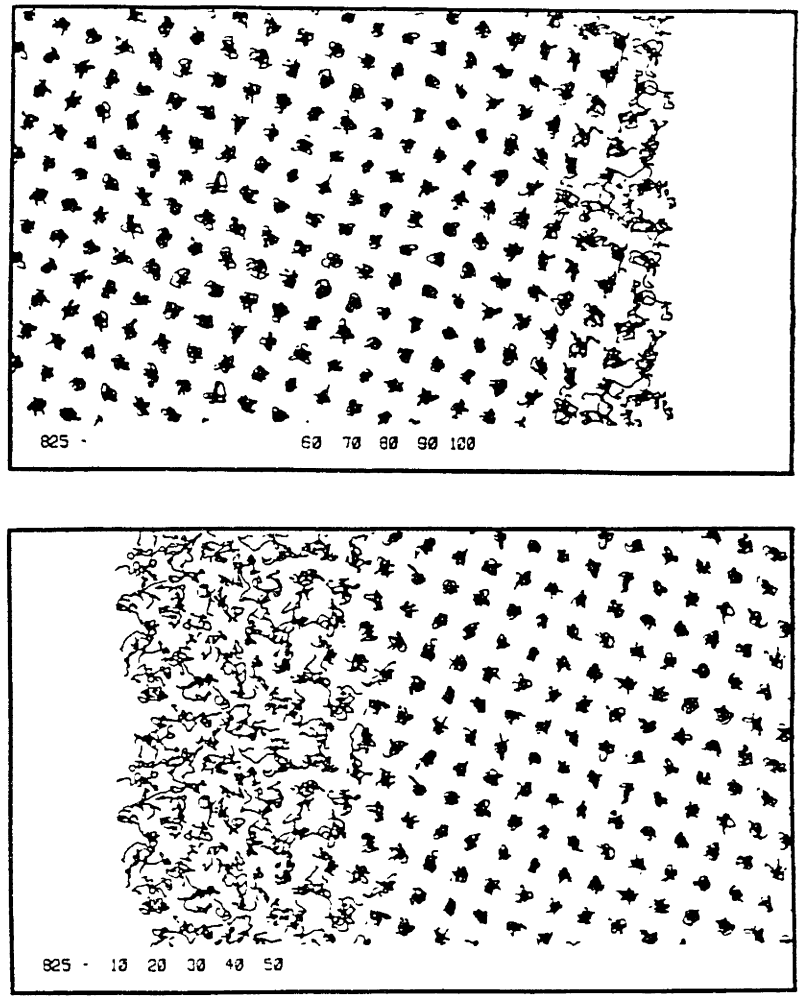

Figure 4-19: Atom trajectories at 825K

Accumulated atom trajectories for the two surfaces at 825K. (a) right surface (b) left surface. The data are at time step 45000 for 500 time steps.

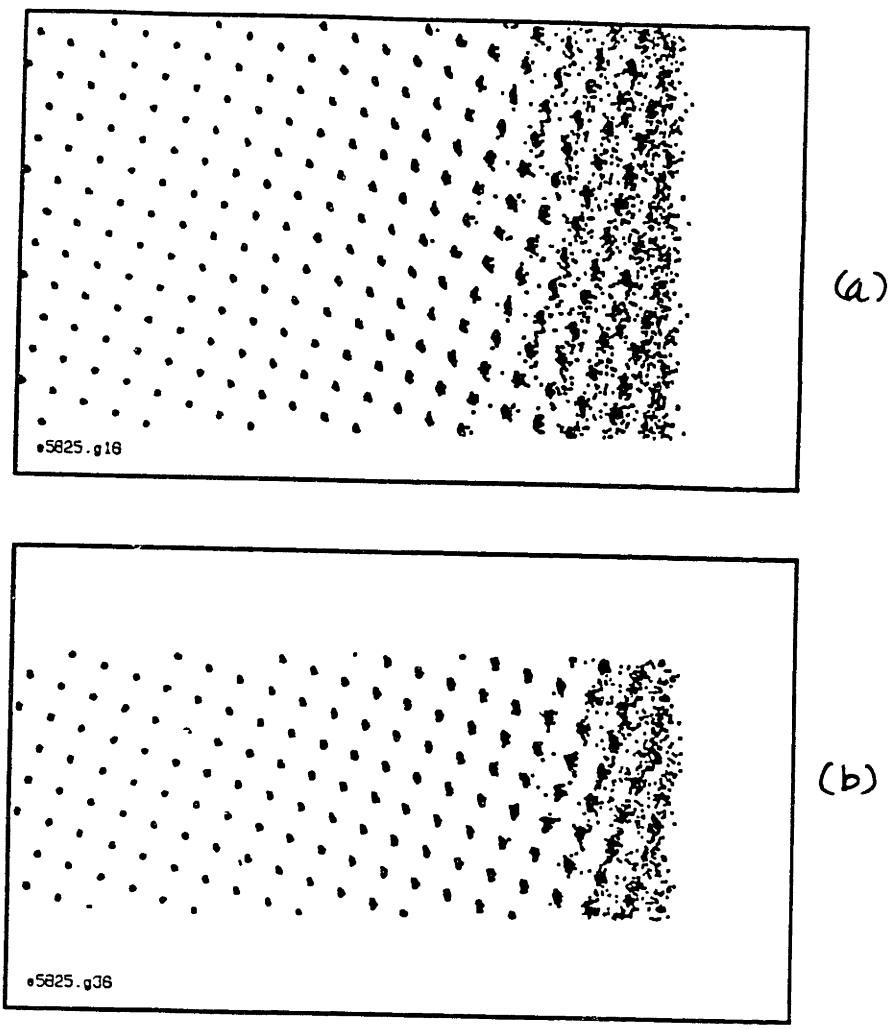

Figure 4-20: Structure at 825K for the right surface

Accumulation of atom positions at the interface for 20000 time steps at 825K for 4 different time steps (a) 25000, (b) 45000 (c) 62000 and (d) 98000. The atom positions are averaged over 1000 time steps.

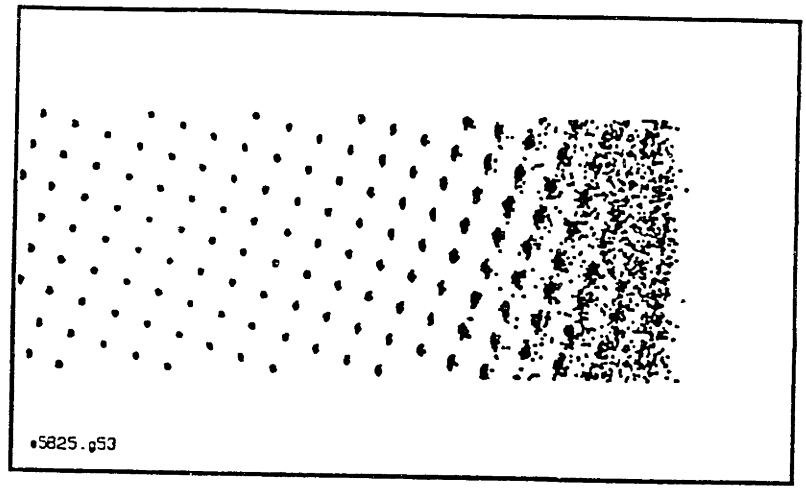

(c)

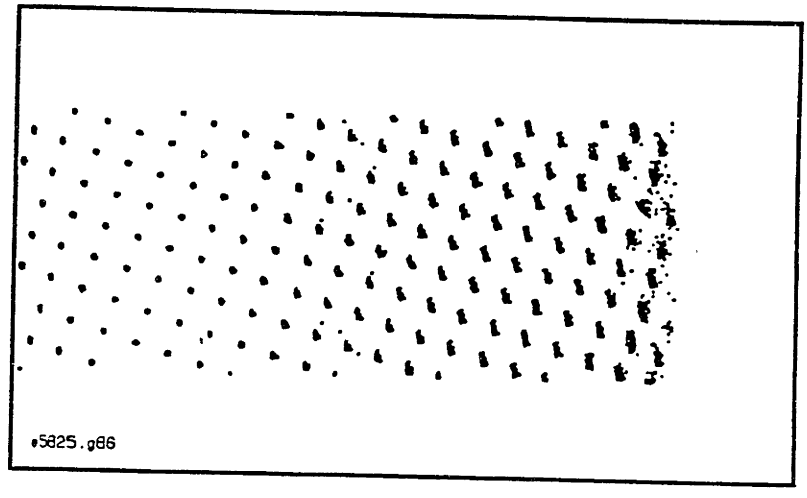

(d)

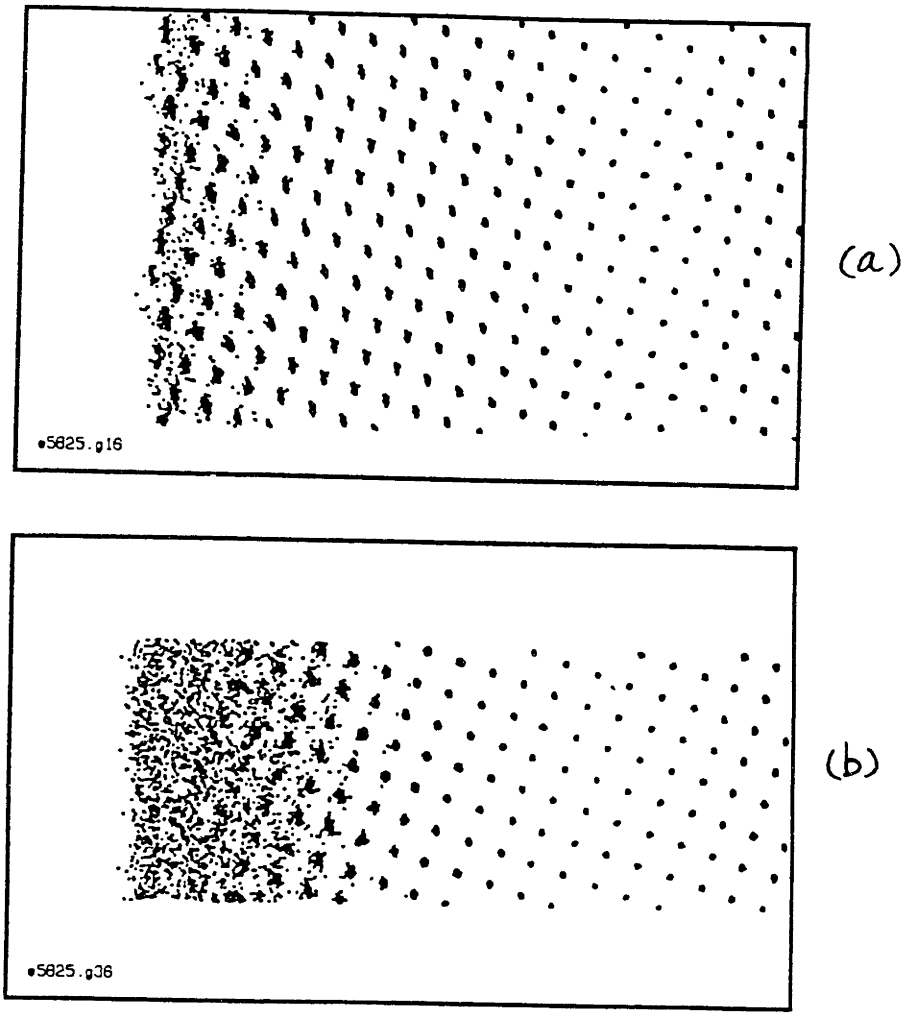

Figure 4-21: Structure at 825K for the left surface

Accumulation of atom positions at the interface for 20000 time steps at 825K for 4 different time steps (a) 25000, (b) 45000 (c) 62000 and (d) 98000. The atom positions are averaged over 1000 time steps.

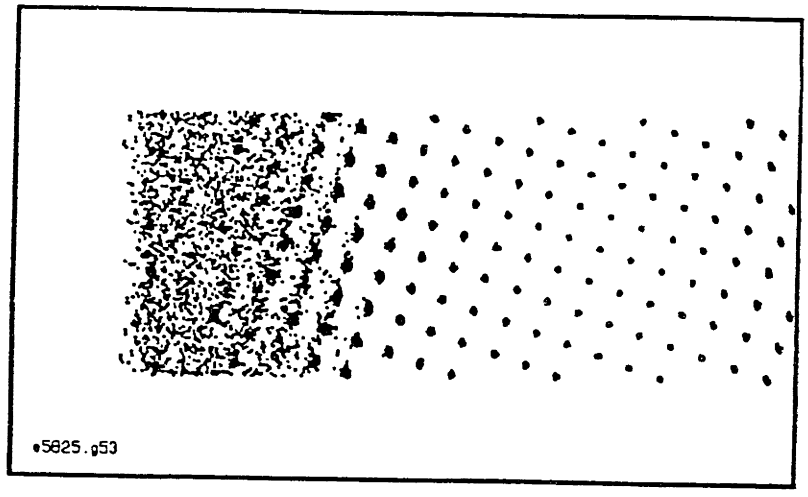

(c)

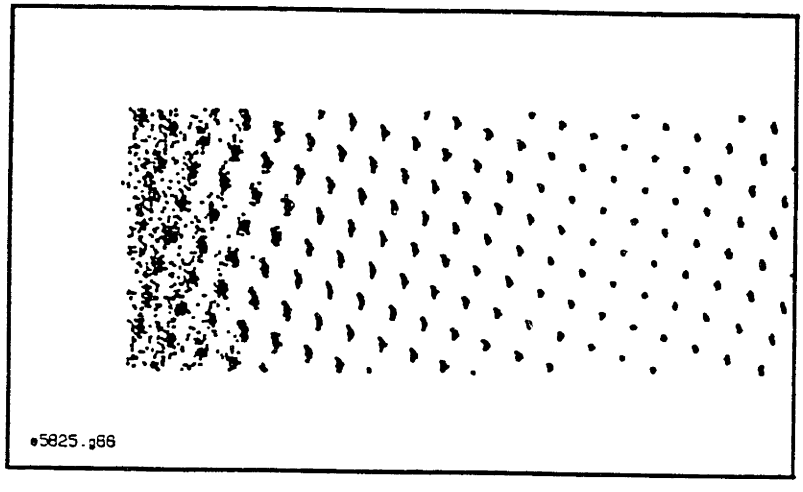

(d)

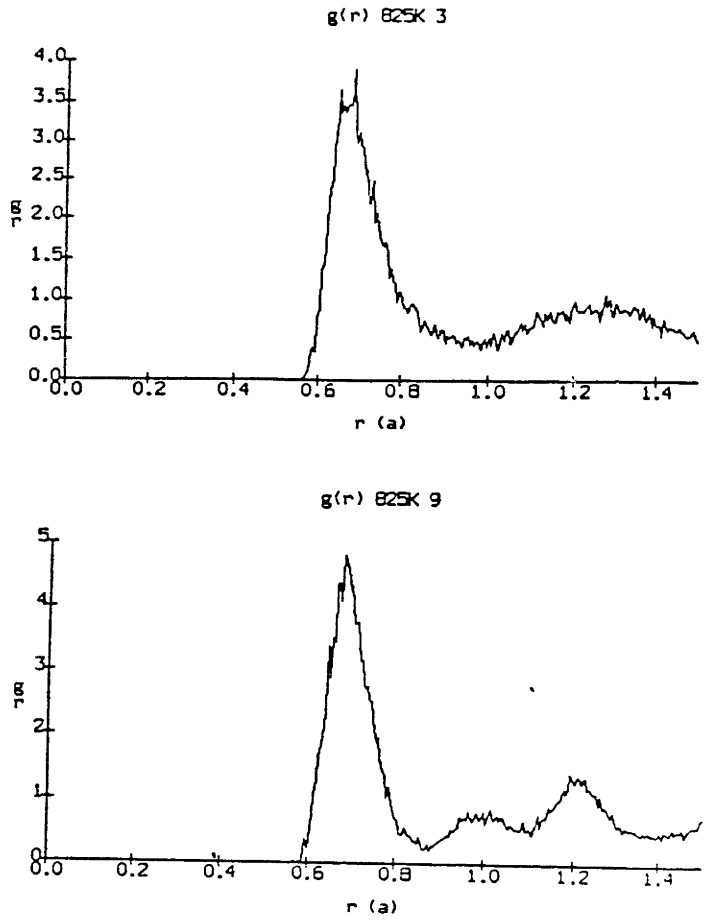

Figure 4-22: Instantaneous radial distribution function at 825K

g(r) for regions across the interface (a) disordered region, (b) ordered region. The data are accumulated for 1000 time steps with 10 time step interval at time step 45000. The atom positions are instantaneous positions.

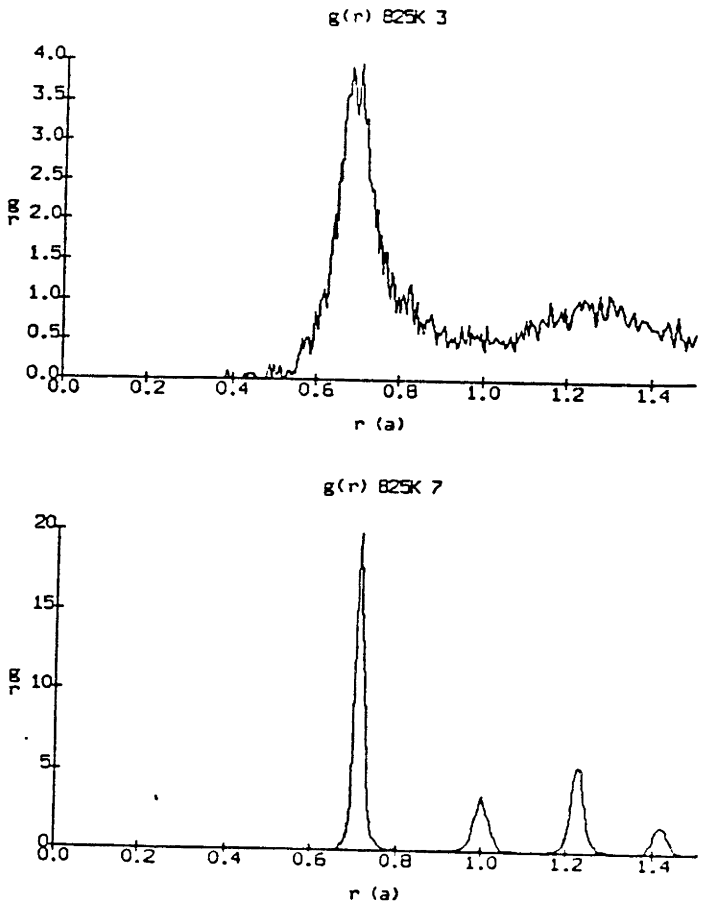

Figure 4-23: Time averaged radial distribution function at 825K at time step 35000

g(r) for regions across the interface (a) disordered region, (b) ordered region. The data are accumulated for 40000 time steps with 1000 time step interval at time step 35000. The atom positions are averaged over 1000 time steps.

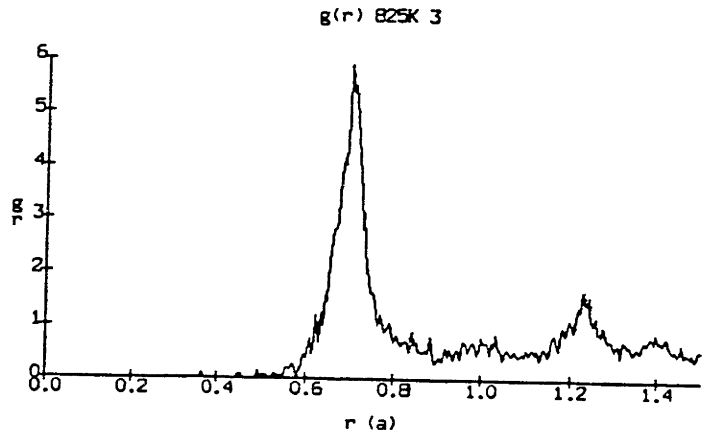

Figure 4-24: Time averaged radial distribution function at 825K at time step 75000

g(r) for disordered region as in Fig. 4-23. The data are accumulated for 40000 time steps with 1000 time step interval at time step 75000. The atom positions are averaged over 1000 time steps.

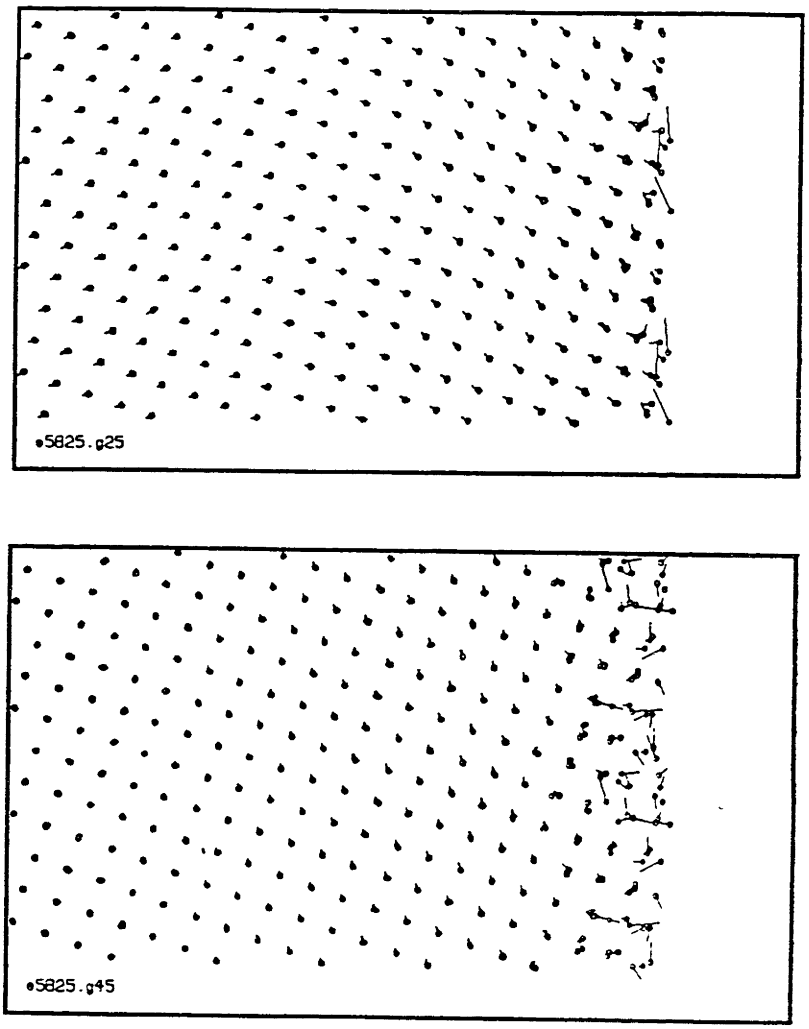

Figure 4-25: Mobility of the right surface at 825K

Mobility of the right surface at 825K at different time steps (a) 25000, (b) 45000 (c) 62000 and (d) 98000. The lines are connecting two consecutive atom positions which are averaged for 1000 time steps.

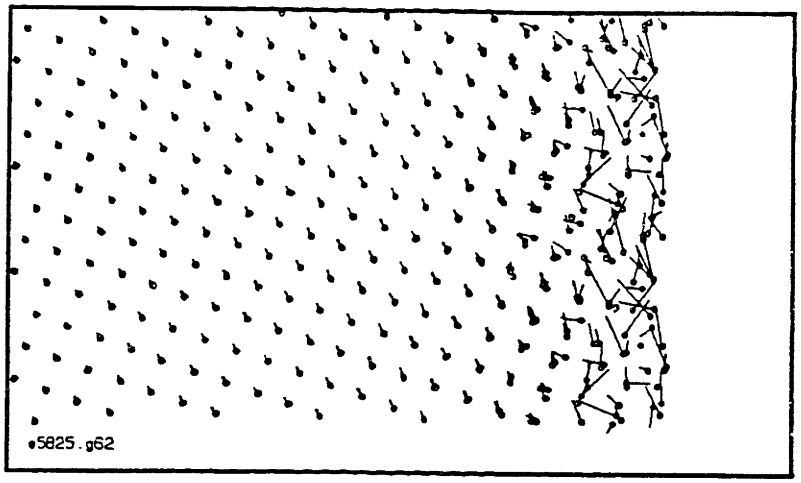

(c)

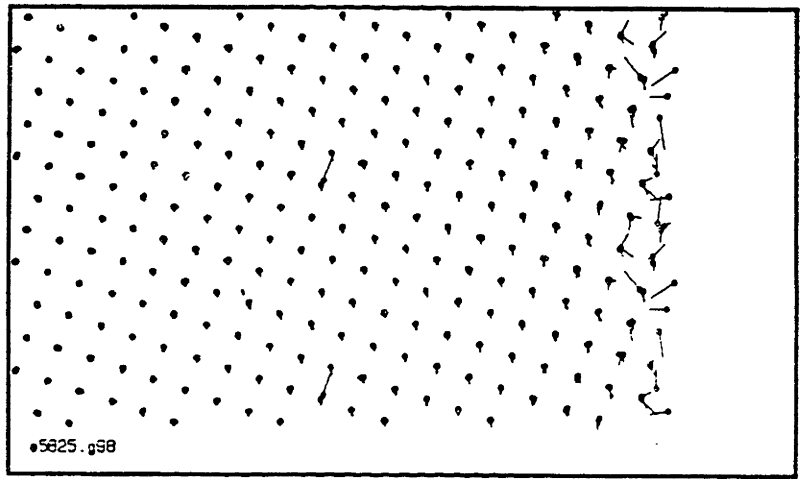

(d)

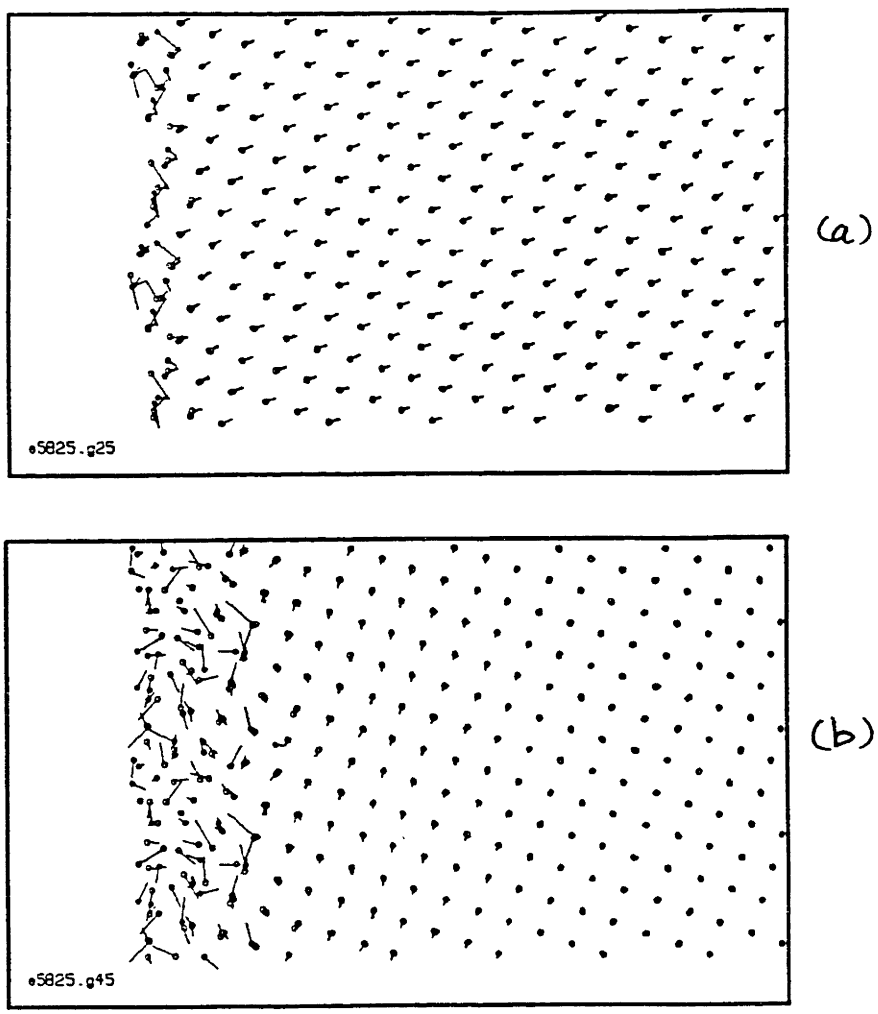

Figure 4-26: Mobility of the left surface at 825K

Mobility of the left surface at 825K at different time steps (a) 25000, (b) 45000 (c) 62000 and (d) 98000. The lines are connecting two consecutive atom positions which are averaged for 1000 time steps.

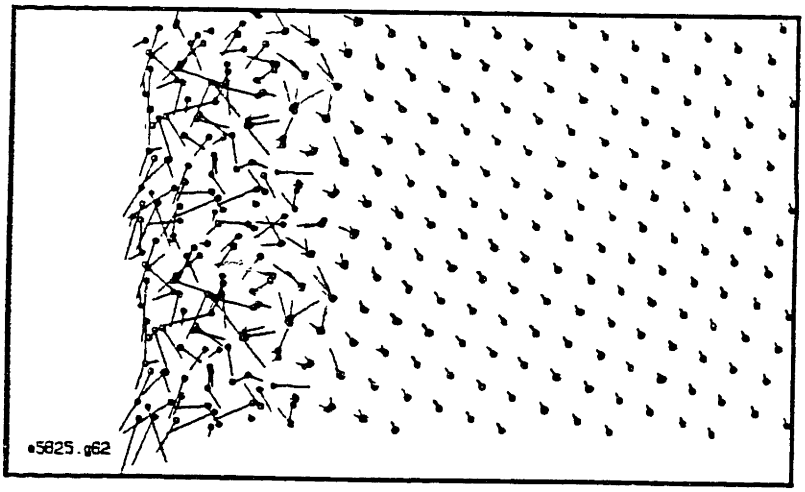

(c)

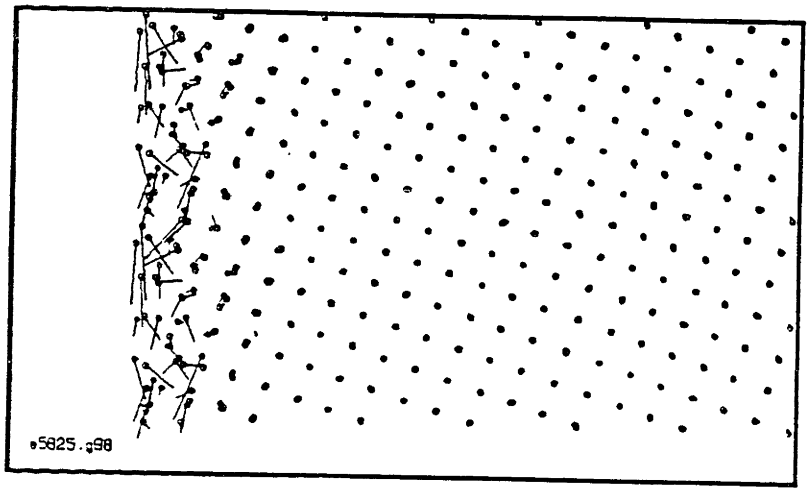

(d)

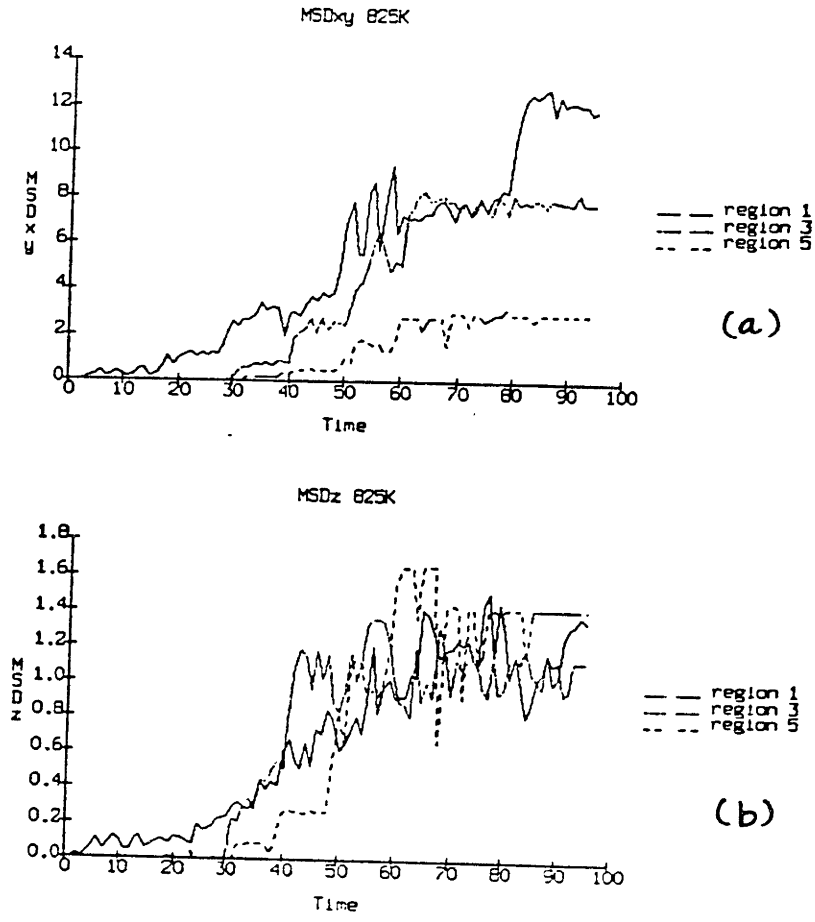

Figure 4-27: MSD at 825K

(a) xy component (b) z component. The data are for different layers in the surface region.

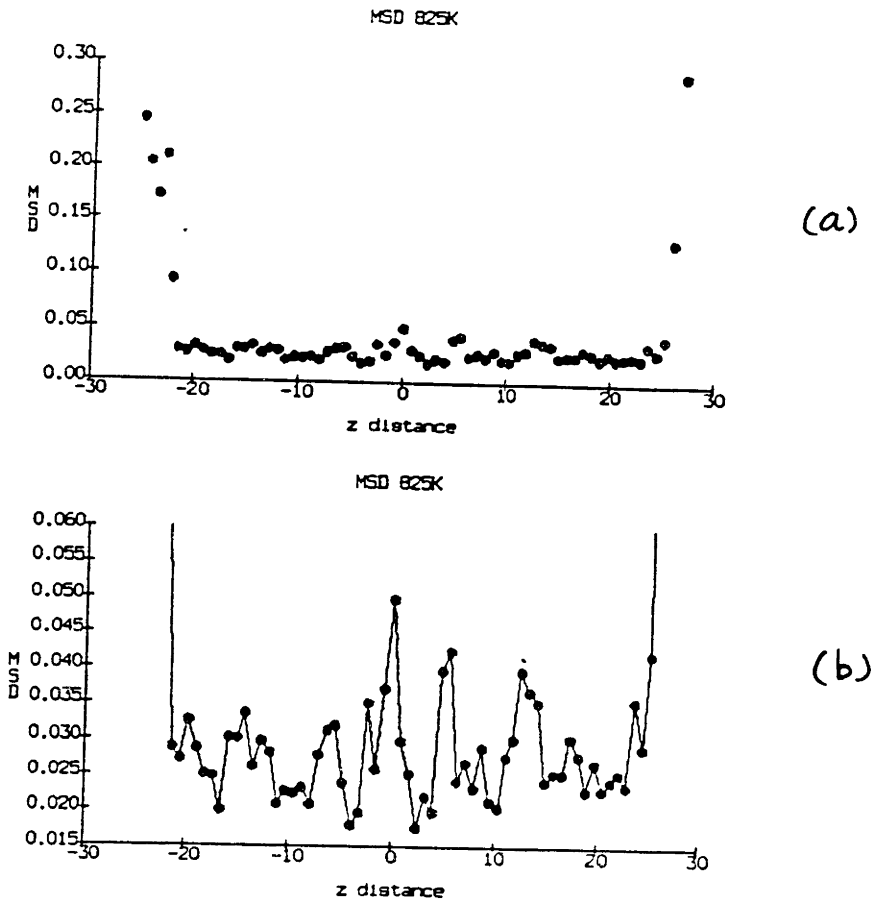

Figure 4-28: MSD profiles at 825K

MSD profiles along the z direction of the simulation cell at 825K. (a) full scale of MSD profile (b) Blow up portion of the MSD in the bulk region.

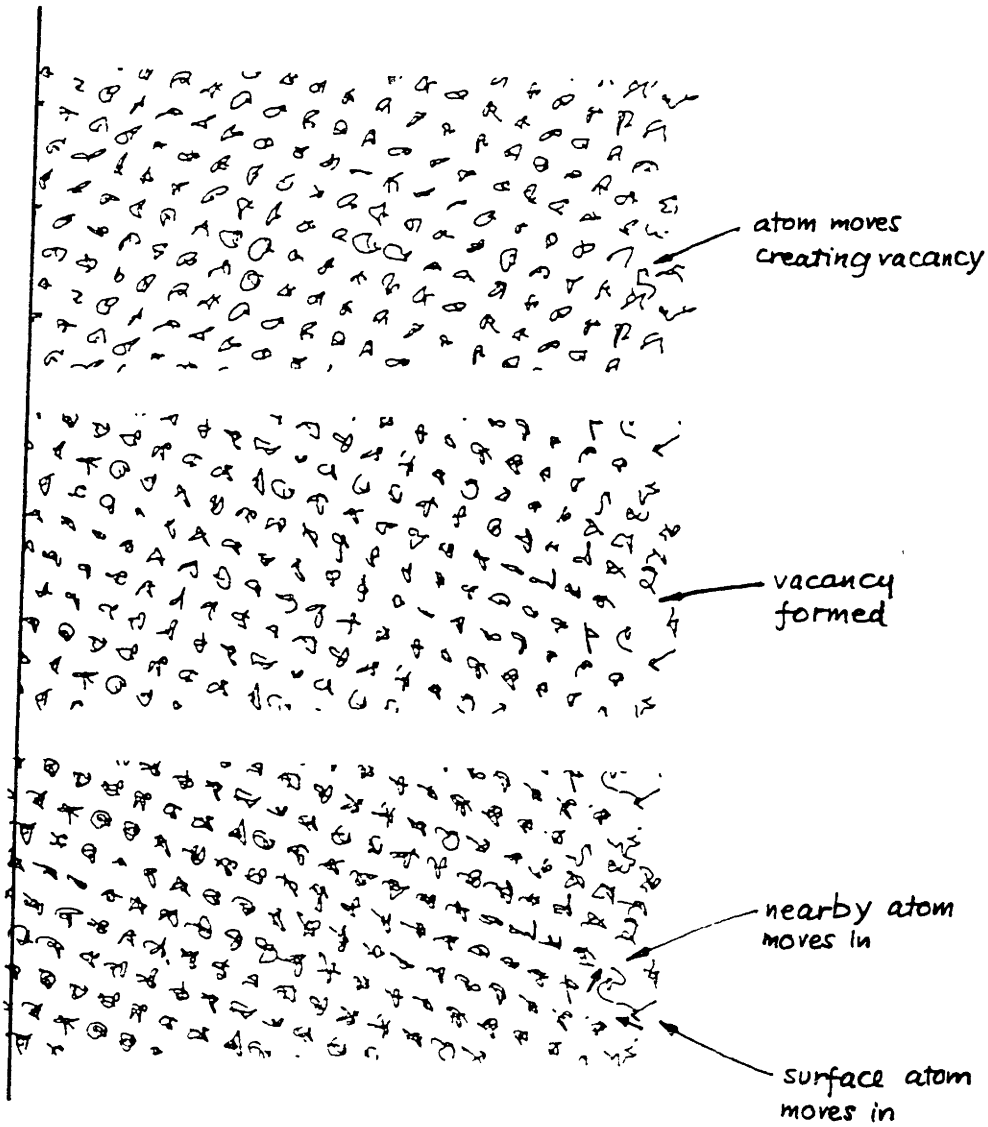

Figure 4-29: Movement of atom through vacancy formation (instantaneous positions)

Atomic trajectories showing the formation of a vacancy and the movement of nearby atom to occupy it at a later time. The atom positions are instantaneous and starting at time step 45000 and cover 1000 time steps.

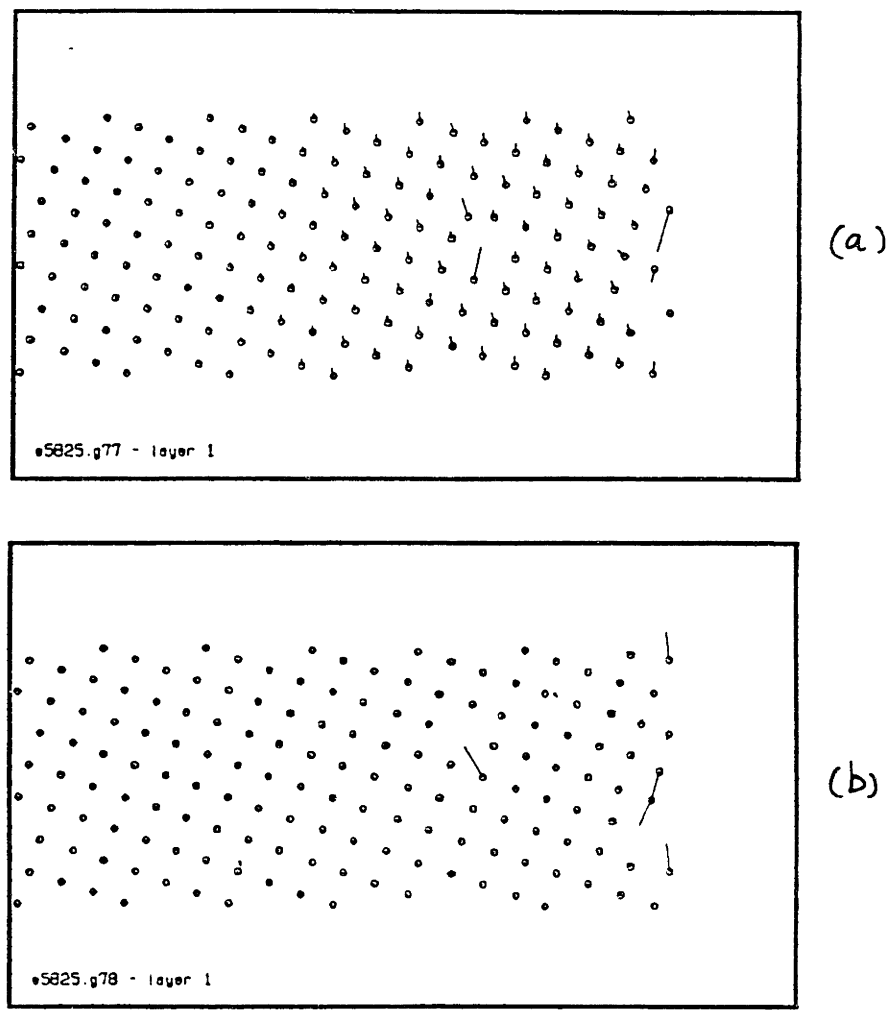

Figure 4-30: Movement of atom through vacancy formation (time averaged positions)

Time averaged positions of atoms showing the movement of vacancies. The atom positions are time averaged over 1000 time steps at time steps (a) 77000 and (b) 78000.

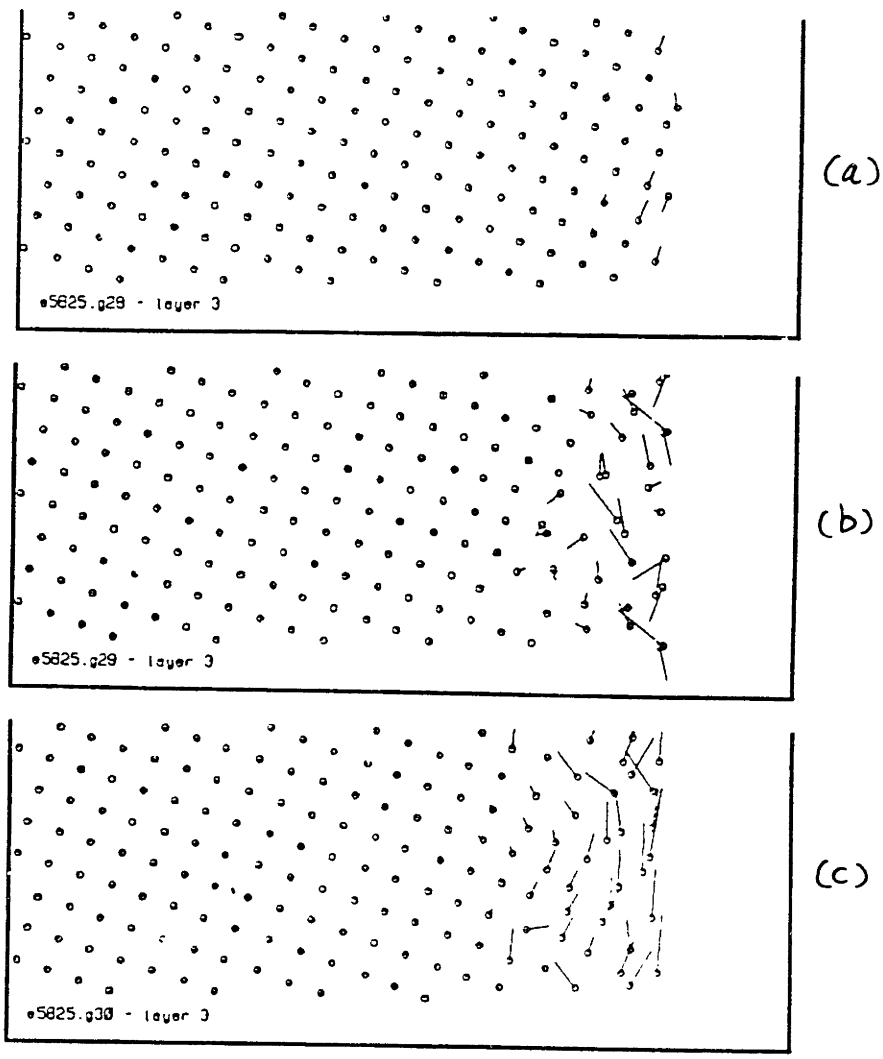

Figure 4-31: Transition from an ordered to disordered surface at 825K

Surface structures at time steps (a) 28000 (b) 29000 and (c) 30000 at 825K showing the rapid change of the surface structure from an ordered surface to a disordered surface.

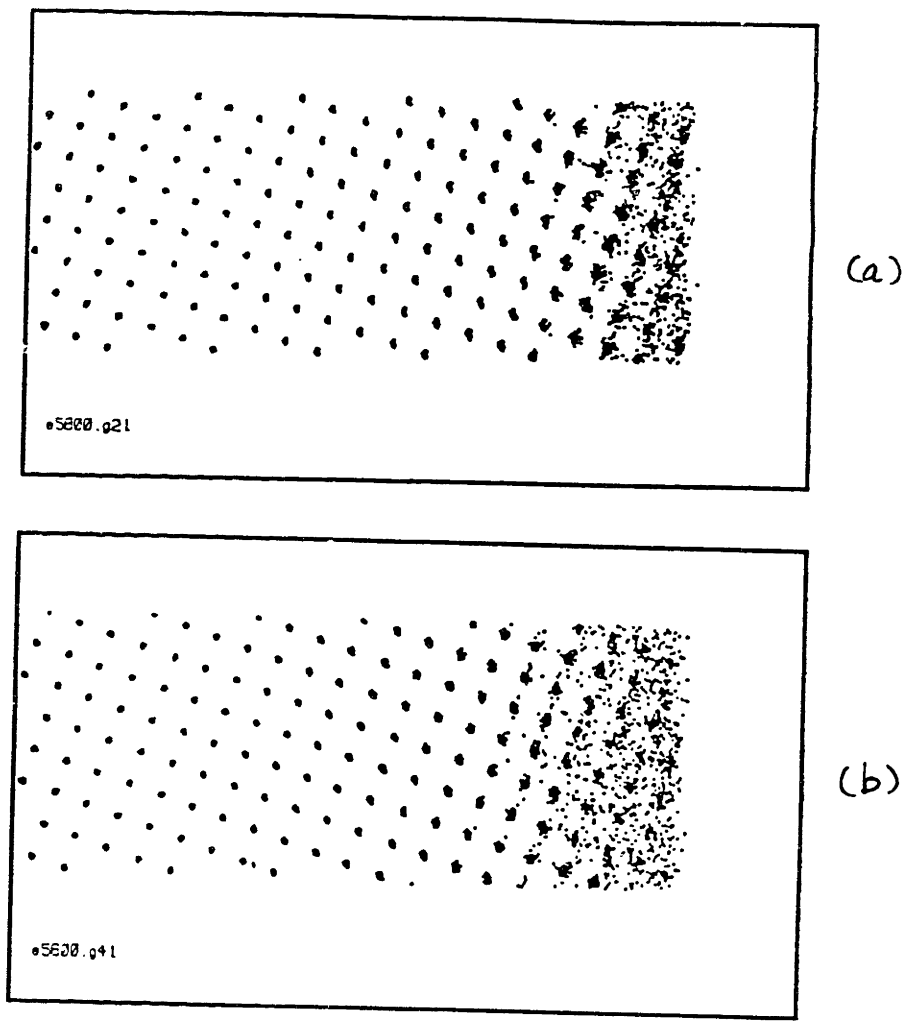

Figure 4-32: Structure at 800K for the right surface

Accumulation of atom positions at the interface for 20000 time steps at 800K for 2 different time steps (a) 20000, (b) 40000. The atom positions are averaged over 1000 time steps.

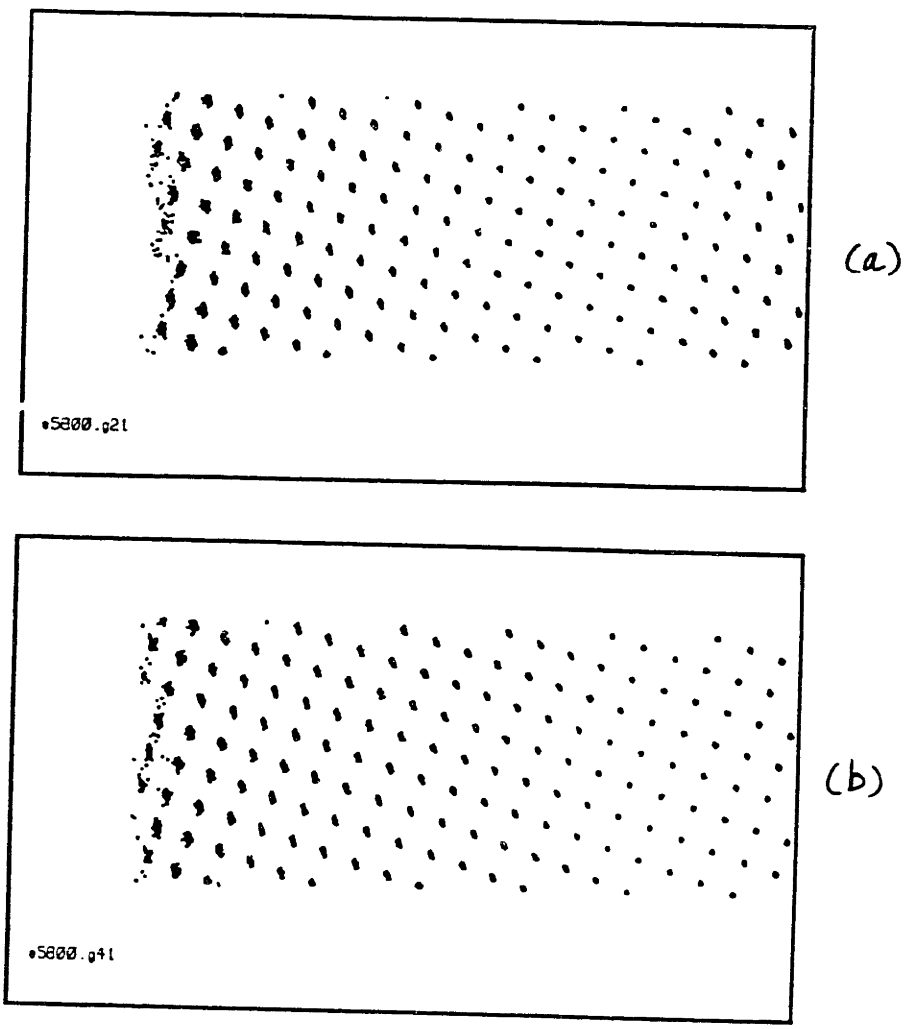

Figure 4-33: Structure at 800K for the left surface

Accumulation of atom positions at the interface for 20000 time steps at 800K for 2 different time steps (a) 20000, (b) 40000. The atom positions are averaged over 1000 time steps.

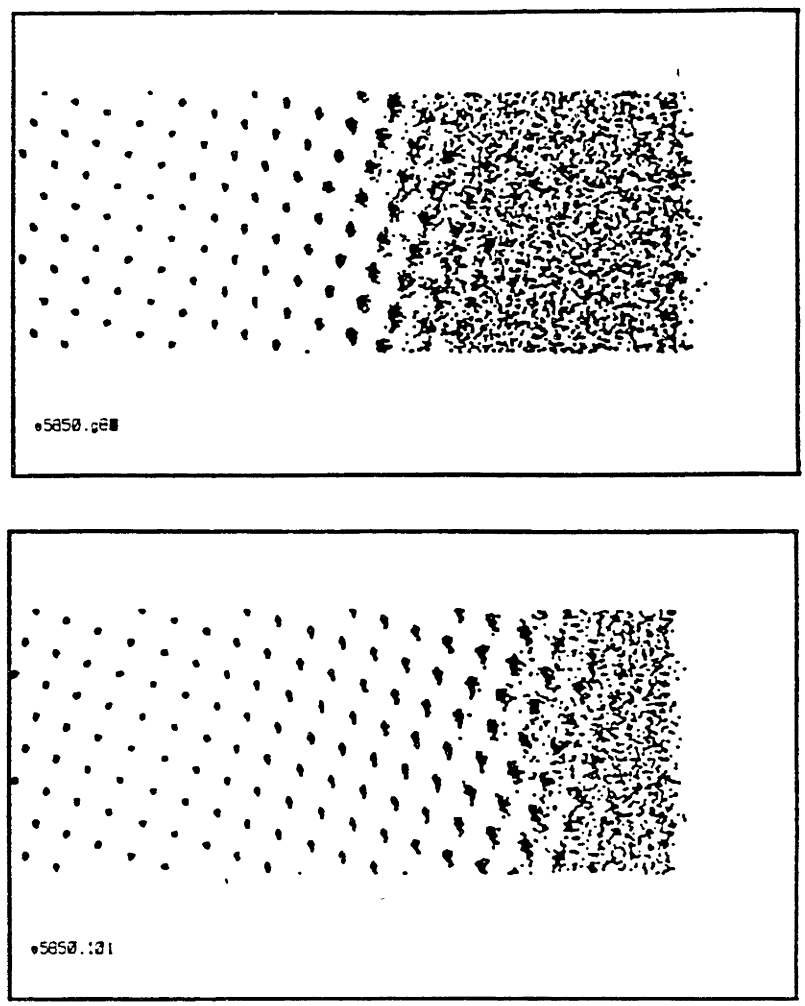

Figure 4-34: Structure at 850K for the right surface

Accumulation of atom positions at the interface for 20000 time steps at 850K for 2 different time steps (a) 80000, (b) 100000. The atom positions are averaged over 1000 time steps.

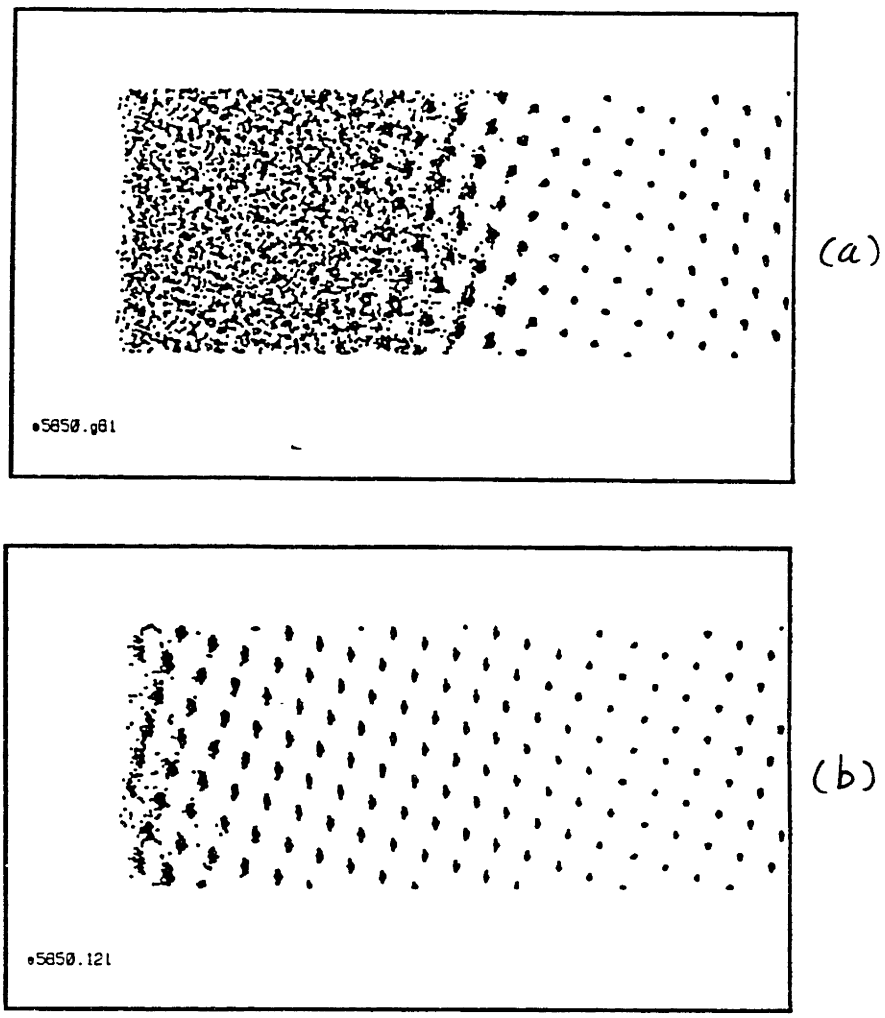

Figure 4-35: Structure at 850K for the left surface

Accumulation of atom positions at the interface for 20000 time steps at 850K for 2 different time steps (a) 80000, (b) 100000. The atom positions are averaged over 1000 time steps.

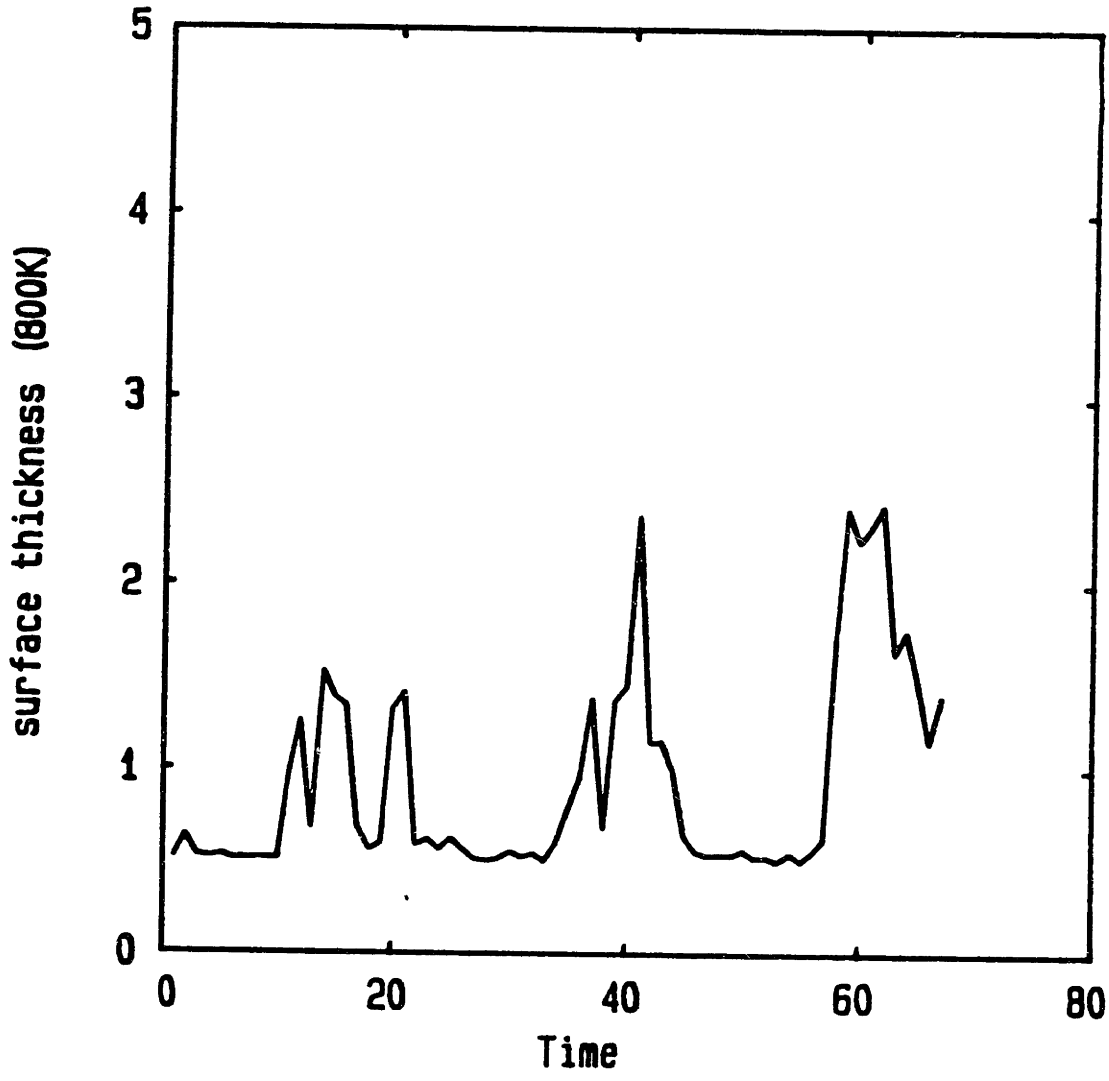

Figure 4-36: Surface disordered thickness at 800K

The thickness is in number of layers or 0.79 a (3.2 A). The time axis is in unit of 1000 time steps or 2.1 psec.

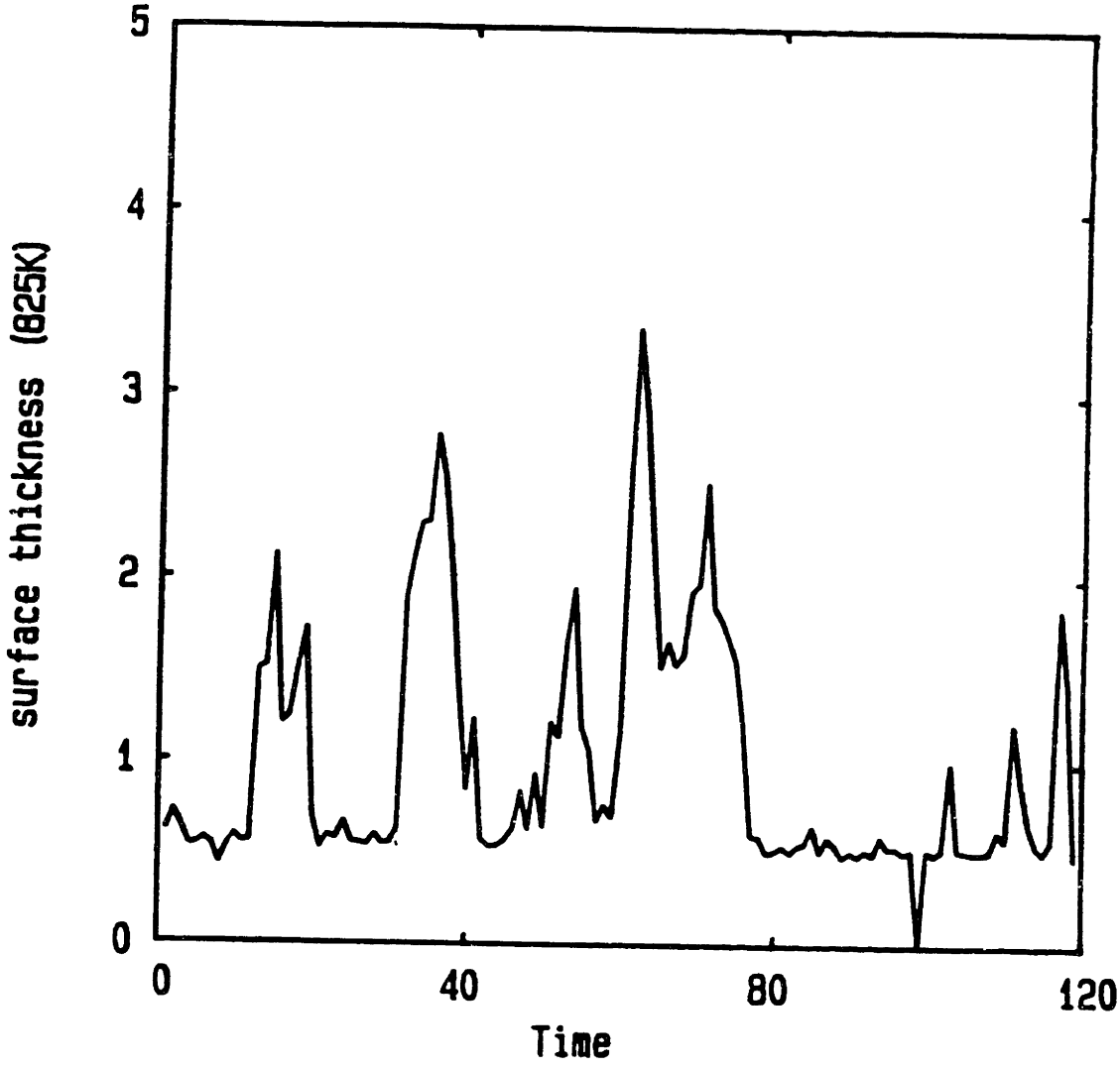

Figure 4-37: Surface disordered thickness at 825K

The thickness is in number of layers or 0.79 a (3.2 A). The time axis is in unit of 1000 time steps or 2.1 psec.

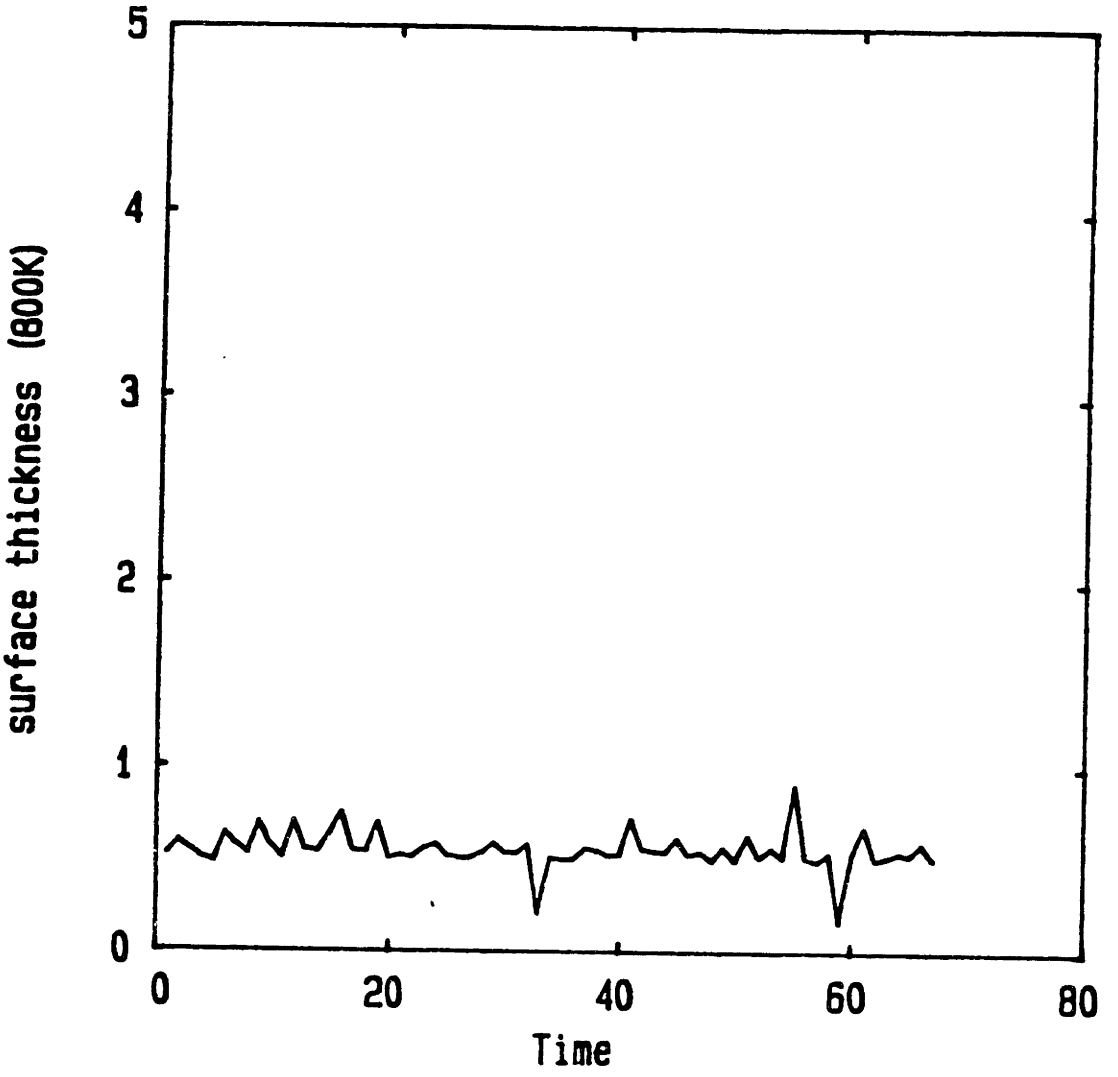

Figure 4-38: Thickness of second surface at 800K

The thickness is in number of layers or 0.79 a (3.2 A). The time axis is in unit of 1000 time steps or 2.1 psec.

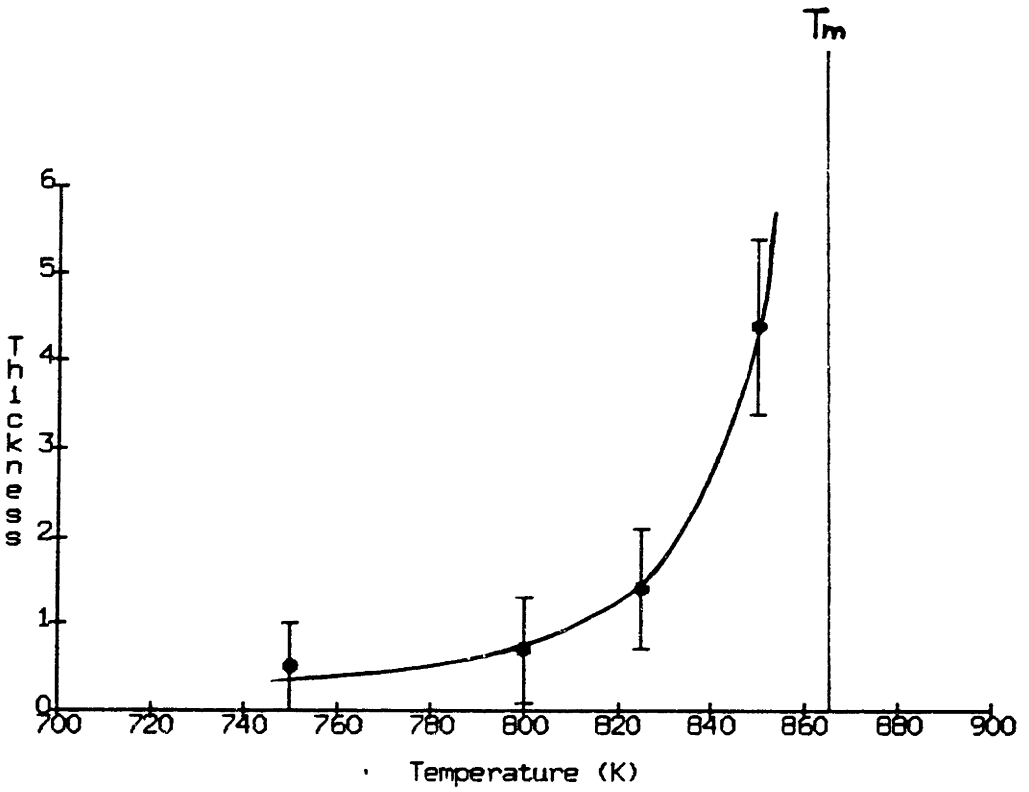

Figure 4-39: Surface thickness vs temperature

The solid line is the fitted $\log(T_m\text{-}T)$ curve.

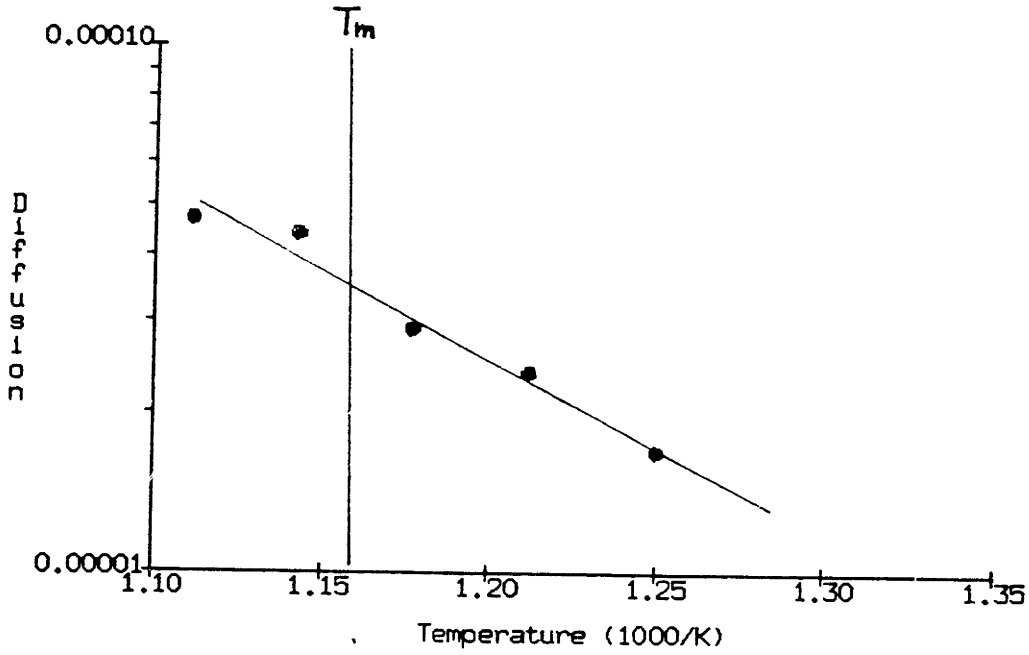

Figure 4-40: Diffusion coefficients vs 1/T

Chapter 5

Thermal disorder in a bicrystal model

The behavior of the bicrystal model described in chapter 2 will be studied in this chapter using MD simulation. To have reliable MD simulation, there are some basic general requirements: reasonable potential function, correct phase diagram and realistic border condition[5] The best potential functions for metals currently available are EAM potentials[28-30]; in this work such a potential will be used.

EAM potentials are an improvement over empirical potentials because they consider also the local environment of the atoms through the electron density calculation. The phase diagram requirement can be satisfied easily by choosing a large enough simulation cell so that far from the gb interface, the material has bulk properties. This could also be used as a criterion to see if a system size is adequate. The border condition requirement is to ensure that a finite size simulation cell (of the order of 10^3 - 10^4 atoms) behaves like a real material (~ 10^{23} atoms). Commonly used in earlier works are periodic border condition (PBC)[18,21] and fixed border condition (FBC)[24,62]. These are not totally satisfactory. PBC could not be used at temperatures close to melting because the gb can migrate toward each other and mutually annihilate[62]. This undesirable effect could be avoided if the simulation cell along the direction perpendicular to the gb plane is sufficiently large. An adequate size for PBC could be impractical so FBC is sometimes used. However FBC could not relieve the stress induced by gb migration, sliding and expansion which in turn might effect the gb behavior.

In this work free border condition model is used. Since this model has only one gb interface, and its upper and lower crystals could move independently, it does not have the weaknesses associated with the PBC or FBC. However since it contains free surfaces,

surface effects need to be studied to ensure that gb behavior is not contaminated by their presence. To accomplish this goal, a reference model, identical to the bicrystal model but without the gb interface, has been constructed and the behavior of the surface has been studied extensively in previous chapter. Comparison of the free surface behavior of the reference and bicrystal models will give the effects and interactions of the free surfaces with the gb.

This chapter is organized as followed. The first section gives a summary of all the bicrystal simulation runs. Temperature and stress distributions are then examined to ensure that these runs are indeed having constant temperature and stress. The second section examines the surface behavior of the bicrystal model. This behavior is then compared with that of the reference model studied in chapter 4 to examine the surface effects on the gb interface of the bicrystal model. The third section is the main focus of this chapter. It examines the thermal disordering of the bicrystal model at temperatures in the vicinity of the melting temperature established earlier using the reference model. The fourth section evaluates the validity of the bicrystal results by examining different border conditions and potentials.

5.1 Summation of bicrystal simulation runs

The simulation runs for the bicrystal model is summarized in Table 5-I. The temperatures examined range from 400K to 925K as in the case of the reference model. The temperature range above melting (875K - 925K) is used to recheck the melting temperature. The temperature range just below the melting temperature (800K - 850K), the main focus of this work, is used to study the bicrystal behavior. The lowest temperature range (400K - 750K) is used mainly to gradually bring the bicrystal to high temperatures.

These simulation runs are under the conditions of constant temperature and stress. Temperature and stress distributions are then examined for all the runs at all temperatures to

Temp (K)	#time step	Total time (psec)	gb energy (eV/atom)	bulk energy (eV/atom)	Pressure (eV/a3)
400	10000	20.84	-3.458(5)	-3.525	-0.030(20)
500	10000	20.91	-3.442(5)	-3.510	-0.015(30)
600	10000	20.98	-3.426(5)	-3.493	-0.033(30)
700	10000	21.05	-3.407(5)	-3.476	-0.021(20)
750	25000	52.73	-3.397(5)	-3.467	-0.025(30)
800	37000	78.20	-3.387(7)	-3.457	-0.023(30)
825	158000	334.34	-3.380(10)	-3.453	-0.021(40)
850	223000	472.43	-3.370(10)	-3.448	-0.025(70)
875	42000	89.08	-3.365(10)	-3.442	-0.026(30)
900	23000	48.84	-3.360(10)	-3.435	-0.025(20)
925	20000	42.52	-3.350(10)	-3.425	-0.020(30)

Table 5-I: Bicrystal model simulation runs

a (4.05A) is the lattice constant of aluminum at room temperature (298K). Pressure unit (eV/a3) is equivalent to 24.1 kbar. The parentheses denote error bars. Ex: -3.458(5) means -3.458 ± 0.005.

ensure of these conditions. Shown in Fig. 5-1 are the temperature distributions of the bicrystal model at temperature 825K at time step 90000. One curve is averaged over 1000 time steps while the other is averaged over 20000 time steps for layers of approximately 30 atoms. The fluctuation in temperature is much smaller with longer time averaging, meaning that the averaged temperature distribution is uniform across the simulation cell. In these temperature distributions, the gb is in the middle of the simulation cell and the two free surfaces are at the ends. One sees that the different regions show no special effects in the temperature profile, as one would expect of a thermally equilibrated system.

The distribution of hydrostatic pressure and three shear components of the stress tensor, σ_{xy}, σ_{xz} and σ_{yz}, are shown in Figs. 5-2 through 5-5 respectively, at temperature 825K and time step 90000. Again, two curves are shown; one is averaged over 1000 time steps while the other is averaged over 20000 time steps. Similar behavior as the temperature distribution is found. The stress distributions are uniform across the simulation cell. 1000 time step averaging stress distributions fluctuate about 0.1 eV/a^3 (equivalent of 2.4 kbar) while the 20000 time step averaging stress distributions have a fluctuation of at least 10 times smaller.

We have just shown that the stress is uniform in the simulation cell at temperature 825K and time step 90000. The same procedure is repeated at other temperatures and time steps and the same behavior is found; the stress distribution is reasonably uniform in the simulation cell.

The system stress is then examined as function of time. Shown in Figs. 5-6 through 5-9 are the time variations of hydrostatic pressure and three shear components σ_{xy}, σ_{xz} and σ_{yz} of the stress tensor at temperature 825K. The data in these figures are averaged over 1000 time steps. The fluctuation in σ_{xy} is much less than in other two shear components σ_{xz} and σ_{yz} because of the periodic border condition along the x and y directions. Also the presence of the gb in the xy plane causes σ_{xz} and σ_{yz} to fluctuate highly because of the

tendency of the upper crystal to slide relative to the lower crystal. One sees fluctuations of the order of 0.005 eV/a^3 for σ_{xy} and about 0.02 eV/a^3 for σ_{xz} and σ_{yz}. The stress tensor behaves in a similar manner at other temperatures. Based on these simulation runs it can be said the system is under uniform temperature and stress distribution.

5.2 Surface behavior in the bicrystal model

A possible weakness of the bicrystal model is the two free surfaces at both ends of the simulation cell. These surfaces could influence the gb interface behavior if the system size is not large enough. Therefore the surface behavior of the bicrystal model has to be examined and compared with that of the reference model. A similarity between the behavior of these two models will show that the bicrystal model size is adequate so that the gb interface does not have any detectable effects on the free surfaces of the bicrystal model. Or using the principle of action - reaction, we could say that the free surface effects on the gb behavior is negligible.

In the low temperature range (400K - 750K), the surface structures are similar in both models. They are well ordered for the entire length of the simulation runs at these temperatures.

In the temperature range above melting (875K - 925K), the liquid region at the surfaces of the bicrystal model is steadily growing, a behavior that signifies melting and observed also in the reference model. The energy, structure and mobility of these liquid regions in the bicrystal model at these temperatures are calculated and found to agree with those of the reference model. One could also determine the melting temperature through the propagation of the liquid regions of the bicrystal model as done previously with the reference model. The plot of the propagation velocities at temperatures above T_m of the bicrystal model is shown in Fig. 5-10 together with those of the reference model. One sees that the values obtained from the bicrystal model and the reference model are very close

and within the error bar of each other. The fiited line is also approximately the same for the new set of data, so the melting temperature determined from the surface data of the bicrystal model is essentially the same as one determined from the reference model. In other words, the presence of the gb interface in the bicrystal model appears not to affect the behavior of the free surfaces at temperatures above T_m.

In the temperature range immediately below T_m (800K - 850K), the disordered region at the surface of the bicrystal model is also in metastable state as one could have expected from the results of chapter 4. Shown in Figs. 5-11 through 5-13 are the thickness of the disordered surface regions of the bicrystal model at temperatures 800K, 825K and 850K respectively. One sees the metastability of the surface regions as the thickness of the disordered region oscillates from small value (ordered surface) to large value (disordered surface). The magnitude of these thicknesses are also comparable to those of the reference model. Also, as in the case of the reference model, the energy, structure and mobility of the surface region in the bicrystal model are highly correlated. When the surface region becomes totally disordered, its energy and mobility also increase to approach those of a liquid, similar to the behavior of the surface region in the reference model. The time averaged thickness of the surface disordered regions of the bicrystal model is plotted as a function of temperature in Fig. 5-14 together with the data from the reference model. One sees similar results from these two models. Therefore the surface behavior in the bicrystal model is not significantly affected by the presence of the gb interface in the middle of the simulation cell.

5.3 Grain boundary behavior in the bicrystal model

It has just been shown that the simulation cell size is adequate based on the similarity of the surface behavior of the bicrystal model and the reference model. We are now ready to study the gb behavior. This section will examine the thermal disordering at the internal interface in the bicrystal model. In the next section we will evaluate the validity of these results through the use of different models and potential functions.

The behavior of the gb above the melting temperature is first examined. One could also calculate the melting temperature from this behavior.[65-66] Then the behavior of the gb at temperatures below T_m is examined in considerable detail. Beside the energy, structure and mobility, gb migration and sliding effects and the elastic response of the gb with respect to shear stress are also studied.

The gb region above T_m behaves as expected; the disordered region originating from the gb steadily grows. Its energy, structure and mobility also agree with those of a liquid. Fig. 5-15 shows the propagation of the liquid region originating from the gb in the bicrystal model together with those from the surfaces of the reference and bicrystal models. The propagation velocity of the gb region agree with that of the surface regions from both models (see Fig. 5-10). The melting temperature extracted from these data is about the same as that determined from the free surface behavior only.

Since the temperature 850K is too close to the melting temperature (this temperature falls within the uncertainty of the melting temperature), the temperature 825K is first chosen to study the time evolution of its gb energy, structure and mobility. Other temperatures will be examined later.

The potential energy and structure factor profiles of the system at 825K are shown in Figs. 5-16 and 5-17 respectively for different time steps, 30000, 60000 and 90000. The region of high energy and low structure factor value at the middle of the profiles is the gb

region. One sees close correlation between the energy and structure of the gb region as the gb migrates and broadens in time. From these profiles one can determine the potential energy of the gb region, defined as the potential energy in the full width at half maximum region of the potential energy profile. The gb thickness is also determined by the full width at half maximum of the structure factor profile. The gb thickness determined in this way is very close to that determined by the potential energy profile.

The gb energy and thickness at 825K, determined as above, are plotted as functions of time in Figs. 5-18 and 5-19 respectively. Again one sees the correlation between the energy and the thickness of the gb region in these two figures. The gb energy is high when the thickness is large. However, the gb thickness, defined using the full width at half maximum of the structure factor profile, does not specify whether the interfacial structure is disordered or not. One has to use the structure factor profiles at these time steps. Generally, they show that if the thickness is more than 3 layers, then it is disordered, while if the thickness is less than 2 layers, it is ordered. The gb structure also can be examined by looking at its configuration. Shown in Fig. 5-20 are the two configurations of the gb region at time steps 60000 and 90000. The atom positions in these figures are averaged over 1000 time steps. These two time steps are chosen because they represent two different states of the gb core region. At time step 60000 the gb has high energy value and large thickness, while at time step 90000 the gb energy is much lower and its thickness is much smaller. One sees that the gb region is very disordered at time step 60000, while at time step 90000 the gb structure is recognizable. Detail configurations of the gb region at these time steps are also shown in Fig. 5-21 through the atomic trajectory plot of atom positions accumulated for 500 time steps. These figures confirm the results in Fig. 5-20 showing at time step 60000 the gb is very much disordered while at time step 90000 it is very ordered and the gb structure is recognizable.

Fig. 5-22 shows the structures of the gb at time steps 60000 and 90000 for 10000

time steps accumulation. One sees large disordered region in the gb at time step 60000 while at time step 90000 the gb structure is still recognizable, though with some amount of disorder. The bulk atoms in these two time steps show local vibrations whereas the gb is seen to be mobile at this temperature. The mobility of the gb atoms is often accompanied by the coupled sliding and migration of the gb region as will be shown later.

The structure of the gb at these time steps is further illustrated by the radial distribution function g(r). One should keep in mind that even for a perfectly ordered gb, g(r) is quite different from the g(r) of the bulk crystal. Therefore g(r) for an ordered gb structure (i.e. low temperature) is needed to serve as a reference for high temperature gb structure study. Shown in Figs. 5-23 and 5-24 are the g(r) for the gb region at temperature 750K which is well ordered. The data in Fig. 5-23 are instantaneous and accumulated for 1000 time steps while the data in Fig. 5-24 are time averaged over 1000 time steps and accumulated for 20000 time steps. In the instantaneous g(r) of Fig. 5-23, one sees the flattening of the second peak in the g(r) distributions in the gb region and the third peak is not too broad as in the case of the g(r) of a liquid. However it is not easy to recognize this as a well ordered gb structure since it also resembles many features of the liquid g(r). The time averaged g(r) of Fig. 5-24 shows much sharper peaks in these distributions. One can tell much more readily the difference between an ordered gb and a liquid-like structure by considering the time averaged g(r) as shown in Fig. 5-24. Therefore the g(r) results at 825K shown below will be time averaged.

The radial distribution function g(r) at time steps 60000 and 90000 for 825K are shown in Figs. 5-25 and 5-26 respectively. As discussed above, these distributions are calculated over time averaged atom positions of 1000 time steps for 30000 time steps. One sees that there are a few layers in the gb region at time step 60000 (in Fig. 5-25) which are disordered, as their g(r) functions are very similar to that of a liquid, i.e. a broad third peak and no second peak. In contrast, all layers in the gb region at time step 90000 (in Fig. 5-26) are quite ordered, as their g(r) functions are very similar to that of as ordered gb structure.

The mobility of the gb region at these time steps is shown in Fig. 5-27. In this figure, two consecutive atom positions, each are averaged over 1000 time steps are connected. One sees large movements in the gb core at time step 60000 and much less movement at time step 90000. The MSD of the gb region at 825K is shown in Fig. 5-28 together with that at 850K. One sees high diffusive motion of the gb region. The diffusion coefficient extracted from this MSD curve is 2.1×10^{-5} cm^2/sec as compared with the value of 2.4×10^{-5} cm^2/sec of the surface region at the same temperature from the reference model.

The above behavior of the gb region at 825K suggests that it is in a metastable state as in the case of the surface region at the same temperature studied earlier in the reference model. The gb region is sometimes liquid-like, i.e. having high energy, disordered structure, and sometimes solid-like, i.e. low energy, ordered structure. The atoms in the gb region is very mobile even when the gb is well ordered because the atoms could move in the gb region by jumping from one lattice position to another.

At temperature 800K and below, the gb region is always ordered for the entire length of the simulation runs at those temperatures. Shown in Fig. 5-29 is the gb thickness at 800K. The thickness shows no changes for the entire length of the simulation run. Fig. 5-30 shows the gb configuration at 800K at time step 20000. The atom positions in this figure is averaged over 1000 time steps. One sees a well ordered gb structure. The gb configuration at 800K is similar to this configuration at all times. Fig. 5-31 shows the trajectory plot of 800K at time step 20000 for 500 time steps. One could easily recognize the gb structure in this figure. However even though the gb structure is well defined and ordered at all times at this temperature, the gb is still very mobile. One already sees this behavior in Fig. 5-31 through the movement of the gb core atoms. Atoms could jump from one lattice position to another at this temperature as shown in Fig. 5-32. In Fig. 5-32 two consecutive atom positions, each averaged over 1000 time steps, are connected to show the movement of atoms.

Gb migration is also important. One already sees the gb migration through the potential energy and structure factor profiles earlier at temperature 825K. At 800K the gb migrates through a series of coupled sliding and migration mechanism.[80] Shown in Fig. 5-33 are two atomic trajectory plots of the gb core at temperature 800K separated by 1500 time steps. The atomic trajectories are accumulated over 500 time steps. One can see the migration of the gb through the coupled sliding and migration as shown in Bishop et al.[80]

The gb structure at 850K is much more disordered than the one at 825K. Shown in Fig. 5-34 is the gb thickness at 850K as a function of time. One observes a sudden jump in the gb thickness to a much higher value at time step 60000. However, the gb structure is apparently stable at the new thickness as it does not change for the next 130000 time steps. Gb migration causes the gb to drift toward one surface, and then interact with it at time step 220000. At this temperature, the bulk region is considerably reduced by the enlargement of the gb region, together with the two disordered surface regions which are also enlarged. The possibility that now gb behavior may be influenced by the free surfaces means that our simulation cell is not large enough for the continued simulation out to longer times.

Based on the behavior of the gb at these temperatures, we conclude that the gb region shows no sign of complete melting at temperatures below T_m.

The behavior of the gb as a function of temperature is studied next. One can see that the gb is in metastable states at 825K through a series of changing states, from ordered to disordered and vice versa. Therefore the gb behavior and properties presented below will be time averaged. Fig. 5-35 shows the potential energies of the gb region together with the solid and liquid branches of the potential energy curve. The potential energies seem to change continuously from its low energy value at 700K to the liquid value at 875K. Fig. 5-36 shows the gb thickness as a function of temperature. One has seen similar behavior earlier at the surface of the reference model. The thickness increases rapidly but continously as the temperature reaches the melting temperature. Fig. 5-37 shows the

diffusion coefficient of the gb region together with those of the surface region from the reference model.

Further behavior of the gb region is studied through its response to an externally applied shear stress. Shear stress is chosen because it would give a pronounced difference in the gb behavior since a liquid cannot support shear stress. Since the gb at high temperatures is in a metastable state and therefore sometimes becomes liquid-like, the upper and lower crystals of the gb under the influence of an externally applied shear stress will be sheared off and in constant motion along the direction of the apllied shear stress.

A summary of the runs designed to study the elastic response of the bicrystal model at high temperatures is presented in Table 5-II. A force along the y direction is applied to a few layers of atoms near the surface region. The stress tensor is therefore having non zero component only in σ_{zy}.

The reference model is first used to calculate the shear modulus of the model. Three runs are made at temperature 750K at different stress values (0.015, 0.030, 0.060 eV/a3). The stress strain curve for this model follow a straight line as shown in Fig. 5-38 where the shear modulus is extracted to be 6.53×10^{10} dynes/cm^2 as compared with the experimental value of 28.2×10^{10} dynes/cm^2 at room temperature (300K). The difference in temperatures (750K for the bicrystal model and 300K for the experimental data) could account for the discrepancy in these two values of the shear modulus since shear modulus decreases rapidly with increasing temperature. Also shown in Fig. 5-38 are the two data points for the elastic response of the gb system at 600K and 750K. From these two data points one could estimate the shear modulus for the gb system at 600K and 750K to be 9.1×10^{10} dynes/cm^2 and 4.3×10^{10} dynes/cm^2 respectively. This is a very rough estimate since there is only one data point for each temperature. One sees a factor of about 1.6 decrease in shear modulus from single crystal to bicrystal at 750K. One also see a factor of 2 increase in shear modulus from 750K to 600K in the bicrystal model. This confirms the suggestion earlier that shear modulus decreases rapidly with increasing temperature.

Temp (K)	#time step	Model	σ_{zy} (eV/a3)	Strain
750	10000	reference	0.015	0.0061
750	10000	reference	0.030	0.0110
750	9000	reference	0.060	0.0220
600	13000	bicrystal	0.015	0.0041
750	20000	bicrystal	0.015	0.0086
750	7000	bicrystal	0.030	*
750	13000	bicrystal	0.060	*
800	16000	bicrystal	0.006	*
800	17000	bicrystal	0.015	*
800	20000	bicrystal	0.030	*
825	20000	bicrystal	0.006	*
825	29000	bicrystal	0.015	*

Table 5-II: Summary of simulation runs of bicrystal model with externally applied shear stress

a (4.05A) is the lattice constant of Al at room temperature (298K). Pressure unit (eV/a3) is equivalent to 24.1 kbar.

* The applied shear stress is larger than critical stress, so the bicrystal is sheared off.

Besides these runs with stable configuration, i.e. finite shear strain for the applied shear stress, there are some runs in which the system fails, i.e. the upper and lower crystals shear off and move at constant velocity in opposite directions. A gb configuration for this case is shown in Fig. 5-39 for the temperature 800K and shear stress 0.015 eV/a^3. From this motion, one could extract the relative velocity of the upper crystal with respect to the lower one. A plot of such velocity vs the applied shear stress for different temperatures (750K, 800K and 825K) is shown in Fig. 5-40. A rough estimate for the critical shear stress, defined as the stress at which the system fails, is the stress where the sliding velocity vanishes. Fig. 5-40 uses linear fit through the data points to estimate the critical shear stress, using the criterion just described. The results suggest that at 825K even a very small applied shear stress could shear off the bicrystal since the extrapolation of the sliding velocity for this temperature intersects the velocity axis. This suggests that the bicrystal totally loses its shear resistance, or equivalently being in liquid state, at about 825K. This result has only qualitative significance since we have not considered system size (gb area) dependence and the effects of the applied stress on the behavior of the gb. We do not know if the system is still in metastable state or has become liquid-like at 825K under the influence of the externally applied shear stress.

5.4 Validity of the bicrystal model results

The thermal disordering of the free border bicrystal model has just been examined. The results show that below the melting temperature, there is a small temperature range ($0.95\ T_m$ - T_m) where the gb region exhibits metastability. The thickness of the disordered region increases rapidly and continuously as the temperature reaches the melting temperature. This is the behavior of the gb using the free border bicrystal model. To evaluate the validity of these results, i.e. to see if these results are general or just for a particular model, different models are constructed and the gb behavior is then studied again

with the new models. The main purpose of this section is to see whether or not the thermal disordering behavior of the gb just seen in previous section depends on the model used.

As discussed in chapter 2, the two basic features of the bicrystal model are border conditions and potential function. We will study next the behavior of the gb behavior using models with two different border conditions (fixed border and semiperiodic border) and a different potential function (empirical Morse potential).

As will be seen below different models gives essentially the same behavior as the bicrystal model with free border.

5.4.1 Model with fixed border condition

This is the simplest bicrystal model beside the periodic border model which cannot be used at temperatures close to melting. The fixed border model has been described in the section regarding border conditions for the bicrystal model in chapter 2, so only a brief description of the model is presented here.

This fixed border bicrystal model is composed of 1920 atoms in the same configuration as the free border model. Everything is the same as in the free border bicrystal model except the free borders. Instead of having free borders at the two ends of the simulation cell, the fixed border model is embedded in fixed atoms arranged in the perfect crystal configuration. The main weakness of the fixed border model is that the fixed border does not allow the expansion of the gb region or the translation of the upper and lower crystals. Lacking the capability to expand could raise the system pressure, thus changing the condition under which the bicrystal is studied (constant temperature and constant stress). Lacking the capability to allow the upper and lower crystals to slide could raise the shear stress, or at least the fluctuation in shear stress, thus leading to storing of excess energy which could result in the disorder of the gb region[3,66]. Thus the stress tensor in the fixed border model is important and needs constant monitoring.

The summary of the simulation runs using the fixed border condition is presented in Table 5-III. All the run conditions in this series are exactly the same as in the free border model, e.g. same potential function, same thermal expansion coefficients, etc. The first check of the simulation results is the temperature distribution. Shown in Fig. 5-41 is the temperature profiles of the run at 825K. Two temperature profiles are shown in this figure. One is time averaged over 1000 time steps starting from time step 64000. The other is time averaged over 20000 time steps starting at time step 64000. One sees a much more uniform distribution of temperature with longer time averaging.

From the data in table 5-III, one sees that the pressure gradually increases at high temperatures and have much higher pressure at temperature 850K. The pressure at 875K is still increasing at the end of the simulation run (30000 time steps). From this data, one could divide the simulation runs in this series into two groups, cutoff at temperature between 825K and 850K. The low temperature group (825K and below) can be considered to be at constant pressure and therefore adequate for data analysis. However one should remember that the pressure at the high end of this temperature range is still slightly increasing. The high temperature group (850K and above) has much higher pressure and therefore are not in the same phase diagram as the other group.

This division is further re-enforced by examining the time variation of the system pressure shown in Figs. 5-42 through 5-45 for the temperatures 800K, 825K, 850K and 875K respectively. The system at 825K has higher fluctuation in the pressure value than the one at 800K and therefore should be regarded as marginally qualified for the constant pressure group. The pressure at 850K fluctuates much more and can be considered as not oscillating around the averaged value since it stays at the high value for some time and then changes to low value. The pressure value at 875K can be regarded as steadily increasing, though the short simulation time makes it difficult to be decisive. Compare with the free border bicrystal model, the behavior at 850K and 875K is consistent because gb expansion is significant at those temperatures.

Temp (K)	#time step	gb energy (eV/atom)	bulk energy (eV/atom)	Pressure (eV/a3)
400	5000	-3.455(5)	-3.525	-0.051(10)
500	5000	-3.442(5)	-3.509	-0.064(10)
600	5000	-3.424(5)	-3.493	-0.052(10)
700	5000	-3.405(5)	-3.475	-0.035(10)
750	70000	-3.397(5)	-3.466	-0.037(20)
800	79000	-3.387(5)	-3.457	-0.032(15)
825	84000	-3.382(7)	-3.452	-0.028(15)
850	70000	-3.374(7)	-3.448	-0.010(40)
875	30000	-3.373(7)	-3.442	0.010*

Table 5-III: Fixed border model simulation runs

a (4.05A) is the lattice constant of aluminum at room temperature (298K). Pressure unit (eV/a3) is equivalent to 24.1 kbar. The parentheses denote error bars. Ex: -3.455(5) means -3.455 ± 0.005.

Spatial distributions of the pressure and the three off diagonal components of the stress tensor σ_{xy}, σ_{xz}, and σ_{yz}, are shown in Figs. 5-46 through 5-49 respectively. The data shown are for the system at 825K at time step 64000 for 1000 time steps averaging and at time step 64000 for 20000 time steps averaging. One sees a much more uniform distribution of the stress tensor with longer time averaging. The magnitudes of the fluctuations of the stress distributions are about the same as in the case of the free border bicrystal model shown in Figs. 5-11 through 5-14. Time variation of the three off diagonal components of the stress tensor σ_{xy}, σ_{xz}, and σ_{yz}, are shown in Figs. 5-50 through 5-52 respectively. The data in these figures are averaged over 1000 time steps. Again the magnitudes of the fluctuations of these stress components are compatible with those of the free border model shown in Figs. 5-16 through 5-18.

Given the similarity of the time variation and spatial variation of the shear stress in the free border and fixed border bicrystal models, it appears that the effect of the fixed border in constraining the gb migration and sliding is not serious. This behavior, if true, would not be consistent with the suggestion of Pontikis et al.[3] that the constraint due to the fixed border could cause high fluctuation in the shear stress, thus leading to gb disorder at low temperatures. Also similar to the behavior from the free border model, gb migration is occurring at all temperatures in the fixed border model. Theoretically, in the free border model, gb can migrate toward the end of the simulation cell while in the fixed border model it is confined in the middle of the cell. However the simulation cells chosen for this work for both the free and fixed border models are sufficiently large so that for the length of the simulation runs, gb migration effects are similar in both models in all temperatures below 850K. At 750K (0.87 T_m) the gb migrates for about 2 lattice constants in 15000 time steps. Time averaged position and time averaged structure factor show well ordered gb structure at all times. This behavior can be compared with that observed by Lutsko et al.[66] who used the instantaneous structure factor values to show that 3d periodic border condition would

inhibit the gb migration process, thus leading to a disordered gb structure at low temperature (0.75 T_m). The comparison suggests that the inhibition is system-size dependent; in a large system (1920 atoms in the present study as compared with 928 atoms for 3d periodic model of Lustko et al., or roughly 464 (928/2) atoms for each gb structure) the inhibition effect for gb migration is minimized.

The energies of the bulk and gb regions of the fixed border model shown in Table 5-III are very similar to those of the free border model shown in Table 5-I. The only noticeable difference is the low energy value of the gb in the fixed border model at 875K. At 825K and 850K, the energy values for the gb region of the fixed border model are also slightly lower than those of the free border model, but in the fixed border model the energy value at 875K is very close to that at 850K. This effect is a consequence of the pressure increase in the model.

The structure of the gb region of the fixed border model is very similar to that of the free border model. Shown in Figs. 5-53 and 5-54 are the gb thickness as function of time for the system at temperatures 800K and 825K respectively. Comparing the gb thickness at this temperature of the fixed border model with that of the free border model shown in Fig. 5-29 at the same temperature, one sees similar behavior. The gb thickness in both models oscillates between 1 and 3 layers. Detailed analysis of the gb structure of the fixed border model shows that it is well ordered at all times as in the case of the free border model. At 825K, the gb region of the fixed border model is also in a metastable state. Its thickness changes from 1-2 layers (meaning well ordered gb structure) to 4-5 layers (disordered structure) and then returns to 1-2 layers, a similar behavior as in the free border model at the same temperature shown in Fig. 5-33.

In summary the gb behaviors of the two models, fixed border and free border, are very similar in the temperature range where the simulation cell of the fixed border is large enough to accommodate the expansion of the gb region. The adequacy of the system size at

high temperatures can be determined by having similar pressure value as the system at low temperatures.

5.4.2 Model with semiperiodic border condition

The semiperiodic border bicrystal model described in chapter 2 is also examined to study the effects of the border conditions on the thermal disorder behavior of the gb interface. The semiperiodic border bicrystal model is also composed of 1920 atoms arranged in exactly the same way as in the free border model. Simulation conditions are also the same as in the case of the free border bicrystal model.

Simulation runs using semiperiodic border bicrystal model are summarized in Table 5-IV. To evaluate this model, temperature and stress profiles are examined. Shown in Fig. 5-55 is the temperature distributions of the system at temperature 825K. One curve in this figure is time averaged over 1000 time steps starting at time step 35000. The other curves is averaged over 20000 time steps also starting at time step 35000. One sees high fluctuation even in the long time averaged values as compared with either the free border or fixed border models. These temperature profiles give a low temperature value at the gb region, thus its effect on the gb behavior could be serious, e.g. the bulk and the gb regions are not at the same temperature, thus leading to the possibility of over stabilization of the gb interface.

The pressure and the three off diagonal components of the stress tensor are shown in Figs. 5-56 through 5-59 respectively for the system at the same temperature and time step. The pressure distributions give the gb region a lower pressure value than in the bulk region even in the long time averaged values. The shear components of the stress tensor behave as expected; uniform distribution along the simulation cell.

Another problem of the semiperiodic border model is that it gives different pressure values than other models, even though they are all runs at identical conditions. The free

Temp (K)	#time step	gb energy (eV/atom)	bulk energy (eV/atom)	Pressure (eV/a3)
400	5000	-3.456(5)	-3.525	0.010(30)
500	5000	-3.443(5)	-3.510	0.040(30)
600	5000	-3.430(5)	-3.494	0.031(30)
700	5000	-3.410(5)	-3.477	0.026(30)
750	5000	-3.402(5)	-3.468	0.042(30)
800	10000	-3.394(5)	-3.458	0.037(30)
825	57000	-3.389(7)	-3.452	0.025(40)
850	110000	-3.383(7)	-3.448	0.035(50)
875	149000	-3.378(8)	-3.442	0.025(60)
900	83000	-3.368(6)	-3.436	0.026(60)
925	37000	-3.367(7)	-3.430	0.034(60)

Table 5-IV: Semiperiodic border model simulation runs

a (4.05A) is the lattice constant of aluminum at room temperature (298K). Pressure unit (eV/a3) is equivalent to 24.1 kbar. The parentheses denote error bars. Ex: -3.456(5) means -3.456 ± 0.005.

border reference and bicrystal models have the averaged pressure value for all temperature runs at about -0.025 eV/a^3 while the fixed border model has the the value of about -0.035 eV/a^3. The pressure value from the semiperiodic border condition of 0.03 eV/a^3 is much different. It even has the opposite sign. This rise in pressure value is definitely an effect of the semiperiodic border condition. Since the pressure is different in the semiperiodic border bicrystal model, direct comparison is not possible. We have to examine the results of this model by themselves and then compare the general behavior.

We first determine the melting temperature. In this model, the gb region is still stable at 875K. It starts to grow at temperature 900K and 925K. Similar analysis to calculate the melting temperature as discussed in chapter 4 shows a melting temperature of (885 ± 15)K as shown in Fig. 5-60. Since the pressure in this model is higher than other models, it is reasonable that it also has a higher melting temperature.

The gb behavior is examined through the variation of the gb thickness with time at temperatures 825K, 850K and 875K as shown in Figs. 5-61 through 5-63 respectively. One sees little variation of the gb thickness at 825K. At 850K and 875K, the gb thickness varies much more, from 2 layers at 850K to 4 layers at 875K. Detailed examination of the gb structures at these temperatures shows that the gb structure at 825K is well ordered all the time and the gb structures at 850K and 875K are in metastable states. Time averaged thickness of the gb region also grows rapidly and continuously as the temperature approaches the melting temperature as shown in Fig. 5-64, a similar behavior as in other models.

Even though the semiperiodic border bicrystal model does generate some questions regarding the uniformity of the temperature and pressure distribution in the simulation cell, its behavior is still similar to that of other models but with T_m is shifted a to higher value. In other words, the thermal disorder behavior of the gb region at high temperature is independent of the bicrystal model used.

5.4.3 Model with Morse potential function

It has been shown that the results of the free border bicrystal model described earlier are independent of the border conditions used. In this section we will examine the bicrystal with different potential functions to see what behavior is also potential independent. Empirical Morse potential function for aluminum with parameters chosen to fit the vacancy formation energy[38] and fixed border bicrystal model are used because of previous works[23,24]. The potential function cutoff is taken to be 1.49 a_0 where a_0 is the lattice constant at T=0K (4.03 A). A shift in the energy and force in the form of equation (2.2) at the cutoff distance is introduced to eliminate the unphysical discontinuity associated with a truncated potential function.

Simulations are first carried out on a single crystal system to study bulk aluminum behavior using Morse potential. Same procedures as in the case of the EAM potential described in chapter 3 for single crystal runs are used. The results are summarized in Table 5-V. The transition temperature for the perfect bulk material for this model is about 950K. As discussed in previous chapter, this temperature is higher than the true thermodynamic melting temperature T_m. This temperature of 950K is the same as in the EAM potential function model, but the cohesive energy of this Morse potential is much smaller (-0.7 eV/atom) as compared with either EAM potential (-3.55 eV/atom) or experimental value (-3.58 eV/atom). This is due to the fact that this Morse potential function is fitted to the vacancy formation energy, not sublimation energy.

Two bicrystal models, differing in number of atoms and system size, are studied in this work. The first model, called model A, is composed of 840 atoms with 2 and 14 CSL units in the x and z directions respectively, and a y dimension of 3 lattice constants. The second model, called model B, is composed of 2520 atoms with the same x and y dimensions but the z dimension is 3 times larger. These two models are constructed similar to the fixed border model of earlier section with the exception of the length in the z direction; model A is shorter and model B is longer than the fixed border model.

Temp (K)	#time step	gb energy (eV/atom)	bulk energy (eV/atom)	Pressure (eV/a3)
500	15000	-.579(10)	-.661(5)	-5.4(3)
600	15000	-.563(10)	-.644(5)	-6.1(3)
700	111000	-.541(10)	-.626(5)	-6.0(9)
800	119000	-.510(10)	-.606(5)	-4.4(12)
825	76000	-.500(10)	-.603(5)	-2.0(20)
850	302000	-.496(09)	-.597(4)	-0.2(20)
875	86000	-.492(08)	-.596(4)	3.6(30)
900	96000	-.492(07)	-.594(5)	9.0(40)
925	105000	-.490(08)	-.588(4)	12.0(50)
950	81000	-.494(09)	-.587(5)	

Table 5-V: Morse potential single crystal simulation runs

a (4.03A) is the lattice constant of aluminum at T=0K. Pressure unit (eV/a3) is equivalent to 24.1 kbar. The parentheses denote error bars. Ex: -.579(10) means -.579 ± 0.010.

Summary of the simulation runs using these two models are shown in Table 5-VI and 5-VII respectively together with their various properties.

The pressure values will give us the indication of the adequacy of the simulation size. From the single crystal pressure in Table 5-V, the pressure values from -7.8 to -4.6 kbar are acceptable. From the pressure data in Table 5-VI, one can see that for model A, the system size is only adequate for the temperature range of 700K and lower. The runs at 800K is marginally acceptable since its pressure is slightly out of this acceptable pressure range. From the pressure data of Table 5-VII, the runs for model B are good for temperatures of 825K and below. The runs at 850K is probably not good because of the high pressure value.

Since we did not determine the melting temperature correctly using the criterion of zero propagation velocity of the liquid region initiated from the interface, we will have to estimate the melting temperature based on the pressure behavior.

The high value of the pressure signifies that the system size is not large enough to accommodate the expansion of the gb region. However if the temperature of the system is above the melting temperature, no system size is adequate because the gb region will steadily grow. This growth will stop when the pressure built up in the bulk region will act as a barrier to prevent further gb expansion. Therefore the pressure and gb thickness at temperature above melting will steadily grow and then level off. This behavior is shown in Fig. 5-65 for the model B at 875K.

This behavior is different from the behavior of the system at temperature below T_m which shows that the simulation cell is not large enough. Below T_m, the gb region does not have the driving force to continually expand, thus the pressure built up in the bulk region will cause the gb region to shrink, and then it will expand again. Thus the pressure and the gb thickness will oscillate in phase. This behavior is shown in Fig. 5-66 for the model A at temperature 825K.

Temp (K)	#time step	gb energy (eV/atom)	bulk energy (eV/atom)	Pressure (eV/a3)
500	15000	-.579(10)	-.661(5)	-5.4(3)
600	15000	-.563(10)	-.644(5)	-6.1(3)
700	111000	-.541(10)	-.626(5)	-6.0(9)
800	119000	-.510(10)	-.606(5)	-4.4(12)
825	76000	-.500(10)	-.603(5)	-2.0(20)
850	302000	-.496(09)	-.597(4)	-0.2(20)
875	86000	-.492(08)	-.596(4)	3.6(30)
900	96000	-.492(07)	-.594(5)	9.0(40)
925	105000	-.490(08)	-.588(4)	12.0(50)
950	81000	-.494(09)	-.587(5)	

Table 5-VI: Morse potential model A simulation runs

a (4.03A) is the lattice constant of aluminum at T=0K. Pressure unit (eV/a3) is equivalent to 24.1 kbar. The parentheses denote error bars. Ex: -.579(10) means -.579 ± 0.010.

Temp (K)	#time step	gb energy (eV/atom)	bulk energy (eV/atom)	Pressure (eV/a3)
500	12000	-.582(10)	-.661(5)	-4.9(2)
600	25000	-.564(10)	-.644(5)	-5.8(3)
700	21000	-.539(10)	-.626(5)	-6.4(3)
800	29000	-.504(10)	-.605(5)	-6.6(3)
825	40000	-.496(10)	-.600(5)	-4.6(5)
850	51000	-.489(09)	-.595(4)	-4.0(5)
875	125000	-.486(08)	-.592(4)	0.1(7)
900	90000	-.483(07)	-.591(5)	4.0(10)
925	96000	-.479(08)	-.586(4)	8.0(10)

Table 5-VII: Morse potential model B simulation runs

a (4.03A) is the lattice constant of aluminum at T=0K. Pressure unit (eV/a3) is equivalent to 24.1 kbar. The parentheses denote error bars. Ex: -.582(10) means -.582 ± 0.010.

Based on this behavior, one could say that the temperature 875K is above the melting temperature. Similar behavior of the pressure and gb thickness is also found at temperature 850K for the model B as shown in Fig. 5-67 but with a much smaller pressure increased. The pressure behavior at the temperature 825K is much more uniform. Therefore the melting temperature is determined to be 850K for this model.

The gb thickness for the system at temperatures 800K and 825K are shown in Fig. 5-68 and 5-69 respectively. One sees similar behavior in these time variations of the gb thickness as in other models: the thickness changes from high value to low value, signified the metastable state of the gb region. The averaged potential energies and thicknesses of the gb region as function of temperature are shown in Fig. 5-70 and 5-71 respectively. One sees a gradual change in the gb energy in the vicinity of the melting temperature and a rapid but apparently continuous change in gb thickness at the temperature approaches the melting temperature. This behavior is the same as in other models.

Different models with different border condition and potential function have been used to study the thermal disorder behavior of the bicrystal. The results from all models are very similar. They show that at temperatures close to the melting temperature, the gb region becomes metastable. This temperature range is approximately above 0.95 T_m. Below this temperature range, the gb region is well ordered at all times even though there is still high mobility in the gb region.

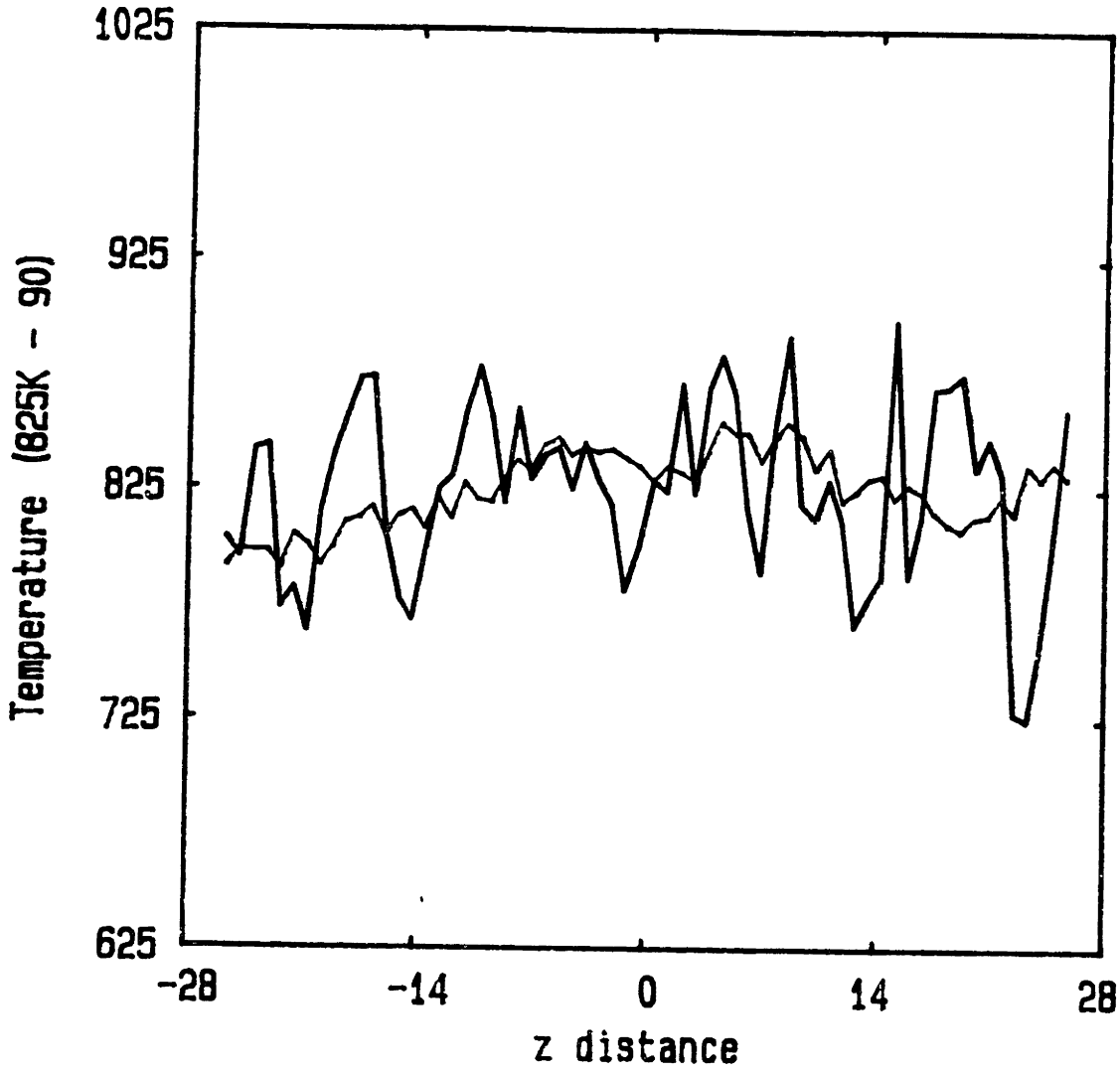

Figure 5-1: Temperature distributions in the bicrystal model

Two temperature distributions (one is averaged over 1000 time steps, the other 20000 time steps) are shown for the bicrytal model at 825K and time step 90000.

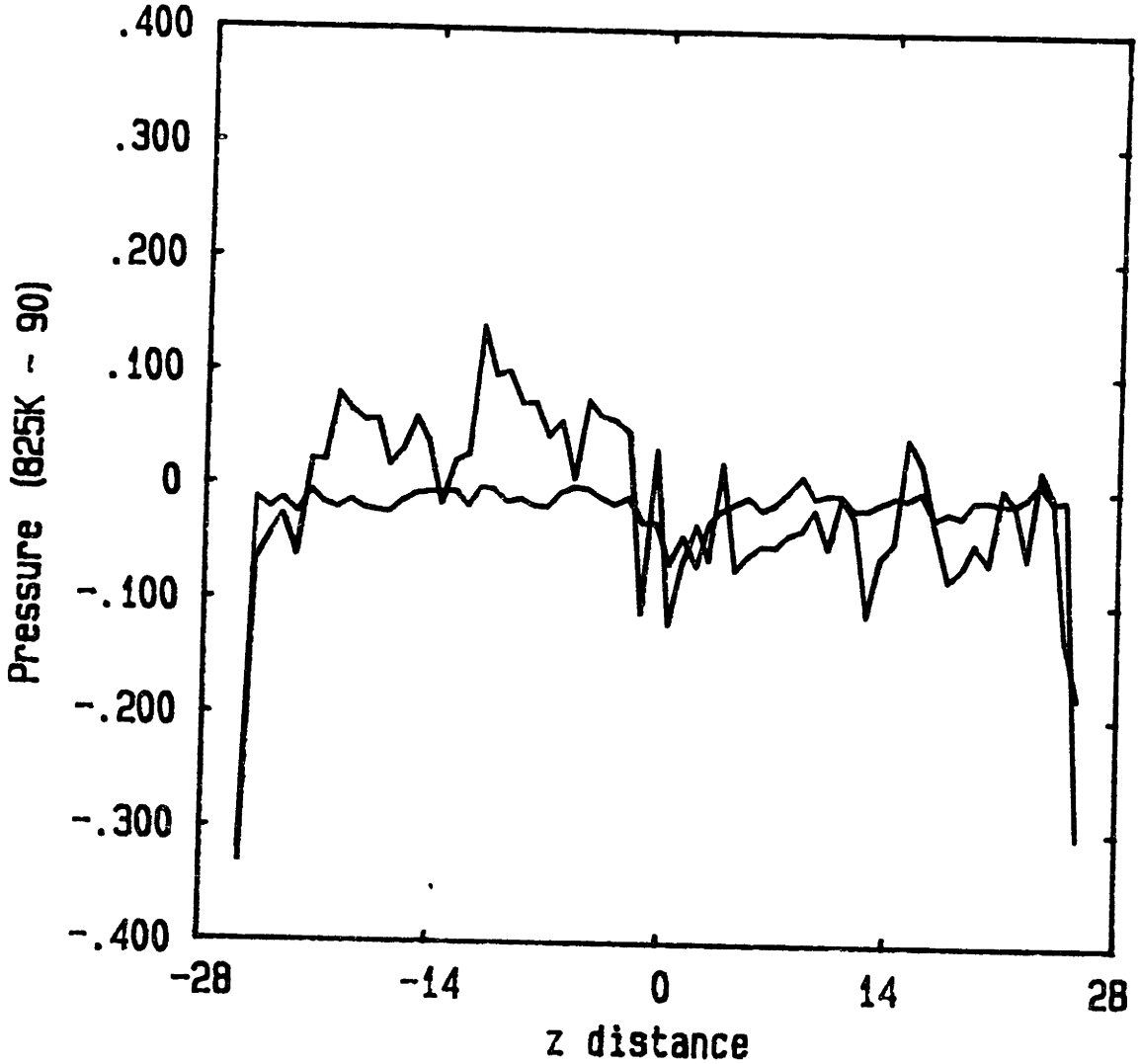

Figure 5-2: Pressure distributions in the bicrystal model

Pressure distri' 'tions are shown for the bicrytal model at 825K and time step 90000. The curve with high fluctuation is averaged over 1000 time steps. The smoother curve is averaged over 20000 time steps.

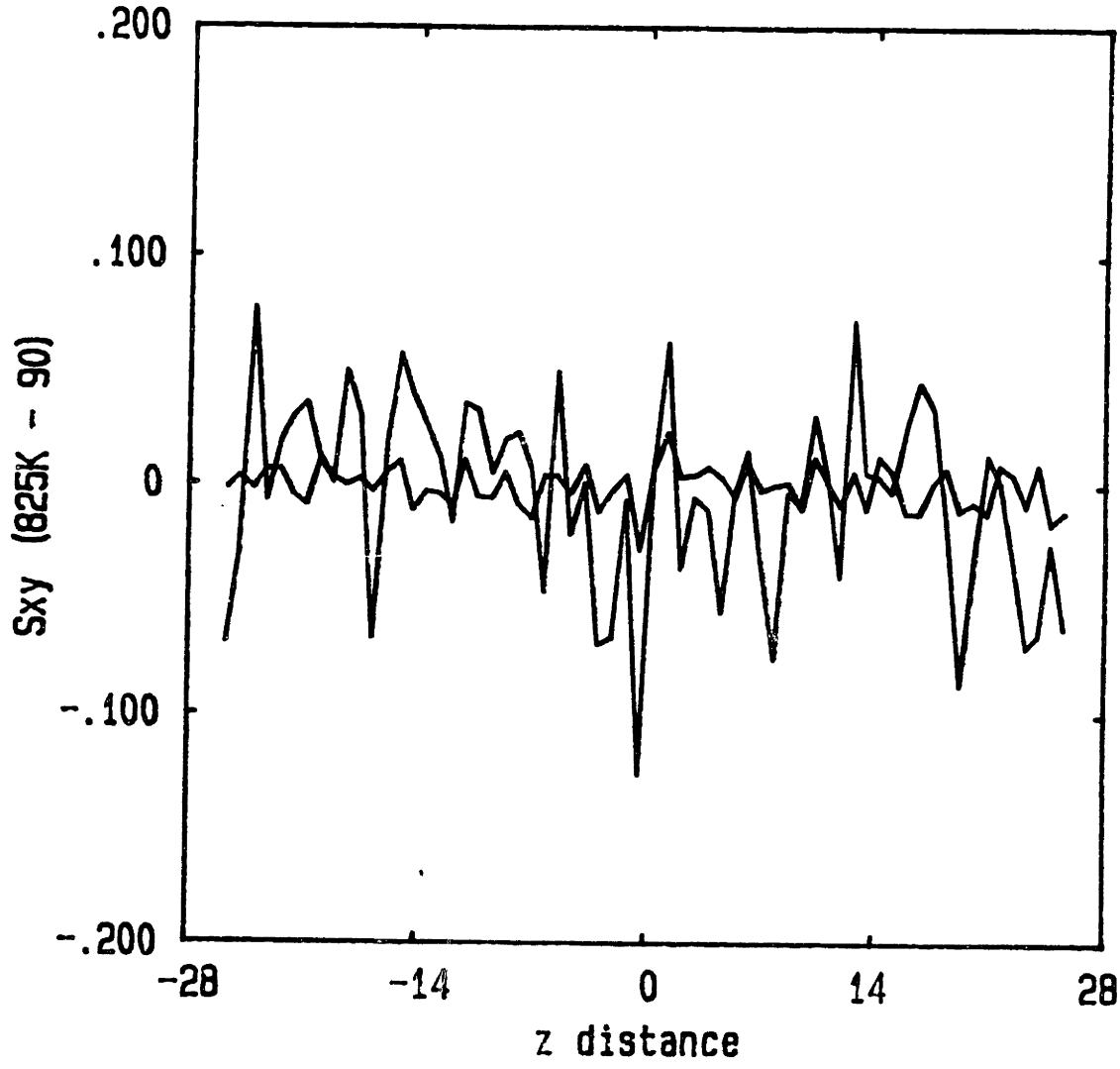

Figure 5-3: σ_{xy} distributions in the bicrystal model

σ_{xy} distributions are shown for the bicrytal model at 825K ar d time step 90000. The curve with high fluctuation is averaged over 1000 time steps. The smoother curve is averaged over 20000 time steps.

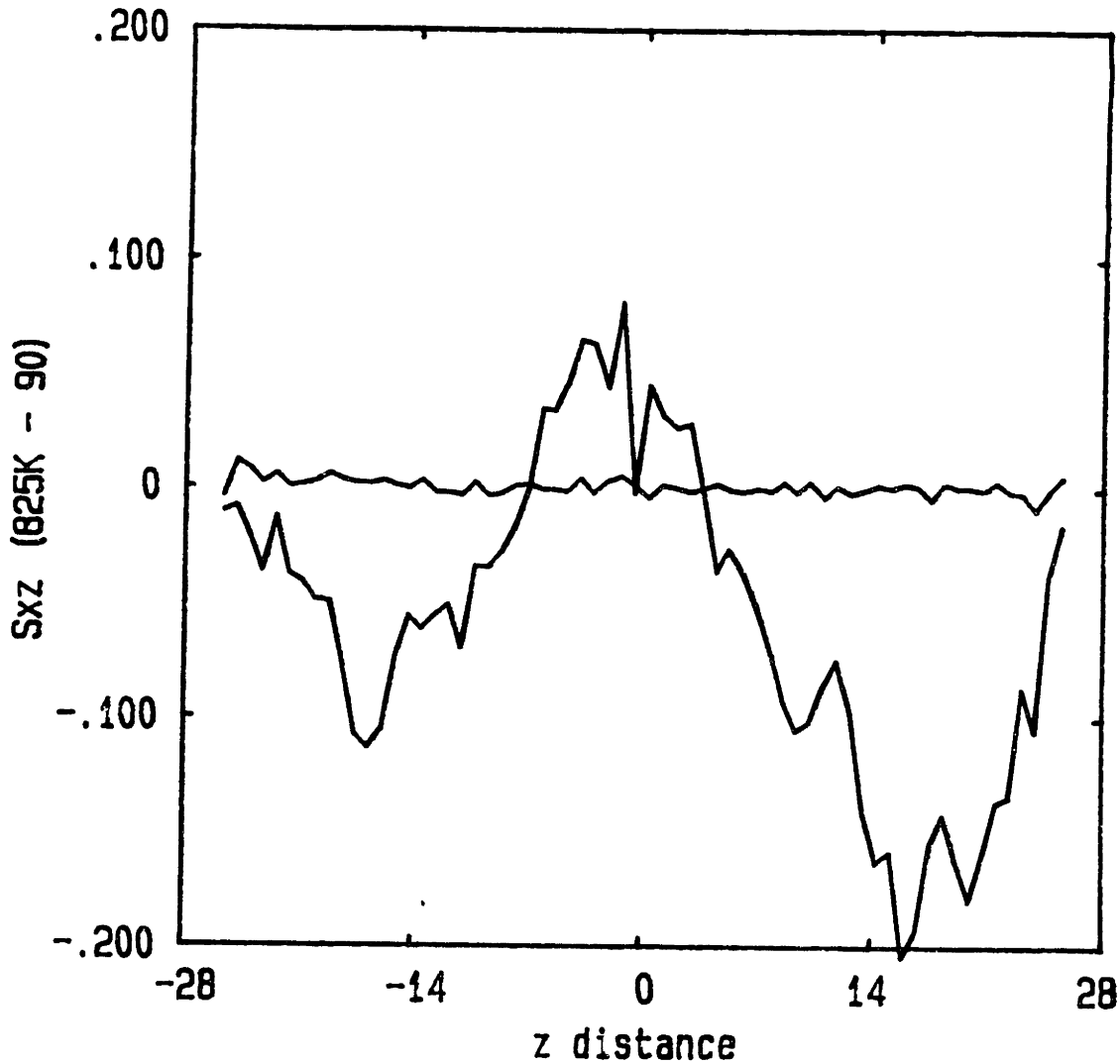

Figure 5-4: σ_{xz} distributions in the bicrystal model

σ_{xz} distributions are shown for the bicrytal model at 825K and time step 90000. The curve with high fluctuation is averaged over 1000 time steps. The smoother curve is averaged over 20000 time steps.

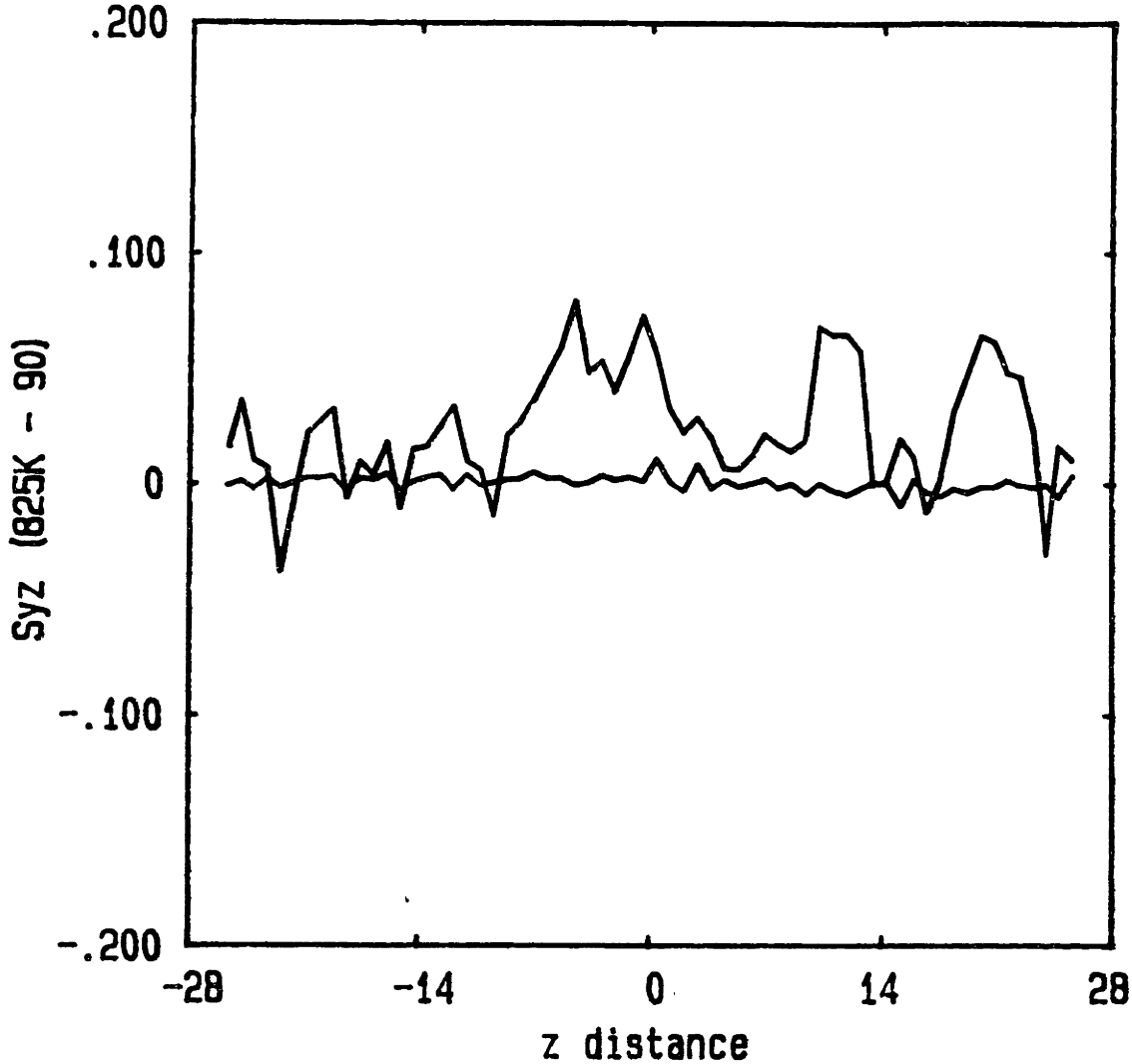

Figure 5-5: σ_{yz} distributions in the bicrystal model

σ_{yz} distributions are shown for the bicrytal model at 825K ınd time step 90000. The curve with high fluctuation is averaged over 1000 time steps. The smoother curve is averaged over 20000 time steps.

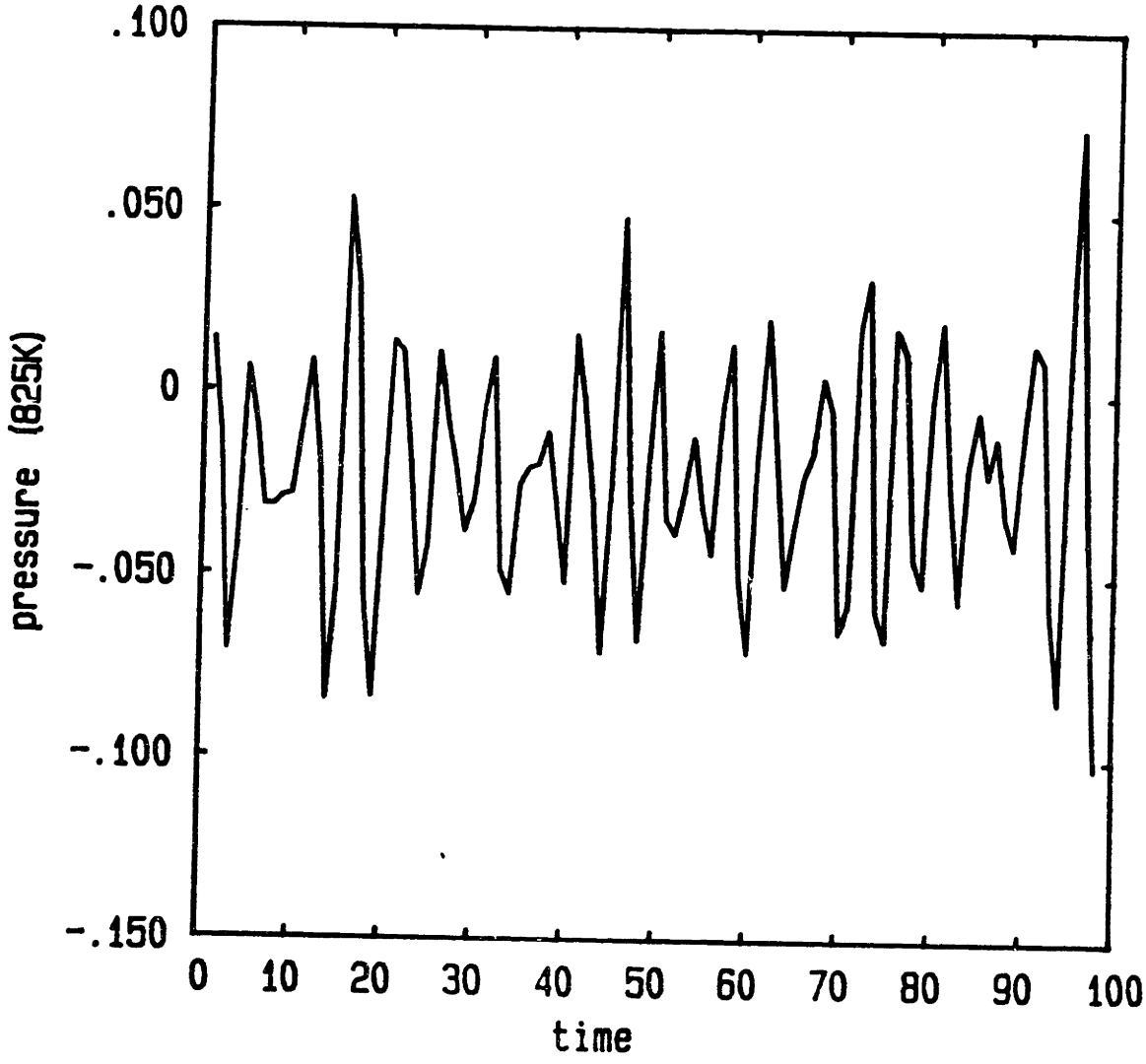

Figure 5-6: Pressure vs time in the bicrystal model

Time variation of the system pressure at temperature 825K.

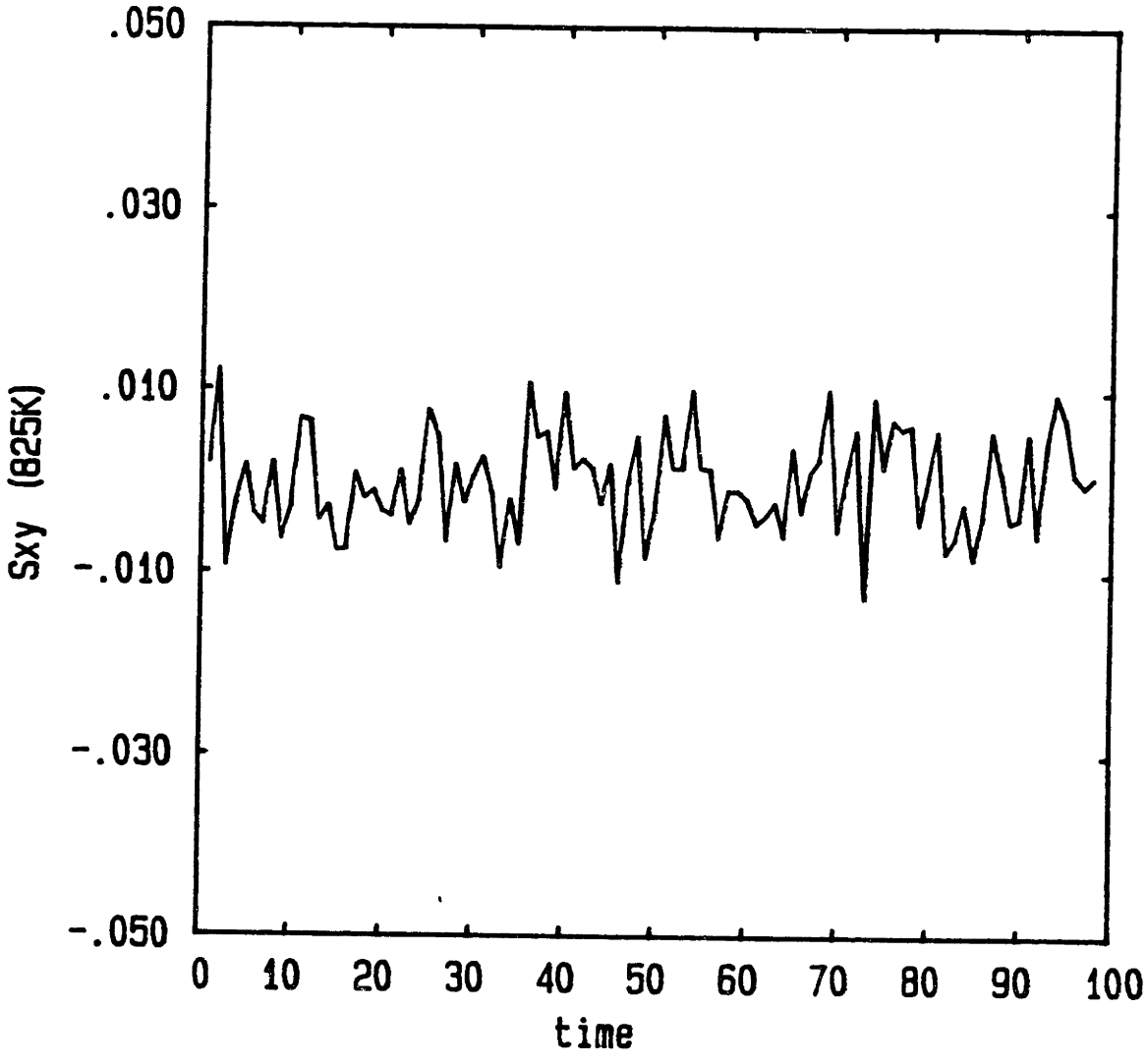

Figure 5-7: σ_{xy} vs time in the bicrystal model

Time variation of the system σ_{xy} at temperature 825K.

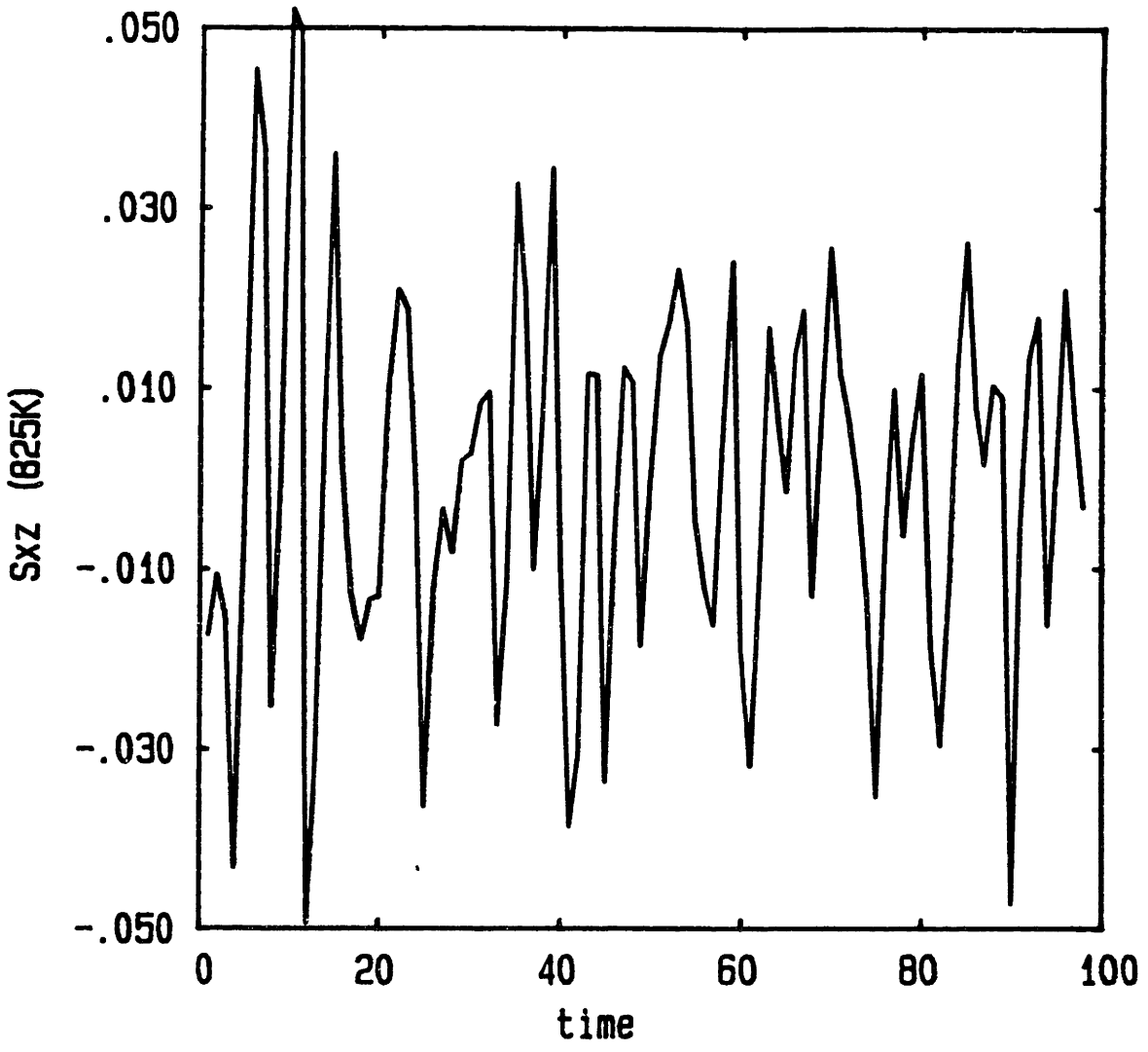

Figure 5-8: σ_{xz} vs time in the bicrystal model

Time variation of the system σ_{xz} at temperature 825K.

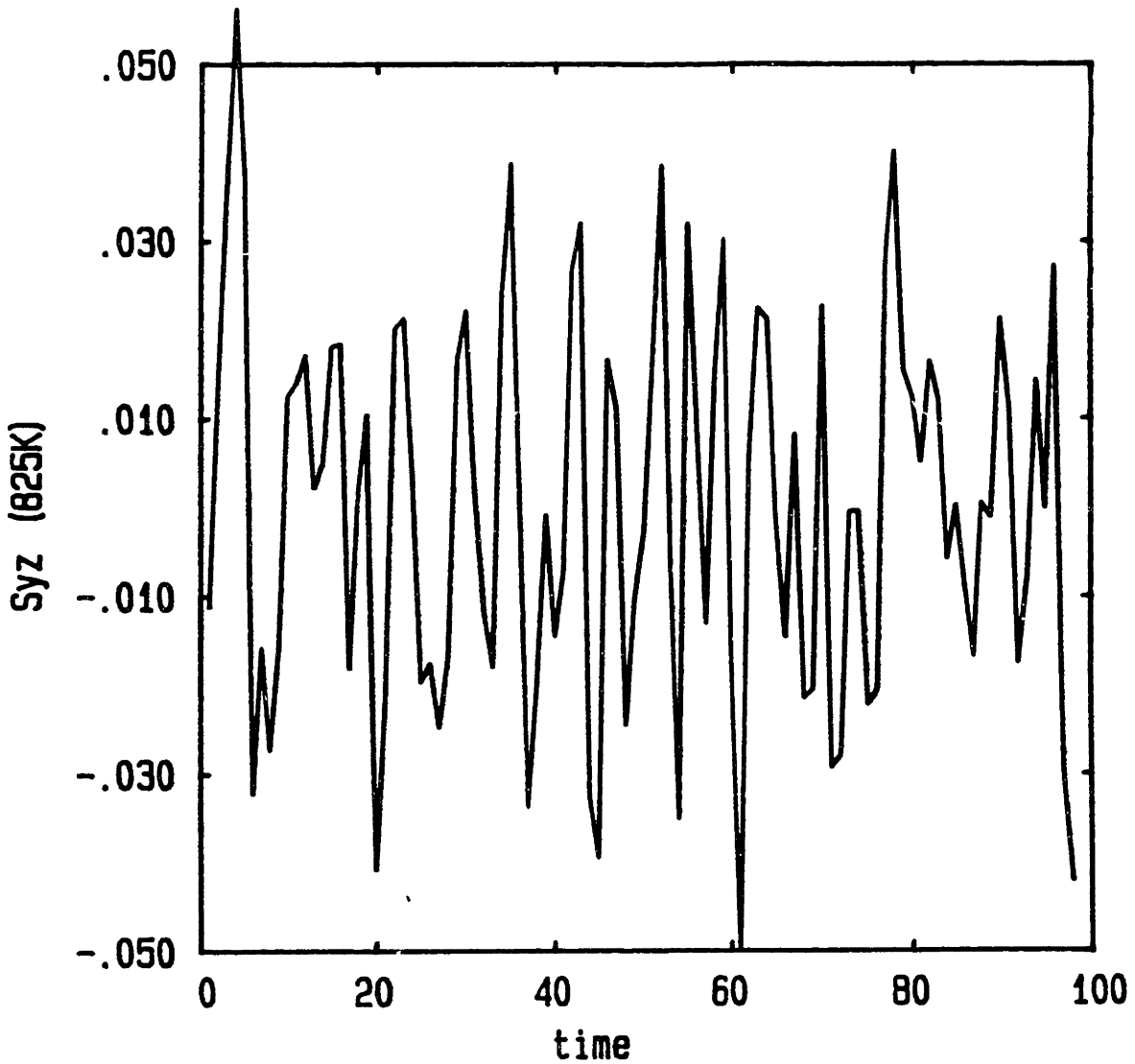

Figure 5-9: σ_{yz} vs time in the bicrystal model

Time variation of the system σ_{yz} at temperature 825K.

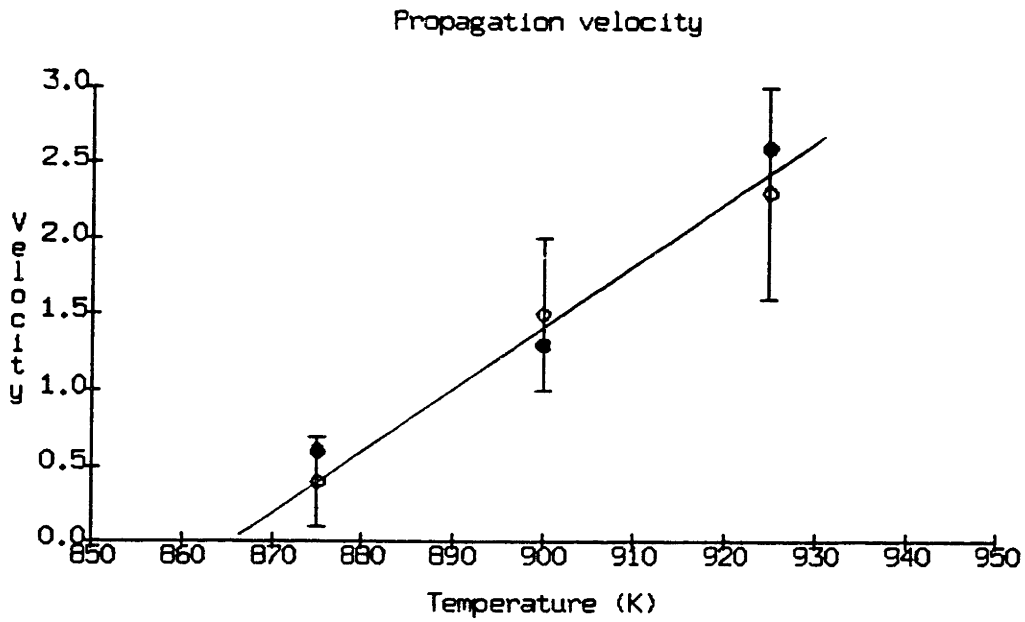

Figure 5-10: Propagation velocities of surface disordered regions

The open circles are data from the reference model. The solid circles are data from the bicrystal model. They all give a melting temperature of approximately 865K.

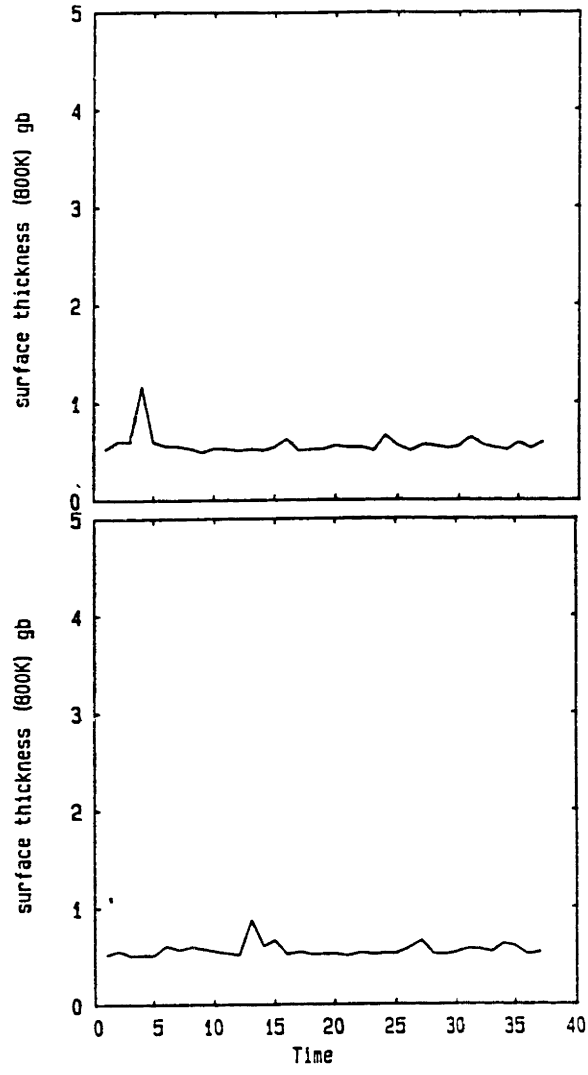

Figure 5-11: Thickness of the disordered surface regions at 800K

The upper and lower figures refer to two difference surfaces at the two ends of the simulation cell. Time axis is in unit of 1000 time steps or about 2 psec. Thickness is in unit of number of layers (0.79 a).

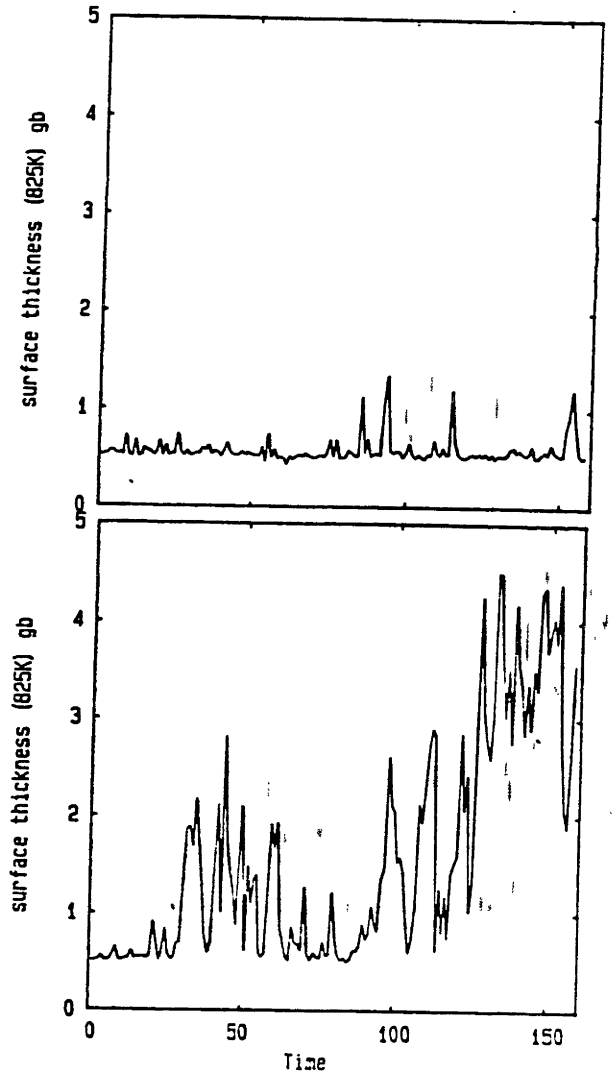

Figure 5-12: Thickness of the disordered surface regions at 825K

The upper and lower figures refer to two difference surfaces at the two ends of the simulation cell. Time axis is in unit of 1000 time steps or about 2 psec. Thickness is in unit of number of layers (0.79 a).

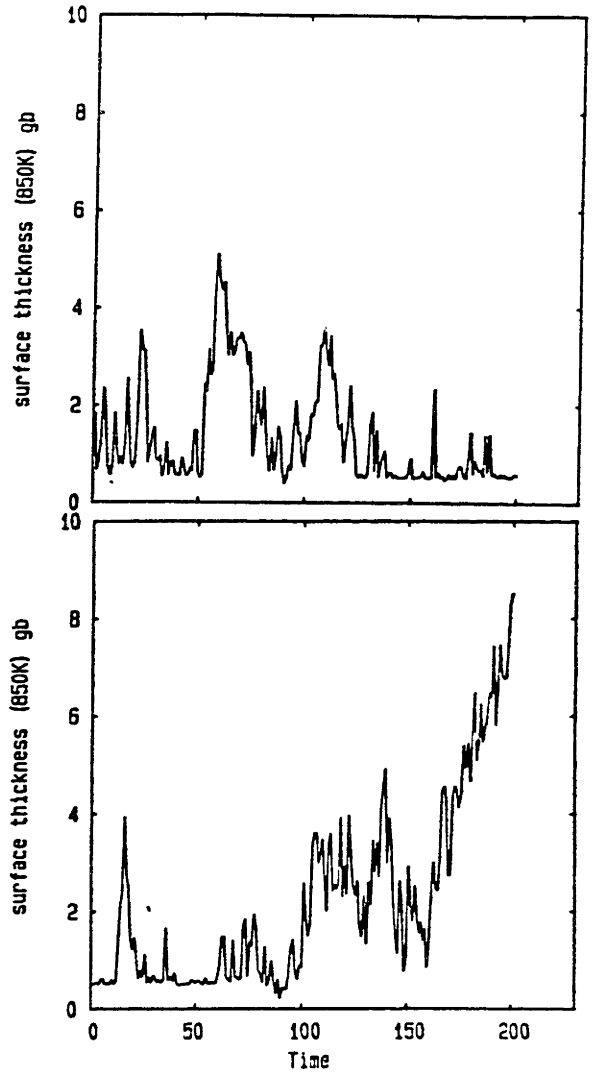

Figure 5-13: Thickness of the disordered surface regions at 850K

The upper and lower figures refer to two difference surfaces at the two ends of the simulation cell. Time axis is in unit of 1000 time steps or about 2 psec. Thickness is in unit of number of layers (0.79 a).

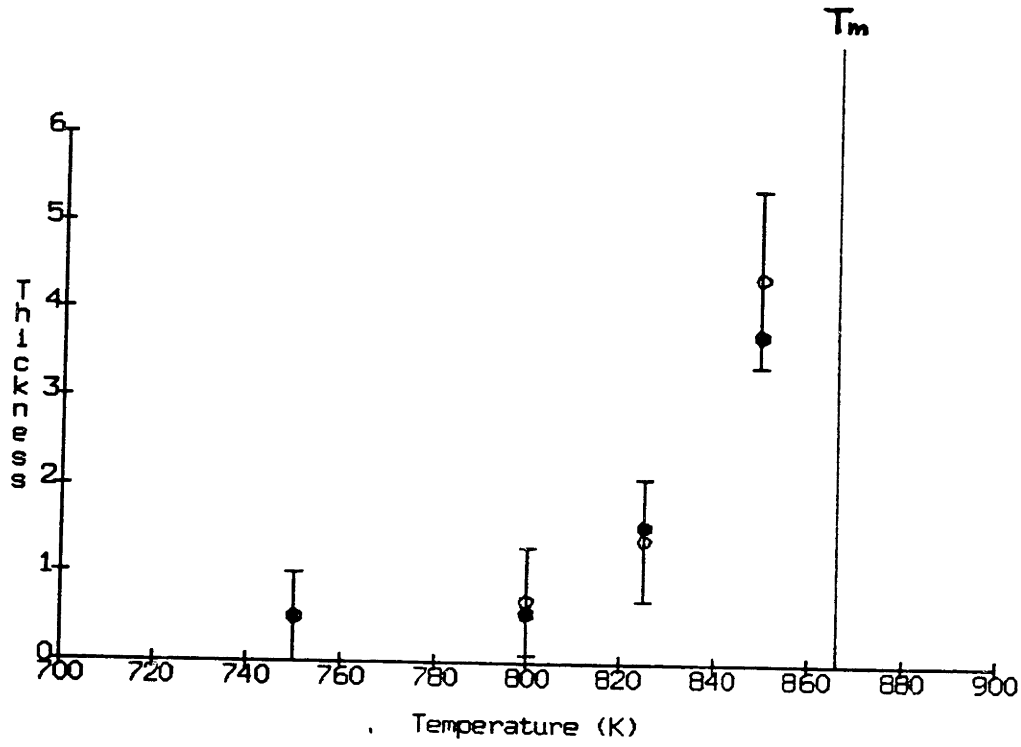

Figure 5-14: Thickness of the disordered surface regions vs temperature

The open circles are data from the reference model. The solid circles are data from the bicrystal model.

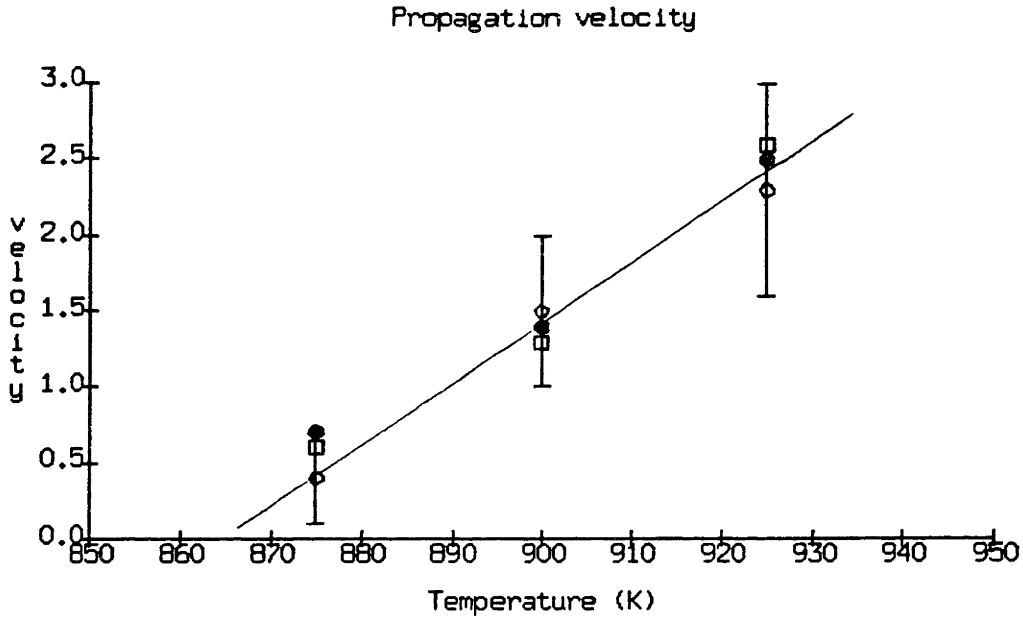

Figure 5-15: Propagation velocities of the gb region

The open circles and squares are data from the surface disordered regions of the reference and bicrystal models. The solid circles are data from the gb region of the bicrystal model.

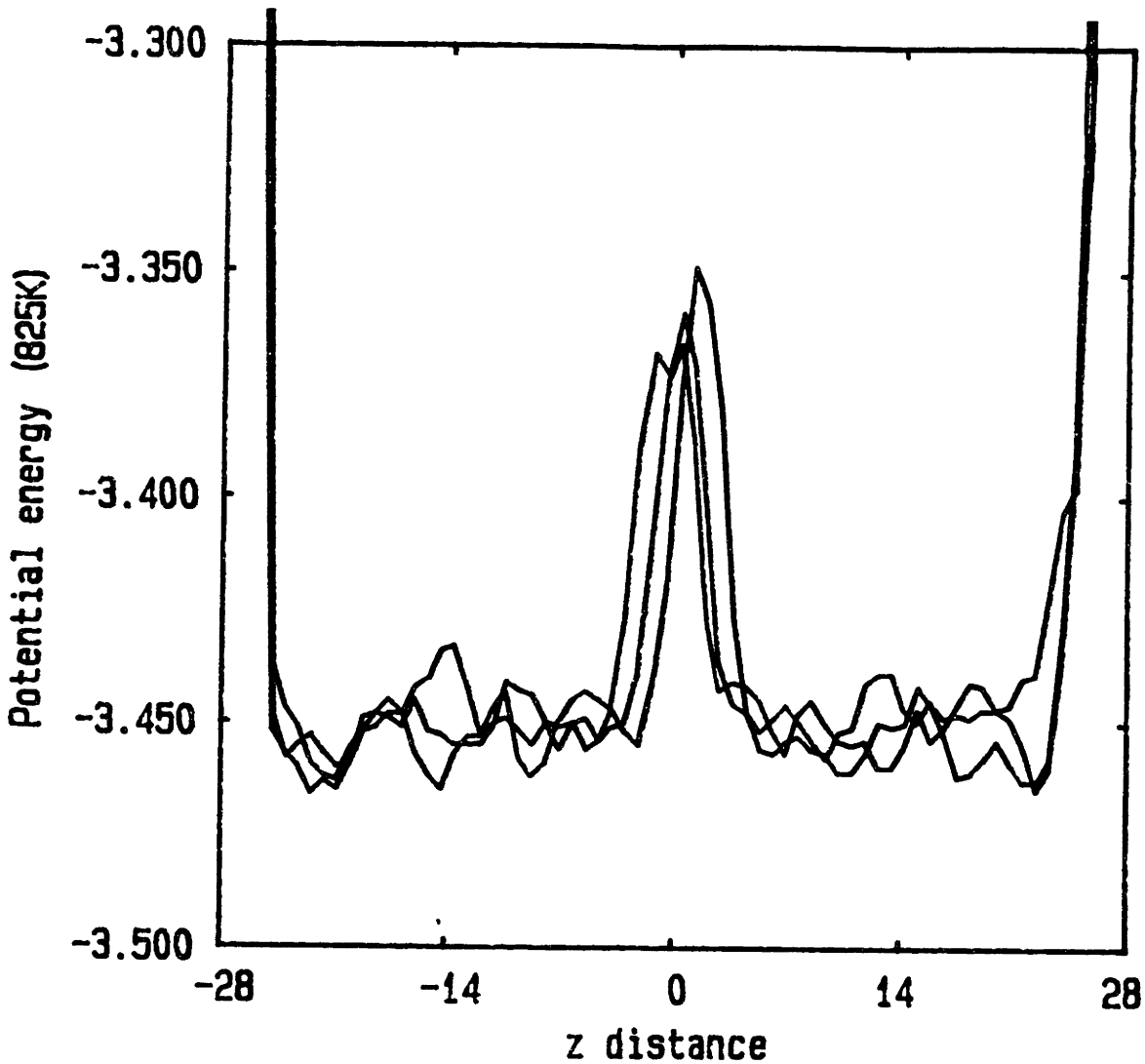

Figure 5-16: Potential energy profiles at 825K at different time steps

Potential energy profiles of the system at 825K and time steps 30000, 60000 and 90000 are shown.

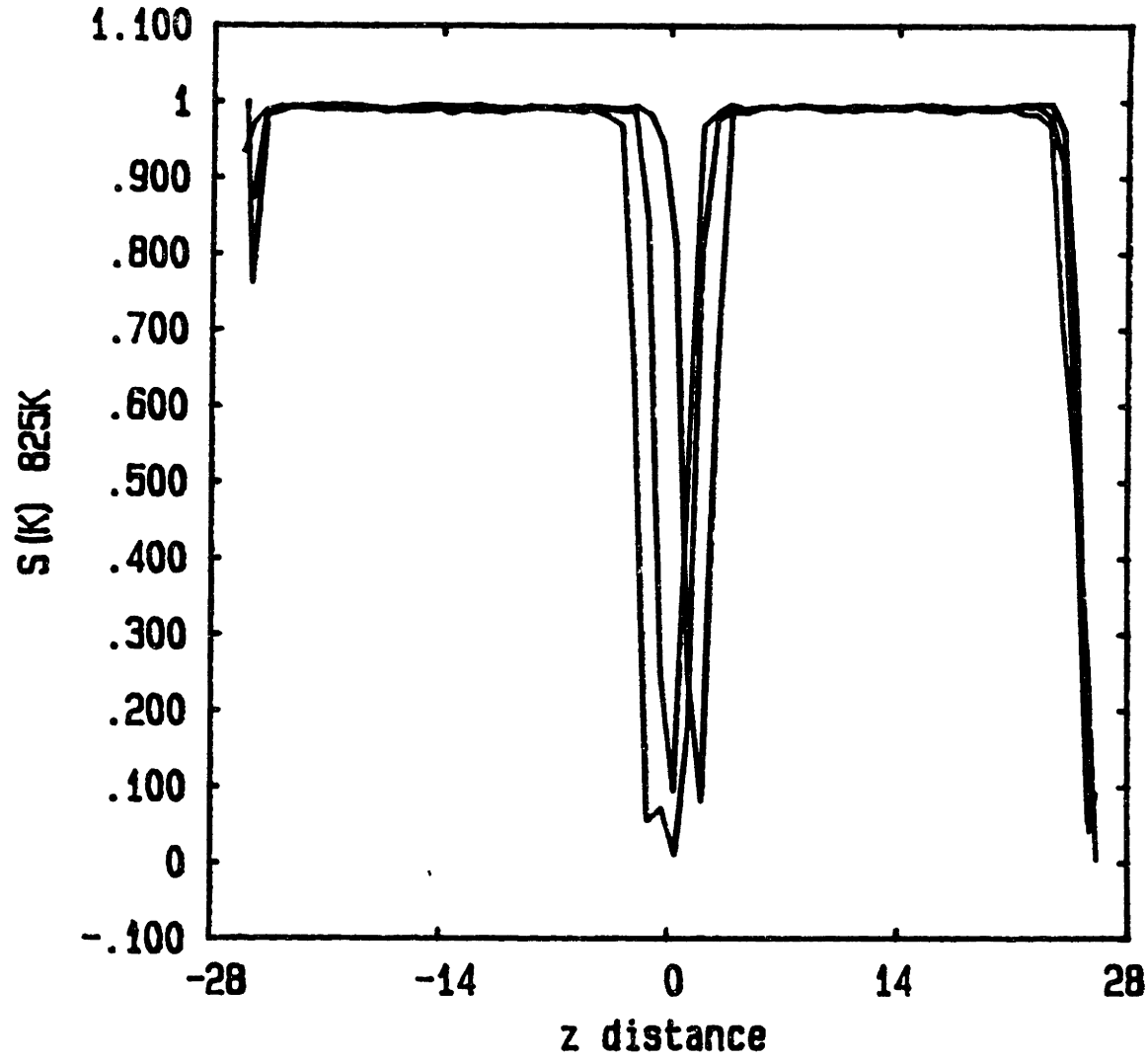

Figure 5-17: Structure factor profiles at 825K at different time steps

Structure factc profiles of the system at 825K and time steps 30000, 60000 and 90000 are shown.

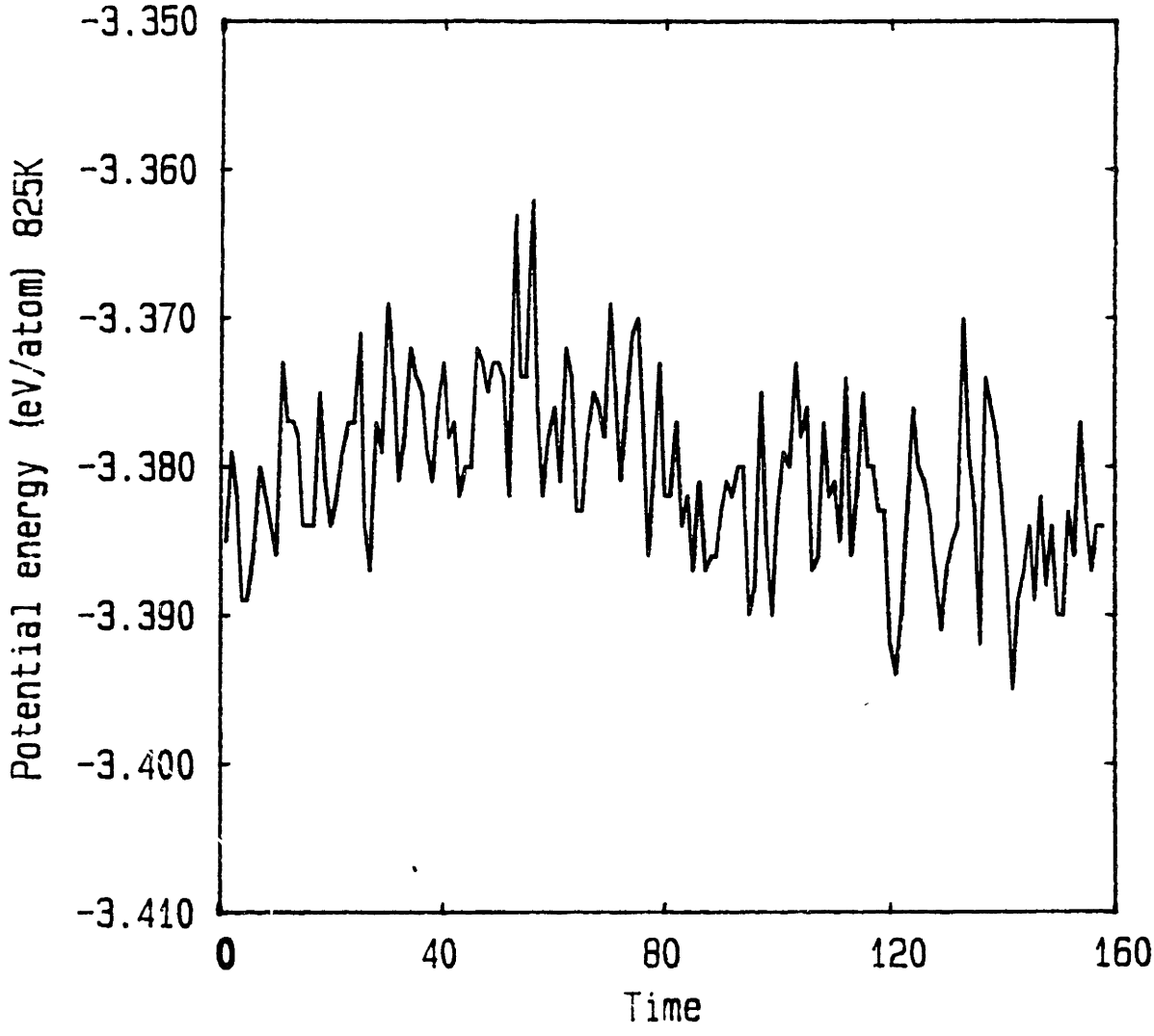

Figure 5-18: Time variation of the gb energy at 825K

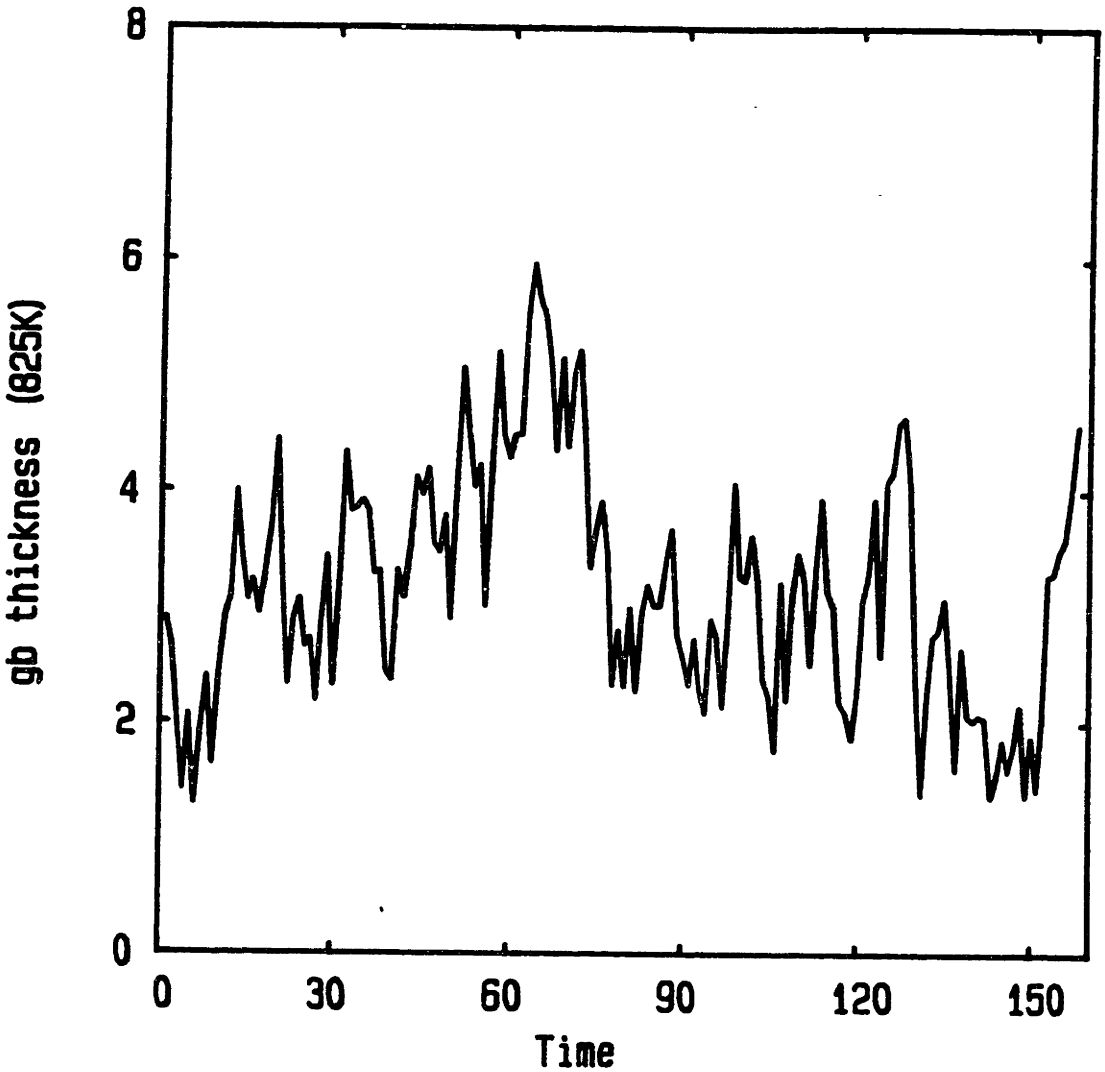

Figure 5-19: Time variation of the gb thickness at 825K

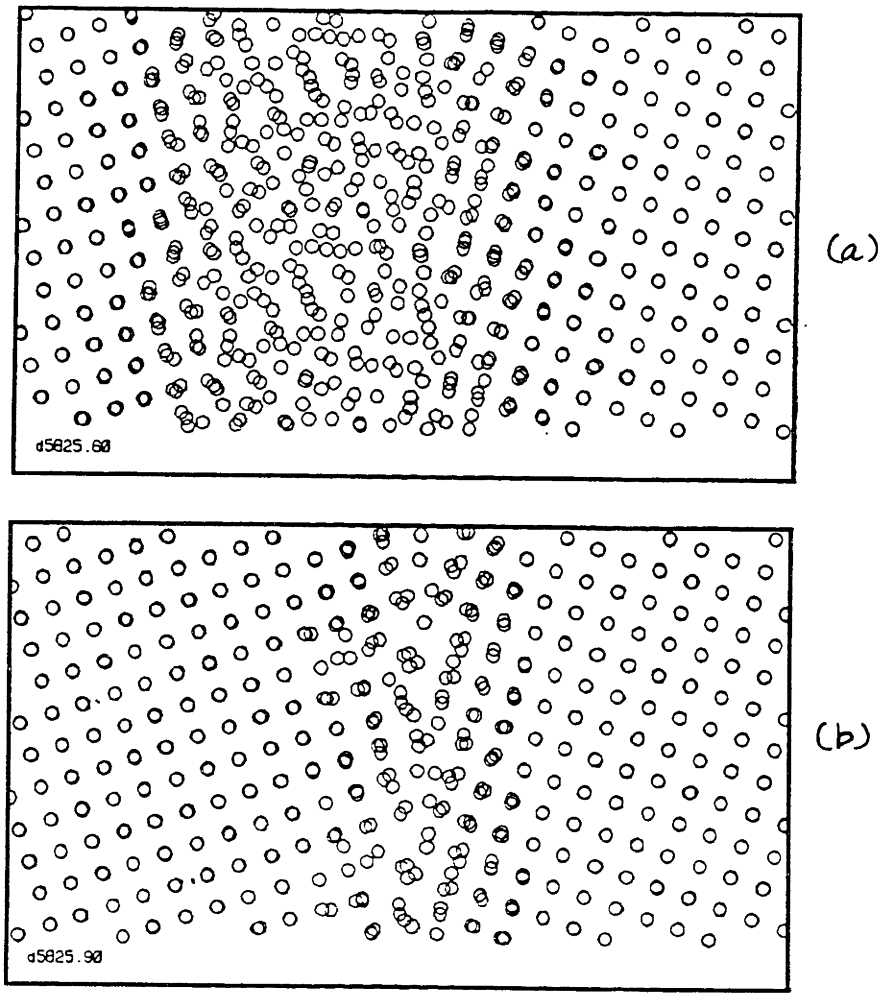

Figure 5-20: Configurations of the gb structure at 825K

The atom positions are time averaged for 1000 time steps at time step (a) 60000 (b) 90000.

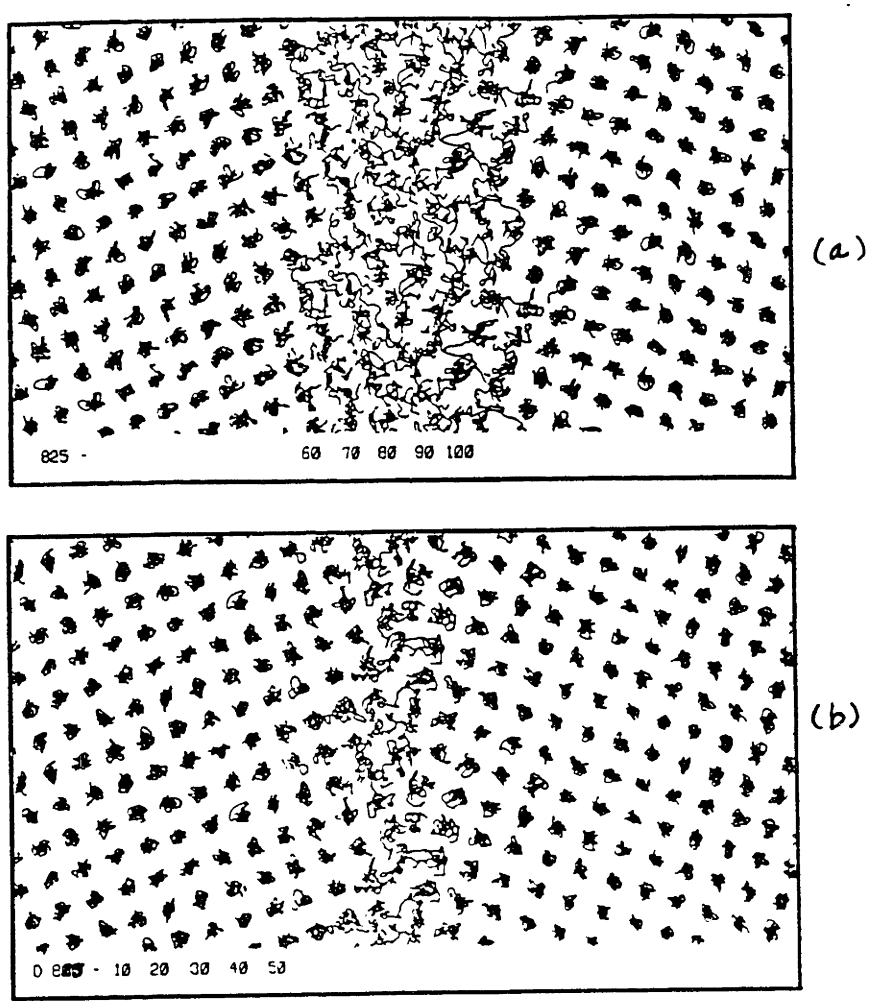

Figure 5-21: Atomic trajectories of the gb structure at 825K

The atom positions are connected for 500 time steps at time step (a) 60000 (b) 90000.

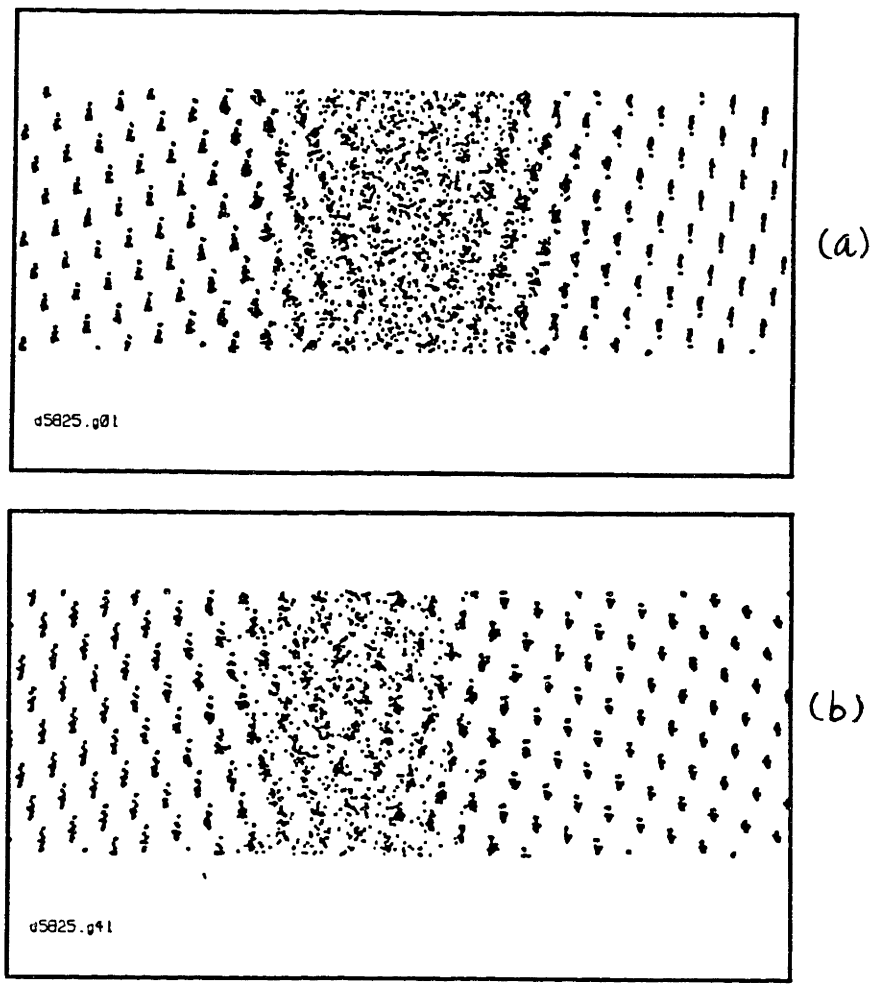

Figure 5-22: Structure of the gb at 825K

10000 time steps accumulation of the gb structure at 825K at time step (a) 60000 (b) 90000.

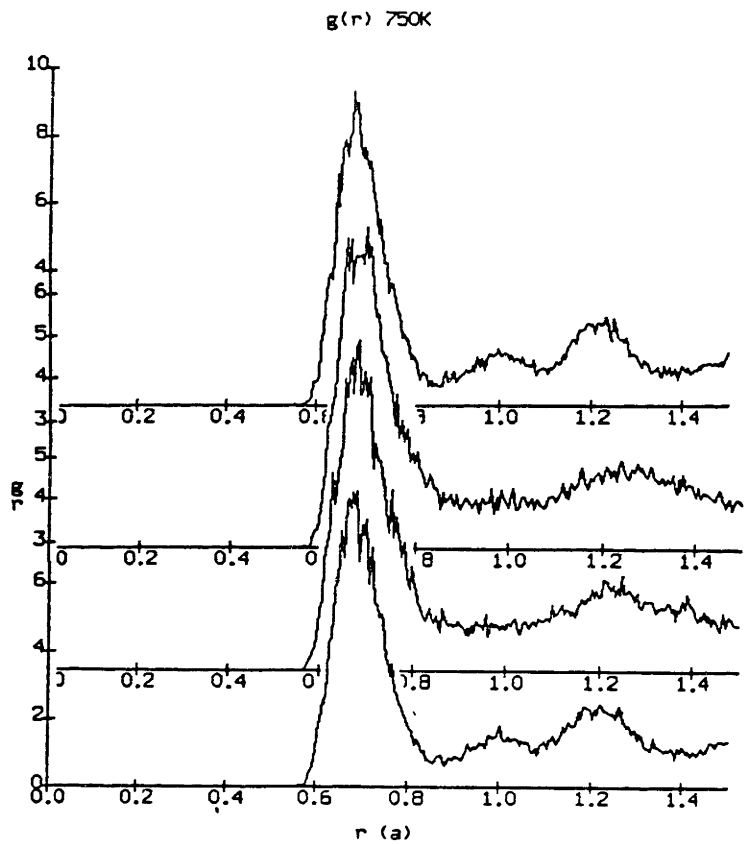

Figure 5-23: Instantaneous g(r) of the gb region at 750K

g(r) for different regions in the gb region are shown. The data are instantaneous and accumulated for 1000 time steps.

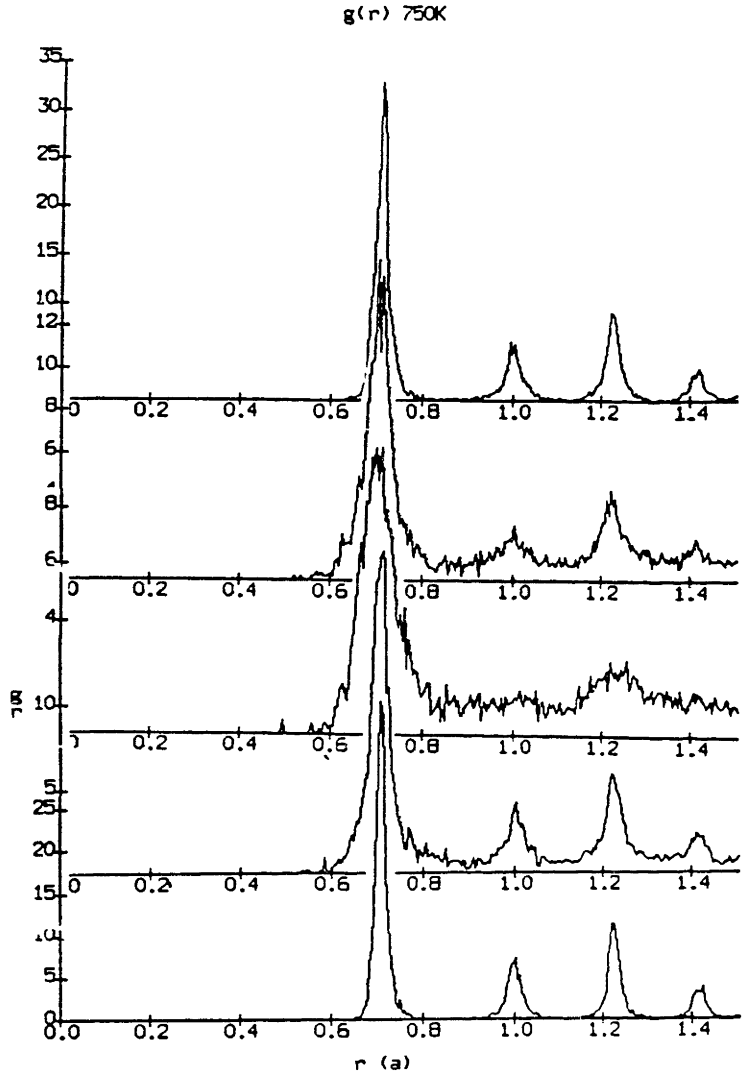

Figure 5-24: Time averaged g(r) of the gb region at 750K

g(r) for different regions in the gb region are shown. The data are time averaged over 1000 time steps and accumulated for 20000 time steps.

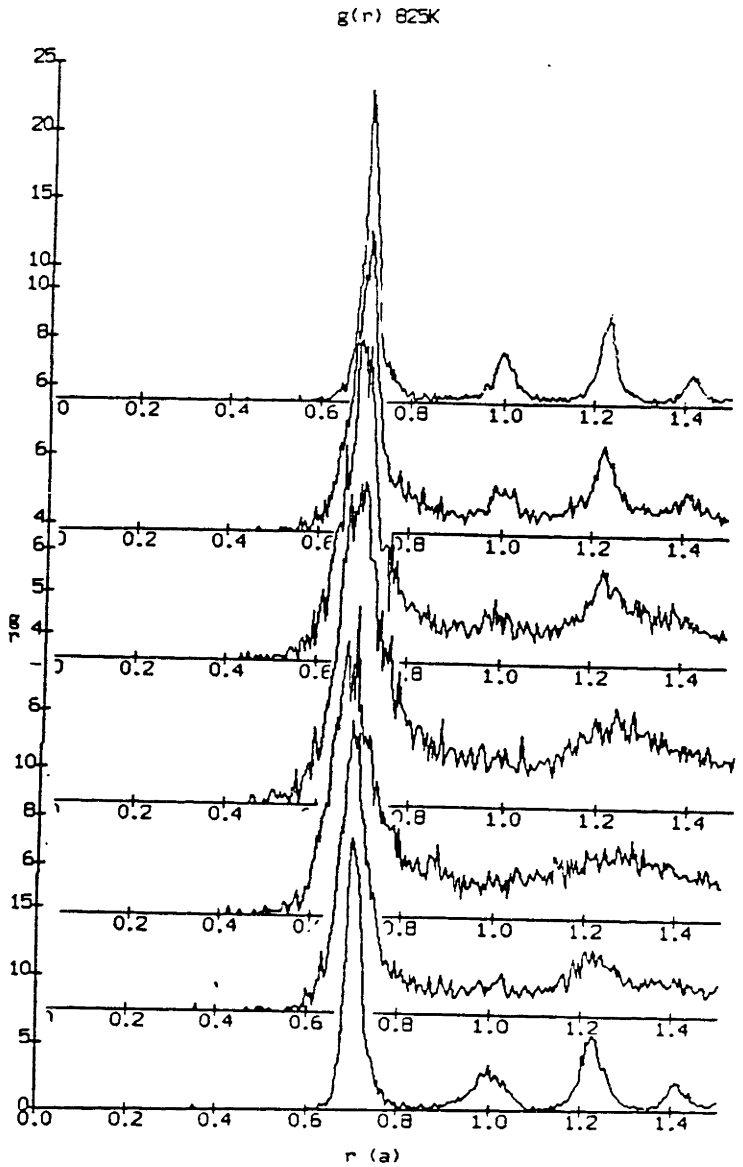

Figure 5-25: g(r) of the gb region at 825K at time step 60000

g(r) for different regions in the gb region are shown. The data are time averaged over 1000 time steps and accumulated for 20000 time steps.

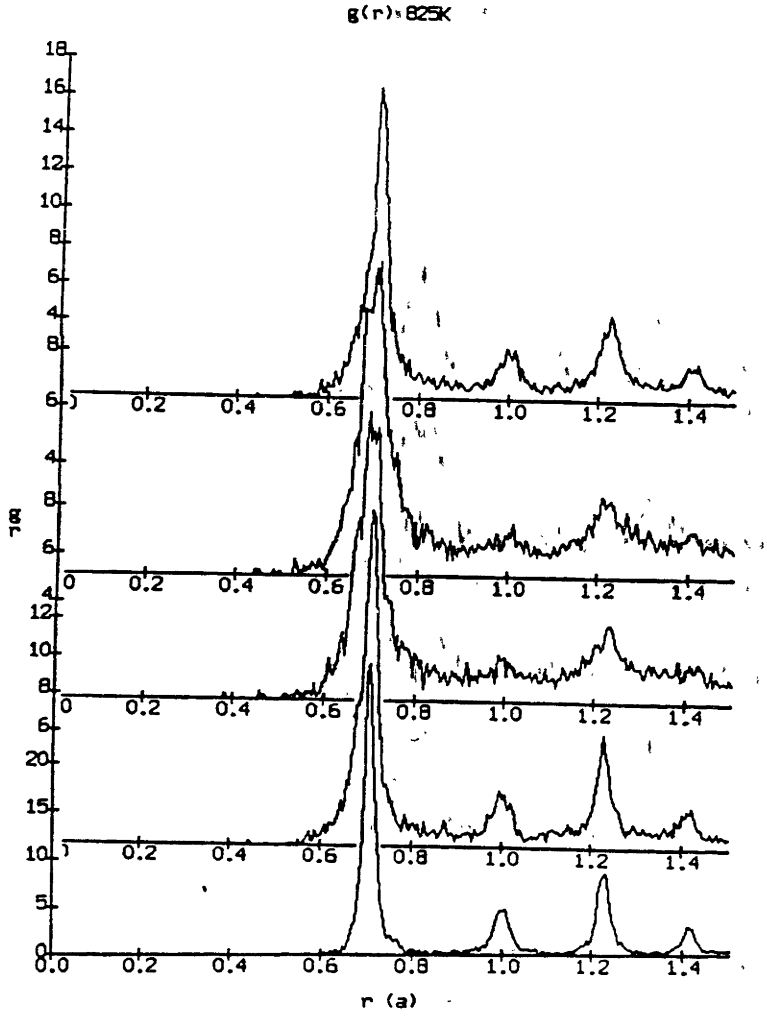

Figure 5-26: g(r) of the gb region at 825K at time step 90000

g(r) for different regions in the gb region are shown. The data are time averaged over 1000 time steps and accumulated for 20000 time steps.

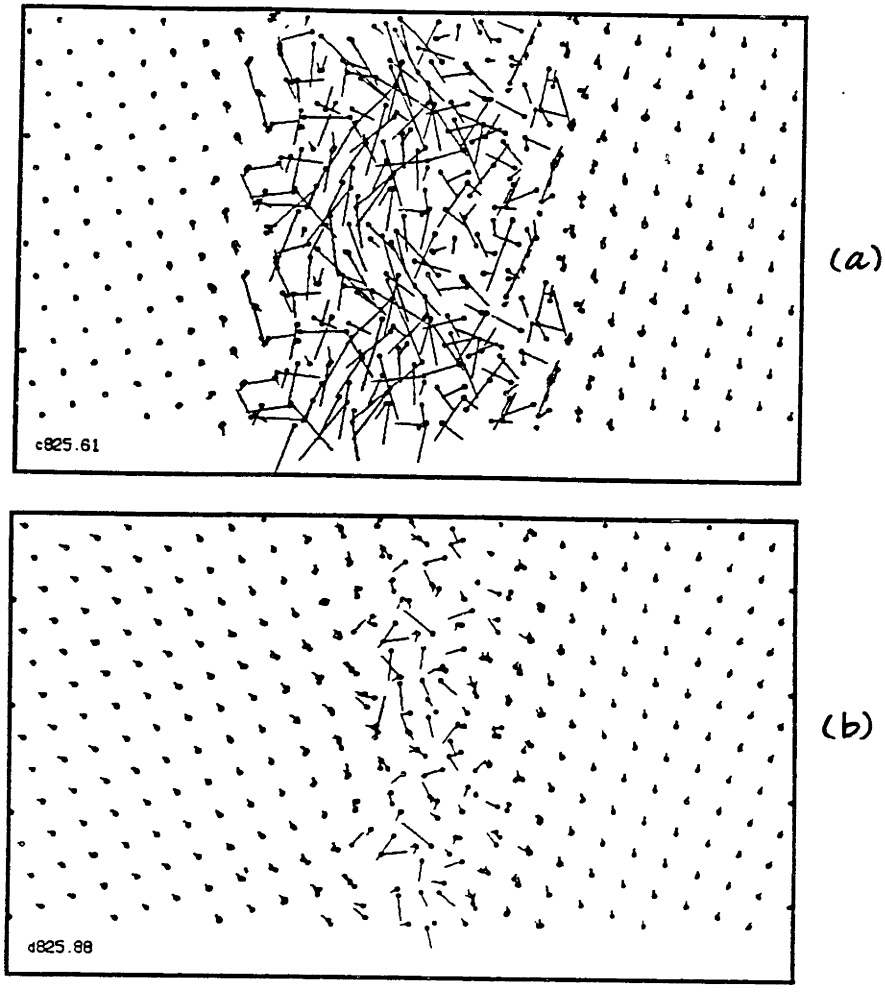

Figure 5-27: Mobility of the gb region at 825K

Two atom positions each are averaged over 1000 time steps are connected to show the movement of the gb atoms at time step (a) 60000 (b) 90000.

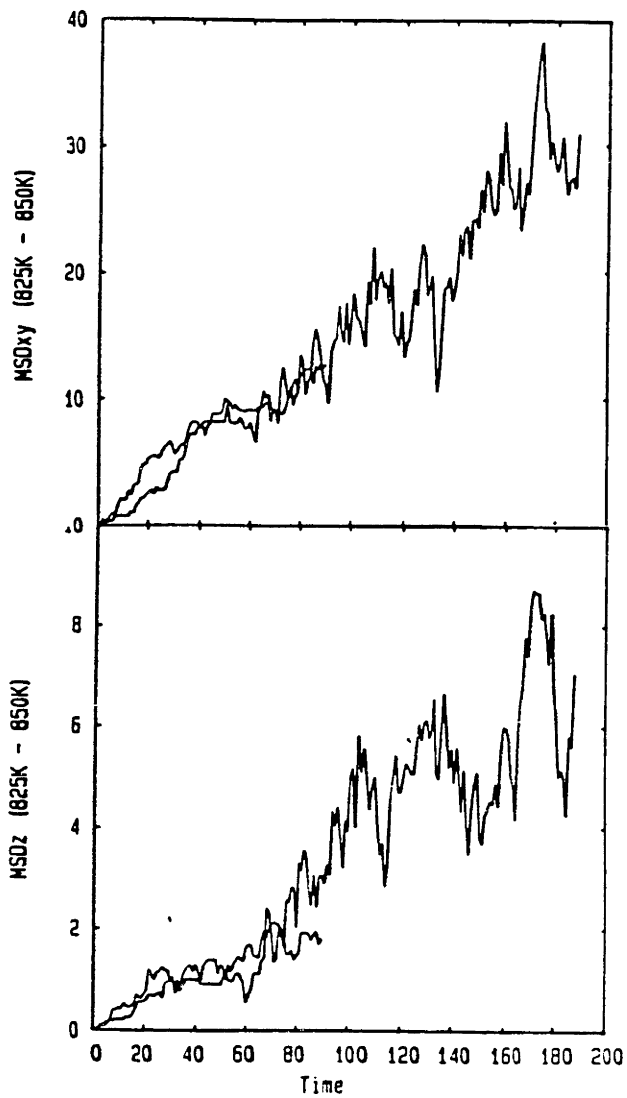

Figure 5-28: MSD of the gb region at 825K and 850K

The 825K MSD curve is plotted up to 90000 time steps. The 850K MSD curve is plotted up to 190000 time steps. (a) xy component (b) z component of the MSD.

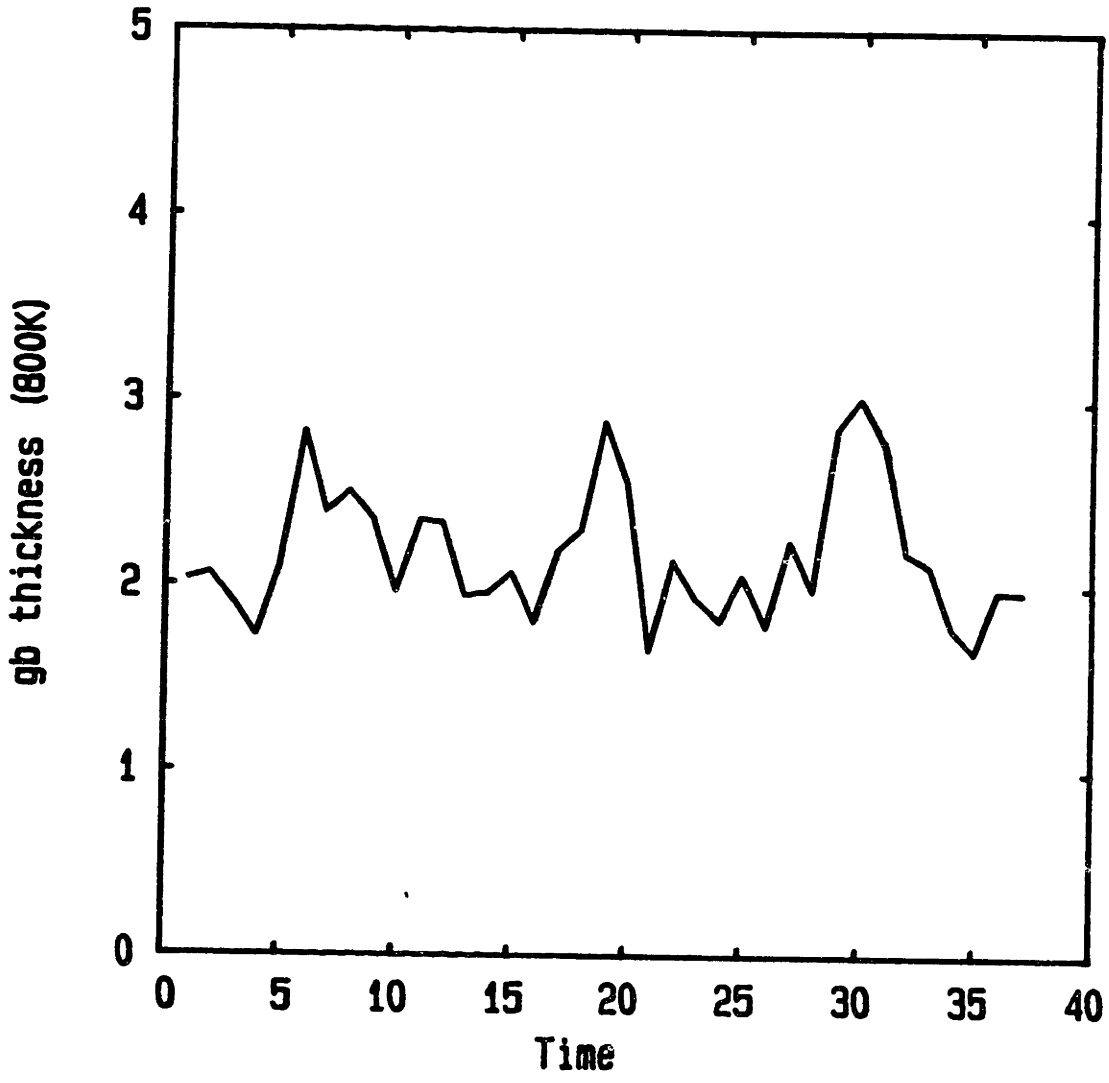

Figure 5-29: Thickness of the gb region at 800K

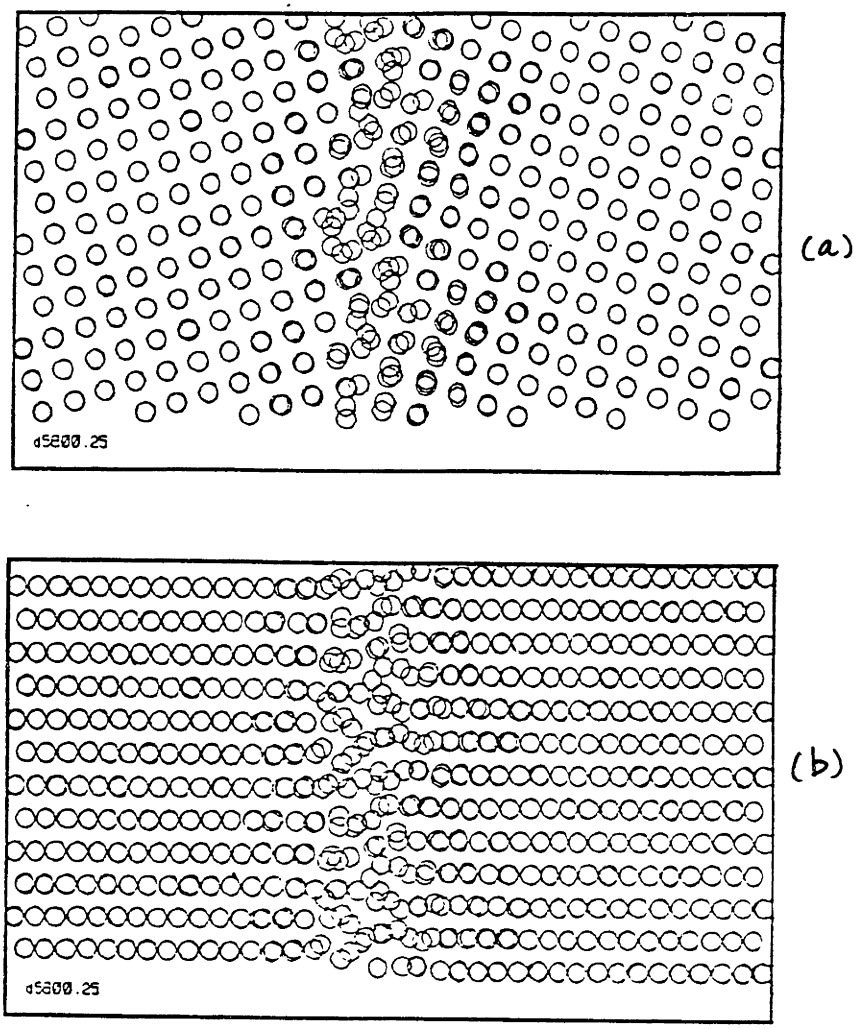

Figure 5-30: Configuration of the gb structure at 800K

gb structure at 800K at time step 20000. The atom positions are averaged over 1000 time steps.

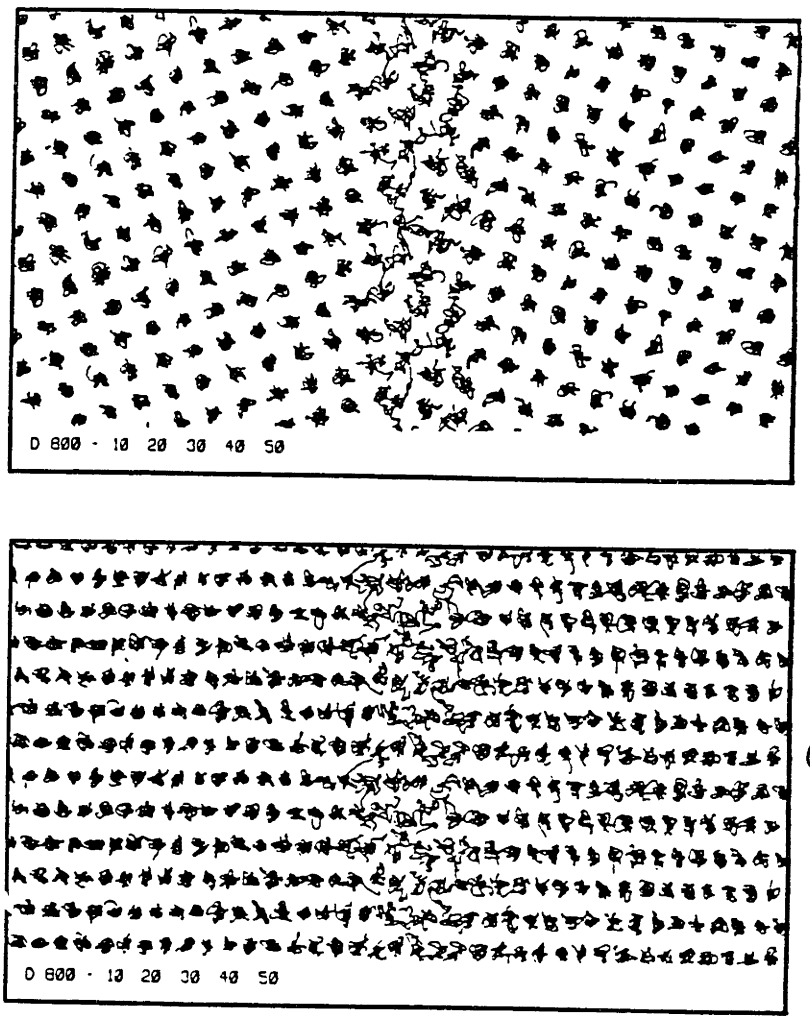

Figure 5-31: Atomic trajectory of the gb structure at 800K

Trajectory of gb atoms for 500 time steps accumulation at time step 20000.

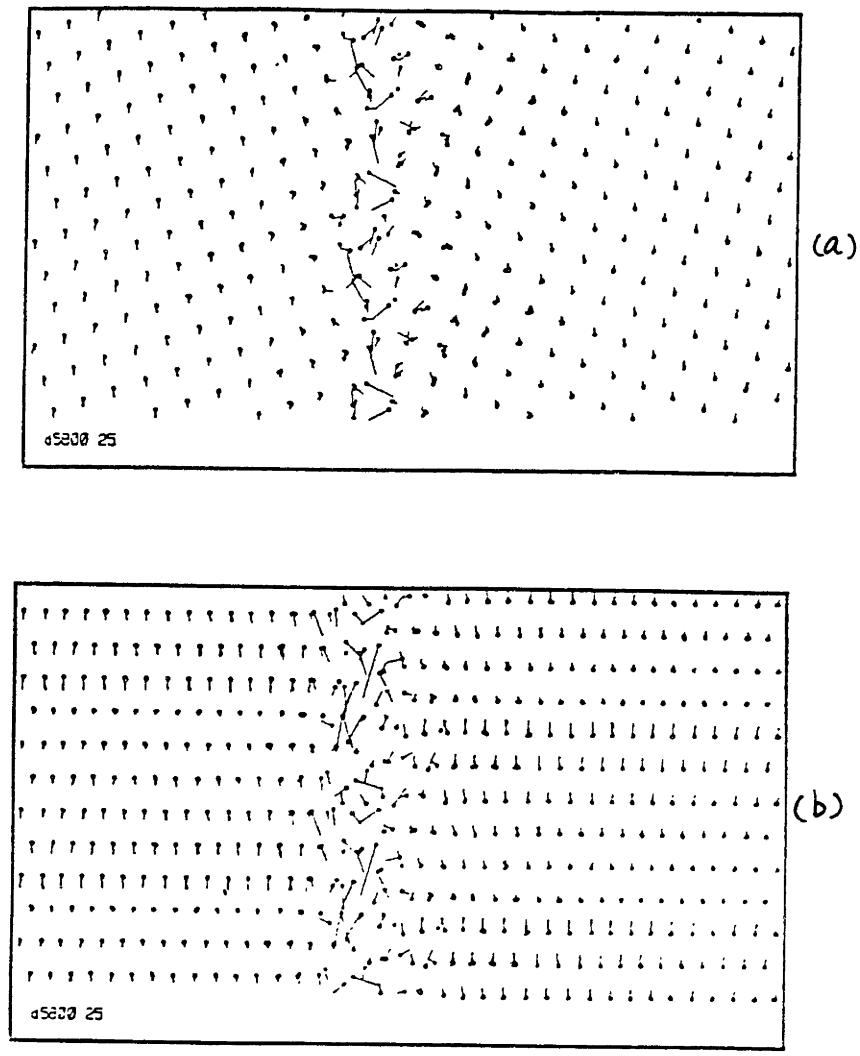

Figure 5-32: Mobility of the gb region at 800K

Two atom positions each are averaged over 1000 time steps are connected to show the movement of the gb atoms at time step 20000

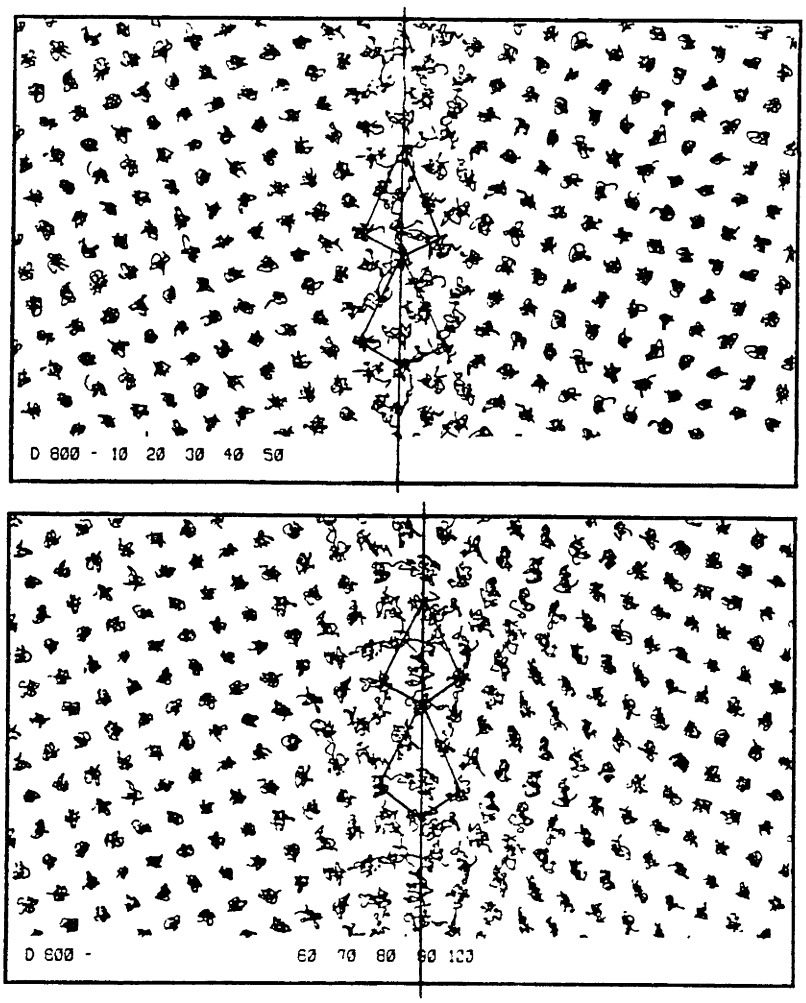

Figure 5-33: Coupled sliding and migration of the gb at 800K

Two atomic trajectory plots of the gb region separated by 1500 time steps are shown. The data is accumulated for 500 time steps.

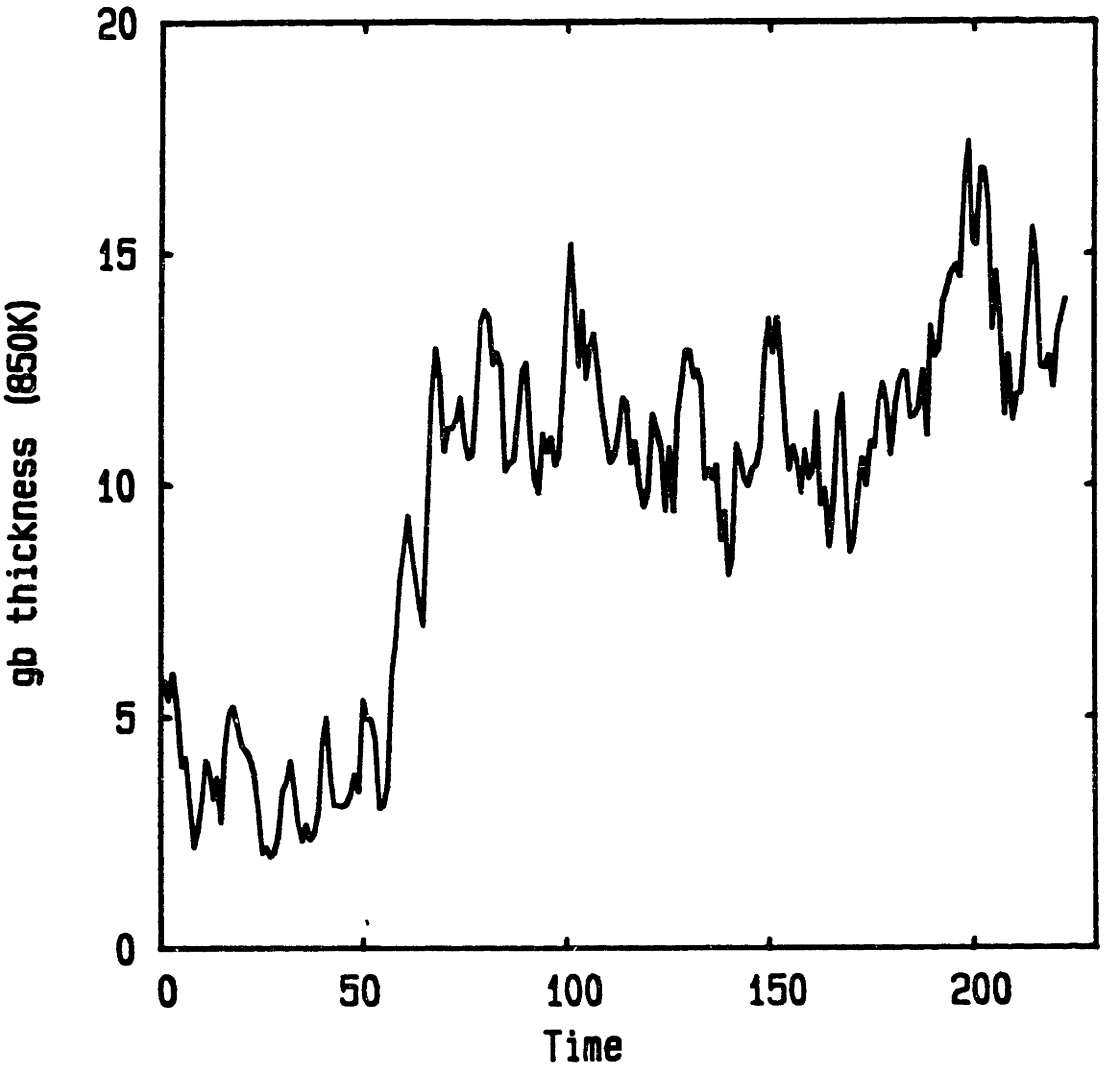

Figure 5-34: Thickness of the gb region at 850K

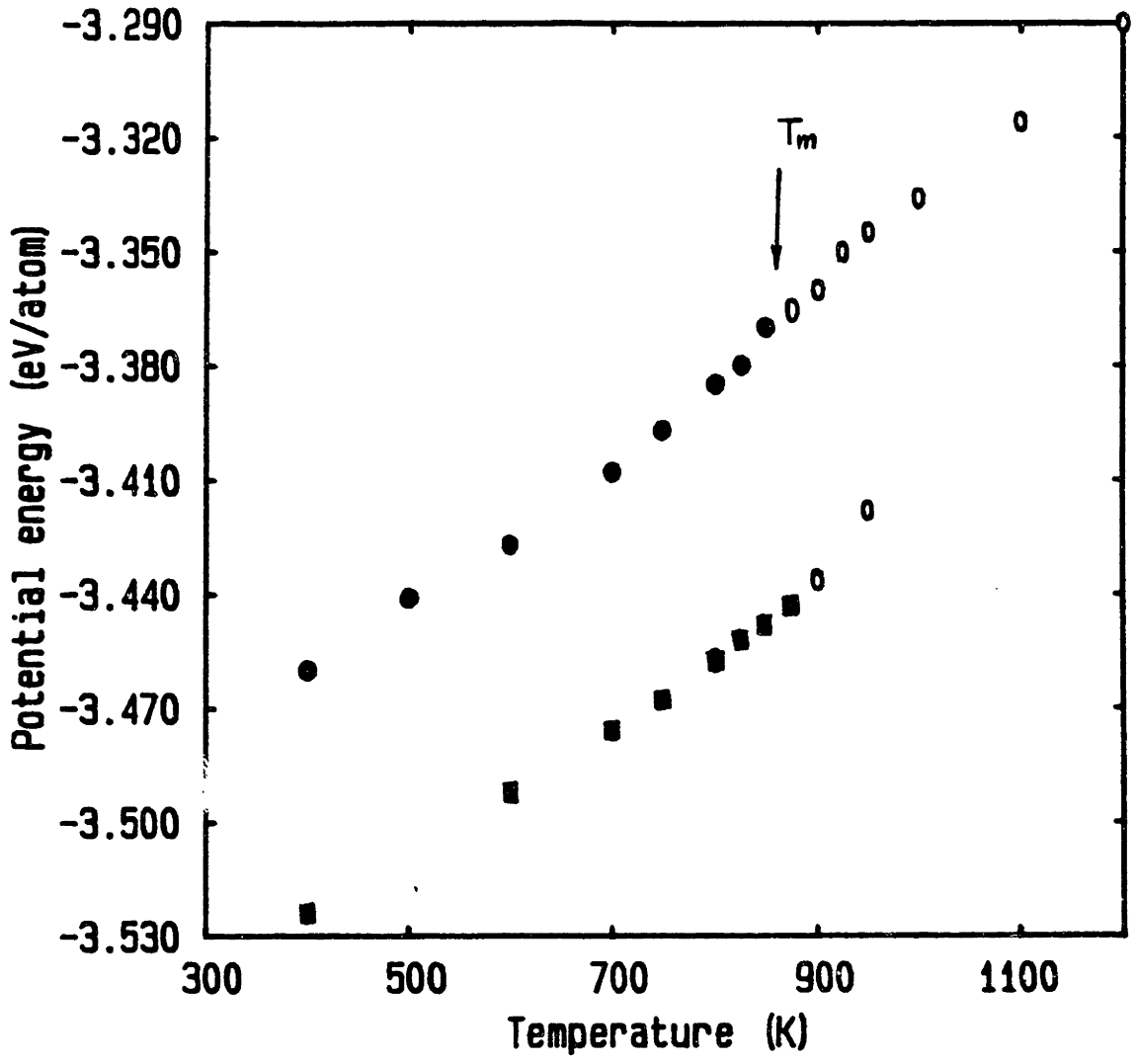

Figure 5-35: Temperature variation of the gb energy

The solid squares are data from the bulk region in the bicrystal model. The solid circles are data for the gb region. The open circles are data from the reference model and single crystal model which constitute the solid and liquid branches of potential energy curve.

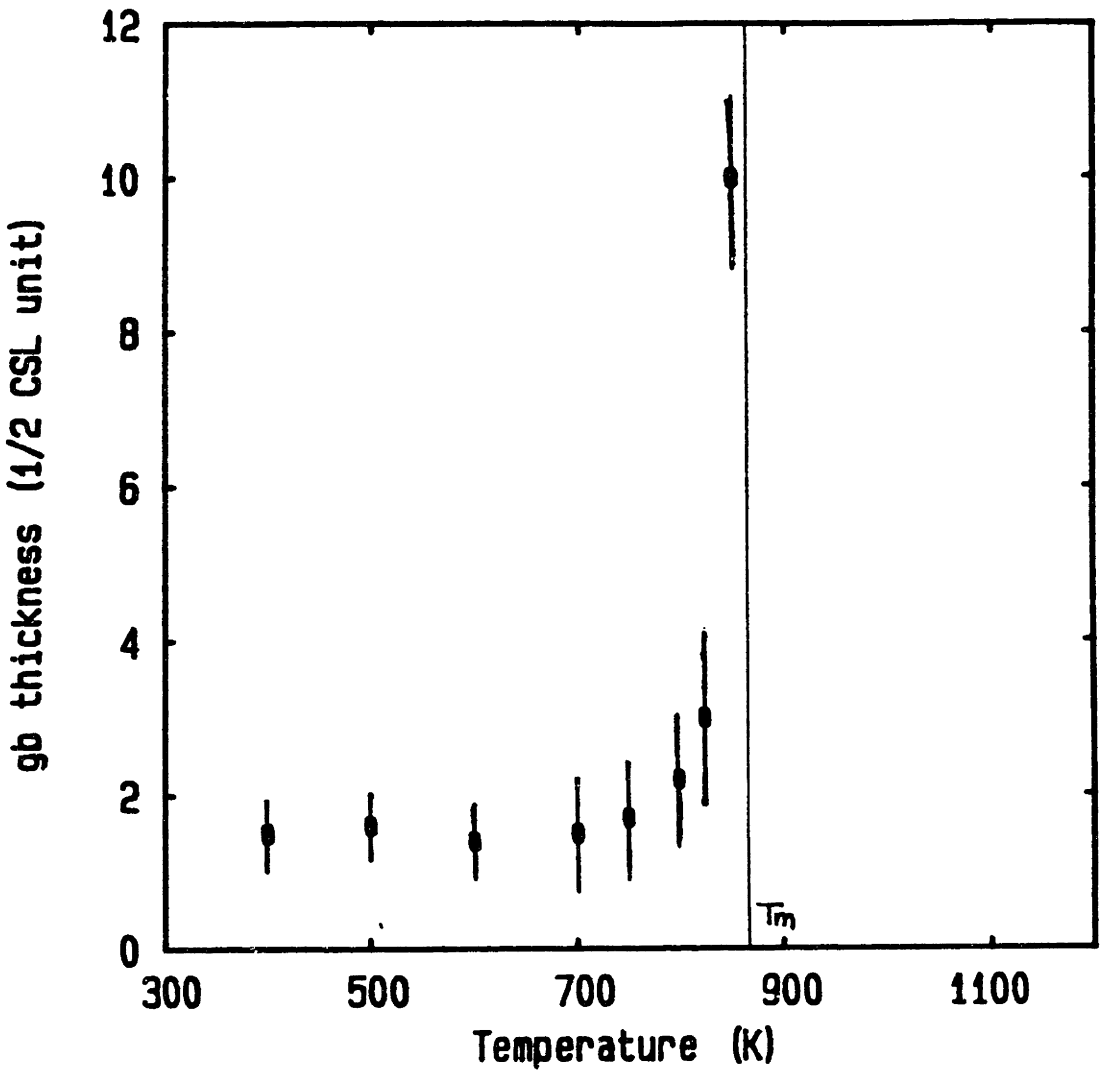

Figure 5-36: Temperature variation of the gb thickness

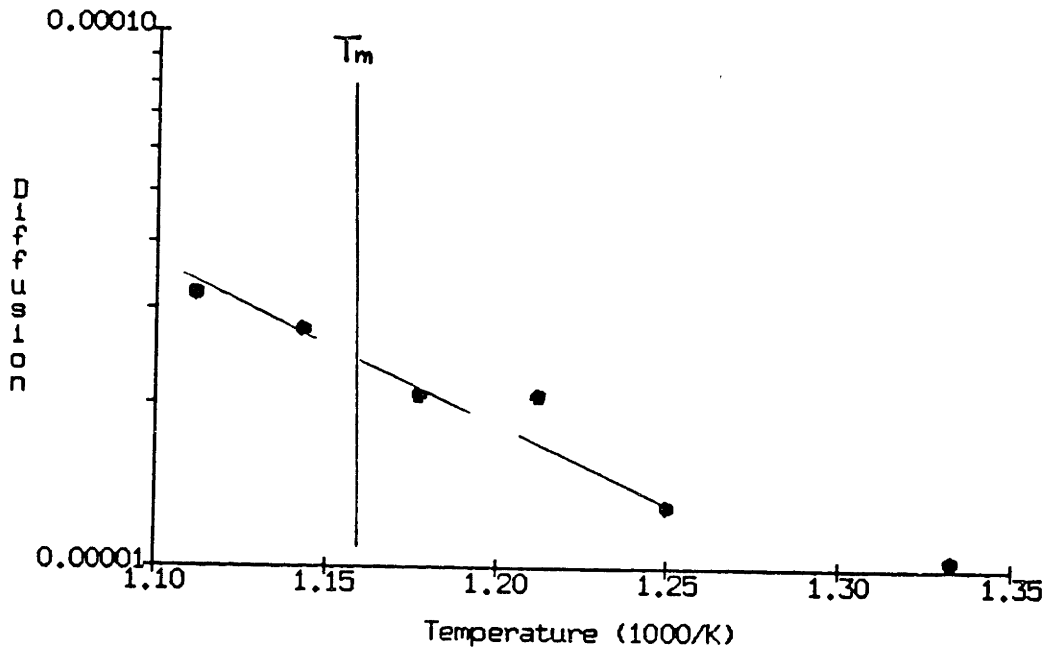

Figure 5-37: Temperature variation of the gb diffusion coefficients

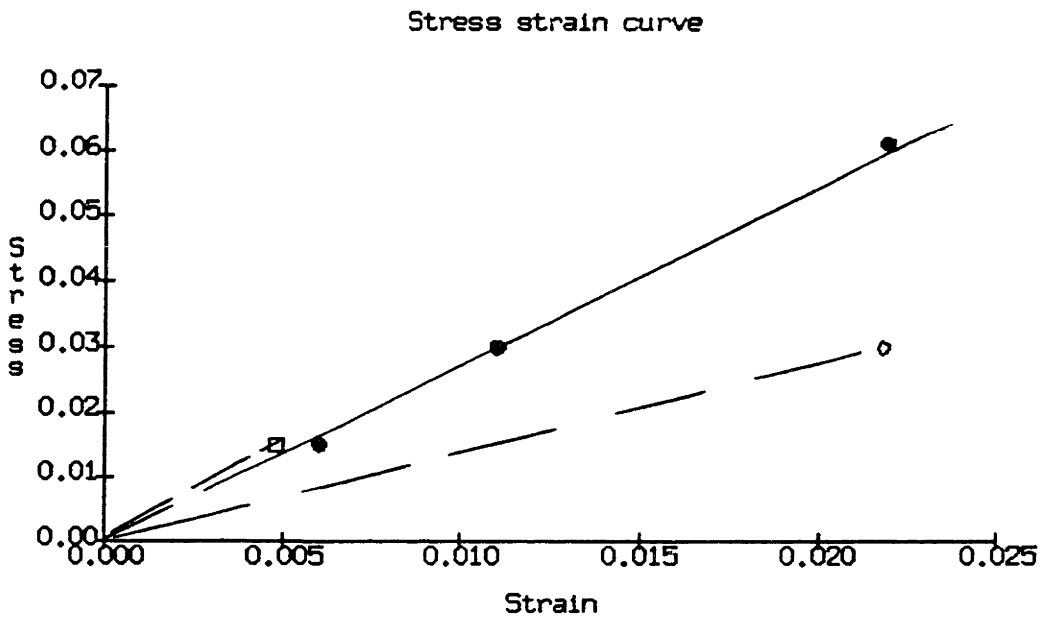

Figure 5-38: Stress strain curves

Solid circles are data for the reference model at 750K. Open circle and square are data for the bicrystal model at 750K and 600K respectively.

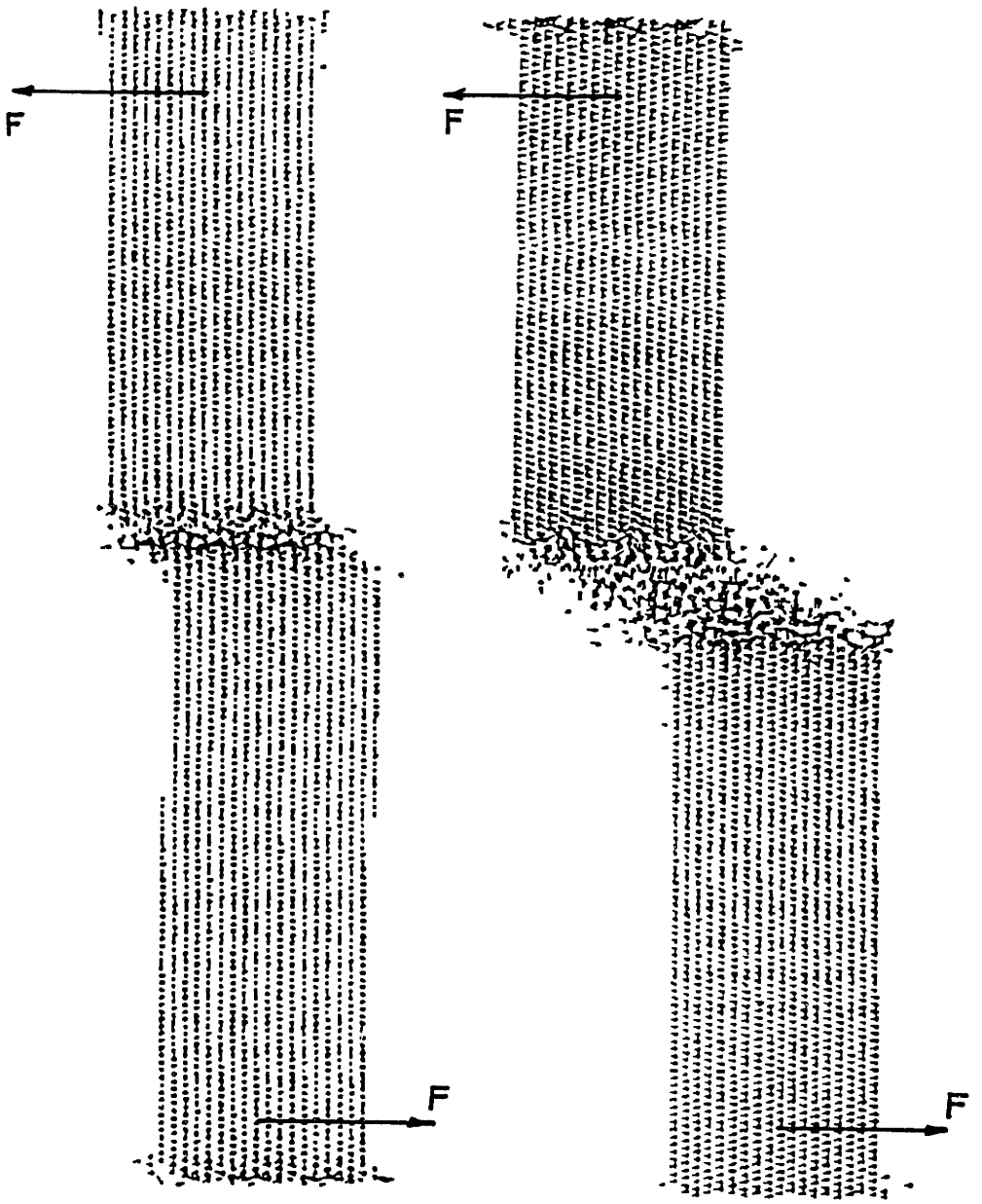

Figure 5-39: Failure of gb at 800K with high shear stress

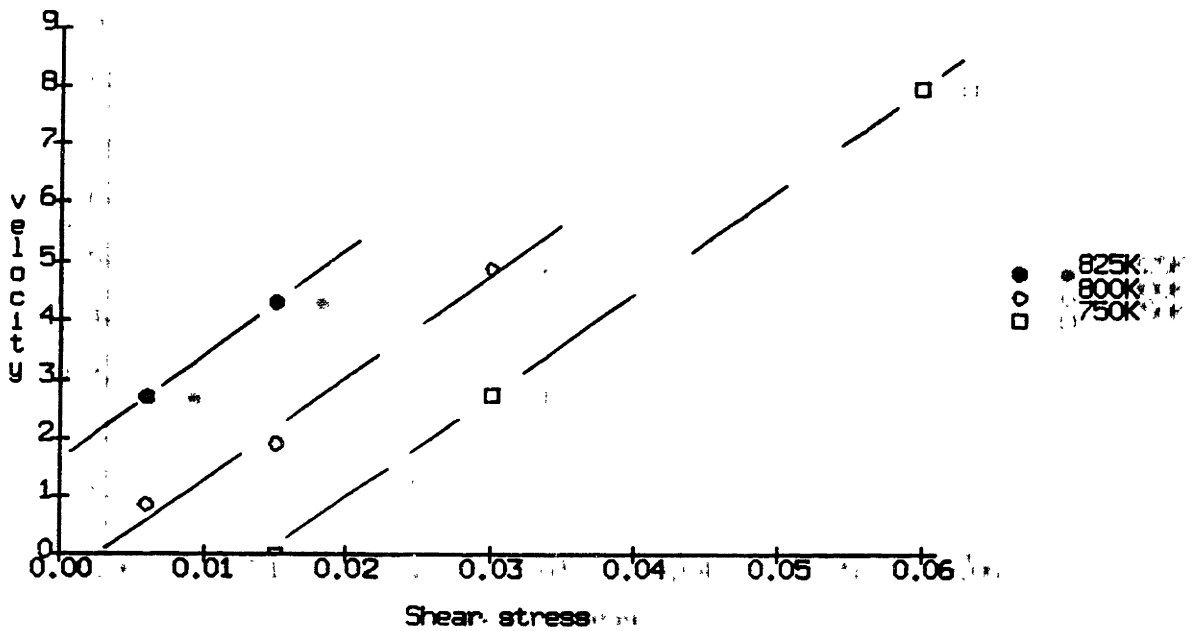

Figure 5-40: Sliding velocity vs applied shear stress

Solid circles are data for 825K. Open circles are data for 800K. Open squares are data for 750K. The straight lines are fitted through these data points.

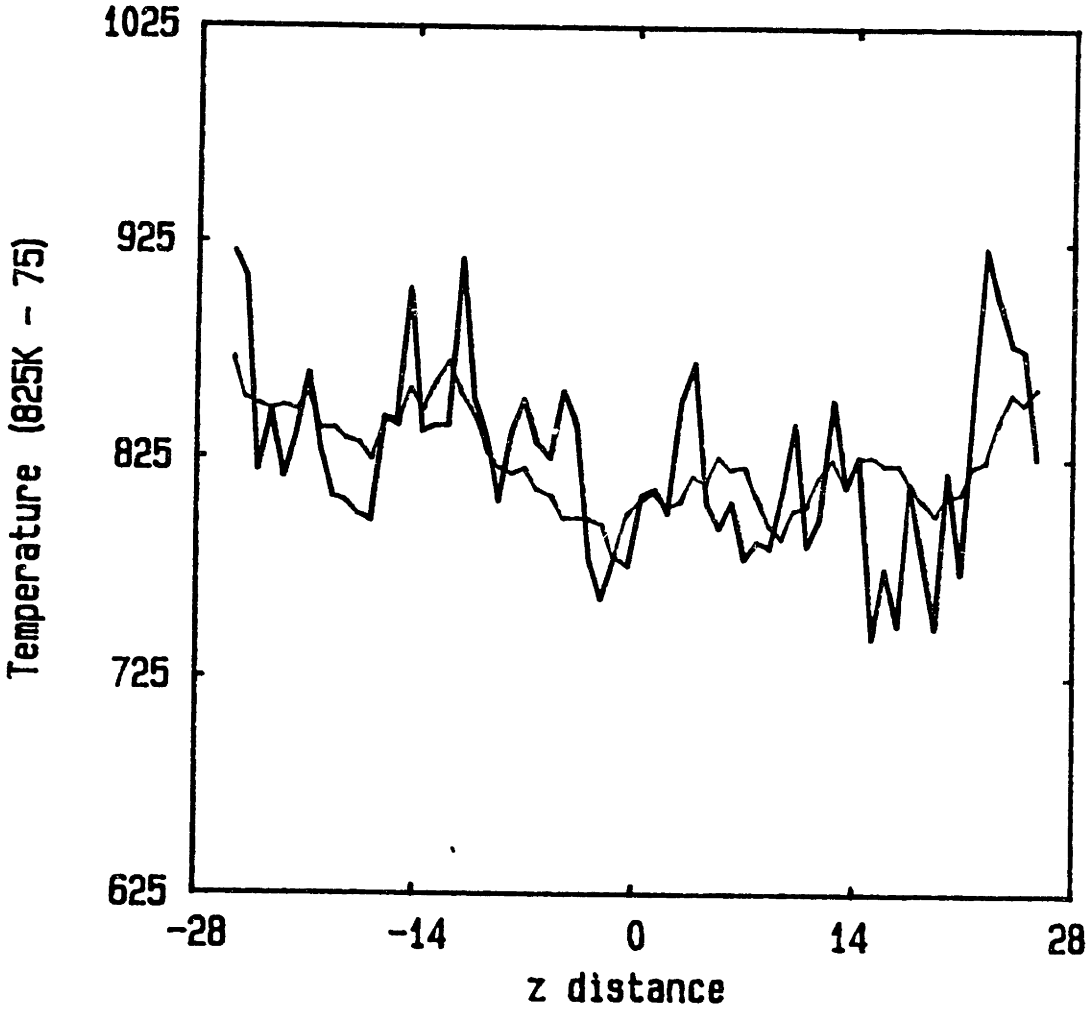

Figure 5-41: Temperature distributions in the fixed border model

Temperature distributions are shown for the fixed border bicrystal model at 825K and time step 64000. The curve with high fluctuation is averaged for 1000 time steps. The smoother curve is averaged for 20000 time steps.

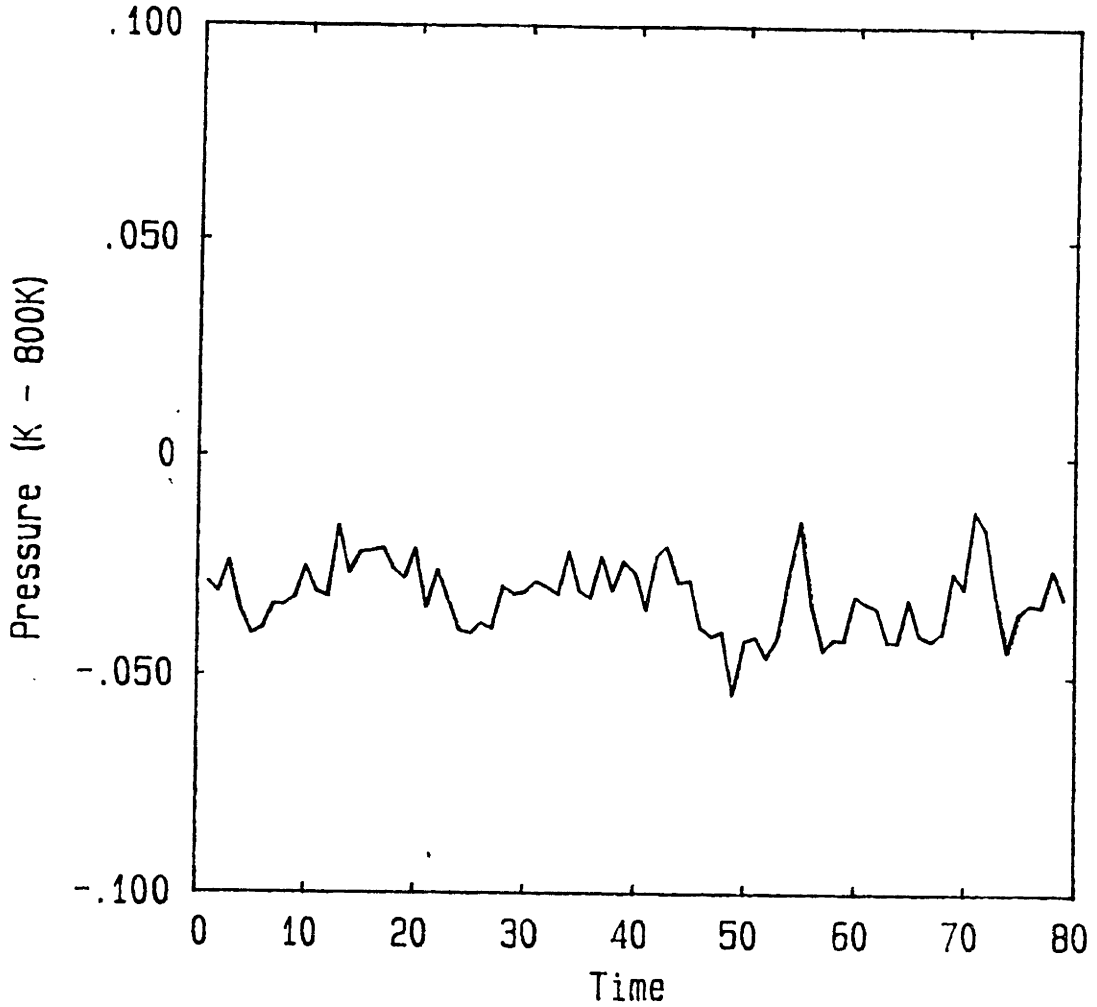

Figure 5-42: Pressure vs time in the fixed border model at 800K

Time variation of the system pressure at temperature 800K.

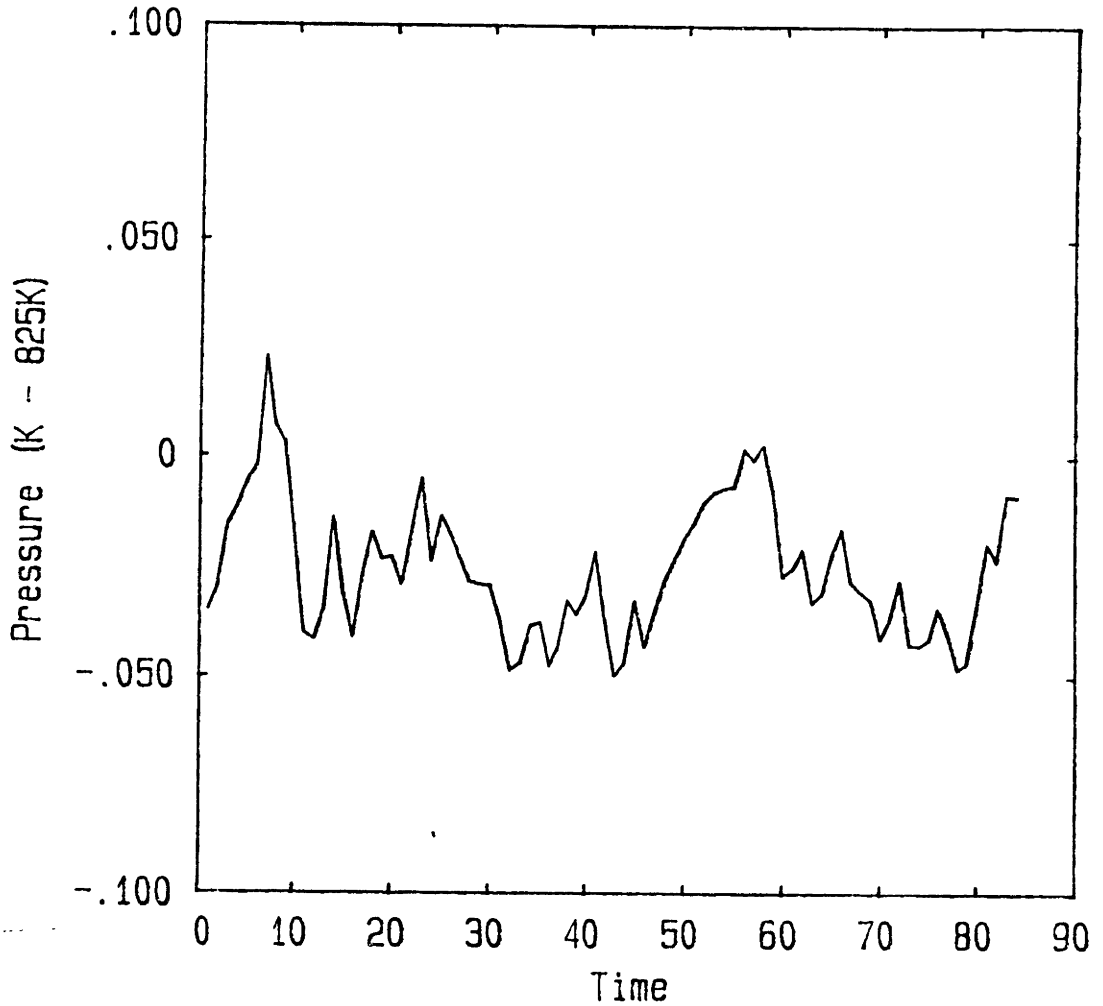

Figure 5-43: Pressure vs time in the fixed border model at 825K

Time variation of the system pressure at temperature 825K

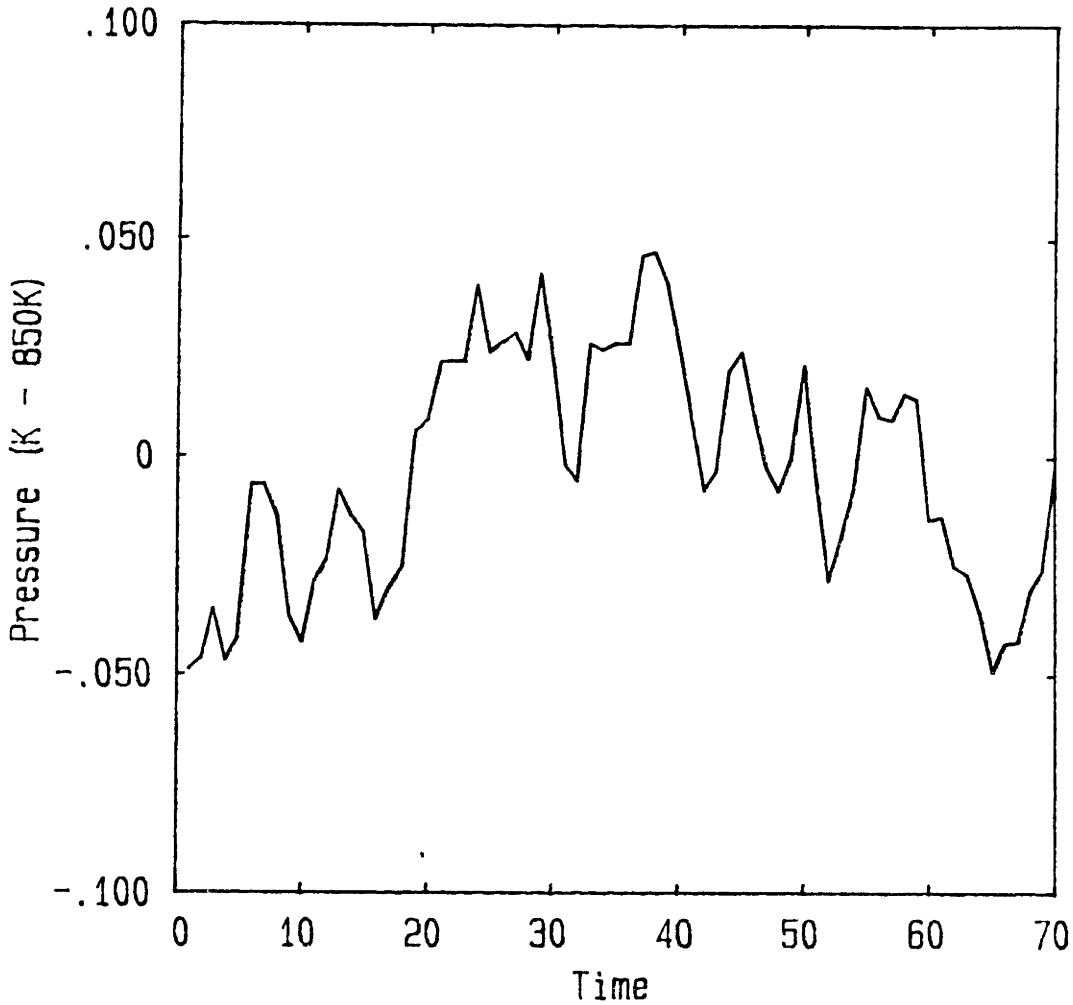

Figure 5-44: Pressure vs time in the fixed border model at 850K

Time variation of the system pressure at temperature 850K.

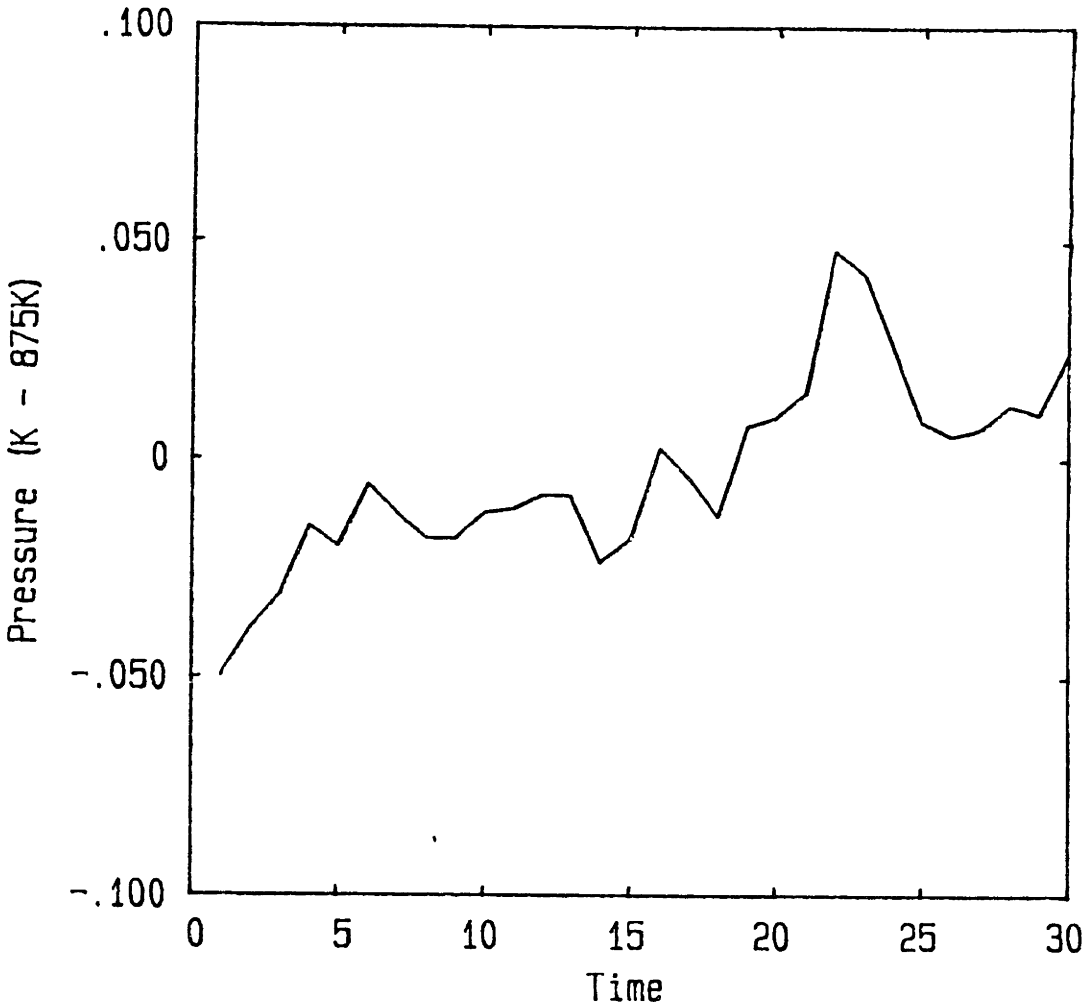

Figure 5-45: Pressure vs time in the fixed border model at 875K

Time variation of the system pressure at temperature 875K.

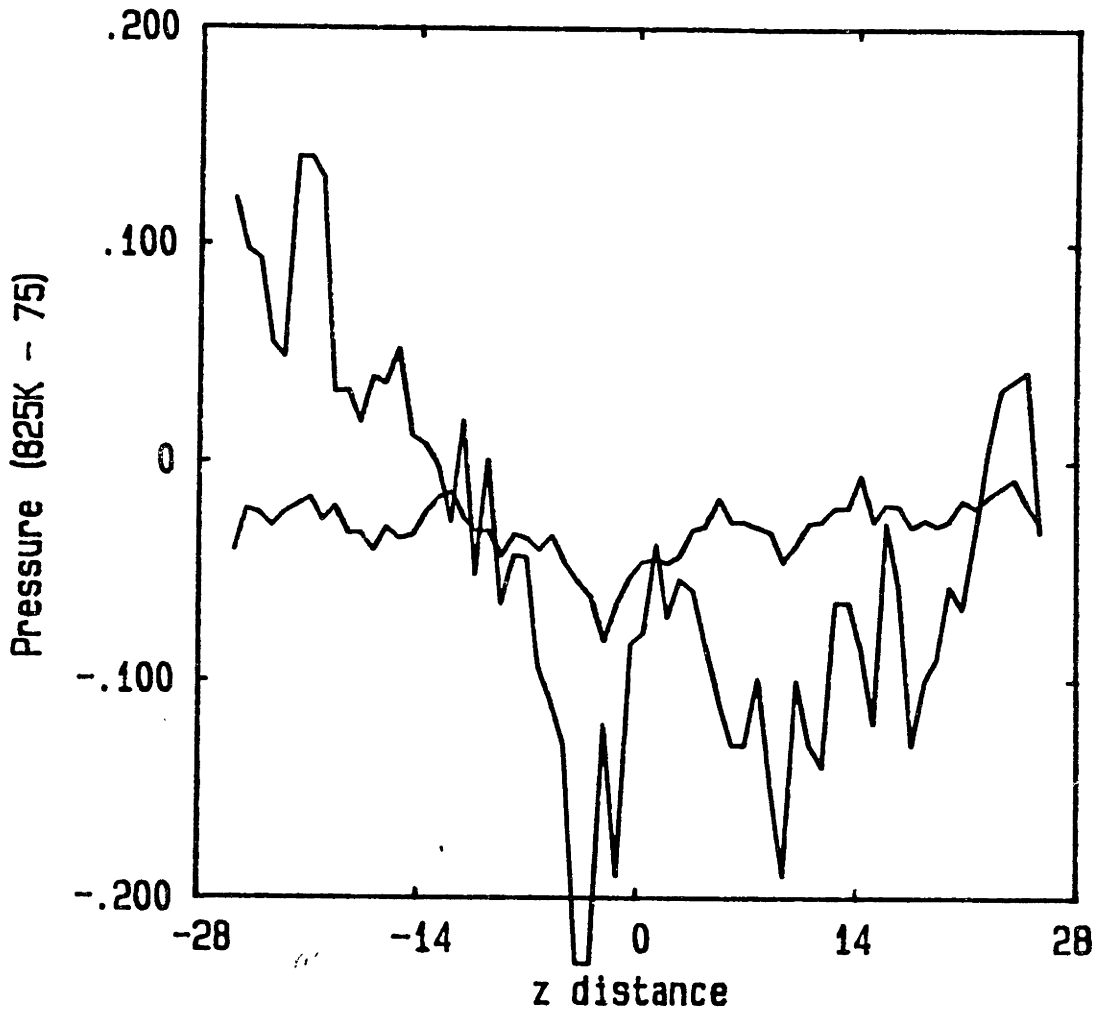

Figure 5-46: Pressure distributions in the fixed border model

Two pressure distributions (one is averaged over 1000 time steps, the other 20000 time steps) are shown for the bicrytal model at 825K and time step 64000.

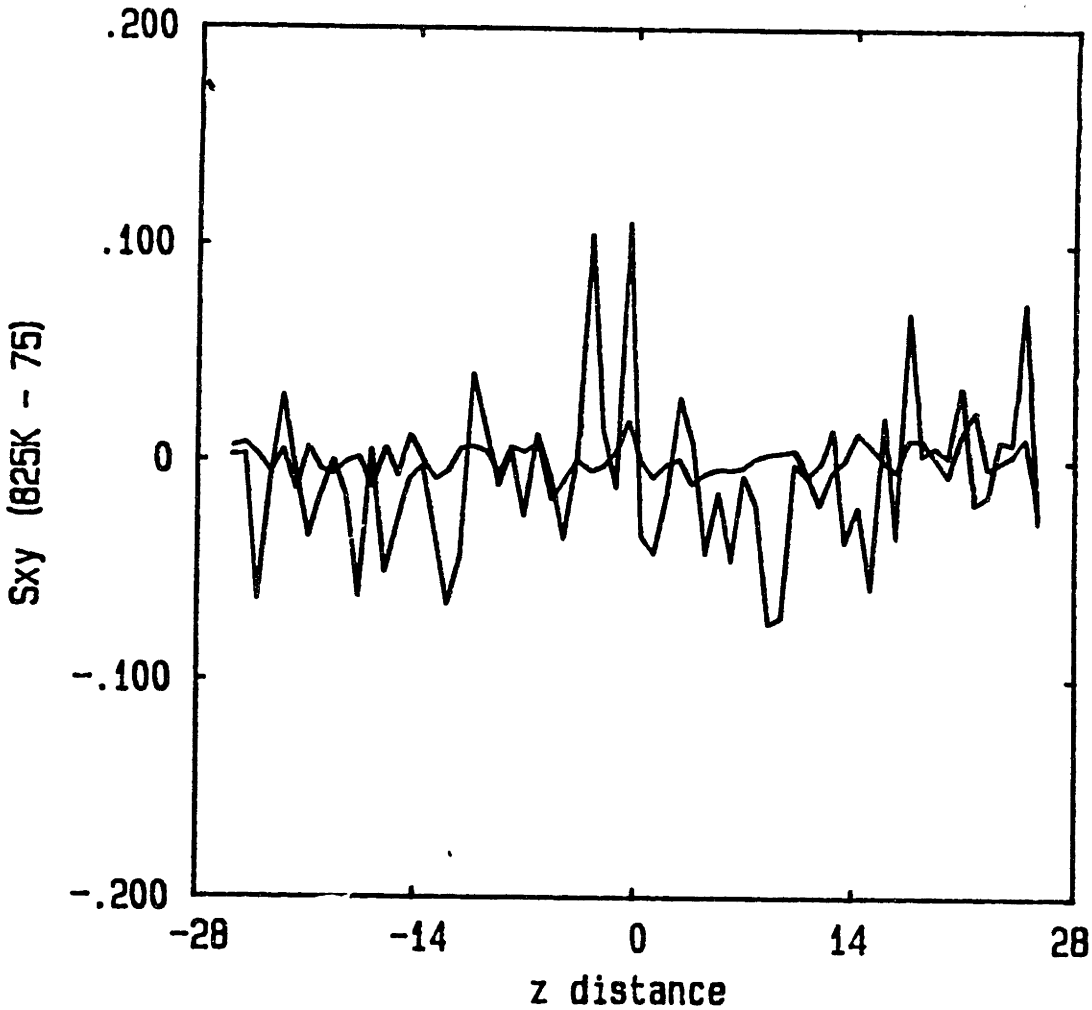

Figure 5-47: σ_{xy} distributions in the fixed border model

Two σ_{xy} distributions (one is averaged over 1000 time steps, the other 20000 time steps) are shown for the bicrytal model at 825K and time step 64000.

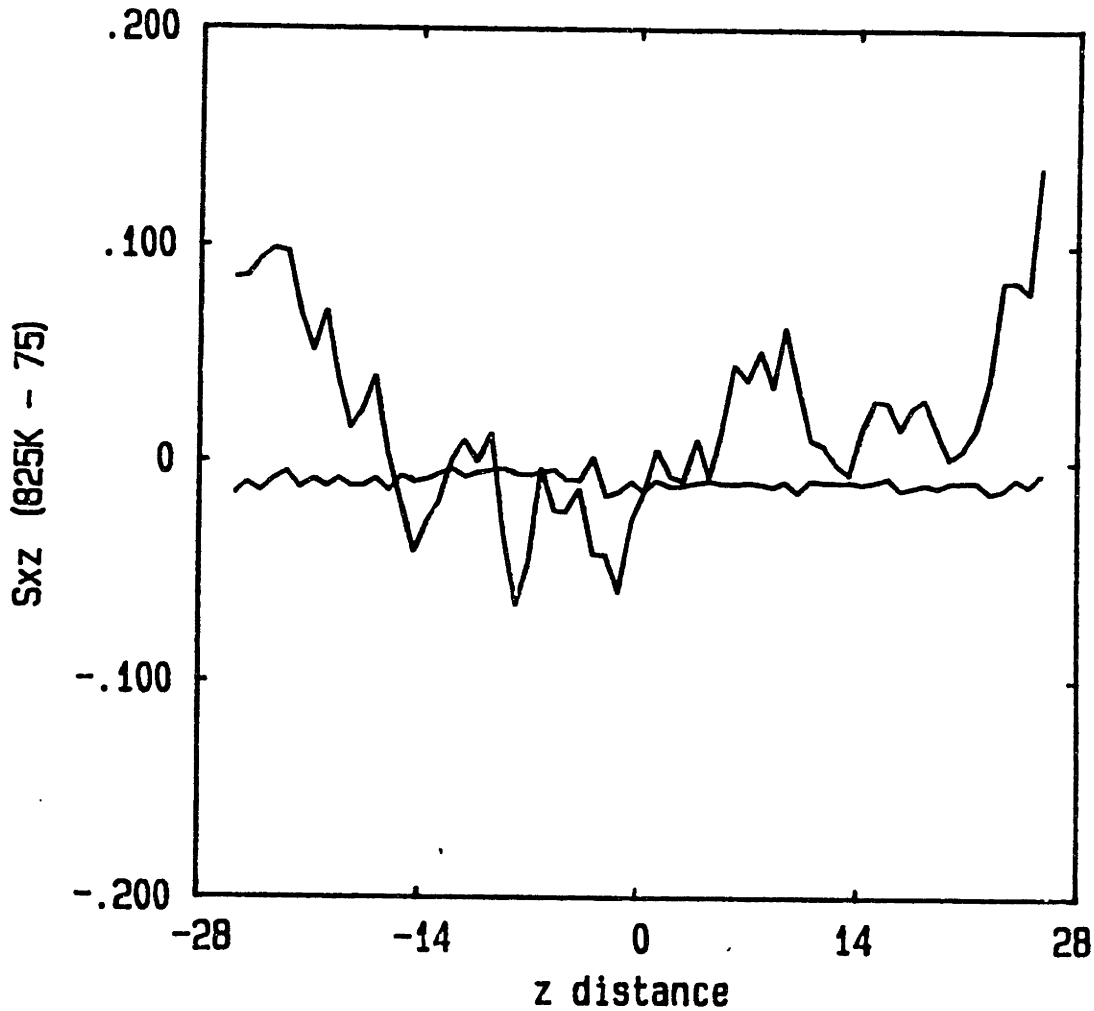

Figure 5-48: σ_{xz} distributions in the fixed border model

Two σ_{xz} distributions (one is averaged over 1000 time steps, the other 20000 time steps) are shown for the bicrytal model at 825K and time step 64000.

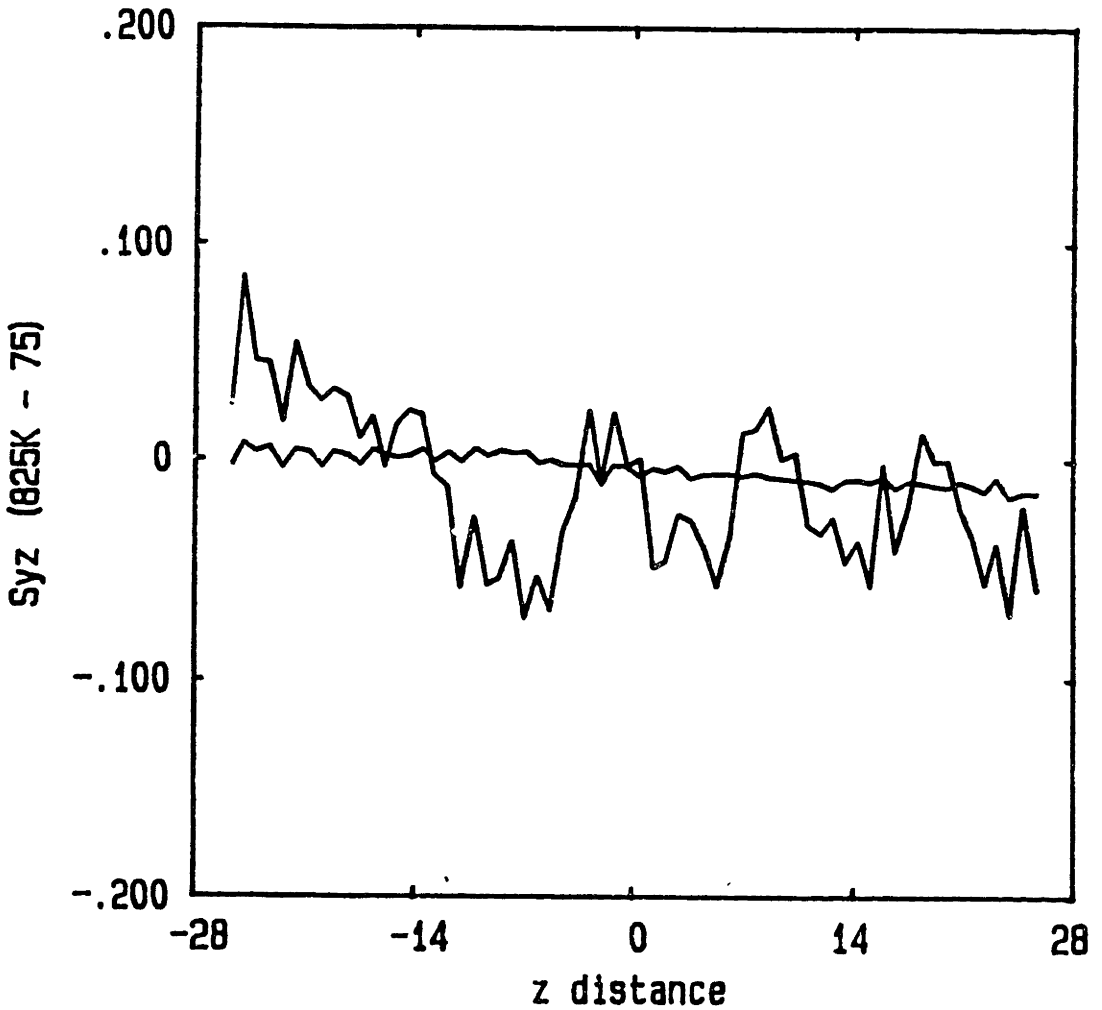

Figure 5-49: σ_{yz} distributions in the fixed border model

Two σ_{yz} distributions (one is averaged over 1000 time steps, the other 20000 time steps) are shown for the bicrytal model at 825K and time step 64000.

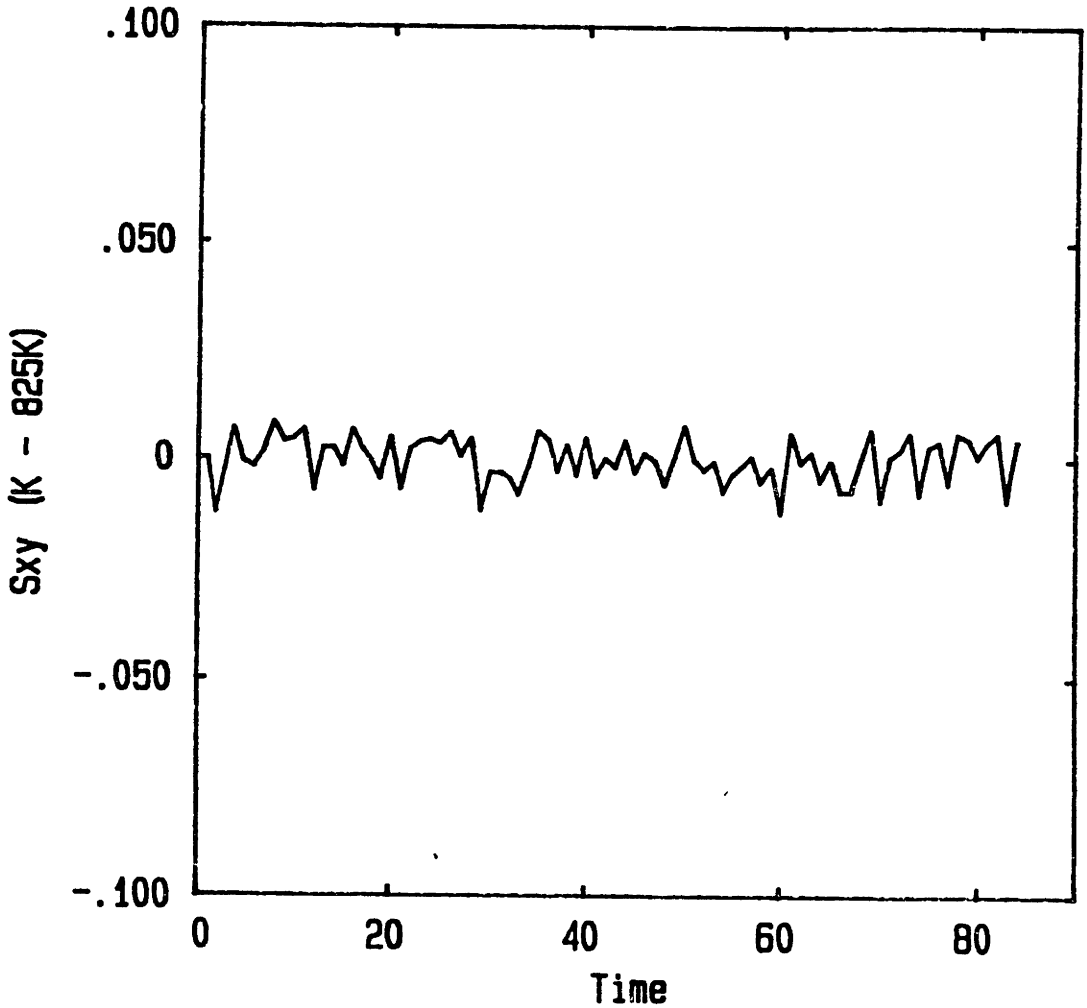

Figure 5-50: σ_{xy} vs time in the fixed border model

Time variation of the system σ_{xy} at temperature 825K.

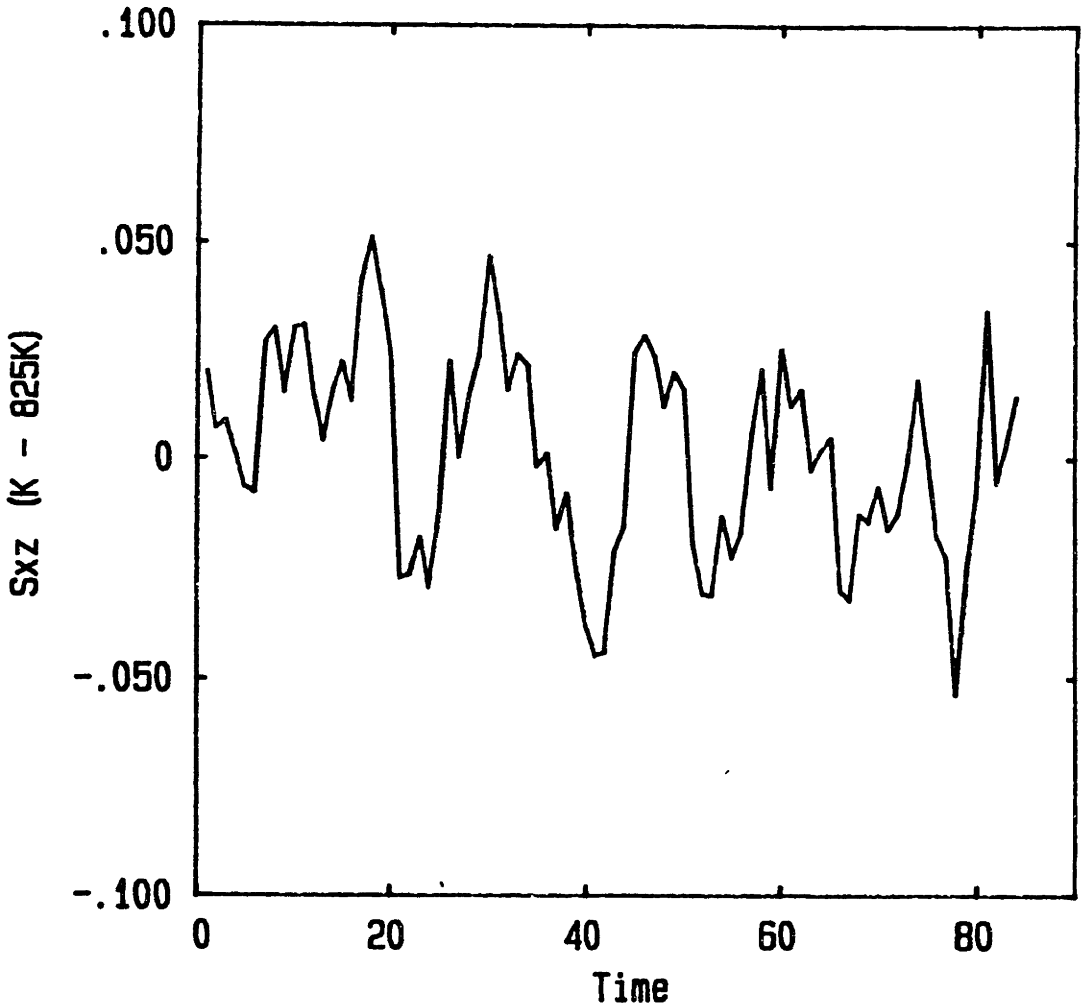

Figure 5-51: σ_{xz} vs time in the fixed border model

Time variation of the system σ_{xz} at temperature 825K.

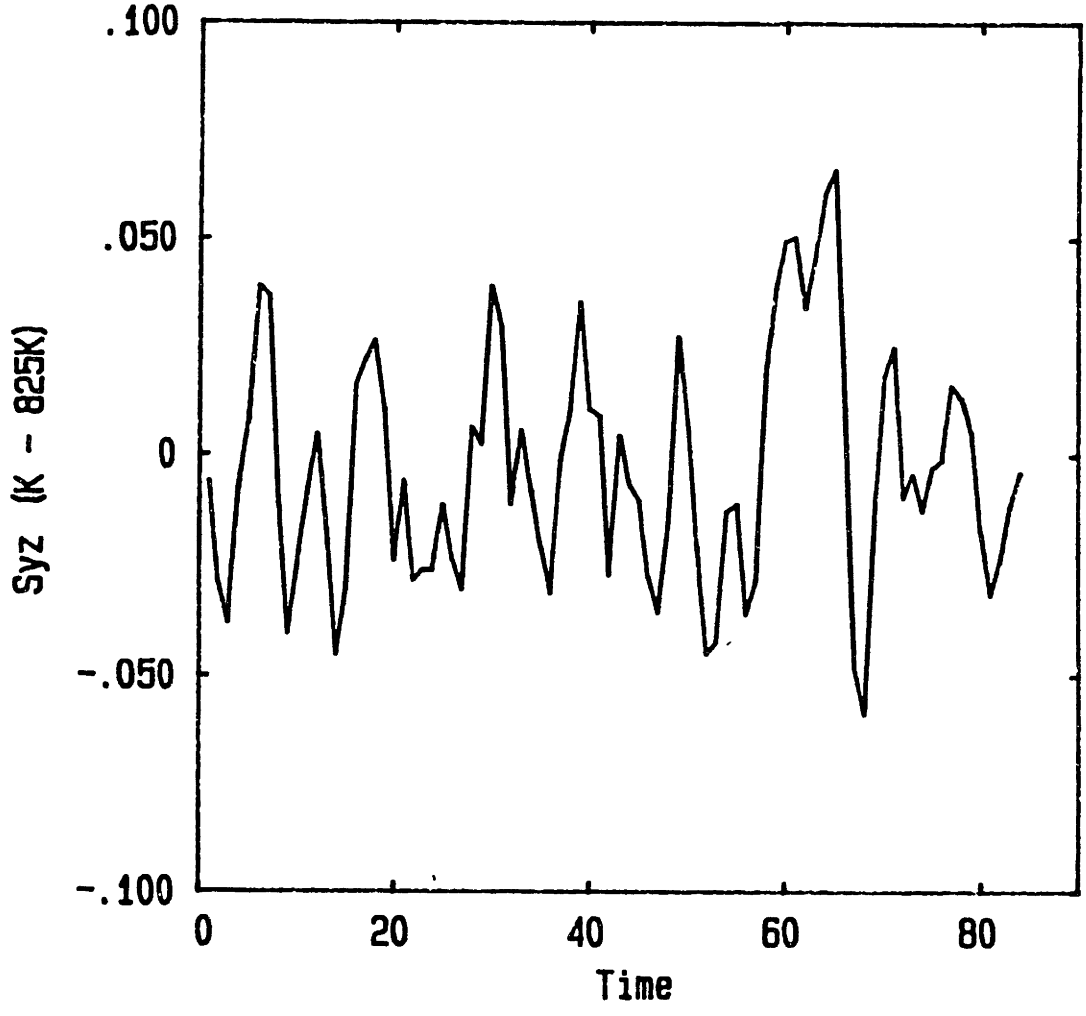

Figure 5-52: σ_{yz} vs time in the fixed border model

Time variation of the system σ_{yz} at temperature 825K.

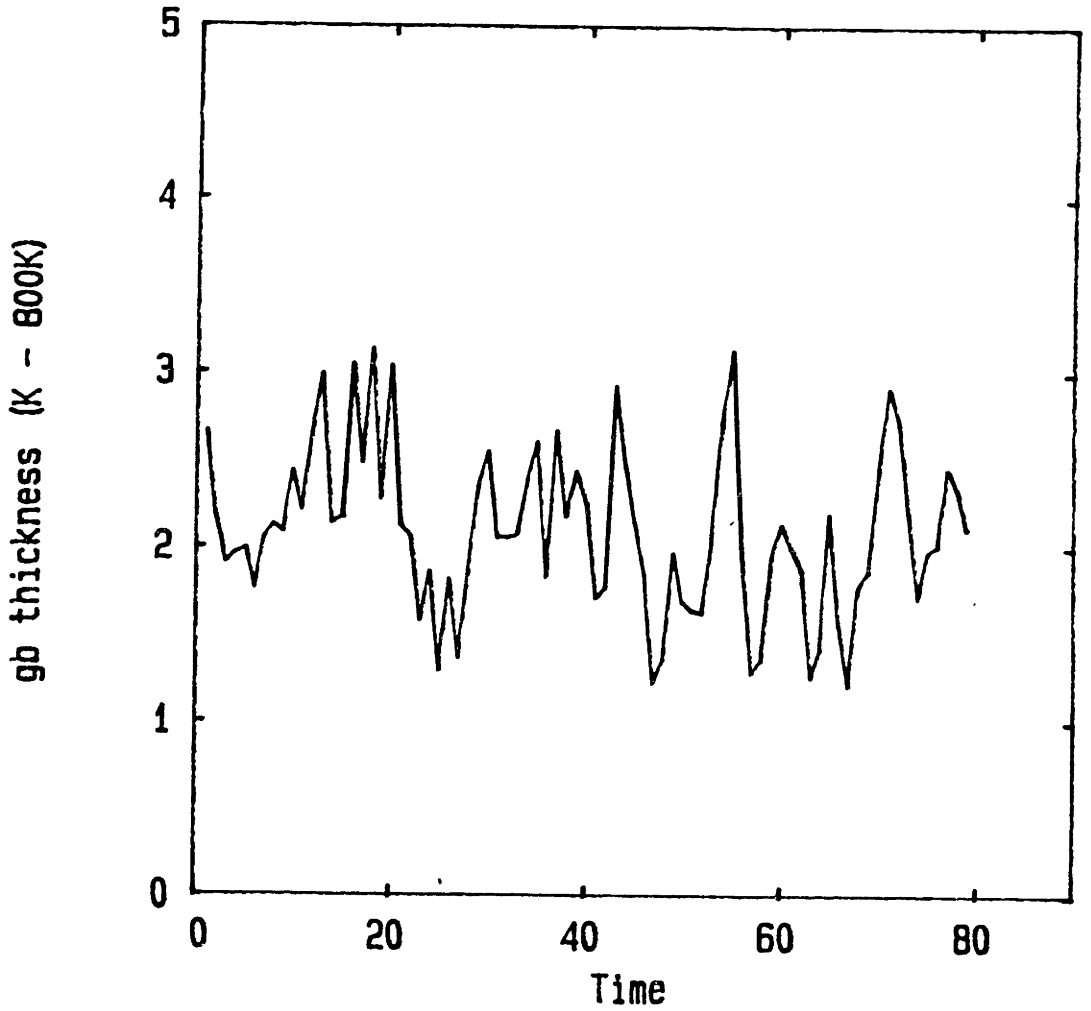

Figure 5-53: Gb thickness at 800K for the fixed border model

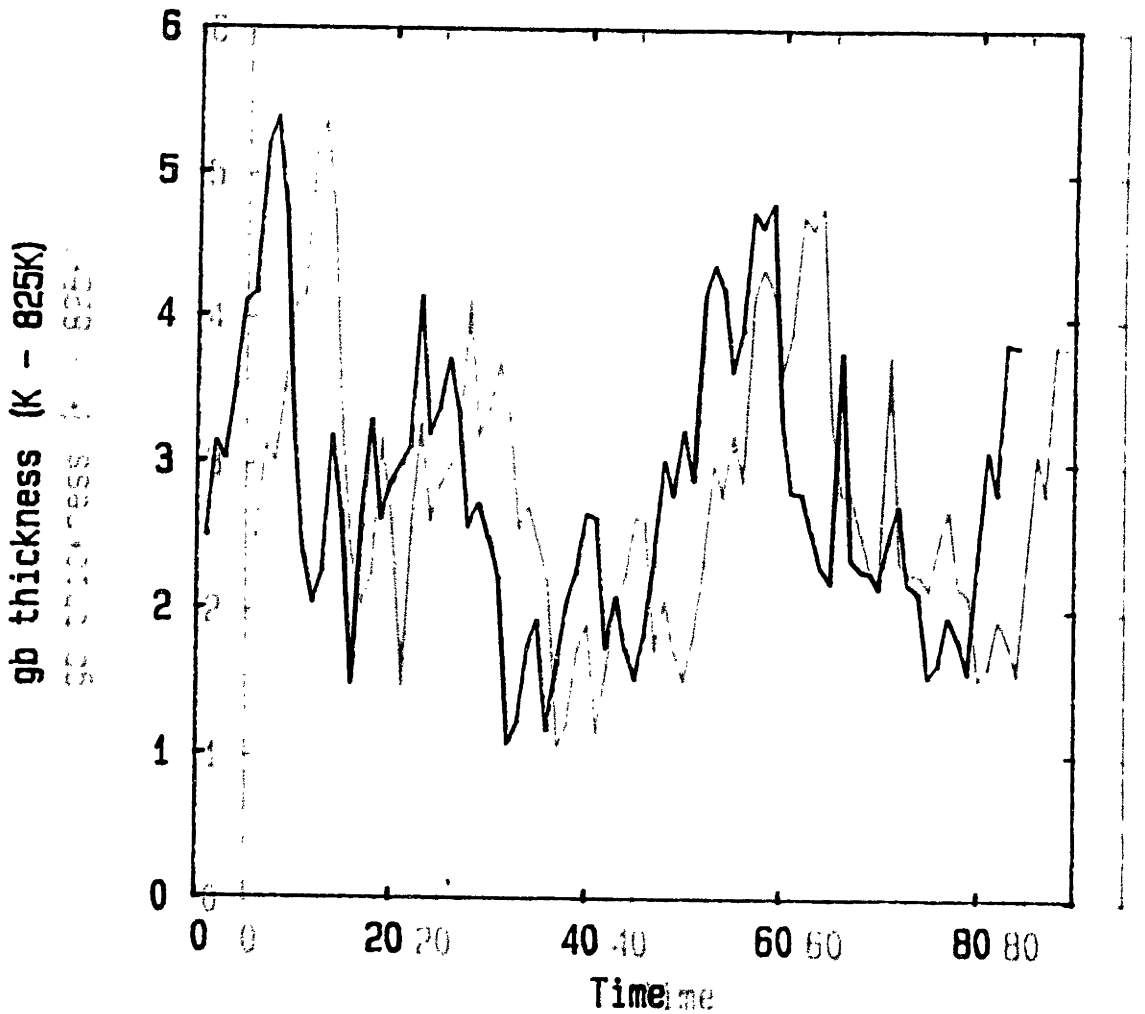

Figure 5-54: Gb thickness at 825K for the fixed border model

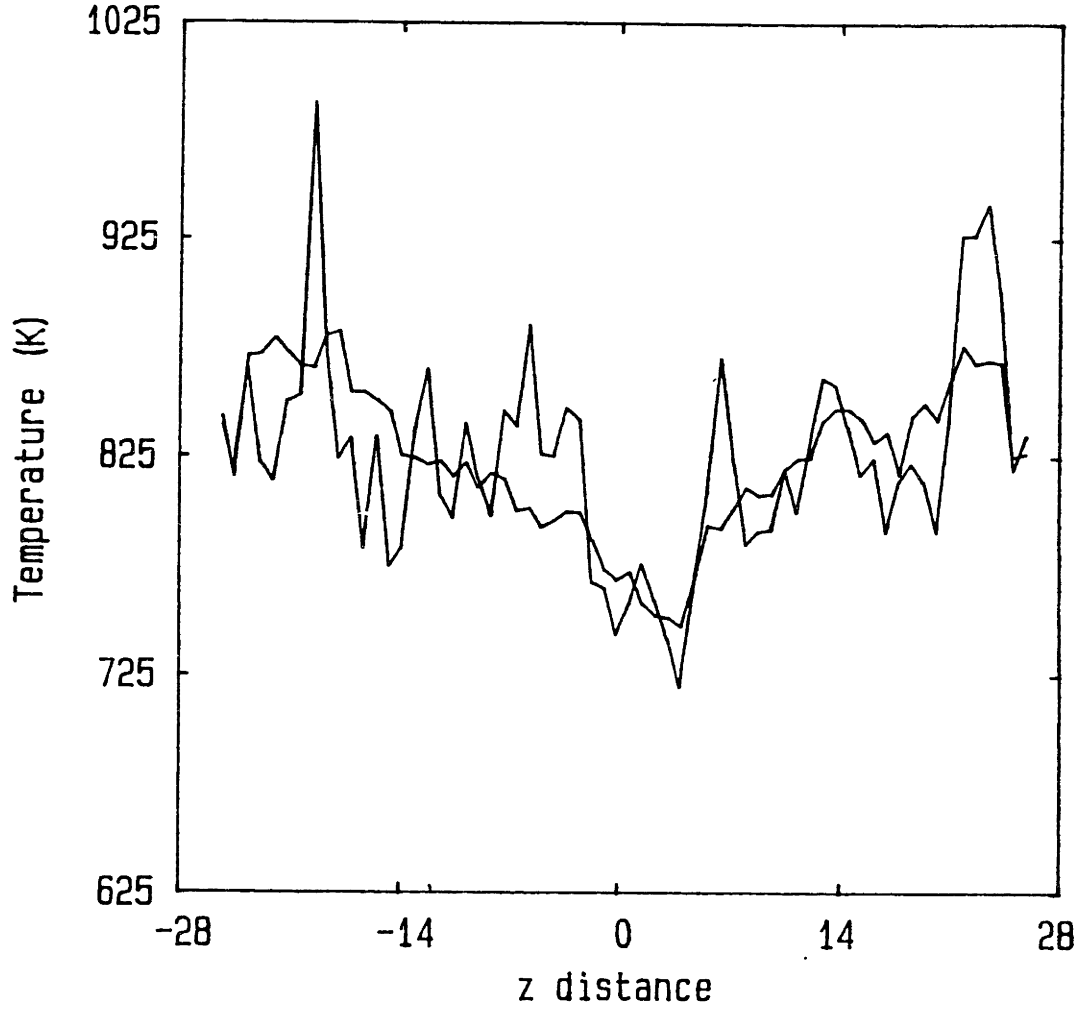

Figure 5-55: Temperature distributions in the semiperiodic border model

Two temperature distributions (one is averaged over 1000 time steps, the other 20000 time steps) are shown for the fixed border bicrytal model at 825K and time step 35000.

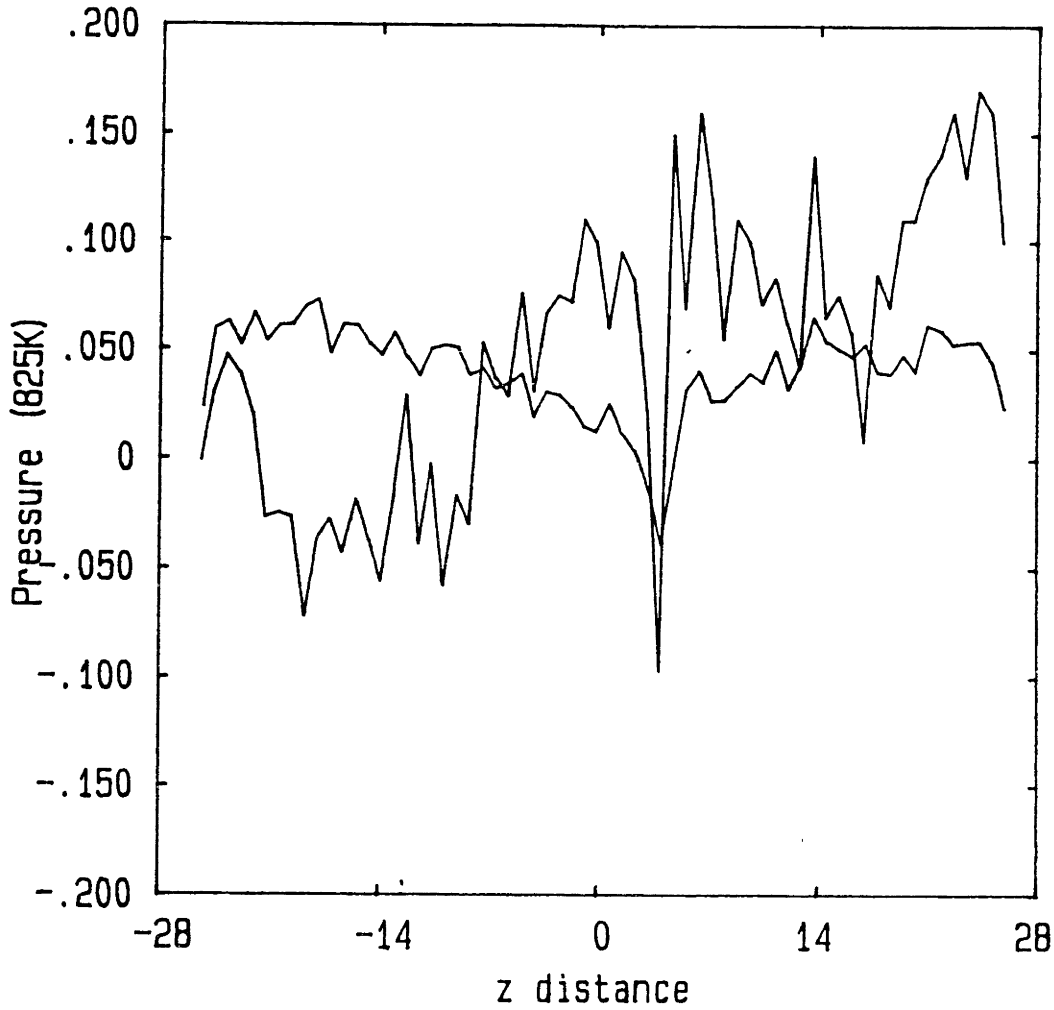

Figure 5-56: Pressure distributions in the semiperiodic border model

Two pressure distributions (one is averaged over 1000 time steps, the other 20000 time steps) are shown for the bicrytal model at 825K and time step 35000.

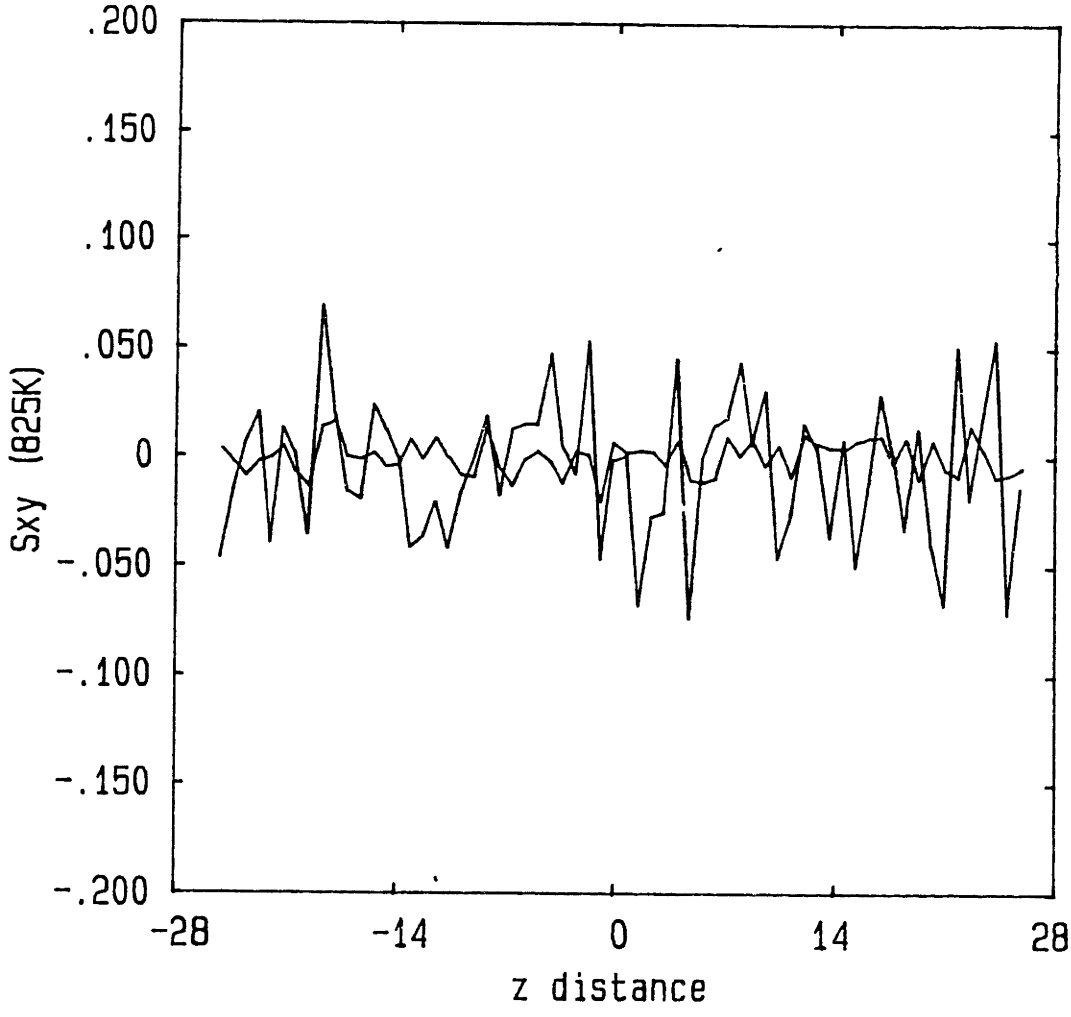

Figure 5-57: σ_{xy} distributions in the semiperiodic border model

Two σ_{xy} distributions (one is averaged over 1000 time steps, the other 20000 time steps) are shown for the bicrytal model at 825K and time step 35000.

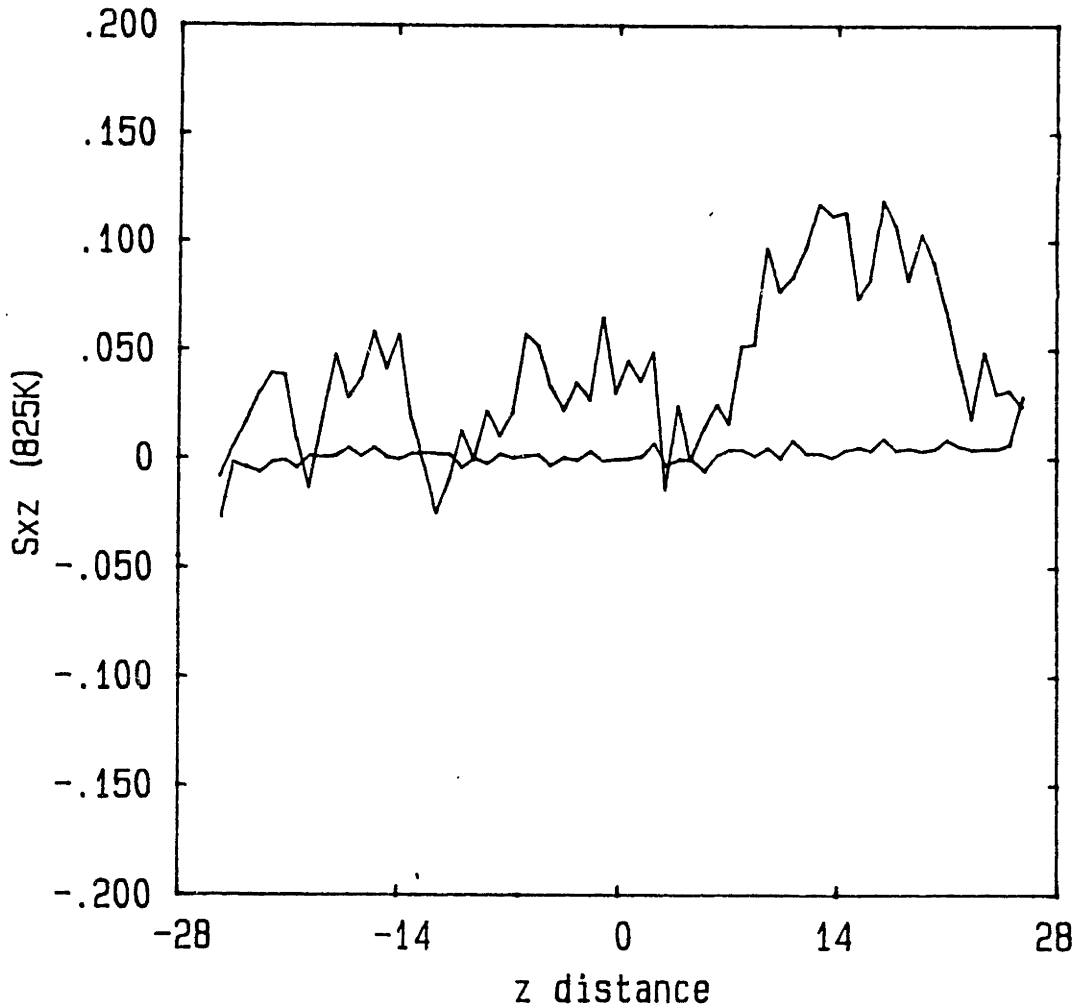

Figure 5-58: σ_{xz} distributions in the semiperiodic border model

Two σ_{xz} distributions (one is averaged over 1000 time steps, the other 20000 time steps) are shown for the bicrytal model at 825K and time step 35000.

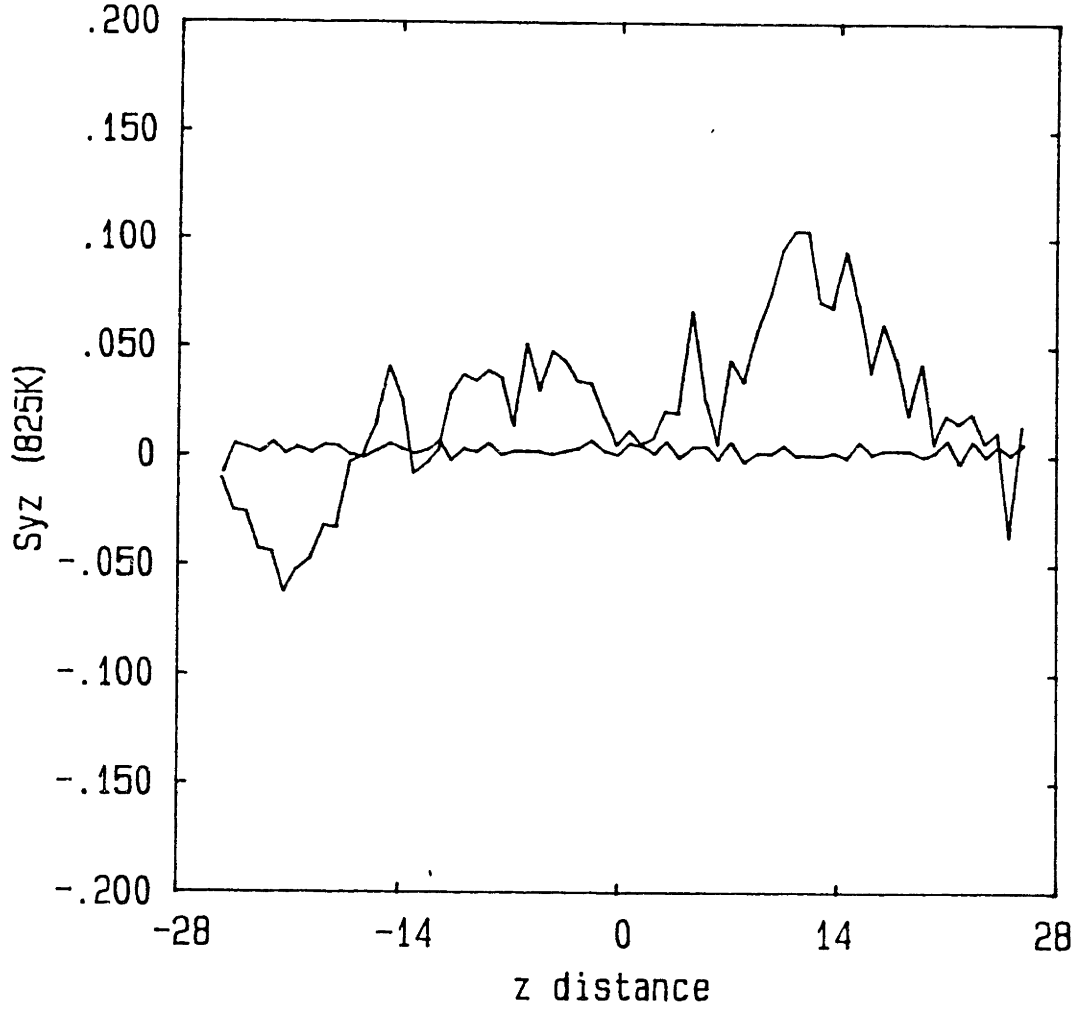

Figure 5-59: σ_{yz} distributions in the semiperiodic border model

Two σ_{yz} distributions (one is averaged over 1000 time steps, the other 20000 time steps) are shown for the bicrytal model at 825K and time step 35000.

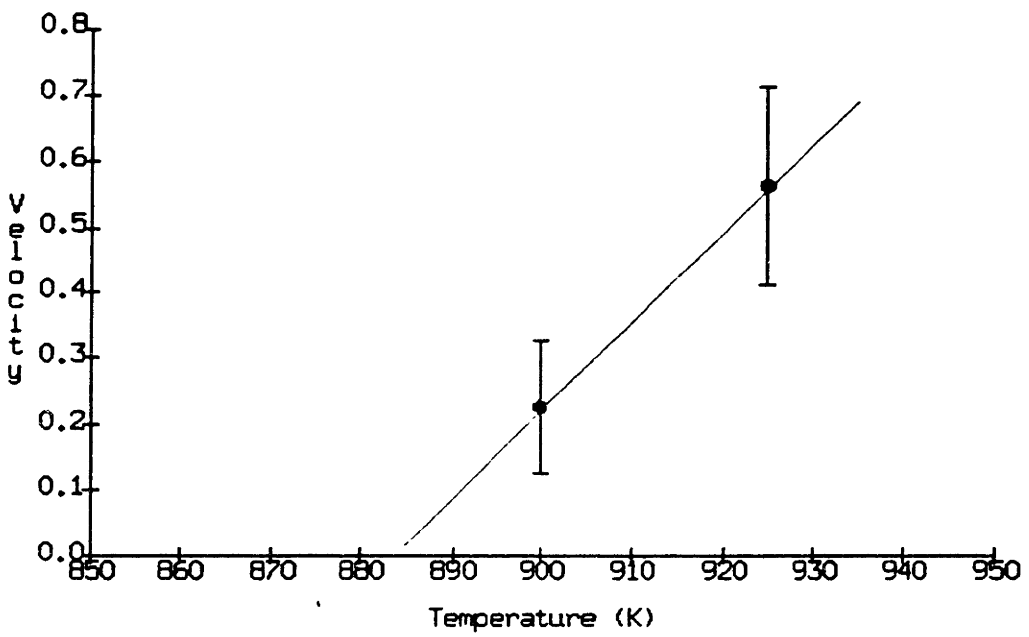

Figure 5-60: Propagation of the gb region in the semiperiodic model

The data are from the gb region of the semiperiodic border bicrystal model.

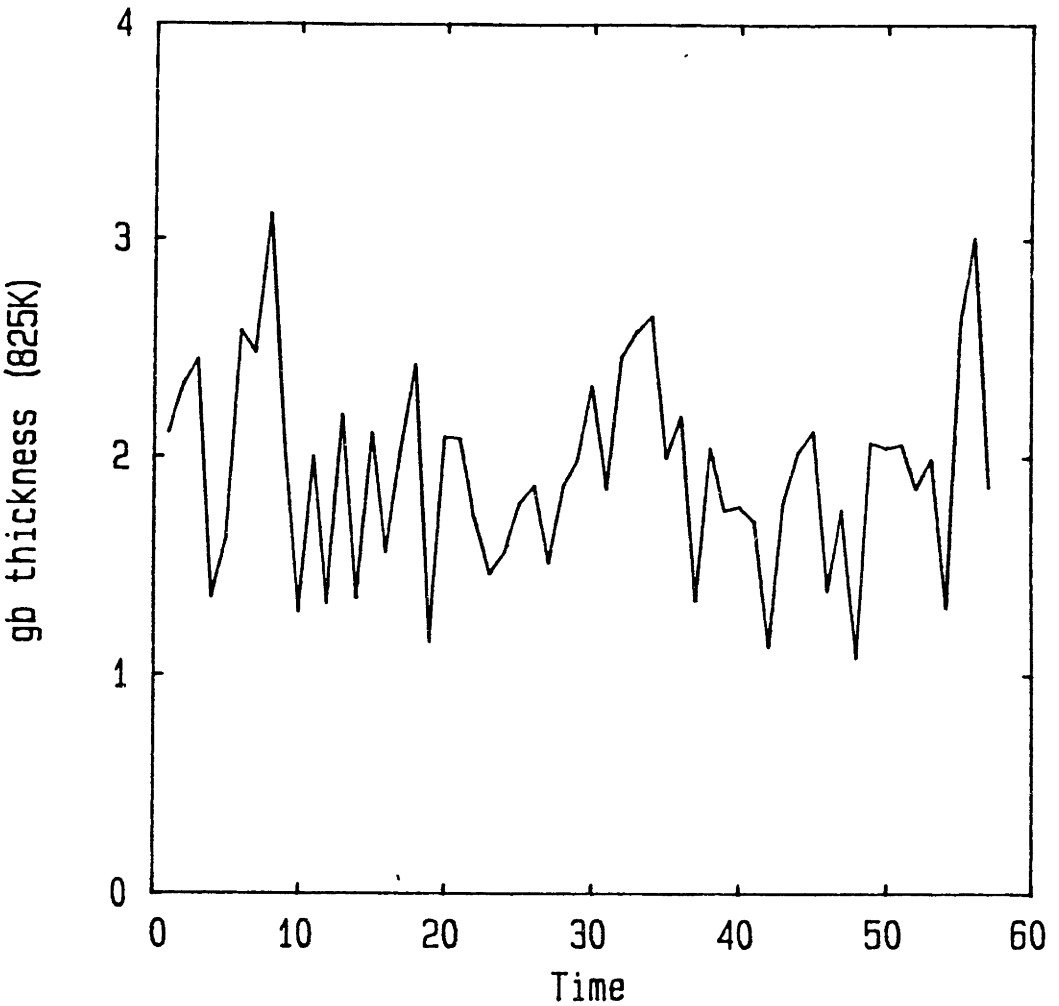

Figure 5-61: Gb thickness at 825K for the semiperiodic border model

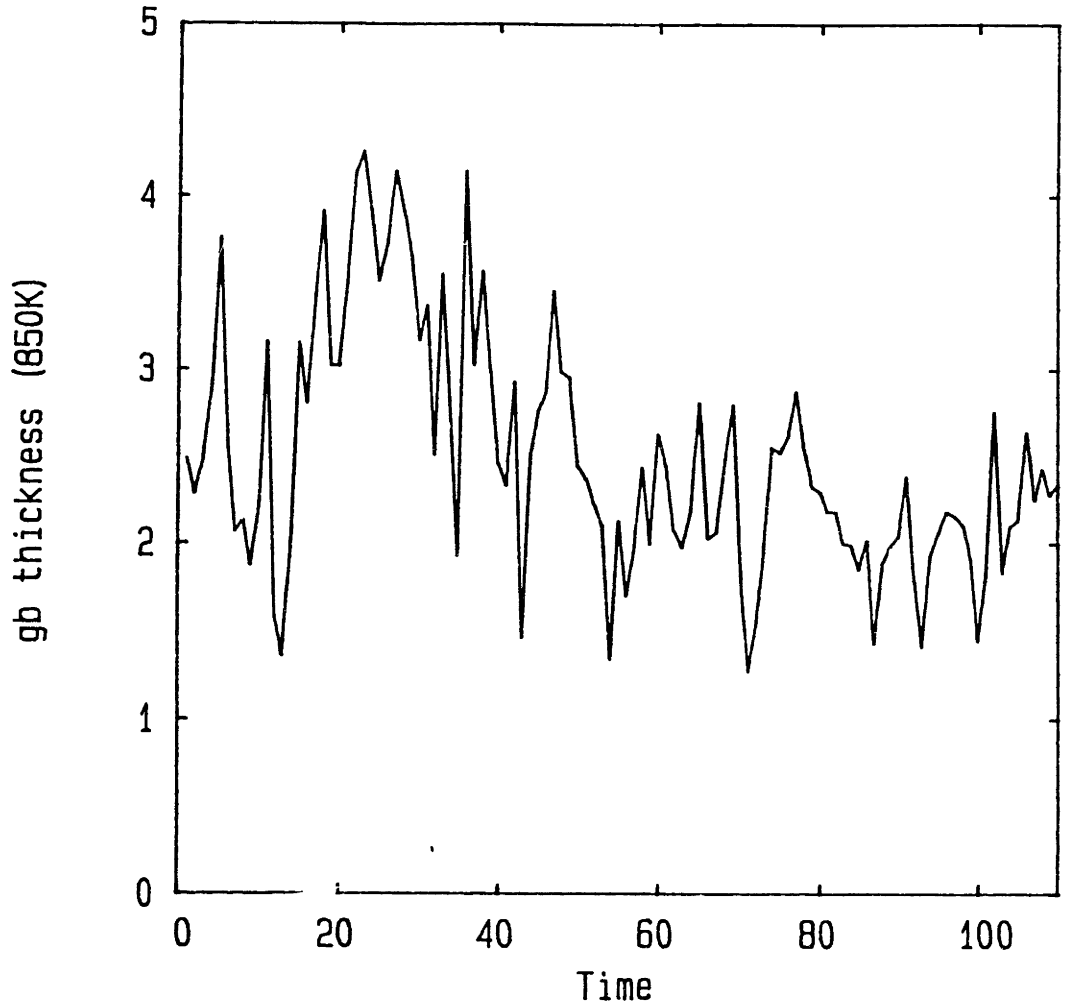

Figure 5-62: Gb thickness at 850K for the semiperiodic border model

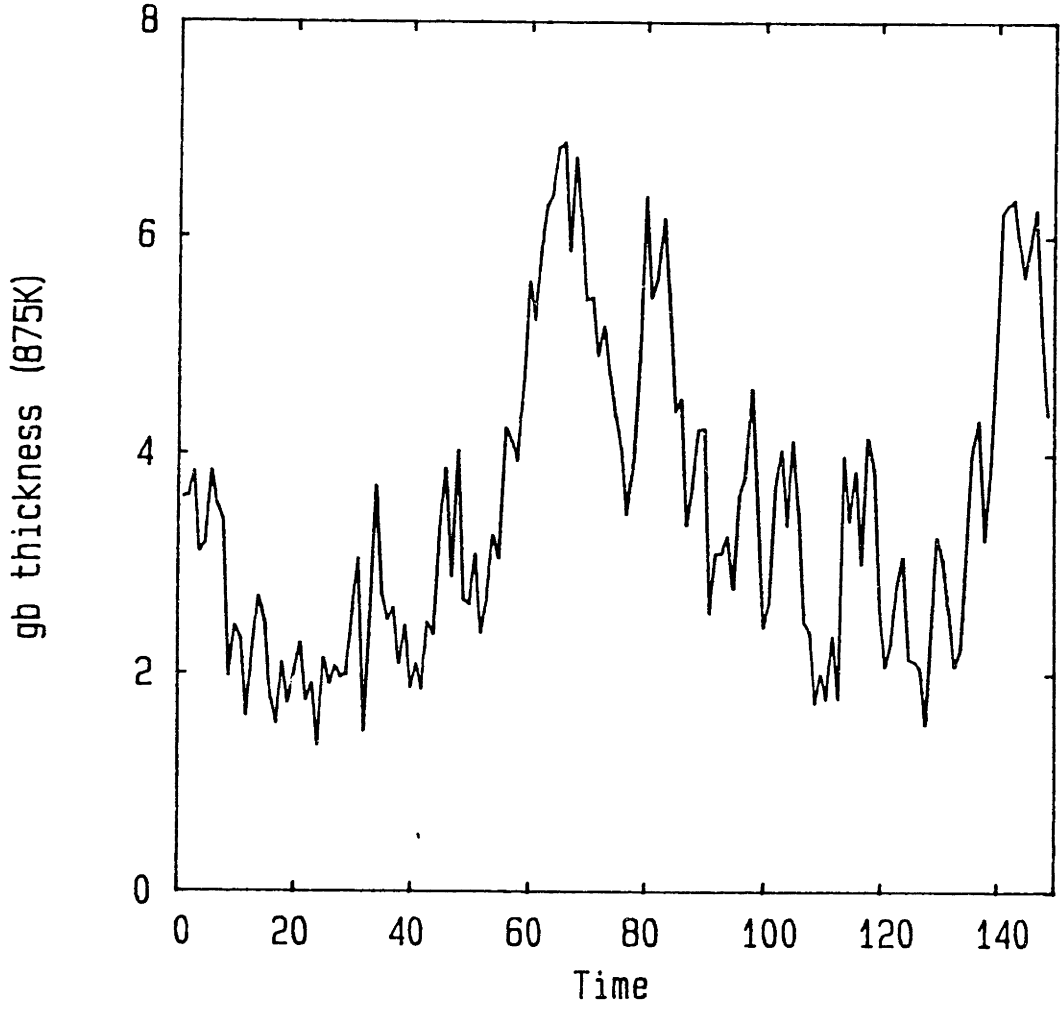

Figure 5-63: Gb thickness at 875K for the semiperiodic border model

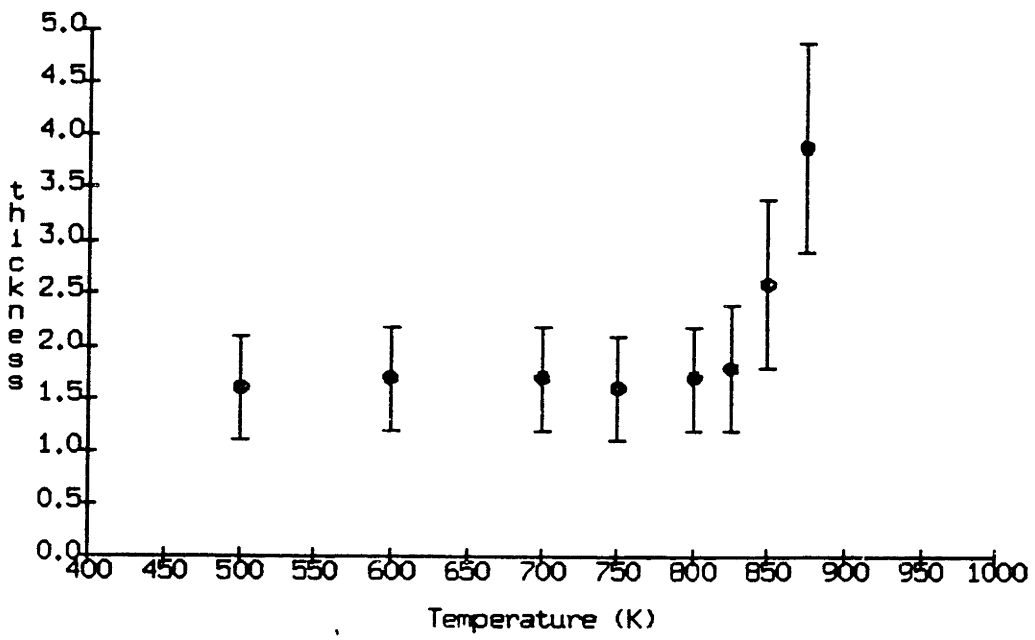

Figure 5-64: Gb thickness vs temperature in semiperiodic border model

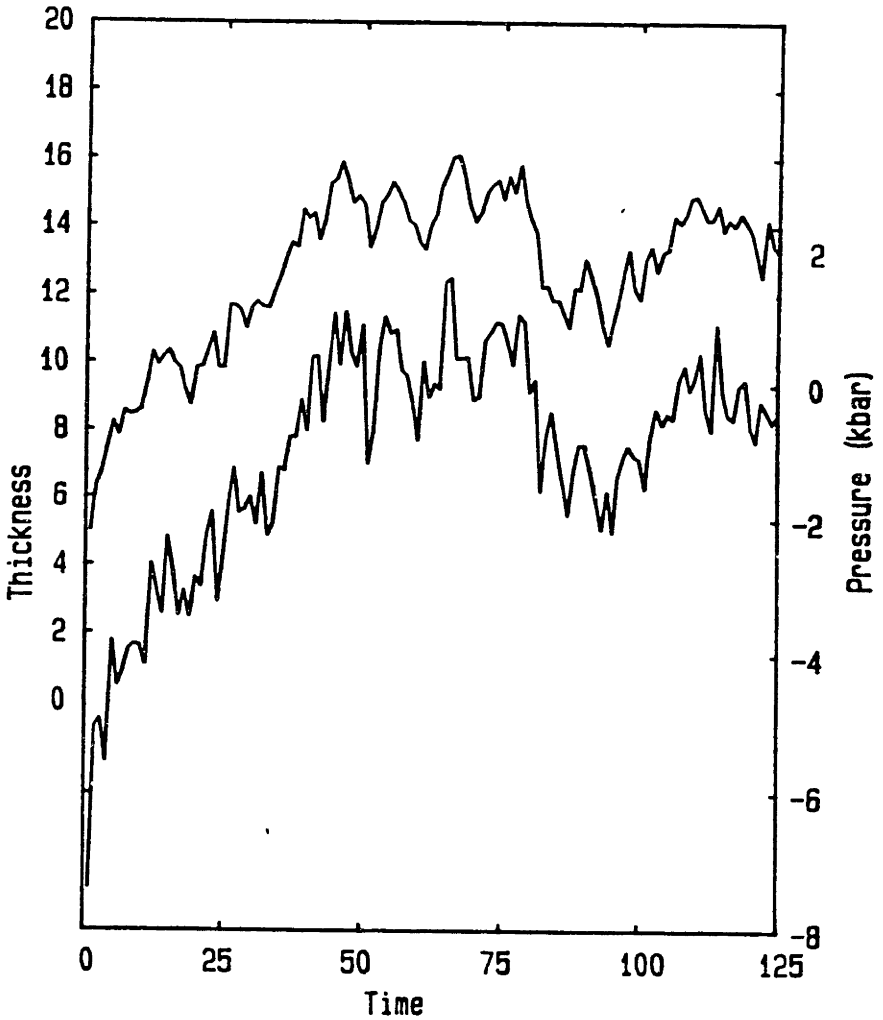

Figure 5-65: Gb thickness and pressure at 875K for Morse potential

The data are from model B. The lower curve is the pressure. The upper curve is the gb thickness.

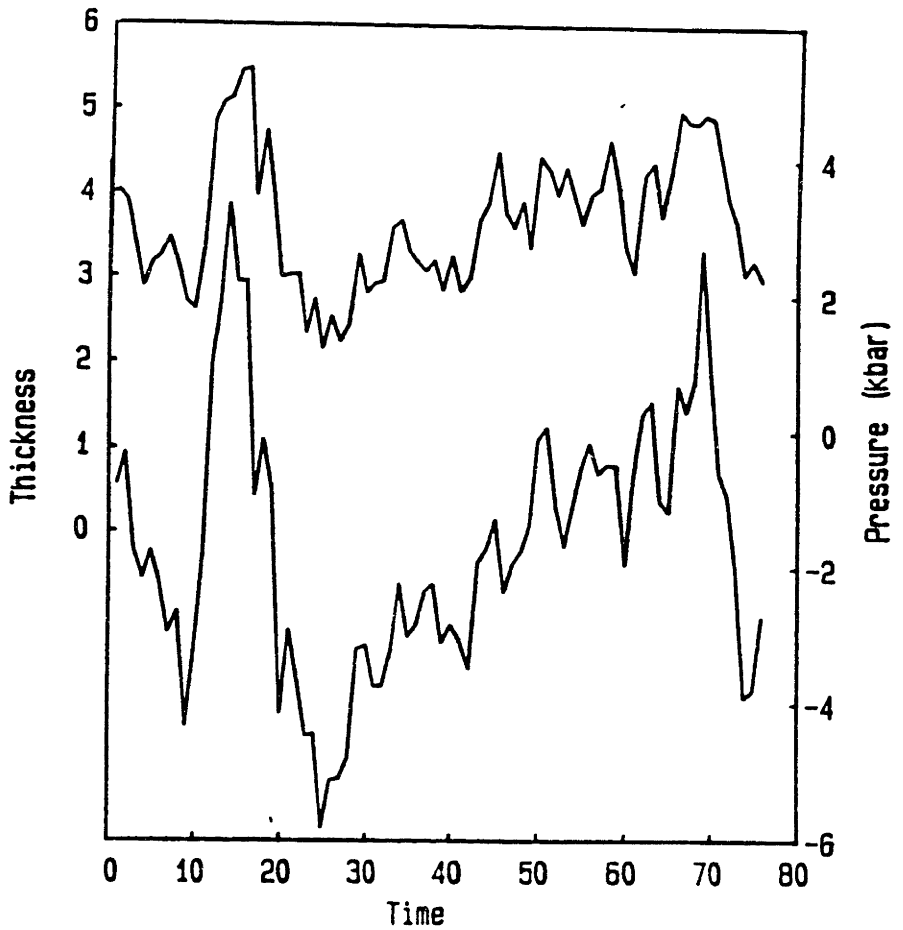

Figure 5-66: Gb thickness and pressure at 825K for Morse potential

The data are from model A. The lower curve is the pressure. The upper curve is the gb thickness.

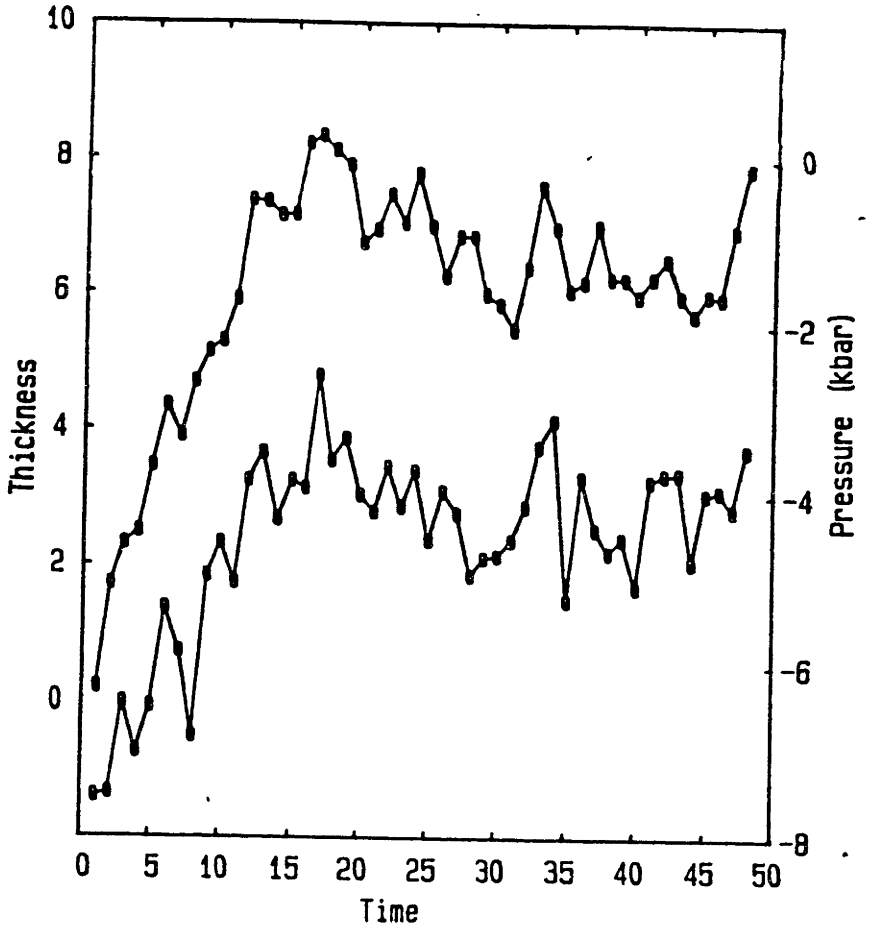

Figure 5-67: Gb thickness and pressure at 850K for Morse potential

The data are from model B. The lower curve is the pressure. The upper curve is the gb thickness.

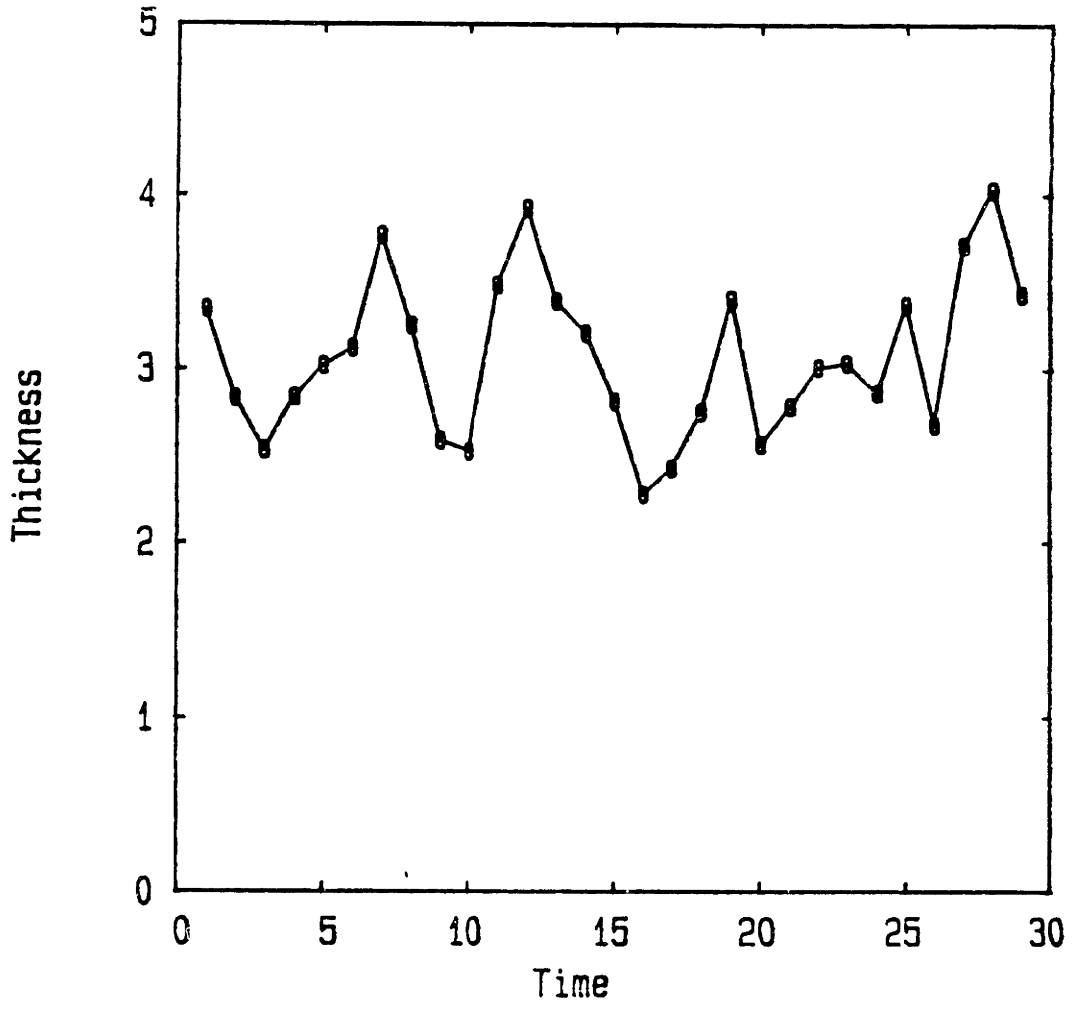

Figure 5-68: Gb thickness at 800K for Morse potential

The data are from model B.

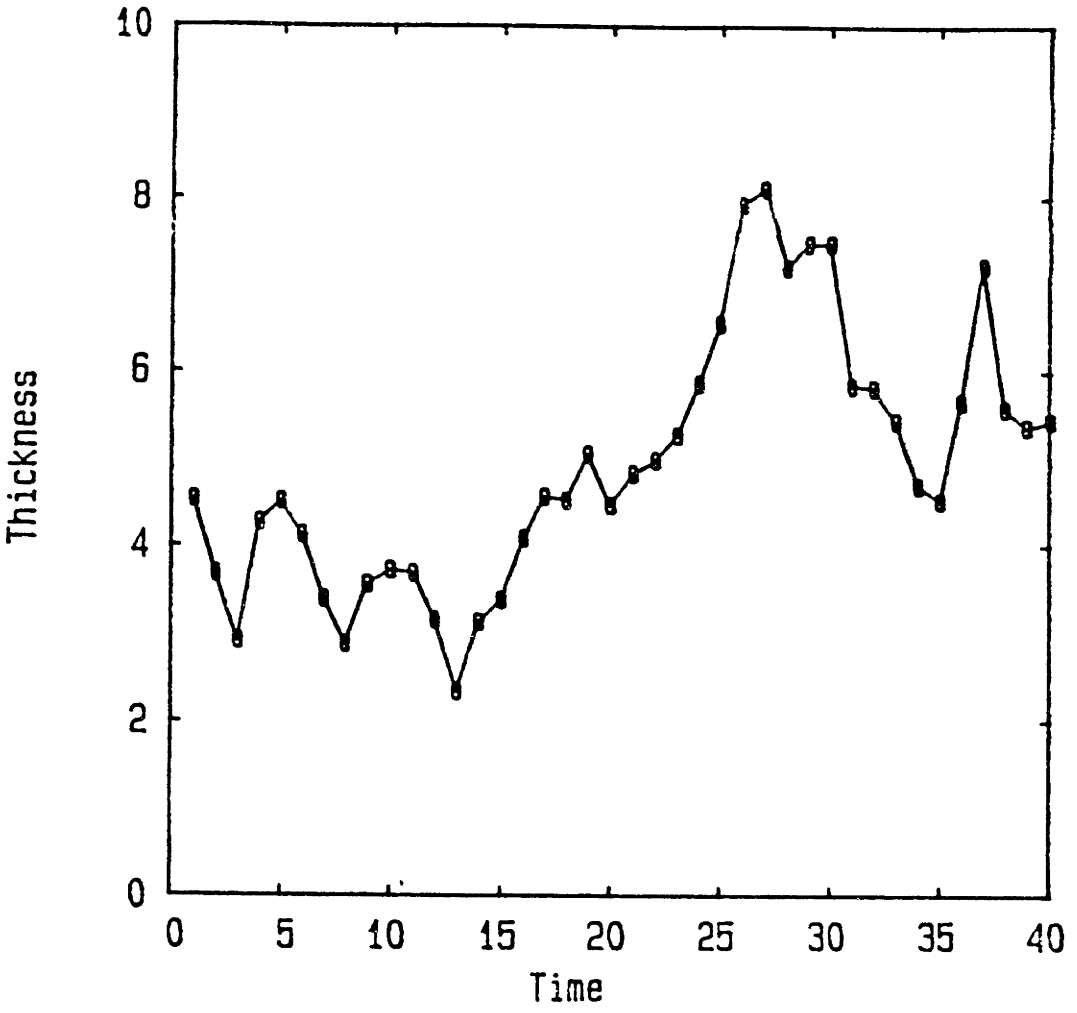

Figure 5-69: Gb thickness at 825K for Morse potential

The data are from model B.

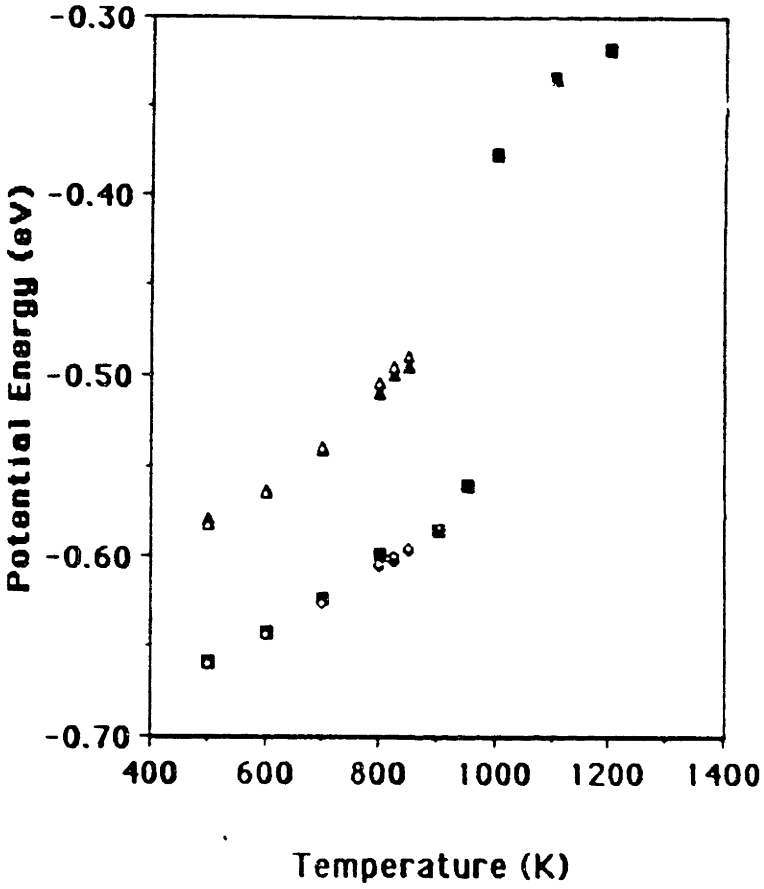

Figure 5-70: Gb energies vs temperature for Morse potential

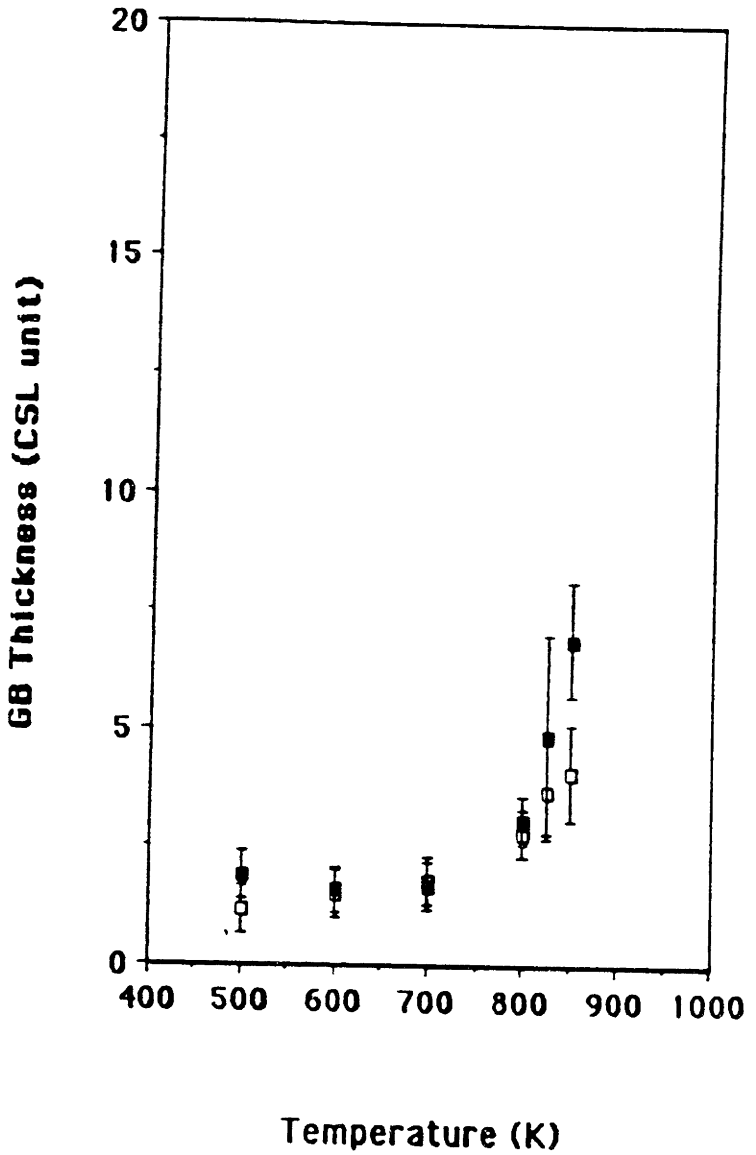

Figure 5-71: Gb thickness vs temperature for Morse potential

Chapter 6

Comparison and interpretation of previous simulation studies

The question of thermal disorder at an interface has been an active field of research in the past few years. Specifically, two interfaces received the most attention, free surface and gb interface. The free surface is an external interface while the gb is an internal interface, but in terms of thermal disorder, they behave in a similar way.

6.1 Thermal disorder in a model with free surface

It is now quite conclusive that melting initiated from the surface. However the question of surface premelting is still not settled. A recent review[5] which critically examined various experimental results and computer modelling results at the surface has concluded that more work is needed to clarify this point. A recent experiment[70] has shown that there is a molten layer at the surface in the temperature range immediately below T_m and the the thickness of this molten layer increase rapidly and continuously as the temperature approaches T_m. These authors have estimated that the surface becomes completely disordered at temperature 0.97 T_m. They also argued that this estimate is probably too conservative, that 0.97 T_m is the upper limit for the temperature at which the surface becomes completely disordered. This behavior is similar to the time averaged behavior of the free surface as presented in chapter 4. Since experimental data are taken for a long period of time (order of seconds) as compared with simulation time scale (order of psec), only time averaged properties could be compared. The simulation results also reveal the process in a much shorter time scale; the molten layer actually is in metastable state.

However, the work of Frenken et al. is not free of criticism. In a critical review by Pontikis et al.[5] of surface melting and roughening transition, they suggest possible

mechanisms which could affect the surface roughness and caution that further investigation of these effects is needed to properly evaluate Frenken's results.

Phenomenological models have been used also to study the problem of surface premelting. Using similar arguments as in the case of gb premelting[75] and thermodynamic analysis of surface excess quantities[81] the quasi liquid layer at the surface is found to be very thin until temperatures very close to melting. Theoretical analysis[71] has shown that the surface order parameter behaves continuously as $|T - T_m|^{\beta}$ with $\beta < 1$.

MD simulation is the only available method of providing atomistic scale information of the surface premelting phenomenon. However different models used have brought different conclusions regarding the thermal disorder of the surface. Broughton and Woodcock[72] using a model with a rigid layer substrate, have presented evidence for successive surface melting at 0.72, 0.80 and 0.99 T_m for the first three surface layers. However Broughton and Gilmer[21] used MD model without the rigid substrate have found no evidence of first order surface premelting transition. They observe continuous changes of the surfae properties in all three surfaces, (111), (110) and (100) up to 0.96 T_m. The premelting results obtained from Broughton and Woodcock are attributed to model artifacts from the rigid layer substrate[21] and also from the large surface to volume ratio of their model[74]. Rosato et al.[74] also studied (110) surface and have shown that surface premelting cannot occur for that surface at temperatures below 0.95 T_m. They have also found that below this temperature, the surface retains its solid-like characters.

These simulation results are consistent with the present work on the thermal disorder at the surface in which we found no premelting up to T_m. These results are also in qualitative agreement with the present work about the onset of the thermal disorder. They have found ordered surface up to 0.96 T_m and 0.95 T_m for stable surfaces such as (111) or (110). In the present work, we have used (310) surface which is more unstable and have found well ordered surface up to 0.93 T_m. It is reasonable to expect that a more stable surface will retain its solid-like characteristics to higher temperatures.

However the present results differ from those of Stoltze et al.[73] in which surface melting was found at temperatures as low as 200K below melting (or an equivalent of 0.75 T_m) for (110) aluminum surface using an effective-medium interaction potential. Their model employed rigid layer substrate which has been discussed by Boughton and Gilmer[21] to be a possible cause for the difference in behavior of the (100) LJ surface between their model and that of Broughton and Woodcock.

6.2 Thermal disorder in gb interface

Thermal disorder at the gb interface has also received much attention. Gb sliding and migration experiments[8] have shown that the activation energy associated with the sliding rate of the bicrystals changes at a certain temperature T_c which ranges between 0.7 to 0.9 T_m for high angle gb. This change was attributed to a gb structural transformation but there is no evidence of gb premelting. The rotating spheres on-a-hot-plate experiments[9,10] have led to the conclusion that essentially all gb could not have been completely melted upto .99 T_m because of the rotation of the spheres due to the dependence of their energy on crystal misorientation. However this does not exclude the possibility that the gb region is highly disordered but still correlated with the single crystal material in the two grains adjoining the boundary.

More recently, direct observations of the gb structures at temperatures near T_m have been performed[12,13] by hot stage TEM to locate grain boundary dislocations (gbd) and to observe the partially melted polycrystalline aluminum specimen. Results from gbd observations indicate that gb structures remain ordered upto .96 T_m. Observations of the partially melted polycrystalline aluminum specimen lead to the conclusion that there is no complete gb melting in aluminum below .999 T_m. However this technique does not offer any information of the thermal disorder of the gb which preceeds the complete melting process.

On the computer modeling side, 2-d lattice gas model study of Kikuchi and Cahn[15] has suggested a gradual transition which leads to complete melting at T_m. Ciccotti et al.[18-20] studied the temperature dependence of a high angle Σ 5 gb using Lennard-Jones (LJ) pair potential and obtained results which appear to be in qualitative agreement with Kikuchi and Cahn. Their results indicated the onset of a gradually disordering transition at 0.5 T_m. However limitations of their border condition (periodic border condition PBC) leads to the mutual annihilation of the gb at 0.9 T_m, thus excluding any information on the gb structure near T_m.

Broughton and Gilmer[21] have also investigated gb premelting in different tilt gb by calculating interface excess free energy through harmonic analysis of the ground state configurations and comparing with MD results. They found gb premelting only in the high angle gb at T_m while other gb remain ordered up to T_m. They concluded that gb premelting is not a true phase transition at temperature below T_m since the thermodynamic parameters are continuous functions of temperature. Also the quasi-liquid (disordered region at the interface) must retain some crystalline symmetry because of the small gb region below T_m. Lutsko and Wolf[25] also studied gb disordering at high temperature and found that twist gb structure is ordered up to 0.85 T_m. They also suggested that the frustration of gb migration in 3d periodic border condition could cause the thermal disordering in the gb structure.

These results are in agreement with the present work in which there is no gb premelting up to T_m. We have also found evidence supporting the suggestion[21] that the thermodynamic parameters should be continuous function of temperature and the disordered gb region must retain some crystalline symmetry because of the finite layer thickness at temperatures below T_m.

However, Deymier et al.[22] have studied 2d and 3d bicrystals and found evidence for a first order phase transition at 0.8 T_m through excess free energy calculations. It has been suggested recently[82] that the frustration of the gb migration may cause the premelting effects in a 3d periodic model.

Chapter 7

Conclusion

In this thesis we have made a systematic molecular dynamics study of the thermal disorder that can occur in a bicrystal and have obtained results that contribute to the resolution of the question of gb premelting. Although our results are specific to a particular gb structure and a certain potential function, we believe it is possible to draw more general conclusions by comparing the present work with experimental findings and other simulation results in the literature.

Based on the explicit results concerning structural order, energy and mobility obtained from the present simulations, we find that our bicrystal model shows no evidence of premelting (complete melting below T_m). Both the surface and the gb interface exhibit thermal disorder at temperatures below T_m with complete melting occurring at or very near T_m.

Concerning the details of the onset of melting, the data show considerable disordering in the interfacial region starting at about 0.93 T_m. The interfaces exhibit metastable behavior in this temperature range, and the temperature variation of the interfacial thickness suggests that the disordering induced by the interface is a continuous transition as predicted by Lipowsky et al.[83] Our results also indicate a close similarity between the disordered behavior at the external surface and at the internal surface (gb) having the same orientation. This is of interest in view of current theoretical and experimental studies of surface disordering; in fact the theoretical connection between gb melting and surface-induced disordering has been pointed out recently[83].

The conclusion of our work regarding the absence of gb premelting is consistent with the most recent experimental observations. Rotating spheres on-a-plate experiments[10] have

shown that essentially all gb could not have been completely melted up to 0.96 T_m because of the rotation of the spheres due to the dependence of their energy on the crystal misorientation. Hot stage TEM observations[12,13] of gb dislocations (gbd) and partially melted polycrystalline aluminum specimen indicated that the gb structure remains ordered up to 0.96 T_m (gbd observations) and no complete gb melting is observed at temperatures below 0.999 T_m.

The present work is also in agreement with various simulation results[18-21] which indicate that gb melting should occur at T_m. The fact that the disordering transition appears to be continuous is a noteworthy piece of evidence supporting the suggestion[21] that the thermodynamic parameters should be continuous function of temperature and the disordered gb region must retain some crystalline symmetry because of the finite layer thickness at temperatures below T_m. On the other hand, our findings do differ from a MD simulation study in which excess free energy is calculated leading to the conclusion that the gb premelting is a first order transition occurring at 0.76 T_m[22]. It has been suggested recently[82] that gb migration effects which can be frustrated by the use of three-dimensional periodic border condition and which can give rise to premelting behavior may play a role.

Reference

[1]R. King, B. Chalmers, Prog. Met. Phys., 1, 127 (1947).

[2]H. Gleiter and B. Chalmers, High Angle Grain Boundaries, (Pergamon Press, Oxford, 1972), chapter 5.

[3]V. Pontikis, presented at Conference on Interface Science and Engineering '87, Lake Placid, NY, July 1987 (in press, J. de Physique).

[4]C. Rothman, presented at Conference on Interface Science and Engineering '87, Lake Placid, NY, July 1987 (in press, J. de Physique).

[5]V. Pontikis, P. Sindzingre, Physica Scripta, T19, 375 (1987).

[6]P. Lagarde, M. Biscondi, Can. Metall. Q, 13, 245 (1974).

[7]P. Lagarde, M. Biscondi, Mem. Sci. Revue Metall., 71, 121 (1974).

[8]T. Watanabe, S-I. Kimura, S. Karashima, Phil. Mag. A, 49, 845 (1984).

[9]U. Erb, H. Gleiter, Scripta Met., 13, 61 (1979).

[10]R.W. Balluffi, R. Maurer, Scripta Met., 22, 709 (1988).

[11]T. Watanabe, S-I. Kimura, S. Karashima, Phil. Mag. A, 49, 845 (1984).

[12]S.W. Chan, J.S. Liu, R.W. Balluffi, Scripta Met., 19 1251 (1985).

[13]T.E. Hsieh, R.W. Balluffi, submitted to Acta Met.

[14]Recently these results have been reviewed by Pontikis (see ref. 3) together with the requirements and difficulties of a reliable MD computations.

[15]R. Kikuchi and J.W. Cahn, Phys. Rev. B, 21, 1893 (1980).

[16]F. Carrion, G. Kalonji, S Yip, Scripta Met. 17, 915 (1983).

[17]P. Deymier, G. Kalonji, R. Najafabadi, S. Yip, Surf. Sci., 144, 67 (1984).

[18]G. Ciccotti, M. Guillope, V. Pontikis, Phys. Rev. B, 27, 5576 (1983).

[19]M. Guillope, G. Ciccotti, V. Pontikis, Surf. Sci., 144, 67 (1984).

[20]M. Guillope, J. Phys. 47, 1347 (1986).

[21]J. Q. Broughton, G. H. Gilmer, Phys. Rev. Letter, 56 2692 (1986).

[22]P. Deymier, A. Taiwo, G. Kalonji, Acta Metall., 35, 2719 (1987).

[23]P. S. Ho, T. Kwok, T. Nguyen, C. Nitta, S. Yip, Scripta Met., 19, 993 (1985).

[24]T. Nguyen, P. S. Ho, T. Kwok, C. Nitta, S. Yip, Phys. Rev. Letter, 57, 1919 (1986).

[25]J. Lutsko, D. Wolf, submitted to Phys. Rev. Lett.

[26]J.M. Haile, A Primer on the Computer Simulation of atomic Fluid by Molecular Dynamics, Clemson University, Clemson, South Carolina, 1980.

[27]G.H. Bishop, R.J. Harrison, T. Kwok, S. Yip, Progress in Mater. Sci., Chalmers Anniversary Vol., J.W. Christian, P. Haasen, T.B. Massalski, eds., (Pergamon Press, NY 1981), p. 49.

[28]M.S. Daw and M.I. Baskes, Phys. Rev. Lett., 50, 1285 (1983).

[29]M.S. Daw and M.I. Baskes, Phys. Rev. B, 29, 6443 (1984).

[30]S.M. Foiles, M.I. Baskes and M.S. Daw, Phys. Rev. B, 33, 7983 (1985).

[31]T. Nguyen, S. Yip, D. Wolf, presented at Conference on Interface Science and Engineering '87, Lake Placid, NY, July 1987 (in press, J. de Physique).

[32]J. Lutsko, D. Wolf, S. Phillpot, S. Yip, T. Nguyen, submitted to Phys. Rev. B

[33]M.J. Weins, H. Gleiter, B. Chalmer, J. Appl. Phys. 42, 2639 (1971).

[34]M. Hashimoto, Y. Ishida, R. Yammamoto, M. Doyama, J. Phys. 10, 1109 (1980).

[35]T. Kwok, P.S. Ho, S. Yip, Phy. Rev. B, 29, 5354 (1984).

[36]H.B. Huntington, Diffusion in Solids - Recent Development, (Academic Press, NY 1975), p.303.

[37]T. Kwok, Proc. of 1st Int'l USLI Science and Technology Symp., ECS. ed., (1987) in press.

[38]R.M.J. Cotterill and M. Doyama, in Lattice Defects and Their Interactions, R. Hasiguti (ed.), Gordon and Breach, New York, 1967, p. 1.

[39]M. Weins, Surf. Sci., 31, 138, (1972).

[40]G. Hasson, J.Y. Boos, I. Herbeuval, M. Biscondi and C. Goux, Surf. Sci., 31, 115 (1972).

[41]M. Hashimoto, Y. Ishida, R. Yamamoto and M. Doyama, Acta Metall., 29, 617 (1981).

[42]M.S. Duesbery, G. Jacucci and R. Taylor, J. Phys. F, 9, 413 (1979).

[43]D. Wolf, Acta Metall, 32, 245 (1984).

[44]R.A. Johnson, in Computer Simulation in Material Science, R.J. Arsenault, J.R. Beeler, Jr., D.M. Esterling, eds., (American Society for Metals, Metals Park, OH 1987), p. 29.

[45]M.W. Finnis, J.E. Sinclair, Philos. Mag., A 50, 45 (1984).

[46]D.J. Oh, R.A. Johnson, J. Mater. Res., 3, 471 (1988).

[47]M. Baskes, M. Daw, B. Dodson and S. Foiles, MRS Bulletin, 13, 28 (1988).

[48]M.S. Daw and R.L. Hatcher, Solid State Comm, 56, 697 (1985).

[49]S.M. Foiles, Phys. Rev. B, 32, 3409 (1985).

[50]S.M. Foiles and M.S. Daw, J. Vac. Sci. Tech. A, 13, 1565 (1985).

[51]S.M. Foiles, Phys. Rev. B, 32, 7685 (1985).

[52]S.M. Foiles, in Computer-Based Microscopic Description of the Structure and Properties of Materials, J. Broughton, W. Krakow and S.T. Pantelides (eds.), Material Research Society Symposia Proceeding, vol 63, 1986, p. 61.

[53]S.M. Foiles and M.S. Daw, J. Mater. Res., 2, 5 (1987).

[54]S.M. Foiles, private communication

[55]E. Clementi, C. Roetti, At. Data Nucl. Data Table, 14, 177 (1974).

[56]J.H. Rose, J.R. Smith, F. Guinea, J. Ferrante, Phys. Rev. B, 29, 2963 (1984).

[57]G. Hasson, M. Biscondi, P. Lagarde, J. Levy and C. Goux, in The Nature and Behaviors of Grain Boundary, H. Hu (ed.), Plenum Press, New York, 1972, p. 3.

[58]W. Bollman, Crystal Defects and Crystalline Interfaces, Springer, Berlin, 1970.

[59]G.H. Bishop and B. Chalmers, Script. Metall., 2, 133 (1968).

[60]D. Wolf, J. Phys. Colloq., C4, 46, 197 (1985).

[61]T. Nguyen and S. Yip, to be published.

[62]G.H. Bishop, R.J. Harrison, T. Kwok, S. Yip, J. Appl. Phys., 53, 5609 (1982).

[63]M. Parrinello, A. Rahman, J. Appl. Phys., 52, 7182 (1981).

[64]B.J. Alder, J.R. Vaisnys, G. Jura, J. Chem. Solids, 11, 182 (1959).

[65]S. Phillpot, J. Lutsko, D. Wolf, submitted to Phys. Rev. Lett.

[66]J. Lutsko, to be published.

[67]R.L. Cormia, J.D. Mackenzie, D.J. Turnbull, J. Phys. Chem., 65, 2239 (1963).

[68]J. Daeges, H. Gleiter and J.H. Perepezko, Phys. Lett. A, 119, 79 (1986).

[69]For a complete discussion, see R.W.Cahn, Nature, 323, 668 (1986).

[70]J.M.W. Frenken, P.M.J. Maree, J.F. van der Veen, Phys. Rev. B, 34, 7506 (1986).

[71]R. Lipowsky, W. Speth, Phys. Rev. B, 28, 3983 (1983).

[72]J. Q. Broughton, L.V. Woodcock, J. Phys. C, 11, 2743 (1978).

[73]P. Stoltze, J.K. Norskov, U. Landman, Phys. Rev. Lett., 61, 440 (1988).

[74]V. Rosato, G. Ciccotti, V. Pontikis, Phys. Rev. B, 33, 1860 (1986).

[75]J.K. Kristensen, R.M. J. Cotterill, Phil. Mag., 36, 437 (1977).

[76]J.Q. Broughton, X.P. Li, Phy. Rev. B, 35, 1920 (1987).

[77]J. Lutsko, private communication.

[78]F.H. Stillinger, T.A. Weber, Phys. Rev. B, 31, 5262 (1985).

[79]I. Ebbsjo, T. Kinell, I. Weller, J. Phys. C, 13, 1865 (1980).

[80]G.H. Bishop, R.J. Harrison, T. Kwok, S. Yip, J. Appl. Phys., 53, 5596 (1982).

[81]D. Nenow, A. Trayanov, J. Crystal Growth, 79, 801 (1986).

[82]J.F. Lutsko, Scripta Met., submitted.

[83]R. Lipowsky, Phys. Rev. Lett., 57, 2683 (1986); R. Lipowsky, W. Speth, Phy. Rev. B, 28, 3983 (1983).